Identification and Biological Characterization of Indoline-Based Autophagy Inhibitors

Dissertation

zur Erlangung des akademischen Grades eines
Doktors der Naturwissenschaften
(Dr. rer. nat.)
der Fakultät für Chemie und Chemische Biologie
der Technischen Universität Dortmund

vorgelegt von
M. Sc. Marjorie A. Rummelt
Geboren am 08.08.1988
in Chiclayo, Peru

Dortmund 2017

Die vorliegende Arbeit entstand im Zeitraum von Oktober 2013 bis Juli 2017 unter der Anleitung von Prof. Dr. Dr. h.c. Herbert Waldmann an der Fakultät für Chemie und Chemische Biologie der Technischen Universität Dortmund und dem Max-Planck-Institut für molekulare Physiologie Dortmund.

1. Gutachter: Prof. Dr. Dr. h.c. Herbert Waldmann

2. Gutachter: Prof. Dr. Martin Engelhard

Para Stephan & mi familia

ACKNOWLEDGEMENTS

First of all, I would like to thank Prof. Dr. Herbert Waldmann for giving me the opportunity to work in this very exciting field and in such a great scientific environment. I highly appreciate his input and support during the course of this thesis.

I am very grateful to Dr. Yaowen Wu, my co-supervisor, for his support, ideas, and valuable collaboration.

I would like to express my gratitude to Prof. Dr. Martin Engelhard for being my second examiner.

I deeply thank Dr. Petra Janning and Dr. Slava Ziegler for their guidance, support, and input during our scientific discussions.

Very special thanks to the whole autophagy team, in particular Dr. Luca Laraia and Lucas Robke, for the numerous and fruitful scientific discussions, great collaboration, and unconditional support. I am furthermore grateful to Dr. Georgios Konstantinidis and Dr. Hana Návarová for their help with the autophagy assay and performing several experiments that contributed to my thesis.

I gratefully acknowledge Dr. Sonja Sievers, Claude Ostermann, and the rest of the COMAS for screening my compounds.

I thank the MS team, in particular Dr. Petra Janning, Andreas Brockmeyer, Malte Metz, and Jens Warmers, for the processing and analysis of the samples produced in my proteomics experiments. Furthermore, I am grateful to Katharina Kuhr and Chantale Martin for the HR-MS measurement of my samples. Big thanks to the NMR department of the TU Dortmund. I am also grateful to the administration, IT department, and facility management of the MPI Dortmund for all the help during the past years. I thank Brigitte Rose in particular, for her support with administrative issues.

I am deeply grateful to the generous funding by the Fonds der chemischen Industrie, in form of a Kekulé fellowship, and the Swiss National Science Foundation, which granted me a Doc.mobility fellowship. I would also like to thank the CGC-supporting companies—AstraZeneca, Bayer, Böhringer Ingelheim, and Merck—for funding this project.

For the careful proofreading of my thesis, I would like to express my gratitude to Dr. Luca Laraia, Dr. Slava Ziegler, and Dr. Stephan Rummelt. Since I did not live in Dortmund anymore at the time, Guillaume Garivet kindly helped me with the entire thesis submission process, for which I am endlessly grateful.

I am immensely grateful to Dr. Luca Laraia–my mentor, colleague, and friend. He was always available to discuss the project's results and progress and patiently guided me through most of the techniques in cell biology and biochemistry required in this project. His enthusiasm and scientific curiosity managed to constantly motivate me. He is the best teacher I know and one of the brightest scientists I have ever met.

Very special thanks to Guillaume Garivet and Javier de Ceballos Cerrajería for the countless hours of scientific discussions. Dr. Glòria Vendrell helped me with enzymatic assays, for which I am very grateful. I would also like to thank Melanie Schwalfenberg, who had an answer to any biology-related question I had. Additionally, I would like to express my gratitude to all my colleagues and coworkers that contributed to my thesis with input or experimental help, in particular: Dr. Silke Brand, Dr. Tim Förster, Dr. Stephanie Gueret, Dr. Peter 't Hart, Nadine Kaiser, Dr. Shobhna Kapoor, Dr. Tatsuro Kawamura, Lea Kremer, Dr. Philipp Küchler, Dr. Pablo Martín-Gago, Nancy Martinez, Dr. Tom Mejuch, Christine Nowak, Elena Reckzeh, Sumersing Patil, Beate Schölermann, Janine Schulte-Zweckel, Julian Wilke, Michael Winzker, and Stefan Zimmermann.

I am deeply grateful to Dr. Stephan Rummelt, for his helpful input in chemistry-related questions and, most importantly, for his moral support during these four years.

I would like to thank the Waldmann group, in particular my labmates, for the great working atmosphere. For the fun times outside of the lab, the lovely memories of Dortmund, and their valuable friendship, I would like to thank especially Dr. Hélène Adihou, Javier de Ceballos Cerrajería, Andreas Christoforow, Guillaume Garivet, Ingrid 't Hart, Dr. Peter 't Hart, Dr. Hilde van Hattum, Zhi-Jun Jia, Nadine Kaiser, Dr. Shobhna Kapoor, Dr. Luca Laraia, Yen-Chun Lee, Nancy Martinez, Dr. Tom Mejuch, Elena Reckzeh, Lucas Robke, Sumersing Patil, Melanie Schwalfenberg, Dr. Glòria Vendrell, Michael Winzker, and, last but not least, Stefan Zimmermann.

I would like to conclude by thanking my family, in particular my husband, my mother, and my sister for their love and support, without which this thesis would not have been possible.

TABLE OF CONTENTS

ABSTRACT .... **I**

KURZZUSAMMENFASSUNG .... **III**

1. PREFACE **5**

2. INTRODUCTION **7**

2.1. Autophagy **7**
- 2.1.1. Autophagy Process and Autophagic Machinery 8
- 2.1.2. Regulation of Autophagy by Upstream Signaling 10
- 2.1.3. Role of Autophagy in Disease 11
- 2.1.4. Small-Molecule Autophagy Modulators 12

2.2. Chemical Genetics **14**
- 2.2.1. Target Identification by Forward Chemical Genetics 15

2.3. Forward Chemical Genetics in Autophagy **23**

3. AIM OF THE THESIS **26**

4. RESULTS AND DISCUSSION **27**

4.1. Identification of an Indoline-Based Autophagy Inhibitor **27**
- 4.1.1. Phenotypic Screen for the Identification of Autophagy Inhibitors 27
- 4.1.2. Effect of Autophagy Inhibitors on Known Regulators of Autophagy 32
- 4.1.3. Validation of Indoline **1a** as an Inhibitor of Starvation-Induced Autophagy 33
- 4.1.4. Conclusion 37

4.2. Synthesis of an Indoline-Based Compound Collection **38**
- 4.2.1. Retrosynthetic Analysis of Indoline **1a** 38
- 4.2.2. Synthesis of Indoline 1a Analogs with Varying Sulfonamide Aryl Groups 38
- 4.2.3. Synthesis of Indoline 1a Analogs with Varying Carboxamide Groups 40
- 4.2.4. Synthesis of Indole Derivatives of Indoline **1a** 42
- 4.2.5. Synthesis of Additional Analogs of Indoline **1a** 43
- 4.2.6. Conclusion 44

4.3. Structure–Activity Studies of an Indoline 1a-Derived Compound Collection **45**
- 4.3.1. Biological Relevance of the Aryl Sulfonamide Functionality 45
- 4.3.2. Biological Relevance of the Carboxamide Functionality 49
- 4.3.3. Biological Relevance of Additional Modifications 50
- 4.3.4. Conclusion 51

4.4. Target Identification by Affinity Chromatography **53**
- 4.4.1. Design and Synthesis of Pull-Down Probes 53
- 4.4.2. Biological Activity and Stability of Pull-Down Probes 65
- 4.4.3. Affinity Chromatography and Subsequent SILAC-Based Quantitative Proteomics . 67

4.4.4. Target Validation ... 68
4.4.5. Conclusion ... 77

4.5. Target identification by Thermal Proteome Profiling ... 79
4.5.1. Thermal Proteome Profiling with Indoline **1a** ... 79
4.5.2. Target Validation ... 81
4.5.3. Conclusion ... 85

4.6. Computational Target Prediction ... 86
4.6.1. Evaluation of Pyruvate Kinase as Target of Indoline **1a** ... 88
4.6.2. Evaluation of RAF and ABL1 Kinases as Targets of Indoline **1a** ... 89
4.6.3. Evaluation of Serotonin Receptors as Targets of Indoline **1a** ... 90
4.6.4. Evaluation of Different GPCR families as Targets of Indoline **1a** ... 94
4.6.5. Conclusion ... 95

5. SUMMARY ... 96

6. EXPERIMENTAL PART ... 103

6.1. Materials used in Biological Experiments ... 103
6.1.1. Buffers and Solutions ... 103
6.1.2. Antibodies for Western blotting ... 104
6.1.3. Software ... 104
6.1.4. Laboratory Equipment ... 105

6.2. Methods used for Biological Experiments ... 106
6.2.1. Methods in Mammalian Cell Culture ... 106
6.2.2. Autophagy-Related Assays ... 108
6.2.3. Affinity-Based Proteomics ... 111
6.2.4. Cellular Thermal Shift and Thermal Proteome Profiling ... 115
6.2.5. Methods in Protein Biochemistry ... 119
6.2.6. Methods to Study Small Molecule–Target Binding ... 121
6.2.7. Profiling Services ... 122

6.3. Materials in Chemical Synthesis ... 127

6.4. Synthesis of Indoline-Based Analogs ... 128

6.5. Synthesis of Pull-Down Probes ... 161

7. LIST OF ABBREVIATIONS ... 181

8. REFERENCES ... 185

9. APPENDIX ... 195

Curriculum Vitae ... 195

Eidesstattliche Erklärung/Affidavit ... 197

ABSTRACT

Autophagy is a vital catabolic process involved in the degradation of cellular components, which plays an important role in cancer and neurodegenerative disorders. Due to their high complexity, the pathways regulating autophagy have not been fully elucidated. The development of specific autophagy modulators and the identification of their cellular targets can provide valuable insight into the regulation of this process and, ultimately, its role in disease.

Herein, a potent inhibitor of starvation-induced autophagy (IC_{50} = 520 ± 550 nM) was identified using a phenotypic screen. In a series of secondary assays, the compound was validated as an autophagy inhibitor. The structure–activity relationship for this compound class was derived from a synthesized compound collection of structural analogs and used for the preparation of a chemical probe for affinity-based proteomics ("pull-down"). Glutamate dehydrogenase (GDH) and calpain-1 were isolated by means of affinity-based proteomics but devalidated as targets of the inhibitor in various biophysical and biochemical assays. The ATP-gated ionotropic receptor P2X4 and the Ragulator component LAMTOR5 were the most promising targets determined by thermal proteome profiling and are currently under evaluation.

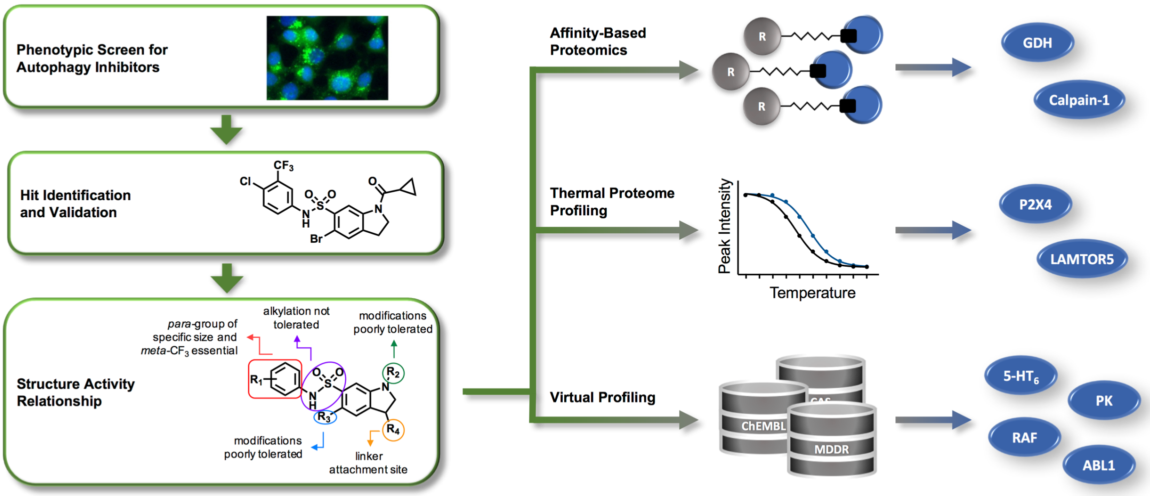
Phenotypic Screen for Autophagy Inhibitors
Hit Identification and Validation
Cl
CF_3
O
S
O
N
H
Br
N
O
Structure Activity Relationship
para-group of specific size and *meta*-CF_3 essential
alkylation not tolerated
modifications poorly tolerated
R_1
R_2
R_3
R_4
modifications poorly tolerated
linker attachment site
Affinity-Based Proteomics
R
Thermal Proteome Profiling
Peak Intensity
Temperature
Virtual Profiling
ChEMBL
MDDR
GDH
Calpain-1
P2X4
LAMTOR5
5-HT$_6$
PK
RAF
ABL1

Targets predicted using a computational approach based on chemical similarity included 5-hydroxytryptamine (5-HT) receptors and multiple kinases—rapidly accelerated fibrosarcoma (RAF1) and related kinases, pyruvate kinase (PK), and abelson murine leukemia viral oncogene homolog 1 (ABL1). Whereas no modulating effect on the predicted kinases was observed, the autophagy inhibitor was a potent antagonist of the G-protein-coupled serotonin receptor 5-HT$_6$ (IC_{50} = 1 µM). However, as known antagonists of the receptor did not inhibit autophagy, 5-HT$_6$ was considered an off-target. Given the strong antagonistic effect seen, G-protein-coupled receptors

need to be further evaluated as potential targets of the identified inhibitor. The successful target identification of this potent inhibitor could help deliver further understanding of the complex mechanisms that regulate autophagy.

KURZZUSAMMENFASSUNG

Autophagie ist ein lebensnotwendiger katabolischer Prozess, der am Abbau zellulärer Komponenten beteiligt ist und eine wichtige Rolle bei Krebs und neurodegenerativen Krankheiten spielt. Aufgrund der hohen Komplexität der Autophagie-regulierenden Signalwege konnten diese noch nicht vollständig entschlüsselt werden. Die Entwicklung spezifischer Autophagie-Modulatoren und die Identifizierung ihrer zellulären Zielproteine können einen wertvollen Einblick in die Regulierung von Autophagie und letztendlich ihre Rolle in Krankheiten gewähren.

Im Rahmen dieser Arbeit wurde mittels phänotypischem Screening ein potenter Inhibitor von durch Aushungern induzierter Autophagie identifiziert (IC_{50} = 520 ± 550 nM). In einer Reihe sekundärer Assays wurde diese Verbindung als echter Autophagie-Inhibitor validiert. Die Struktur-Aktivitätsbeziehung für diese Verbindungsklasse wurde aus einer hergestellten Substanzkollektion abgeleitet, anhand derer eine chemische Sonde synthetisiert wurde. Glutamatdehydrogenase (GDH) und Calpain-1 wurden durch Affinitätschromatographie isoliert, allerdings anschließend in verschiedenen biophysikalischen und biochemischen Assays als Zielproteine des Autophagie-Inhibitors devalidiert. Mittels thermischem Proteomprofiling wurden der ATP-abhängige Ionenkanal P2X4 und die Ragulator-Komponente LAMTOR5 als vielversprechendste Zielproteine identifiziert und werden derzeit untersucht.

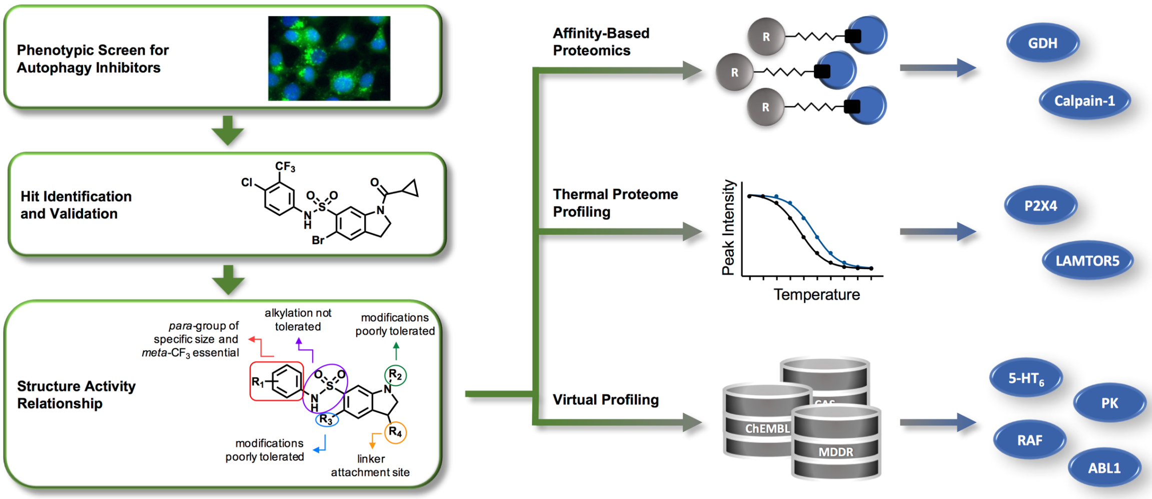
Phenotypic Screen for Autophagy Inhibitors
Hit Identification and Validation
CF_3
Cl
O
S
N
H
Br
Structure Activity Relationship
para-group of specific size and *meta*-CF_3 essential
alkylation not tolerated
modifications poorly tolerated
R_1
R_2
R_3
R_4
modifications poorly tolerated
linker attachment site
Affinity-Based Proteomics
R
GDH
Calpain-1
Thermal Proteome Profiling
Peak Intensity
Temperature
P2X4
LAMTOR5
Virtual Profiling
ChEMBL
CAS
MDDR
5-HT$_6$
PK
RAF
ABL1

5-Hydroxytryptaminrezeptoren und mehrere Kinasen—rapidly accelerated fibrosarcoma (RAF1) und verwandte Kinasen, Pyruvatkinase (PK) und abelson murine leukemia viral oncogene homolog 1 (ABL1)—waren unter den Zielproteinen, die durch rechnergestützte Ansätze anhand von strukturellen Ähnlichkeiten vorausgesagt wurden. Während kein Effekt auf die PK beobachtet wurde, war der Autophagie-Inhibitor ein potenter Antagonist des G-Protein-gekoppelten

Serotoninrezeptors 5-HT_6 (IC_{50} = 1 µM). Da allerdings bekannte Antagonisten dieses Rezeptors Autophagie nicht inhibierten, wurde 5-HT_6 als „Off-Target“ bezeichnet. Angesichts des beobachteten starken antagonistischen Effekts, müssen G-Protein-gekoppelte Rezeptoren genauer als mögliche Zielproteine des identifizierten Inhibitors untersucht werden. Die erfolgreiche Identifizierung des Zielproteins dieses Inhibitors könnte dazu beitragen, weitere Einsicht in die komplexen Autophagie-regulierenden Mechanismen zu ermöglichen.

1. PREFACE

Almost a century ago, Spemann and Mangold discovered what proved to be the foundation for understanding cell communication: When they transplanted a blastopore lip from an amphibian gastrula into the opposite side of another embryo, the authors noticed that gastrulation was induced in the surrounding tissue of the host, leading to the formation of a Siamese twin.[1]

Today we know that cell behavior is strongly influenced by external stimuli, which not only allow intercellular communication, but also regulate numerous processes throughout the life of a cell, e.g. division, differentiation, homeostasis, and programmed death. Extracellular signaling molecules ("ligands") are, together with proteins and phospholipids, part of complex networks called signal transduction pathways, which are orchestrated in a tightly regulated fashion to maintain cellular function.

A signal transduction cascade generally starts with binding of an extracellular ligand to a transmembrane receptor. The bound receptor then triggers a series of activation events, resulting in the specific modulation of gene transcription and, ultimately, cellular response.[2] To date, numerous signaling pathways have been discovered, of which only few govern the vast majority of cellular processes.[3] Indeed, the induction or inhibition of such processes is also highly influenced by the cell competence, signal intensity, and cross-regulation between different pathways.[4]

Defects in cell signaling are responsible for various types of diseases, including immunodeficiency, neurodegenerative disorders, diabetes, and cancer.[5-6] The latter is a good example of how aberrant signaling pathways can have a major impact on health. A synergism of often more than one oncogene with abnormal expression causes uncontrolled proliferation, inhibition of tumor suppressor genes, and metastasis regardless of the nutrient levels or oxygen supply in the cell.

Recent work has shown that metabolic perturbations are a frequent cause for numerous human diseases.[7] Extensive research in this area has provided a large number of therapeutic targets and valuable insight into metabolic signaling pathways.[8] However, the complexity of cellular processes makes their study a significant challenge, posing many riddles, which can only be deciphered through an interdisciplinary approach.

2. INTRODUCTION

Cell metabolism encompasses all the processes by which energy is converted inside a cell and is therefore involved in numerous key cellular functions. This strictly regulated equilibrium of constant synthesis and degradation of material allows for the proper functioning of cells.

Before the 1950s, it was believed that proteins were stable *in vivo* and did not give catabolism the importance it has nowadays.[9] The understanding of metabolism only began with the discovery of protein degradation in lysosomes by de Duve *et al*.[10] Shortly after, irregularly shaped, double membraned vacuoles filled with cytoplasm and organelles were observed,[11-12] which were subsequently transformed into lysosomal-like structures.[13] It became evident that these vacuoles served for the degradation of cellular components and were hence named *autophagosomes*, Greek for "self-eating bodies."[14]

2.1. Autophagy

Autophagy is a eukaryotic cellular process that mediates the degradation of cytosolic components to maintain homeostasis. This dynamic process acts primarily as a highly conserved response to nutrient deprivation—i.e., starved cells induce autophagy as a recycling mechanism to temporarily compensate for the lack of extracellular nutrients. Furthermore, autophagy is involved in the clearance of long-lived or unnecessary proteins and organelles.[15] For example, autophagy is responsible for the elimination of paternal mitochondria after fertilization.[15] The degradation of dysfunctional mitochondria is another important function of this process, as it prevents the release of reactive oxygen species and other toxic proteins to the cytosol.[15] The clearance of protein aggregates is also crucial to protect cells from toxic cellular waste. Apart from its role as a response to cellular stress, basal levels of autophagy are necessary for maintaining cellular homeostasis.[16] Autophagy is therefore a vital catabolic process in the development, differentiation, and survival of cells.[15, 17-19]

Three types of autophagy have been identified to date: chaperone-mediated autophagy, microautophagy, and macroautophagy. The former delivers soluble proteins containing a specific pentapeptide motif (i.e., KFERQ) to the lysosome using cytosolic chaperones.[20-22] Microautophagy refers to the direct engulfment of cytosolic components by invagination of lysosomal membranes.[21] The best characterized form of autophagy is macroautophagy, which, as microautophagy, involves the removal of cytosolic components. The difference lies in the sequestration mode: in macroautophagy, double-membraned vesicles called autophagosomes are responsible for engulfing large cytosolic portions.[22] Macroautophagy and microautophagy can be both selective or non-selective. Selective modes are triggered by the recognition of autophagy substrates by specific receptors. One example is mitophagy, the degradation of unnecessary and damaged mitochondria.[22] Non-selective autophagy, on the other hand, is mainly responsible for the recycling of biomolecules for the production of nutrients and energy. Given that it is the main route to the lysosome and therefore the most prominent form of autophagy, this work focuses on the study of non-selective macroautophagy (hereafter autophagy).[9]

2.1.1. Autophagy Process and Autophagic Machinery

Autophagy starts with the formation of the autophagophore (or "pre-autophagosomal structures" in yeast), a double-membraned structure responsible for the sequestration of autophagic cargo. Autophagophores form in mammals predominantly at the contact sites between mitochondria and the endoplasmatic reticulum (ER).[22] However, the exact lipid source for membrane formation of autophagophores remains unclear. Autophagosomes are built upon the elongation and closure of autophagophores. These transient organelles have a diameter of approximately 1 μm and no hydrolytic activity.[22] For their maturation, autophagosomes are transported to the lysosomes along microtubules by dynein motor proteins. Once at the lysosome site, they fuse to endosomes and later lysosomes, generating autolysosomes, where the autophagic cargo is finally degraded (Figure 1).[21] This process requires a complex machinery acting in a coordinated fashion at each stage.

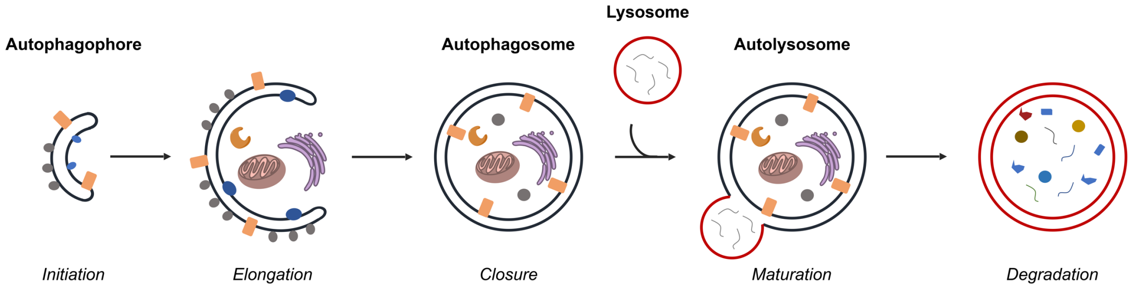

Figure 1. Formation, elongation, and maturation of autophagosomes. Adaptation from Yang and Klionsky.[18]

The identification of yeast autophagy-related (ATGs) genes in the early 1990s by Ohsumi and coworkers provided a breakthrough in the understanding of the molecular basis of autophagy.

With the discovery of the first mammalian ATG genes by Mizushima *et al.* it was demonstrated that this process is highly conserved from humans to yeast.[23]

In mammals, the autophagic machinery comprises over 20 so-called autophagy-related (ATG) proteins, responsible for autophagosome formation and maturation. They can be divided in three functional units: the unc-51 like autophagy activating kinase 1 (ULK1) and its effectors and two ubiquitin-like conjugating systems (Figure 2).[24] ULK1 is the mammalian homolog of the yeast Atg1 protein and the most upstream ATG kinase. It activates class III phosphoinositide 3-kinase (PI3K, also named vacuolar protein sorting 34 [VPS34]) complex, which is essential in every step of autophagic flux. For example, VPS34 mediates the recruitment of the autophagic machinery to the growing autophagophore.

The key protein of the first conjugating system is light chain 3 (LC3), the mammalian homolog of Atg8, which is responsible for the autophagophore elongation and closure. The cysteine protease ATG4 cleaves a C-terminal sequence of pro-LC3 to form LC3-I, which is then activated by the ubiquitin-like conjugating enzyme (E1-like) ATG7, and subsequently transferred to the E2-like enzyme ATG3. LC3-I is then lipidated with phosphatidylethanolamine (PE) to form LC3-II, allowing its recruitment to the autophagophore. This last step is mediated by the ATG12 conjugating system. ATG12 is activated by ATG7 and subsequently transferred to ATG10 to allow the formation of the ATG5–ATG12 conjugate. This conjugate forms a homodimer with ATG16L, which mediates the lipidation of LC3-I. Given the complexity of this process, upstream signaling is crucial for the regulation of the autophagic machinery at numerous stages.

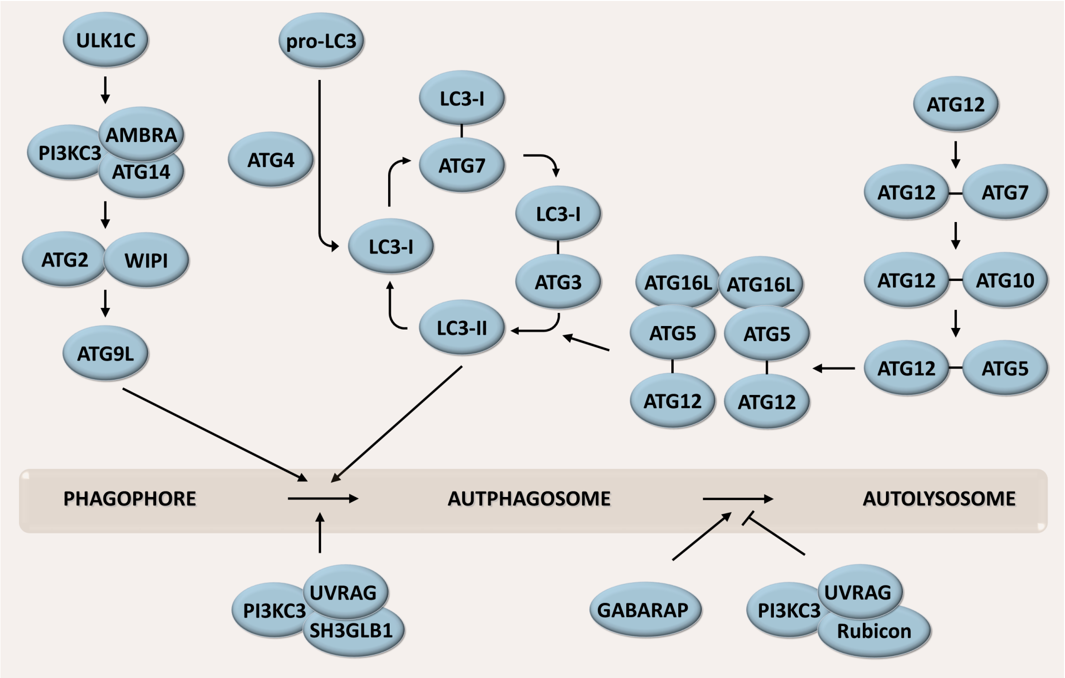
ULK1C
pro-LC3
LC3-I
ATG12
PI3KC3
AMBRA
ATG14
ATG4
ATG7
ATG12
ATG7
LC3-I
ATG2
WIPI
LC3-I
ATG16L
ATG16L
ATG3
ATG12
ATG10
ATG5
ATG5
LC3-II
ATG9L
ATG12
ATG12
ATG12
ATG5
PHAGOPHORE
AUTPHAGOSOME
AUTOLYSOSOME
PI3KC3
UVRAG
SH3GLB1
GABARAP
PI3KC3
UVRAG
Rubicon

Figure 2. Mechanism of the autophagic machinery. AMBRA = Activating molecule in BECN1-regulated autophagy protein 1; WIPI = WD repeat domain phosphoinositide-interacting protein; UVRAG = UV radiation resistance-associated gene protein; SH3GLB1 = endophilin-B1; GABARAP = Gamma-aminobutyric acid receptor-associated protein.

2.1.2. Regulation of Autophagy by Upstream Signaling

Autophagosome formation is a multistep process, which is regulated by upstream signaling. Signal transduction can be triggered by nutrient levels, growth factors and amino acids. Though not yet fully elucidated, two main autophagy-regulating pathways have been discovered, referred to here as mammalian target of rapamycin (mTOR)-dependent pathway and phospholipase Cε (PLCε) pathway (Figure 3).[15] The mTOR-dependent pathway acts via class I PI3K, protein kinase B (PKB) and the mTOR complex 1 (mTORC1). The activation of mTORC1 blocks autophagy by inhibiting the components of autophagosome formation directly.[25] Consequently, inhibition of mTOR by rapamycin induces autophagy. This canonical pathway is sensitive to nutrient levels and can therefore be activated by withdrawal of amino acids or glucose. In the second pathway, elevated levels of cyclic AMP (cAMP) and Ca^{2+} inhibit autophagy by activating PLCε.[26] Additional regulators of autophagy are B cell lymphoma 2 (Bcl-2), which blocks autophagy by sequestering Beclin-1 from the Beclin-1/PI3K complex,[27] and transcription factor EB (TFEB), which induces autophagy upon dephosphorylation.[28]

Although several signaling pathways that regulate autophagy and their key players have been identified, these remain unclear. Numerous missing links within each pathway and lacking information about the cross-talk between these urge the discovery of novel proteins involved in the regulation of this catabolic process. This knowledge can ultimately provide important information about the role of autophagy in disease and its potential in therapy.

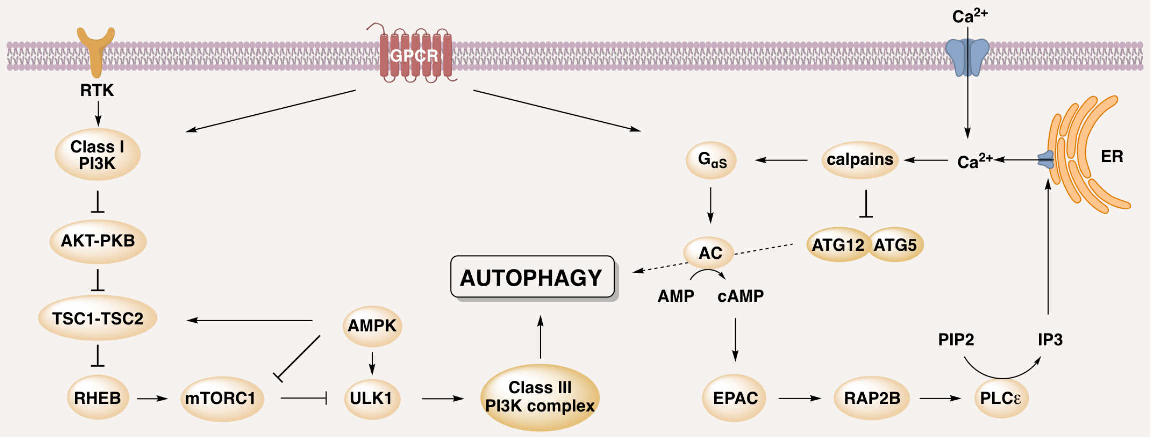

Figure 3. Representation of the two major pathways regulating autophagosome formation. Right: PLCε-dependent pathway; left = mTOR-dependent pathway. ER = endoplasmatic reticulum; GPCR = G-protein coupled receptor; RTK = receptor tyrosine kinase; AC = adenylate cyclase; EPAC = exchange protein directly activated by cAMP; PIP_2 = phosphatidylinositol 4,5-bisphosphate; IP_3 = inositol 1,4,5-trisphosphate; TSC = tuberous sclerosis; RHEB = Ras homolog enriched in brain; AMPK = 5'-AMP-activated protein kinase. Adaptation from Rubinsztein et al.[15]

2.1.3. Role of Autophagy in Disease

Because of its important role in numerous cellular functions, altered levels of autophagy and genetic defects in the autophagic machinery have been linked to the development and onset of diseases, such as neurodegenerative disorders, cancer, and diabetes.[15, 29] For instance, physical exercise has been proven to induce autophagy and protect mice from diabetes.[30]

Most late-onset neurodegenerative diseases can arise from toxic protein aggregates failing to be cleared in neurons. For example, aggregates of β-amyloid and mutant forms of huntingtin and α-synuclein are responsible for Alzheimer's, Huntington's, and Parkinson's disease, respectively. Recent studies show that the clearance of these aggregates is enhanced when autophagy is induced. Furthermore, their accumulation is observed at low levels of autophagy.[31-33] Consistent with these findings, an impairment of autophagosome formation and degradation has been reported in Alzheimer's disease.[15, 34]

Evidence suggests a dual role of autophagy in cancer, depending on the stage of tumorigenesis.[35] The increased clearance of toxic cellular waste acts as a preventive mechanism against cancer. E.g., tumor suppressor genes such as tuberous sclerosis (TSC) 1 and 2 stimulate autophagy. Moreover, the mitophagy-mediated clearance of damaged mitochondria prevents ROS generation, which has a known tumorigenic potential. On the other hand, autophagy can promote tumor cell survival by providing these with energy despite the nutrient-limiting conditions of tumor microenvironments.[15, 35] Consequently, whereas autophagy upregulation might serve as a preventive strategy against cancer, autophagy inhibition is a potential approach in cancer therapy.

2.1.4. Small-Molecule Autophagy Modulators

Of the numerous autophagy modulators identified to date, several have entered clinical trials (Table 1). The mTOR-inhibitor rapamycin is widely used for specific induction of autophagy and has been shown to reduce amyloid-β levels.[36] Further examples of autophagy activators are lithium and metformin, which are currently in phase II clinical trials for Alzheimer's disease.[29] Inhibitors of autophagy include bafilomycin A1 and the unselective PI3K inhibitor Wortmannin.[15] Due to their off-target effects and high cytotoxicity, these compounds are only utilized in research. Only recently, selective inhibitors of the mTOR upstream kinases AMPK, ULK1, and VPS34 were developed, which, as expected, inhibit autophagy. Other important tools for the modulation of autophagy are the autophagy flux inhibitor chloroquine and its derivative hydroxychloroquine. These quinoline-derived modulators act by inhibiting autophagosome–lysosome fusion, thereby leading to an accumulation of autophagosomes. Surprisingly, chloroquine and hydroxychloroquine are the only autophagy inhibitors in advanced clinical trials, which highlights the need for new modulators of this process.

Table 1. Examples of autophagy modulators in research and clinics.[29, 37-38]

	Modulator	Structure	Mode of Action	Clinics/Model
Activators	**Rapamycin**	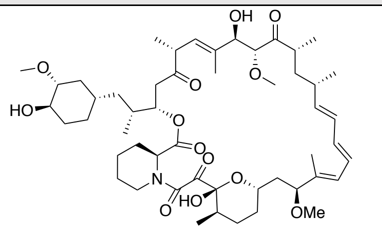	inhibits of mTOR	Alzheimer's disease, animal models
	Lithium	Li^+	reduces IP_3 levels	Alzheimer's disease, phase II
	Metformin	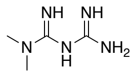	upregulates AMPK	Alzheimer's disease, phase II
	Carbamazepine	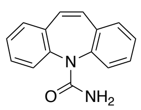	reduces IP_3 levels	α1-antitrypsin deficiency liver cirrhosis, phase II
	Trehalose	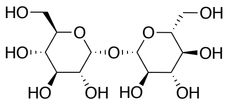	unknown	Huntington's disease, animal models
Inhibitors	**(Hydroxy)chloroquine**[a]	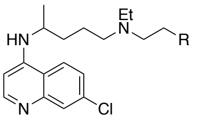	inhibits autophagosome–lysosome fusion	various cancers
	Bafilomycin A1	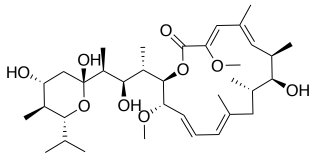	inhibits vATPase and autophagosome–lysosome fusion	experimental agent
	Dorsomorphin	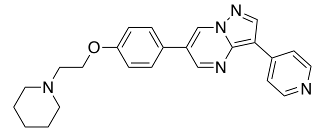	inhibits AMPK	in preclinical evaluation
	SAR405	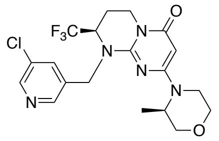	inhibits class III PI3K	in preclinical evaluation
	SBI-0206965	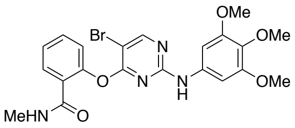	Inhibits ULK1	in preclinical evaluation
	Spautin	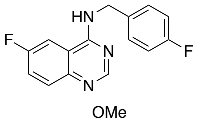	lowers beclin-1 levels	experimental agent
	Wortmannin	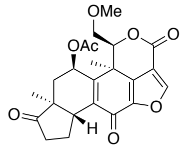	inhibits PI3K	experimental agent

a) R = H: chloroquine; R = OH: hydroxychloroquine.

As many questions remain open regarding the function of autophagy in disease, there is a strong need for a deeper understanding of the mechanisms underlying this cellular process. Therefore, the development of novel autophagy small-molecule activators and inhibitors is of great importance in areas beyond therapeutic research. For example, the specific modulation of autophagy at the various stages of the process enables the detailed study of its function in different cellular environments. Furthermore, identification of the cellular targets of modulators in an approach called forward chemical genetics enables the discovery of new autophagy regulators and can ultimately reveal new targets for drug discovery.

2.2. Chemical Genetics

Classical and chemical genetics are biological tools used in the study of the function of a signaling pathway, protein, or gene. In classical genetics, genes that play a role in a specific pathway can be identified and their function determined by screening mutant libraries of an organism and evaluating their phenotype. Its chemical-biological equivalent uses libraries of small molecules to perturb the function of a protein.[39] Unlike in the study of genetic effects, modulation by small molecules allows a temporal and much more rapid readout, as compounds can trigger a phenotypic response within seconds. In addition, the extent of the phenotypic response can be fine-tuned by varying the concentration of the compound utilized, which is not feasible when conducting a genetic experiment.[40-41] Further advantages of the chemical approach include the ability of small molecules to disrupt protein-protein interactions and perturb a single function of a multifunctional protein.[42] The major limitation of chemical genetics is that small molecules are often not specific for one single protein. Moreover, whereas every gene can be manipulated, selective modulators are available only for a fraction of all proteins.[39]

Similarly to classical genetics, the chemical approach distinguishes between forward and reverse chemical genetics. The goal in forward chemical genetics (FCG) is to identify proteins that regulate a given cellular process. In reverse chemical genetics (RCG), the function of a protein is determined by identifying a selective small-molecule modulator of a protein and subsequently using this compound to analyze the triggered phenotypic response and hence understand the function of the protein (Figure 4).[41, 43]

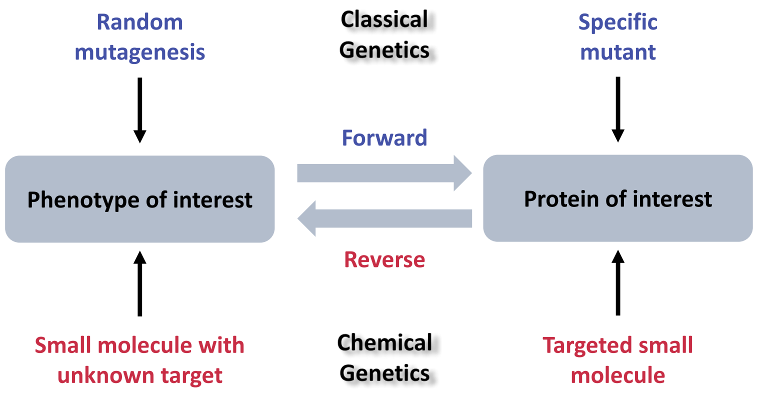
Random mutagenesis
Classical Genetics
Specific mutant
Forward
Phenotype of interest
Protein of interest
Reverse
Small molecule with unknown target
Chemical Genetics
Targeted small molecule

Figure 4. Difference between forward and reverse classical and chemical genetics. Adaptation from Lehar et al. [41]

2.2.1. Target Identification by Forward Chemical Genetics

The discovery of proteins involved in a signaling pathway can give great insight into important cellular processes and provide the basis for new drug discovery programs. To this end, the targets of small molecules with a desired phenotypic effect can be identified using FCG.

A typical FCG experiment starts with the screening of a compound library for the desired phenotypic response in cells or organisms. The use of libraries consisting of bioactive compounds with known targets, such as the library of pharmaceutically active compounds (LOPAC®), can significantly accelerate the identification of new regulators of a pathway. On the other hand, screening of unbiased libraries may lead to novel targets for which no specific modulators are known or that are poorly characterized.

Once a compound is identified that triggers the desired response, the hit is tested in orthogonal assays to discard the possibility of a false-positive. The validated hit compound is then optimized to obtain more potent modulators with enhanced properties. For this step, it is necessary to generate a compound collection of structurally derived analogs of the parent hit. The structural analogs are then tested in the initial phenotypic screen to obtain information about the structure–activity relationship (SAR) of the compound class. The target of the small-molecule modulator can be identified by performing e.g. proteomics experiments or computational target prediction and subsequently validated in target engagement assays (Figure 5).

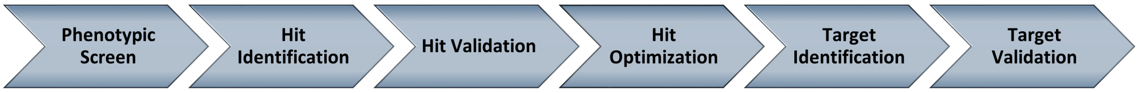

Figure 5. Workflow of forward chemical genetics for the target identification of a small-molecule that modulates a cellular process.

i. Phenotypic Screening

Common methods employed in phenotypic assays include cell viability, genetic engineering, and fluorescence-based techniques.[40, 44]

Viability screens with cancer vs. healthy cells allow the identification of compounds that are selectively toxic towards cancer cells. Most approaches assessing cell viability use reagents that are metabolized only in viable cells with an intact metabolism or protease activity to produce a fluorescent or colorimetric product.[45]

To investigate pathways that involve the activation of specific transcription factors, the sequence of an intracellular reporter that produces a measurable signal is fused to the promoter region of the gene of interest.[46] One example is the broadly applied luciferase-based phenotypic screen to study the Wnt/β-catenin signaling pathway. When this pathway is active, a cascade triggers the translocation of β-catenin into the nucleus, which then binds to T-cell factor/lymphoid enhancer factor (TCF/LEF) transcription factors, leading to the transcription of the target genes. To detect the activation of the pathway, a vector containing the TCF/LEF-binding promoter sequence fused to the firefly luciferase gene can be transfected into cells. Hence, activation of the Wnt signaling cascade leads to the transcription of luciferase, which catalyzes the reaction of luciferin to the fluorescent oxyluciferin.[47] Additional reporter proteins utilized are β-galactosidase and green fluorescent protein (GFP). The latter has been optimized to produce higher intensity emission upon excitation with blue light. This enhanced GFP (eGFP) allows, besides its use as a reporter protein, the localization of eGFP-tagged proteins *in vivo* and is hence a powerful tool in phenotypic screening.[48-49]

In addition to fluorescently tagged proteins, specific organelles or biomolecules can be visualized using selective cellular dyes. The readout of multiple parameters, e.g. cell morphology or multiple fluorescence signals can be performed by high-content screening (HCS). This technique has gained great importance over the past two decades and is nowadays a standard procedure for drug discovery, as it incorporates cellular imaging into a high-throughput strategies.[50]

ii. Proteomic Hit Identification Strategies

The most challenging and time-consuming steps of an FCG project are the target identification and validation of a small-molecule. The human genome encodes around 20,000 proteins,[51] 600 lipids,[52] and 10,000–20,000 carbohydrate epitopes for glycan-binding proteins,[53] all of which, including nucleic acids, could be the target of a small molecule.[40] Given this vast diversity and the distinct chemical properties of each small molecule present in a chemical library, no general method can be applied to the target identification of a compound hit. For instance, the identification of integral membrane proteins requires different techniques than the one of cytosolic proteins. Moreover, the chemical nature of a small molecule or natural product may not allow the modifications required for various proteomics experiments. Despite these limitations, the most widely applied target identification methodology is affinity-based chromatography, which has provided the cellular targets for numerous compounds over the past decades.[40]

a) Affinity-Based Proteomics

In a so-called "pull-down" experiment, the modulator is immobilized to a solid support and subsequently exposed to a cell lysate, thereby allowing binding to its target. Stringent washing removes non-specific binding, and the remaining bound proteins are analyzed by mass spectrometry (MS) (Figure 6)

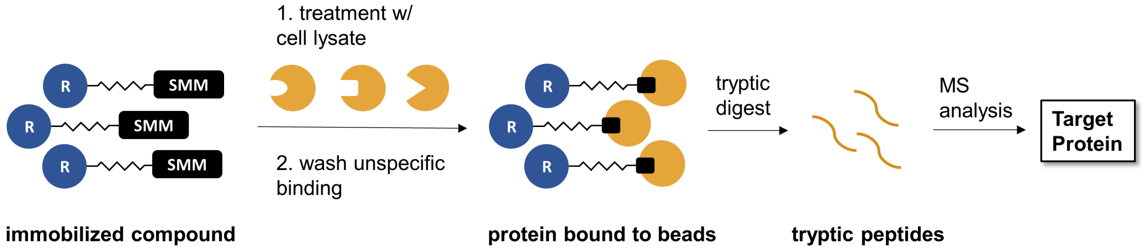

Figure 6. Principle of an affinity-based proteomics experiment ("pull-down"). R = resin; SMM = small-molecule modulator.

For the immobilization to a solid support, a linker needs to be attached to the compound. To identify a site that allows modifications without compromising the activity of the parent compound, the information derived from the SAR study is necessary. Depending on its chemical nature, the compound can be attached to the linker directly, i.e. through a functional group already present in the molecule, or via a spacer bearing a reactive group, such as an amine, a carboxylic acid, or an alcohol. In addition to the active chemical probe, a negative control probe is required, which is derived from an inactive analog.

The use of a linker is essential, as it prevents steric hindrance between the target and the solid support. Furthermore, it can allow the compound to enter a potentially unexposed binding site of a protein. Depending on its composition, hydrophilic linkers can enhance the solubility of the small molecule and prevent non-specific binding to the target. Commonly used linkers are two- and three-unit polyethylene glycol (PEG)-based, as they meet all the above-mentioned criteria. Other linkers with enhanced properties include polyproline and tartaric acid linkers.[54-55] The pull-down probe can be immobilized to the beads either covalently or by affinity. For a covalent attachment, beads bearing activated groups, e.g. *N*-hydroxysuccinimide (NHS), are employed, which readily react with alcohols and amines. Affinity binding can be performed with the well-established biotin/streptavidin or a similar system.[40]

When bound to the matrix, the proteins can be eluted using an excess of unmodified compound. Alternatively, release of the bound proteins can be accomplished by denaturation with detergents (e.g. sodium dodecyl sulfate [SDS]). This method is utilized for gel-based proteomics, in which the proteins in the elution sample are separated by SDS-polyacrylamide gel electrophoresis (PAGE) and the bands cut, tryptically digested, and analyzed by MS. For a quantitative analysis, the proteins are directly digested while still immobilized to the beads and the released tryptic peptides analyzed by high resolution MS. In liquid chromatography (LC)-MS/MS (tandem MS), the peptides are separated by reversed-phase LC prior to MS analysis. A tandem mass spectrometer detects peptide ions and their fragmentation products, resulting in an ultra-high-resolution spectrum. The results are then compared to a protein database, e.g. UniProt, to identify the proteins isolated. Proteins enriched by the active probe when compared to the negative control are considered as potential targets.[56]

Carr and coworkers developed a quantitative approach for affinity-based proteomics that combines stable isotope labeling with amino acids in cell culture (SILAC)[57] with affinity enrichment.[58] This technique has, next to the recent advances in mass spectrometry, greatly enhanced the capabilities of affinity-based proteomics.[40, 56] As the name implies, cells are cultured with medium containing heavy isotope-labeled amino acids, e.g. $^{13}C_6$,$^{15}N_2$-L-lysine and $^{13}C_6$,$^{15}N_4$-L-arginine, leading to the incorporation of these into their proteins. The “heavy” lysate is then incubated with the active probe, and a normal lysate, i.e. with isotopically unlabeled proteins, is incubated with the control. Subsequently, both samples are combined and analyzed by tandem MS. The labelling results in a characteristic mass shift, i.e. 8 Da for lysine- and 10 Da for arginine-labeled peptides.[58] A protein enriched by the active probe exhibits “heavy” mass peaks with a higher intensity than the "light" peaks and is thus identified as potential target of the small molecule (Figure 7).

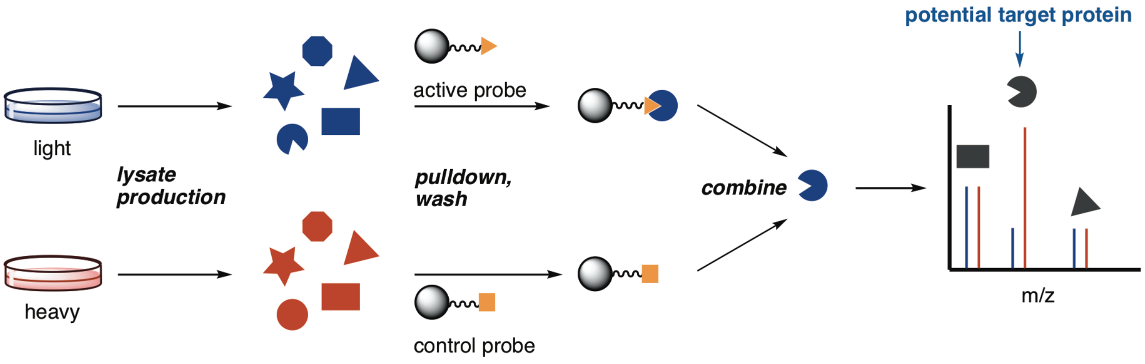

Figure 7. Principle of quantitative affinity-based proteomics by SILAC. Adaptation of Ziegler et al.*[40]*

b) Label-Free Methods

Target identification technologies that require labeling of the bioactive molecule have certain drawbacks. For instance, modifications on the hit compound may not be tolerated, leading to inactive pull-down probes.[59] In addition, the incorporation of a linker can result in off-target binding or lower solubility. These limitations can be overcome by employing linker-free techniques. Some of these methods rely on the fact that proteins are stabilized when bound to a compound. One example is the drug affinity responsive target stability (DARTS), which takes advantage of the lower susceptibility of a ligand-bound protein towards proteases than when in the unbound state.

Thermal proteome profiling (TPP) is an alternative label-free approach, which combines the cellular thermal shift assay (CETSA) with quantitative proteomics.[60] The main principle behind this strategy is based on the changes in thermostability of a protein when bound to a ligand. With increasing temperature, the interactions within a protein that stabilize its tertiary structure break, and the protein unfolds or "melts". Binding to a compound can result in a measureable shift of a protein's melting temperature. In a TPP, cell lysate is incubated with either compound or a control and each sample is divided into ten aliquots. The aliquots are incubated at different temperatures, and the soluble fraction of each is analyzed by tandem MS. Since a protein precipitates upon unfolding, the intensity of a protein peak will decrease with increasing temperature, resulting in a melting curve. Proteins displaying a shift in the curve upon incubation with the compound are identified as potential targets. By using different neutron-encoded isobaric mass tagging reagents

(TMT10) for each aliquot, the ten samples of each set can be combined and analyzed simultaneously, thereby reducing the measurement time significantly (Figure 8).[60-61]

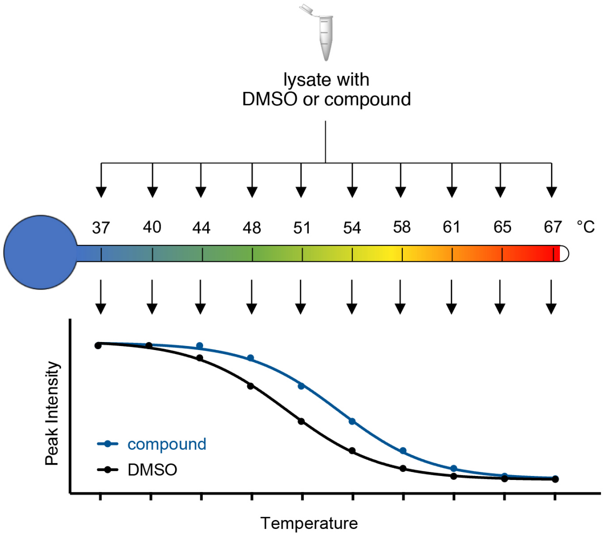

Figure 8. Principle of TPP. Compound- and DMSO-treated lysates are aliquoted into ten samples, and each set is incubated in a temperature gradient. The soluble fractions are TMT-labeled and analyzed by MS/MS. Adaptation from Savitski et al.*[60]*

Despite the remarkable advances in proteomics, the need for a cell lysate restricts the diversity of the pool containing potential targets to soluble and highly abundant proteins. For example, multispan-membrane proteins, such as membrane receptors and channels, represent a major obstacle in proteomics, as mild detergents are not capable of solubilizing these, and strong detergents can disrupt their structure.[56] Therefore, strategies for which protein solubilization is not necessary serve as attractive alternatives, in particular when a membrane protein is suspected as the target of a compound. Along these lines, a method that has been applied for the identification of membrane proteins involves *in situ* labeling with a chemical probe that can bind to their targets covalently *in vivo*, either through their intrinsic chemical reactivity or photocrosslinking. For in-gel fluorescence purposes, a second requirement is a probe that has a fluorescent tag in addition to the covalent or photo-tag. After incubation with the trifunctional probe and irradiation, the cells can be lysed with a strong detergent, such as SDS, and the samples analyzed by gel electrophoresis and fluorescence scanning.[56]

iii. Genetic Hit Identification

Yeast is a model system for the study of cellular mechanisms in humans, as at least one third of the encoded proteins are homologous in both organisms.[40] An effective method for target identification of small molecules is drug-induced haploinsufficiency profiling (HIP).[62] This genetic approach uses a set of bar-coded heterozygous yeast deletion strains, each of which has one specific monoallelic deletion and hence a lower concentration of the respective encoded protein. Consequently, each strain is highly sensitive to the interference of the function of the deleted gene. Thus, a small molecule targeting the locus of a gene leads to growth inhibition of the corresponding mutant strain, and the target can be identified by quantification thereof. A complementary strategy is the multicopy suppression profiling, which is based on the opposite principle to HIP. Here, a strain with the overexpressed target becomes more tolerant to the modulating small molecule.[40]

In most cases, a genetic profiling identifies not only the sought-after target, but also proteins involved in the same pathway. Thus, it can provide additional information, e.g. about the upstream regulation of the target. However, further experiments are necessary in this case to isolate the target.[40]

iv. Computational Hit Identification Strategies

Targets can be predicted using computational tools that compare the structural similarity of the query small molecule with a database of compounds whose cellular targets are known. One example is the Similarity Ensemble Approach (SEA), an algorithm that calculates the two-dimensional similarity developed by Shoichet and coworkers.[63] Using this powerful tool, the authors were able to confirm reported targets and identify new targets for numerous pharmaceutical compounds and U.S. Food and Drug Administration (FDA)-approved drugs, thereby demonstrating the value and reliability of computational methods.[64] Other algorithms, such as SwissTargetPrediction use the three-dimensional similarity to compare the shape of a pair of ligands,[65] which performs better when these display a low structural similarity.[66]

The downside of computational strategies lies in the dependence of similarity-based algorithms on existing protein-targeting ligands. Hence, a target for which either no or only structurally unrelated small-molecule modulators have been developed will not be identified.[66]

v. Validation of Identified Targets

The last step in forward chemical genetics consists in the confirmation of the identified protein as target of the small-molecule modulator in binding, functional, and genetic assays. This is the most important part of a target identification project, as it rules out off-target binding and proves an existing role of the target in the studied cellular process. Given that most target identification experiments deliver lists of numerous potential targets, validation studies need to prioritize according to whether their function can be relevant in the studied process.

Depending on whether a chemical probe is available or not, different methodologies can be applied. For example, binding of the molecular target can be confirmed by performing a competitive pull-down experiment with the linker-free compound, followed by immune-blotting.[40] When the lysate is incubated with the active probe together with the unmodified compound at high concentrations, the latter can outcompete binding of the active probe to the target, and thus less protein is isolated. However, proof of binding alone does not suffice to validate the potential target, since the protein may not be involved in the regulation of the studied pathway. To address this question, potent, selective modulators of the identified target, if available, can be tested in the initial phenotypic screen and should elicit the same response as the hit compound.

Binding affinity can be determined in biophysical assays. Commonly used techniques that do not require the modification of the compound or the protein include isothermal titration calorimetry (ITC) and differential scanning fluorimetry (DSF). The former measures the heat generated or required upon protein-compound binding and allows the determination of the dissociation constant (K_D). DSF uses the principle of the thermal shift assay (TSA) and thus determines the changes in protein thermostability. If a chemical probe of the compound is accessible, additional methods can be employed such as fluorescence polarization (FP) of surface plasmon resonance (SPR).[40] Binding studies, as well as co-crystallization of the protein-compound target, can give solid evidence of target engagement. However, all these approaches can be hampered by the poor accessibility of the target protein.

As binding of the compound may not affect the function of the target, orthogonal assays are mandatory for target confirmation. In this respect, functional assays can be conducted to investigate whether the compound modulates the activity of the putative target, provided that this is a protein whose function can be measured directly, such as an enzyme or a receptor. However, non-cellular biochemical assays may deliver conflicting information due to cell permeability, compound solubility, and cross-talk between different pathways.[40]

Small interfering RNA (siRNA) and complementary DNA (cDNA) are more accessible than the corresponding purified protein and allow the cellular knock-down and overexpression of the target, respectively. A genetic knock-down should display the same phenotype as an inhibitor of the studied pathway and an increased sensitivity towards treatment with the small molecule, leading to a shift in the IC_{50}. Inversely, cells with the overexpressed target should be more tolerant towards the treatment with the compound and display the same phenotype as an activator.

If no link between the identified target and the studied pathway has been established or the cellular function of the protein is unknown, the protein needs to be extensively characterized in order to understand its regulating role. The study of an uncharacterized protein is highly challenging but ultimately delivers novel regulators of a pathway and consequently valuable information for untangling the puzzle of cell biology.

2.3. Forward Chemical Genetics in Autophagy

As described in Chapter 2.1, the molecular mechanisms of autophagy regulation are poorly understood, despite the extensive research performed to counteract this lack of information. Nevertheless, the application of methods in both classical and chemical genetics have given rise to a significant number of modulators[15] and allowed the identification of multiple autophagy regulators.[67]

Cell-based screening is a useful starting point in the discovery of pathway regulators. Most screens monitor autophagy by determining the levels or localization of specific markers, e.g. LC3, a cytosolic protein essential in the formation and maturation of autophagosomes (Chapter 2.1.1). The development of GFP-LC3 transgenic mice to analyze autophagy *in vivo* by Mizushima *et al.*[68] revolutionized the field and provided a basis for the identification of autophagy modulators. This technique is based on the observation that, upon autophagy activation, LC3-I is conjugated to PE and consequently recruited to the isolation membrane. Therefore, whereas at basal conditions the GFP-LC3-I fluorescence is distributed throughout the cytoplasm, GFP-LC3-II accumulates to the autophagosomes when the autophagic response is active, and green fluorescent puncta can be detected (Figure 9).

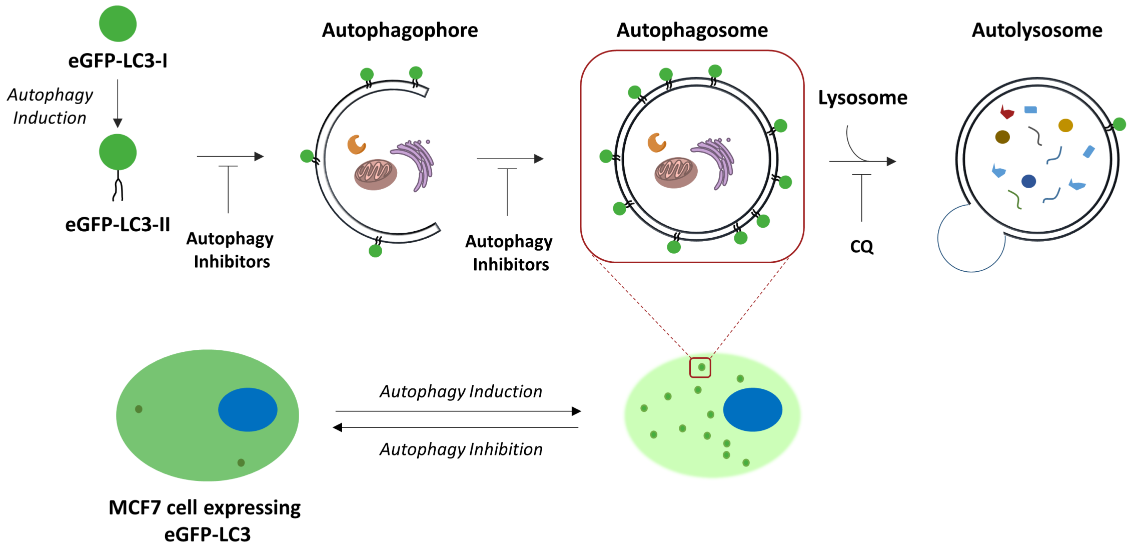

Figure 9. Schematic representation of the principle of the GFP-LC3-based phenotypic assay. Cells with basal levels of autophagy have a diffuse GFP signal. The GFP-tagged autophagy marker LC3-I is lipidated with PE upon induction of autophagy to form LC3-II and consequently recruited to the membrane of growing autophagophores. Autophagosomes can be detected as green puncta using fluorescence microscopy and quantified. Autophagy can be artificially induced by amino acid starvation or by inhibition of mTOR using rapamycin. Inhibition of the fusion to lysosomes by chloroquine causes an accumulation of puncta and thus an enhanced signal-to-noise ratio. Autophagy inhibitors reverse this phenotype, leading to a diffuse fluorescence signal.

Subsequently, Balgi *et al*. established the first automated phenotypic screen using the GFP-LC3 system in human cells, through which they identified numerous inducers of autophagy.[69] This method has been adapted for high-throughput screening and led to the discovery of numerous FDA-approved and GPCR-targeting compounds that modulate autophagy.[70-72] Moreover, the screening of unbiased chemical libraries has enabled the identification of compounds with novel chemotypes and targets that are yet to be discovered, including oxautins and autophagonizer.[73-75] Recently, Park and coworkers presented an alternative high-throughput screening approach to identify autophagy modulators that monitors lipid droplets. This methodology allows the direct measurement of a late-stage phenotypic effect of autophagy, and hence autophagic flux, by quantifying lipid droplets.[76]

Following a pilot phenotypic screen, hit validation is performed in a series of secondary screens and assays. Common techniques to confirm modulation of autophagy include the repetition of the phenotypic assay in different cell lines or in a tandem monomeric red fluorescent protein (mRFP)-GFP-LC3-based assay and immunoblotting for LC3-II or other autophagy markers.[67, 71] Further proof for autophagy modulation can be obtained by determining the levels or localization of downstream targets of autophagy regulators, e.g. the mTOR targets S6K1 and eukaryotic initiation factor 4E-binding protein 1 (4EPB1) and the phosphatidylinositol 3-phosphate (PI3P) sensors FYVE and WIPI2.[70-71, 73]

For the numerous autophagy modulators discovered in unbiased phenotypic screens, only few targets have been identified, most likely because of the recentness of the various assays required for this purpose. Using affinity-based proteomics, Sasazawa *et al*. identified valosin-containing protein (VCS) as the target of xanthohumol.[77] The label-free approach DARTS was applied in the identification of Cathepsin D and (TXNL1) as potential targets of dichloroacetate.[78] Most recently, Waldmann *et al*. discovered the potent autophagy inhibitor Autophinib and identified VPS34 as its target using target deconvolution.[79] The latter example represents one of the few target identifications of a synthetic modulator of autophagy and thereby highlights the importance of using target-agnostic phenotypic screens for the discovery of modulators with novel chemotypes. An unbiased strategy is therefore an effective way to identify novel regulators of autophagy.

3. AIM OF THE THESIS

Autophagy is an emerging therapeutic target for neurodegenerative disorders and cancer. Therefore, unraveling the mechanisms underlying autophagy is crucial to understand cell catabolism and its role in disease.

For this purpose, an autophagy inhibitor, identified in an in-house medium-throughput screen, was selected for further studies because of its potency and chemotype. The goal of this thesis was to validate the hit as an autophagy inhibitor in secondary assays and to identify its target(s) by means of forward chemical genetics. For this purpose, a compound collection of structural analogs should be generated and biologically evaluated to derive the SAR of the compound class. Based on the knowledge gained from the SAR analysis, a chemical probe for affinity-based proteomics should be prepared. Moreover, alternative target identification strategies, e.g. thermal proteome profiling and computational methods, should be exploited. The putative targets identified should be confirmed in biochemical and biophysical assays and evaluated for their role in autophagy. The identification of modulators is a useful way to study cellular pathways and can provide the basis for the discovery of autophagy regulators and ultimately novel targets for therapy.

4. RESULTS AND DISCUSSION

4.1. Identification of an Indoline-Based Autophagy Inhibitor

Specific modulation is a widely-used tool to study the effect of abnormal levels of autophagy on homeostasis and other vital processes in cells. The discovery of potent, specific autophagy modulators allows not only the study of this process, but also provides the foundation for its specific therapeutic targeting. Furthermore, by identifying the targets of specific autophagy modulators, further insight into the mechanisms regulating this vital signaling pathway can be gained.

4.1.1. Phenotypic Screen for the Identification of Autophagy Inhibitors

To discover new autophagy modulators, a medium-throughput screen for autophagy inhibition was established at the Compound Management and Screening Center (COMAS) of the Max Planck Institute of Molecular Physiology. Compounds that were able to inhibit artificially induced autophagy were identified as hits.

To monitor autophagy levels, the procedure developed by Balgi *et al.*[69] was employed in human MCF7 breast carcinoma cells stably expressing eGFP-LC3 (Chapter 2.3). In the assay, autophagy is induced in cells either by replacing full growing medium by Earle's balanced salt solution (EBSS), which triggers acute amino acid starvation, or by using the mTOR inhibitor rapamycin. In fed conditions, the fluorescence is distributed throughout the cytoplasm, and when the autophagic response is active, eGFP-LC3 accumulates to the autophagosomes and green fluorescent puncta can be detected (Figure 10). Inhibitors of autophagosome formation can reverse this phenotype. By using chloroquine (CQ), an inhibitor of the autophagosome-lysosome fusion, the degradation of autophagosomes can be blocked and the fluorescent signal enhanced.

Initially, 150,000 compounds were screened at a single concentration against starvation-induced autophagy. Compounds displaying an inhibition $\geq$ 70% (5,500 compounds) were rescreened in starvation-mode and for inhibition of autophagy induced by targeting mTOR using rapamycin. The dose-dependent inhibitory effect was determined for compounds exhibiting an average inhibition of $\geq$ 70%. Autophagy inhibitors with an $IC_{50} \leq 5$ µM were divided into two categories: active in starvation-induced autophagy (profile "S", 128 compounds) and active in starvation- and rapamycin-induced autophagy (profile "SR", 118 compounds). Given that S-inhibitors are not able to elicit an inhibitory response if autophagy is induced by inhibiting mTOR, they are expected to act upstream of mTORC1 or via an orthogonal pathway. In contrast, SR-inhibitors are expected to act either downstream of mTOR or through an mTOR-independent pathway. This strategy facilitates an early classification of autophagy inhibitors according to their modes of action.

Indoline **1a** was identified as a potent inhibitor of autophagic flux of the S-class (Figure 10, middle row), as it does not inhibit rapamycin-induced autophagosome formation at 10 μM (Figure 10, bottom row). Moreover, it was shown that **1a** inhibits autophagy dose-dependently with an IC_{50} = 520 ± 550 nM (Figure 11).

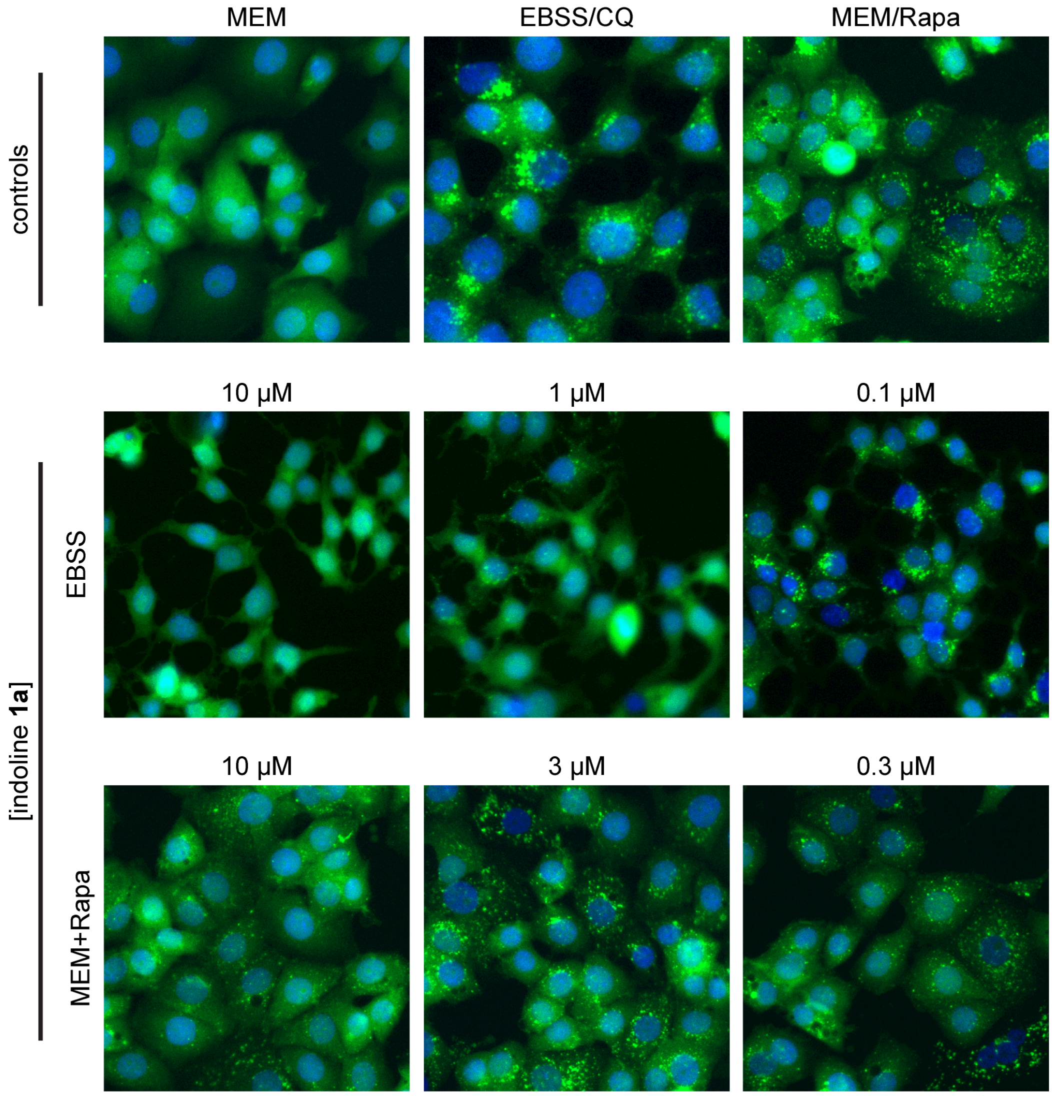
MEM
EBSS/CQ
MEM/Rapa
controls
10 µM
1 µM
0.1 µM
EBSS
[indoline **1a**]
10 µM
3 µM
0.3 µM
MEM+Rapa

Figure 10. Phenotypic assay employed to identify autophagy inhibitors using eGFP-LC3. MCF7 cells stably expressing eGFP-LC3 were either treated with rapamycin or starved of amino acids with EBSS, simultaneously treated with compound, and incubated for 3 h. The cells were fixed with formaldehyde and the nuclei stained blue with the DNA-binding reagent Hoechst. The green-fluorescent puncta are quantified and normalized to the MEM and EBSS or rapamycin controls. MEM = minimal essential medium; Rapa = rapamycin. Representative images shown (n = 4, each in N = 3).

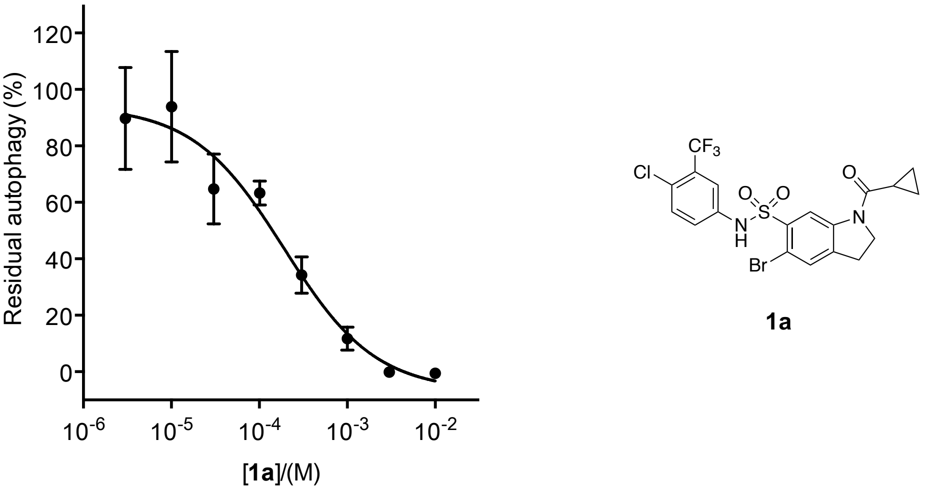

Figure 11. Indoline ***1a*** *(right) inhibits starvation-induced autophagy in a dose-dependent manner in the phenotypic assay described in Figure 10 (left). Autophagy is quantified by the number of puncta per nucleus and normalized to the MEM and EBSS controls. Data shown are mean values ± SEM (n = 4). Representative graph shown.*

GFP is prone to proteolytic degradation is the lysosomes, which can decrease its fluorescence when autophagosomes fuse to lysosomes. Moreover, its fluorescence is sensitive to the acidic lysosomal milieu.[80] Therefore, an apparent inhibitory effect observed in the GFP-based phenotypic screen can arise from enhancement of autophagosome–lysosome fusion leading to false positives.[81-82] In contrast, the mCherry signal is not affected by acidic pH. Consequently, the use of mCherry-GFP-tagged LC3 enables the visualization of autophagosomes and autolysosomes. In this tandem assay, whereas colocalization of the signals represents intact autophagosomes, an mCherry signal indicates the presence of autolysosomes. A true inhibitor of autophagosome formation should be able to decrease the number of both autophagosomes and autolysosomes.

As a first approach in the validation as an autophagy inhibitor, **1a** was tested in the above-described tandem mCherry-eGFP assay. The confocal images reveal that **1a** strongly inhibits autophagosome and hence autolysosome formation dose-dependently (Figure 12, Figure 13), thereby supporting the findings of the primary phenotypic assay.

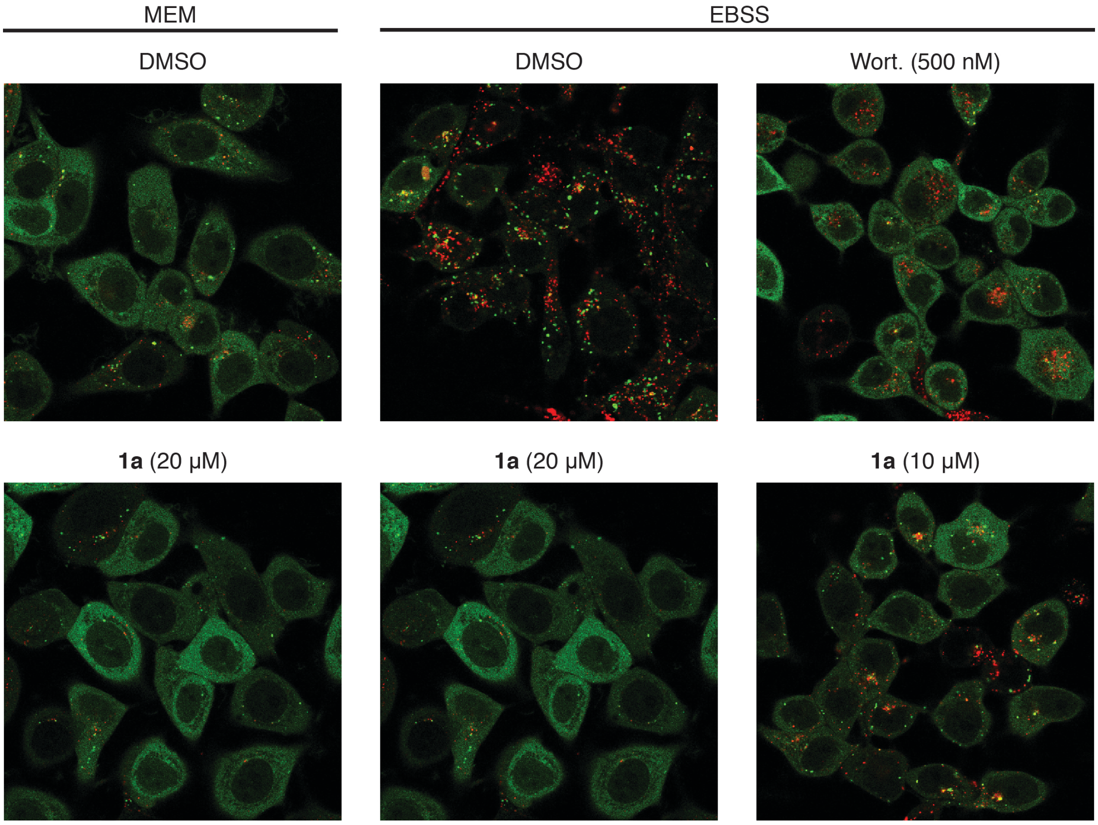

*Figure 12. Indoline **1a** inhibits the formation of autophagosomes. Effect of **1a** on autophagosomes (yellow) and autolysosomes (red) on starved MCF7 cells stably expressing mCherry-eGFP-LC3. Cells were incubated with **1a** either in MEM or EBSS, incubated for 3 h, and imaged. Representative images shown (N = 5).*

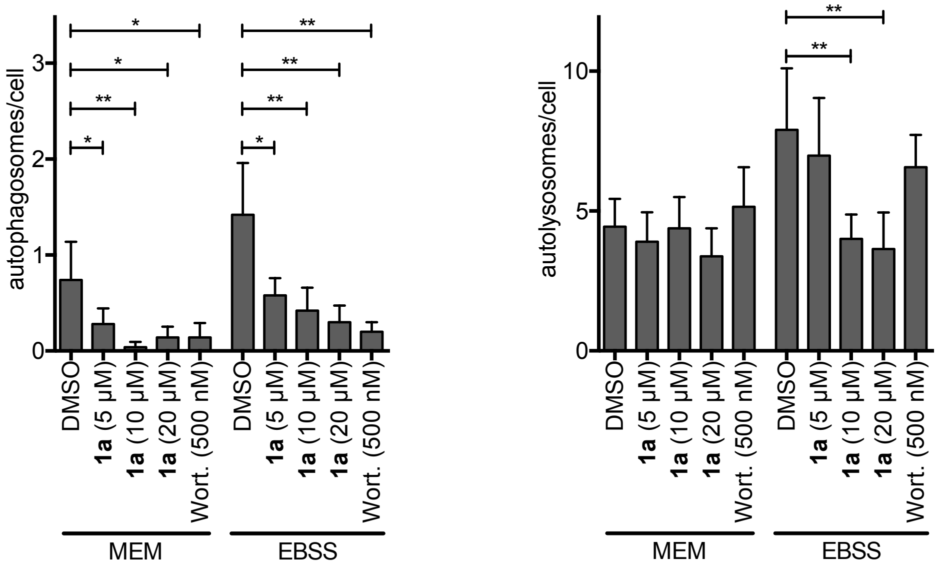

*Figure 13. Indoline **1a** inhibits autophagosome formation in a dose-dependent manner. Left: quantification of GFP puncta showed a decrease in autophagosomes in fed and starved conditions. Right: quantification of mCherry puncta showed a decrease in autolysosomes in starved and fed conditions.*

4.1.2. Effect of Autophagy Inhibitors on Known Regulators of Autophagy

Prior to performing target identification with resource- and time-intensive methods, such as affinity-based proteomics, it is crucial to determine whether the identified inhibitors act on known regulators of autophagy that are easily accessible for functional or binding assays. Therefore, the most potent inhibitors ($IC_{50} \leq 5$ μM) were selected for testing against a number of targets. Given that phosphorylation processes play a major role in autophagy, three kinases and a small panel of phosphatases were evaluated.

Phosphorylation events by the kinases VPS34, ULK1, and AMPK activate autophagy (Figure 3). Being, directly involved in the formation of autophagosomes, VPS34 is the most downstream kinase in the regulation pathway of autophagy. It produces PI3P in a localized manner,[83] which triggers the recruitment of WIPI-1 (the mammalian orthologue of Atg18) and other effector proteins to the growing autophagosomal membrane.[84-86] Activation of VPS34 complexes is caused by the phosphorylation of Beclin-1 by ULK1,[87] which is itself phosphorylated by AMPK and mTOR.[25] AMPK can additionally inhibit the repressive function of mTOR on autophagy by phosphorylating TSC2,[88] a negative regulator of mTOR, and the mTORC component raptor.[89]

According to their mode of action, 42 S-type and 45 SR-type inhibitors were assayed against the mTOR upstream kinase AMPK or the mTOR downstream kinases ULK1 and Vps34, respectively. In addition, the four most potent S-type inhibitors were evaluated against a panel of 23 phosphatases. Most of the compounds, including **1a**, showed no or little effect on the activity of the tested targets (Figure 14) and thus remain promising tools for finding novel regulators of autophagy.

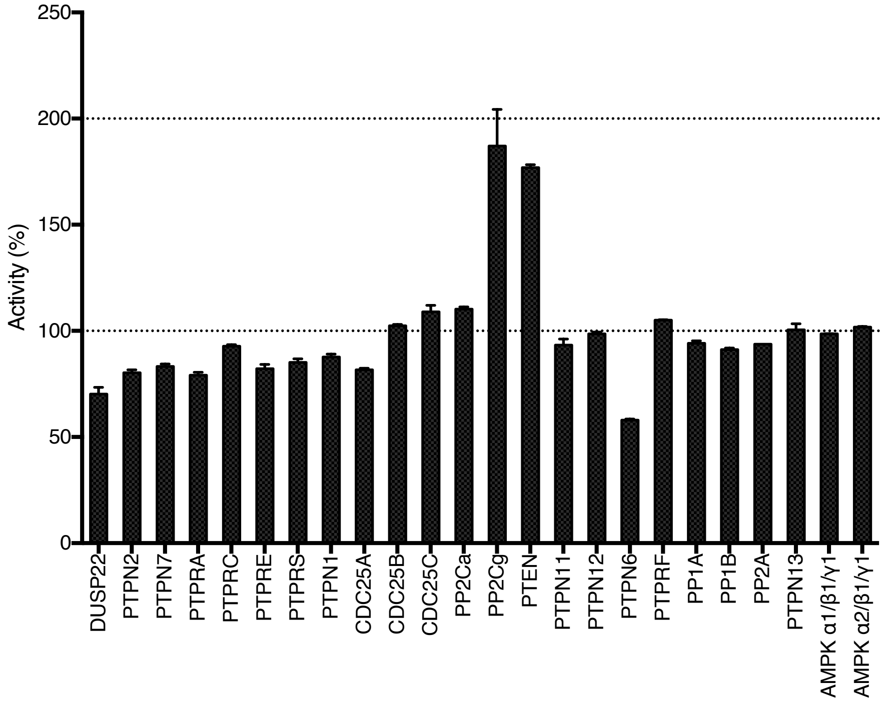

*Figure 14. Indoline **1a** has no effect on the activity of most of the phosphatases tested and AMPK at 10 µM. Phosphatase activities were determined in a colorimetric assay using purified phosphatase targets and* p-*nitrophenylphosphate or BIOMOL® Green reagent. AMPK activities were determined in a radiometric assay using purified AMPK and ^{33}P-ATP. Performed by SignalChem. Data shown are mean ± SEM (N = 2).*

4.1.3. Validation of Indoline 1a as an Inhibitor of Starvation-Induced Autophagy

To confirm the findings of the phenotypic screen and evaluate its toxicity, **1a** was tested in three independent assays.

GFP-based phenotypic screens can have certain limitations. As described in the previous chapter, GFP is sensitive to lysosomal environment. Furthermore, as a non-native protein, GFP is a target for proteasomal degradation and can affect the function of LC3 because of its size.[90] Therefore, an independent analysis of LC3 levels is necessary in parallel to the phenotypic screens. One strategy is to monitor the levels of LC3-II by immunoblotting, which increase upon activation of autophagy due to the lipidation of LC3-I. Another widely used marker is the ubiquitin-binding protein p62 (also known as sequestosome-1), which is degraded when the autophagic response is active. Using similar conditions as for the phenotypic screen, it was demonstrated that **1a** inhibits the accumulation of lipidated LC3 and the degradation of p62 in amino acid-starved cells in a dose-dependent manner (Figure 15).

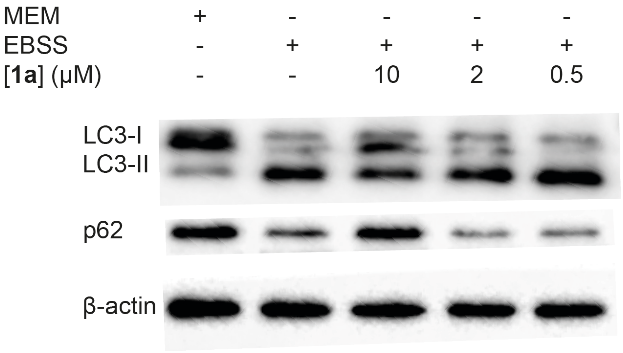

Figure 15. Indoline ***1a*** *inhibits the autophagy-induced accumulation of LC3-II and degradation of p62 in MCF7-eGFP-LC3 cells. MCF7 cells stably expressing eGFP-LC3 were incubated with either MEM, EBSS, or EBSS and compound for 3 h and lysed with Laemmli buffer. Denatured proteins were resolved on SDS-PAGE, transferred to a polyvinylidene fluoride (PVDF) membrane and probed for LC3-B (Cell Signaling, cat# 2775), p62 (MBL international, cat# PM045), and β-actin (Abcam, cat# ab8227) (n = 4).*

In order to study any cellular pathway using chemical genetics, it is essential to determine the toxicity of the biologically active compounds on the cell lines employed, as cytotoxic compounds can generate false-positive results. Moreover, as starved cells are not able to produce energy when autophagy is blocked, non-toxic autophagy inhibitors should be selectively toxic towards nutrient-deprived cells.

A common method to assess cell viability monitors the cleavage of water soluble tetrazolium salt 1 (WST-1) by mitochondrial dehydrogenases, which generates the dye formazan. The overall activity of these enzymes and hence the formation of formazan directly correlates with cell growth and can be monitored over time. By performing a WST-1 assay, it could be demonstrated that **1a** inhibits growth selectively in amino acid-starved MCF7 cells with an IC_{50} = 3.0 ± 0.4 µM (Figure 16).

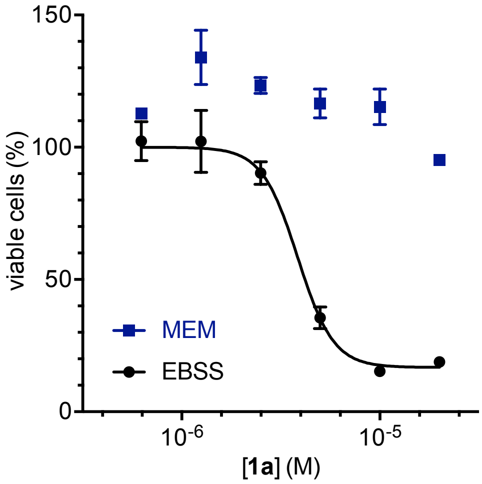

*Figure 16. Indoline **1a** is selectively toxic towards starved MCF7 cells. MCF7 cells in either full medium (MEM, blue) or under starvation conditions (EBSS, black) were treated with **1a**, and the viability was determined after 48 h by monitoring the absorbance for 1 h after addition of WST-1 reagent. Data shown are mean ± SEM (n = 3).*

To determine the mechanism of cell death, the apoptosis rate of MCF7 cells in the presence of **1a** was evaluated using an IncuCyte® analysis system. This automated platform combines contrast/fluorescence microscopy with cell incubation for time-dependent live-cell imaging of multiple samples and hence allows cell monitoring in the presence of compound under various conditions. The method employed here makes use of a DNA-intercalating agent, which is fluorescent when cleaved by active caspase 3/7 upon induction of apoptosis. Analysis of the cell confluence and fluorescence over 72 h revealed that **1a** has no effect on fed cells but induces apoptosis in amino acid-starved cells dose-dependently ($EC_{50} = 4.4 \pm 0.3$ μM, Figure 17), indicating that nutrient-deprived cells undergo cell death by means of apoptosis when autophagy is inhibited by **1a**.

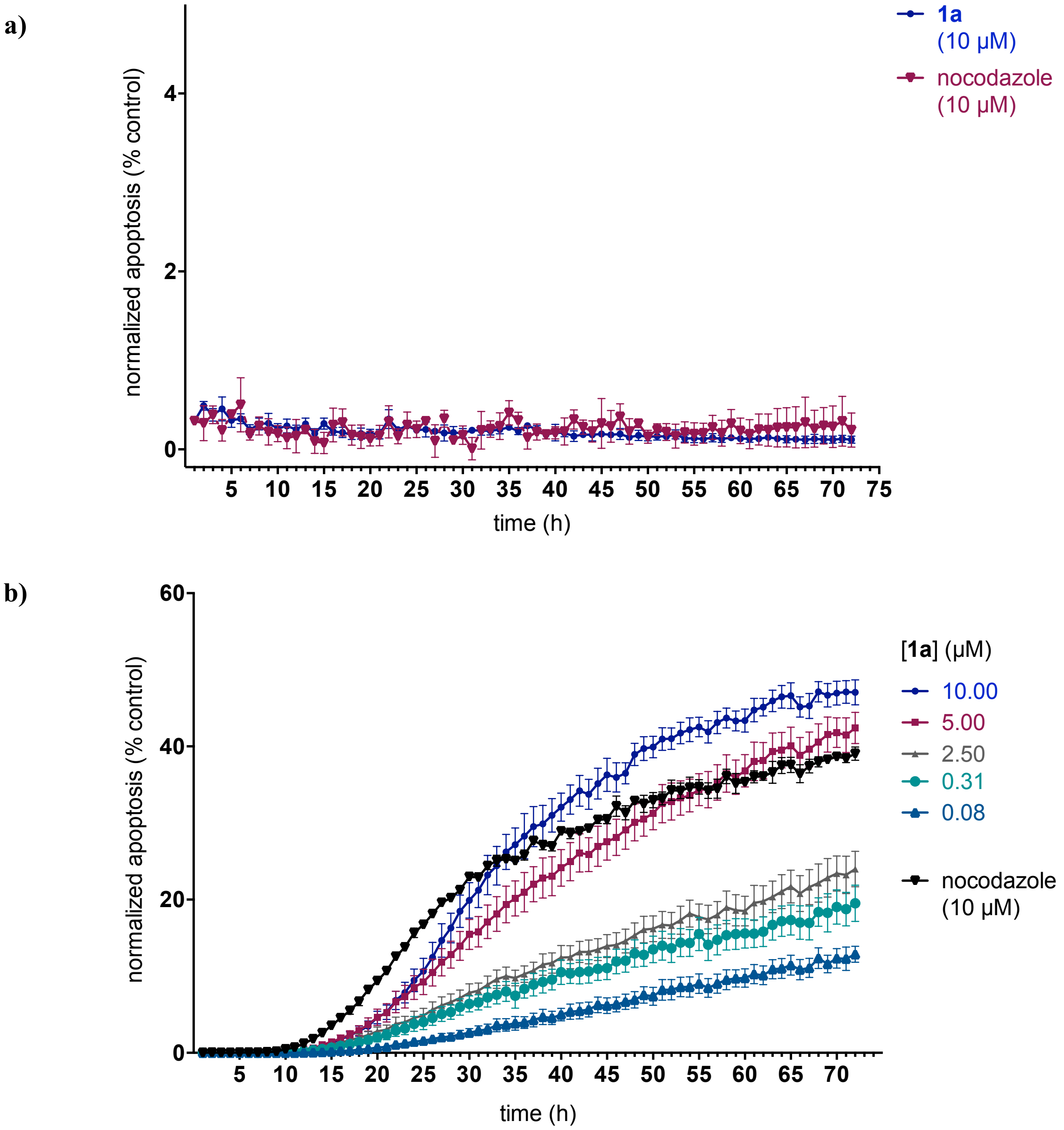

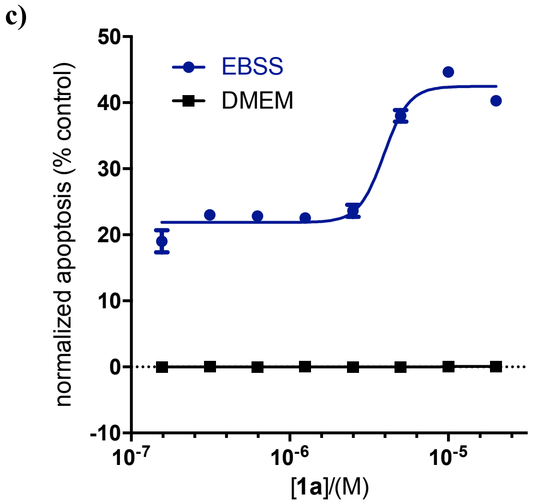

*Figure 17. Indoline **1a** selectively induces apoptosis in starved MCF7 cells. MCF7 cells in either **a)** full medium (DMEM) or **b)** under starvation conditions (EBSS) were treated with **1a** and the apoptotic cells were monitored over 48 h using the green fluorescent dye IncuCyte™ Kinetic Caspase-3/7 Apoptosis Assay Reagent in the Incucyte Zoom. The ratio of apoptotic cells was defined as green fluorescence confluence as a percentage of phase contrast confluence and is normalized to the DMSO control. Only relevant concentrations shown for clarity. **c)** The graph shows the dose-response influence of **1a** after 48 h of treatment. Data shown are mean values ± SEM (n = 3, N = 3).*

4.1.4. Conclusion

Using a GFP-based and a tandem mCherry-GFP-based assay, it was demonstrated that **1a** is a potent inhibitor of starvation-induced autophagy. Furthermore, its inability to inhibit rapamycin-induced autophagy indicates that **1a** acts presumably upstream of mTOR. The inhibitor was validated by immunoblotting and cell viability assays, which show that its cytotoxicity is selective for starved cells. Since it did not target any of the known regulators tested, different approaches to identify its target were applied, which will be discussed in the next chapters.

4.2. Synthesis of an Indoline-Based Compound Collection

Given its strong potency and inhibitory profile, **1a** was selected for further studies. As only few structural analogs of **1a** were present in the COMAS library or commercially available, a compound collection derived from **1a** was synthesized in order to delineate the SAR. In this chapter, the synthetic routes employed in the preparation of the compounds will be described in detail. The derivation of the SAR based on the biological evaluation of the analogs will be illustrated in Chapter 4.3.

4.2.1. Retrosynthetic Analysis of Indoline 1a

Indoline **1a** can be disconnected at the sulfonamide moiety to an amine and a suitable sulfonyl indoline, such as a sulfonyl chloride. The groups at C5 and C6 in **2** can be derived from acyl indoline **3** by bromination and chlorosulfonylation, using the directing properties of the acyl group **3**, which in turn can be traced back to commercially available indoline (**4**) (Scheme 1).

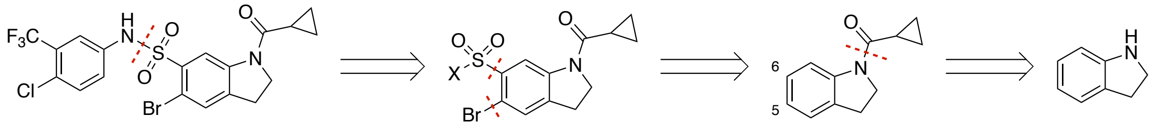

1a **2** **3** **4**

*Scheme 1. Retrosynthetic analysis for autophagy inhibitor **1a** from commercially available indoline (4).*

When studying the SAR of a compound class, it is important to compare single modifications of each site, while keeping the rest of the molecule intact. To generate compound collections bearing only one modification at the same site in an efficient way, two divergent synthetic routes were employed, which allowed the introduction of either the acyl or the sulfonamide functionalities at the last step.

4.2.2. Synthesis of Indoline 1a Analogs with Varying Sulfonamide Aryl Groups

In the first route towards analogs of **1a**, early installation the cyclopropanecarbonyl group allowed the generation of an aryl sulfonamide series **1a–x** in four steps from **4** (Scheme 2).

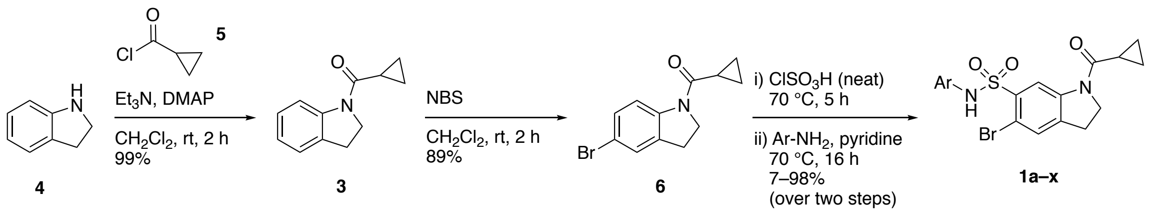

Scheme 2. Synthesis of aryl sulfonamide series ***1a-x*** *from commercially available indoline (4) via acylation, bromination, chlorosulfonylation, and aminolysis. DMAP = 4-dimethylamino pyridine; NBS =* N-*bromosuccinimide.*

Acylation of **4** was accomplished by treatment with cyclopropanecarbonyl chloride (**5**) using Et$_3$N as a base and a catalytic amount of DMAP in excellent yield. Subsequent bromination with NBS gave the C5-bromide **6**, which is in agreement with the selectivity reported for aromatic amines, including acyl indolines.[91-95] Acyl bromoindoline **6** was sulfonylated using chlorosulfonic acid and the resulting crude product reacted with various anilines in pyridine, leading to target compounds **1a–x**. The yields of this reaction strongly correlated with the electronic properties of the substituents, i.e., the more electron donating the substituents, the higher the yield. Furthermore, aminolysis with anilines bearing substituents *ortho* to the amine resulted in lower yields, most likely due to steric effects. However, this was not studied in detail in the context of this thesis.

Though not fully understood, the regioselective chlorosulfonylation of **6** at C6 of acyl bromoindolines, which is contradictory to the *ortho*/*para*-directing effect of amides, has been previously reported.[96] This regioselectivity can be rationalized by the *ortho*-directing effect of the C5-bromide or steric hindrance caused by the *N*-acyl group. Another explanation is a possible complexation between chlorosulfonic acid and the amide functionality, which would render the nitrogen more electron-deficient and hence *meta*-directing.[96] Likewise, consistent with the reported reactivity of non-brominated indolines, chlorosulfonylation of *N*-acyl indoline **3** occurred exclusively at C6, affording **7** in good yield (Scheme 3).

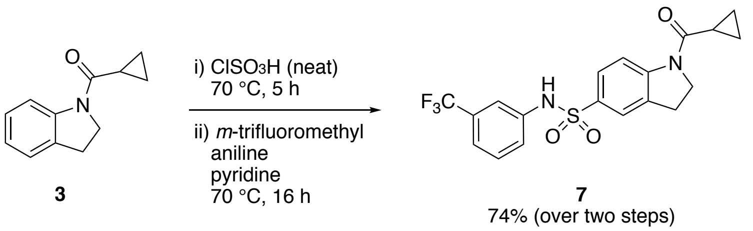

Scheme 3. C6-selective chlorosulfonylation of acyl indoline ***3*** *and subsequent aminolysis with* m-*trifluoromethyl aniline.*

4.2.3. Synthesis of Indoline 1a Analogs with Varying Carboxamide Groups

A slightly different route from the one described in the previous chapter allowed late-stage functionalization of the indoline-N with varying carboxy substituents (Scheme 4). Starting from commercially available *N*-acetylindoline (**8**), sulfonamide **9** was prepared the same way as **1**, employing *p*-chloro-*m*-trifluoromethyl aniline (**10**) for the aminolysis step, in good overall yield (81%). Saponification of **9** lead to free indoline **11**. Additionally, the preparation of *m*-trifluoromethyl analog **12** was conducted following the procedure employed for **11** and used as a precursor of a second carboxamide series.

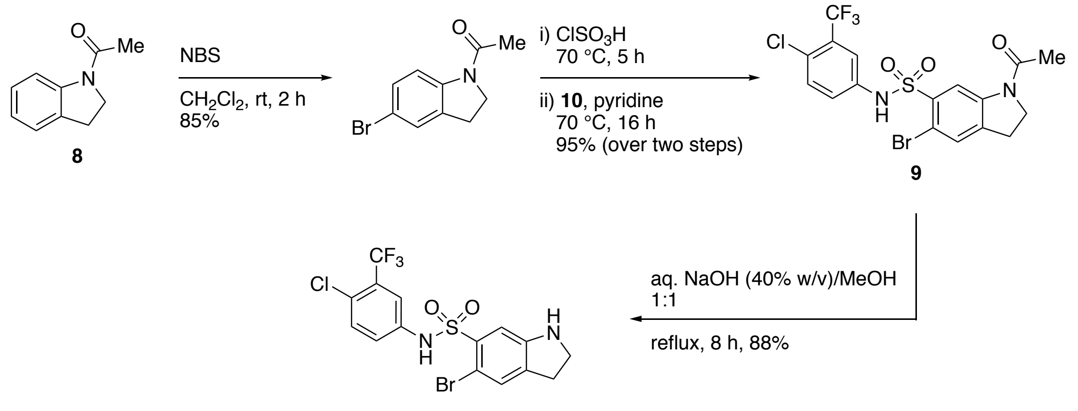

11

*Scheme 4. Route employed in the synthesis of the precursor **11** of an indoline carboxamide series, starting from commercially available* N*-acetylindoline (**8**). Deacetylation and reacylation with different carboxy reagents allowed late stage functionalization.*

Acylation of NH-indoline **12** should give the target amides **13**. However, when **12** was reacted with acyl chlorides using the same conditions as for the synthesis of **3**, only the double acylation product **14** was observed (Table 2, entry 1). Lowering the equivalents of the acyl chloride, as well as slow addition of the reagent and higher dilution had the same outcome (entry 2). Therefore, introduction of the carboxy moiety was attempted using the carboxylic acid analogs and standard amide coupling conditions with 1-ethyl-3-(3-dimethylaminopropyl)carbodiimide (EDC)/DMAP, dicyclohexyl-carbodiimide (DCC)/DMAP, and (1-cyano-2-ethoxy-2-oxoethyliden-aminooxy)dimethylamino-morpholino-carbenium hexafluorophosphate (COMU)/oxyma as coupling reagents, which resulted in no conversion of starting material **12**. Only the use of benzotriazol-1-yl-oxytripyrrolidinophosphonium hexafluorophosphate (PyBOP) with *N*-methyl-morpholine (NMM) as base gave traces of the desired product **13** (entry 6).

Table 2. Optimization of reaction conditions for the N-acylation of bromosulfonamide indolines.

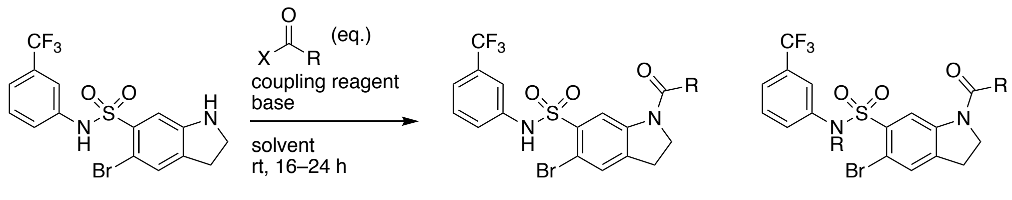

12 **13** **14**

Entry	X	R	Equivalents Acyl Source	Coupling Reagent(s)	Base	Solvent	Products
1	Cl[a]	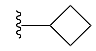	2.3	DMAP	Et_3N	CH_2Cl_2	**13**, **14** (1:1)[c]
2	Cl[a]	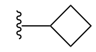	1.1	DMAP	Et_3N	CH_2Cl_2	**13**, **14** (1:1)[c]
3	OH[b]	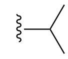	2.0–4.0	EDC, DMAP	DIPEA	CH_2Cl_2	no conversion[d]
4	OH[b]	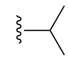	2.0	DCC, DMAP	DIPEA	CH_2Cl_2	no conversion[d]
5	OH[b]	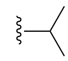	4.0	COMU, oxyma	–	DMF	no conversion[d]
6	OH[b]	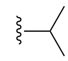	4.0	PyBOP	NMM	DMF	traces of **13**[d]
7	OH[b]	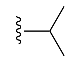	4.0	PyBOP, DMAP	DIPEA	DMF	**13** (57%)
8	OH[b]	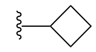	1.5	T3P	DIPEA	EtOAc	**13** (58%)

*[a] To a mixture of **12** in the indicated solvent, the coupling reagent, the base and the acyl chloride were added successively. [b] To a mixture of the acid (chloride) and the coupling reagent(s) in the indicated solvent under an argon atmosphere, **12** and the base were added successively. [c] Product/side product ratio determined by ^{1}H NMR. [d] Monitored by ultra-high-performance column chromatography (U-HPLC). DIPEA =* N,N-*diisopropylethylamine; T3P = propylphosphonic anhydride.*

Reaction with the reagents PyBOP/DMAP or T3P gave the desired products **13** in moderate yields (entries 7 and 8). Therefore, these conditions were employed in the generation of series **13** and **15** (Scheme 5).

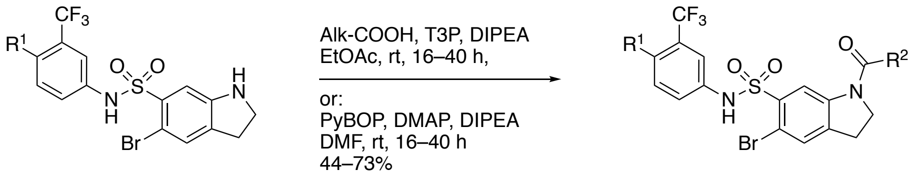

11: R^1 = Cl
12: R^1 = H

15b–j: R^1 = Cl
13a–l: R^1 = H
R^2 = Alk

*Scheme 5. Optimized conditions employed in the synthesis of carboxamide series **13** and **15**.*

The optimal conditions found for the regioselective acylation of free indolines were not applicable to the reaction with pivalic acid (Table 3, entry 1). No conversion of **11** was observed when using pivalic acid anhydride or pivalic acid chloride in CH_2Cl_2 under basic conditions (entries 2 and 3). Increasing the effect of the base by performing the reaction in pyridine as solvent led to the desired pivalic acid analog **15h** in moderate yield (entry 4).

*Table 3. Optimization of reaction conditions for the preparation of pivalic analog **15h**.*[a]

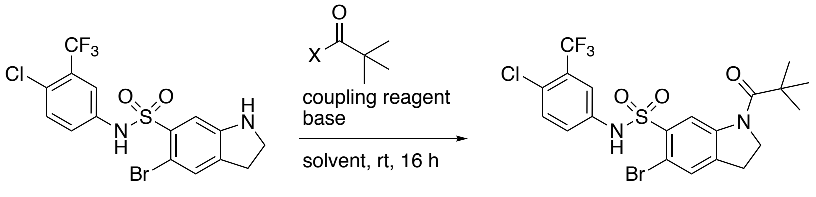

11 **15a**

Entry	X	Coupling reagent(s)	Base (eq.)	Solvent	Yield
1	OH	T3P	DIPEA (8.0)	EtOAc	–[b]
2	piv. anh	DMAP	Et_3N (2.0)	CH_2Cl_2	–[b]
3	Cl	DMAP	Et_3N (3.0)	CH_2Cl_2	–[b]
4	Cl	–	–	pyridine	65%

*[a] To a mixture of **11** in the indicated solvent under an argon atmosphere, the coupling reagents, the base, and the pivalic acid (chloride/anhydride) were added successively. [b] Monitored by U-HPLC. Piv. anh. = pivalic anhydride.*

4.2.4. Synthesis of Indole Derivatives of Indoline 1a

Indole scaffolds are ubiquitous structures found in numerous natural products, including the amino acid tryptophan, a major constituent of proteins. Its presence in a variety of alkaloids and the neurotransmitter serotonin has driven pharmaceutical companies to synthesize indole-containing libraries for targeting GPCRs, enzymes, and ion channels.[97-98] Due to its structural similarity to indoline, the indole analogs **16a** and **16b** were considered as an interesting addition to the compound collection, which should be prepared via oxidation of **1a** and **1b**, respectively.

First attempts to oxidize **1b** with 2,3-dichloro-5,6-dicyano-1,4-benzoquinone (DDQ) in different solvents at a range of temperatures resulted in little or no conversion (Table 4, entries 1–3). Increasing the number of equivalents of the oxidant had no effect on the outcome (entries 4–6). Therefore, different oxidizing agents were tested. Whereas no conversion was observed when using

$Mn(OAc)_3$ (entry 7), better results were obtained with MnO_2 as an oxidant (entry 8). Using the latter, an increase of the reaction temperature gave the desired indole **16b** in excellent yield (entry 9). The synthesis of indole **16a** was performed analogously in comparable yield (92%). NH-indolines, such as **11**, were considerably more reactive and were readily oxidized with MnO_2 to **17** at lower temperatures (CH_2Cl_2, reflux).

*Table 4. Optimization of reaction conditions for the oxidation of **1b**.*[a]

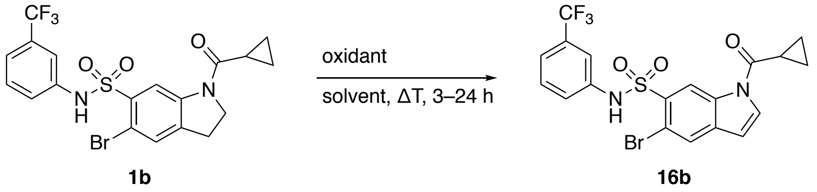

Entry	Oxidant (eq.)	Solvent	Temperature	Heat Source	Time	Yield
1	DDQ (1.1)	MeCN	rt	–	3 h	no conversion[b]
2	DDQ (1.1)	toluene	rt, reflux	c	24 h	traces[b]
3	DDQ (1.1)	toluene/CH_2Cl_2	rt, reflux	c	16 h	9%
4	DDQ (2.0)	DMF	rt, 80 °C, reflux	c	16 h	no conversion[b]
5	DDQ (2.0)	toluene	150 °C	mw	1 h	18%
6	DDQ (5.0)	dioxane	150 °C	mw	3 h	19%
7	$Mn(OAc)_3$ (1.2)	toluene	reflux	c	4 h	no conversion[b]
8	MnO_2 (10.0)	CH_2Cl_2	reflux	c	4 h	31%
9	MnO_2 (10.0)	toluene	reflux	c	4 h	94%

*[a] A mixture of **1b** and the oxidant in the indicated solvent were heated to the indicated temperature. [b] Determined by ^1H nuclear magnetic resonance (NMR). c = conventional heating; mw = microwave irradiation.*

4.2.5. Synthesis of Additional Analogs of Indoline 1a

To study the effect of the bromide group on the activity of aryl sulfonamide indoline analogs, **1a** and **b** were submitted to Pd/C-catalyzed hydrogenolysis in the presence of Et_3N, giving compounds **18a** and **b** in excellent yields (Scheme 6).

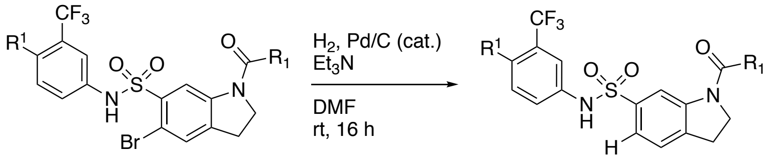

R^1 = Cl: **1a**
R^1 = H: **1b**

R^1 = Cl: **18a**, 95%
R^1 = H: **18b**, 96%

*Scheme 6. Synthesis of dehalogenated derivatives **18a** and **b**, via hydrogenolysis of **1a** and **b**.*

The last analog described in this section consists in oxetane **19**. Oxetanes are considered carbonyl bioisosteres, but have enhanced physicochemical and pharmacological properties compared to carbonyl moieties, which makes them attractive functional groups in medicinal chemistry.[99] To determine the influence of a carbonyl-to-oxetane replacement on the activity profile of the indoline compound class, oxetane **19** was synthesized following a reported procedure from **11** and 3-oxetanone via reductive amination (Scheme 7).[100] Interestingly, the ethyl substituted analog **20** was formed as a side product. However, the mechanism of this reaction was not investigated in the context of this thesis.

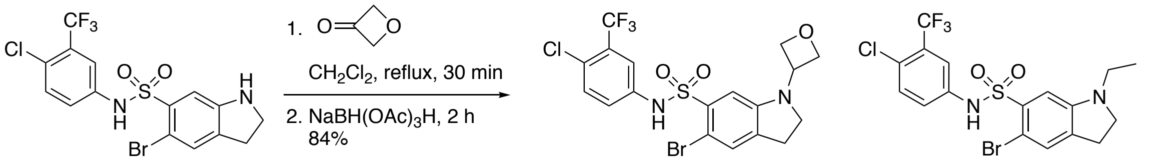

11

19
84%

20
12%

*Scheme 7. Preparation of oxetane **18** from **11** via reductive amination, using 3-oxetanone, following a reported procedure.[100]*

4.2.6. Conclusion

A compound collection of structural analogs of **1a** was successfully generated. The first steps leading to the common precursors **6**, **10**, and **11** were conducted in multi-gram scale, and obstacles in the later steps of the routes were overcome by successful optimization of reaction conditions. Using divergent synthetic routes, two series of compounds were produced, which consisted in analogs with varying sulfonamide aryl groups or carboxamide moieties. The preparation of further analogs was accomplished via oxidation or hydrogenation of **1a** and **1b**, or via reductive amination of **11**. The biological evaluation of the compound collection will be discussed in the next chapter.

4.3. Structure–Activity Studies of an Indoline 1a-Derived Compound Collection

Hit optimization using the SAR of a compound class can give rise to equally or more potent inhibitors with enhanced physicochemical and biological properties. Furthermore, SAR can provide information on functional group and site tolerability for the design of a chemical probe for affinity-based chromatography experiments. For this purpose, the activity of the compound collection described in Chapter 4.2 was evaluated in the phenotypic assay described in Chapter 4.1.1. To identify the impact of each functional group of **1a** and corresponding modifications thereof, the activities of compounds with single-site modifications were compared among each other (Scheme 8).

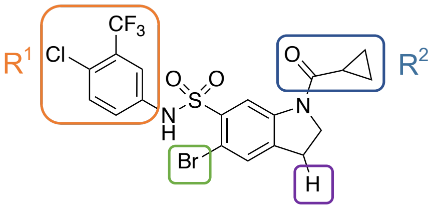

1a

*Scheme 8. Functional groups modified to study the SAR of the compound collection derived from **1a**.*

4.3.1. Biological Relevance of the Aryl Sulfonamide Functionality

A preliminary SAR study with ten analogs of **1a** already present in the COMAS library revealed that an aromatic moiety directly attached to the sulfonamide is essential for activity. For example, an isopropyl sulfonamide indoline showed no inhibition (Table 5, entry 1). Analogs with larger groups, such as a piperidine or a piperazine linked through a C_2H_4 spacer, display a weak potency as well (entries 2 and 3). Analogs with aromatic groups attached to the sulfonamide through an alkane spacer, such as thiophene, *o*-chlorophenyl, or *N*-ethylaniline, did not inhibit autophagy or only weakly.

Table 5. Analogs of ***1a*** *in the COMAS library lacking an aryl sulfonamide moiety and their corresponding inhibition potencies towards starvation-induced autophagy at 10 µM.*

Entry	Molecule	Inhibition (%)
1	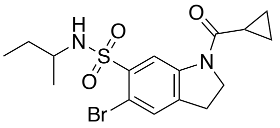	11
2	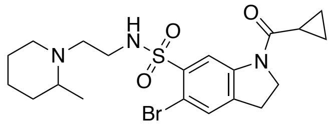	54
3	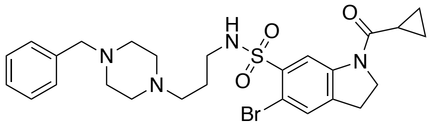	-11
4	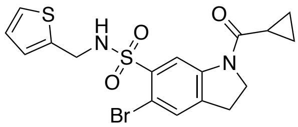	6
5	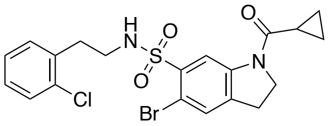	64
6	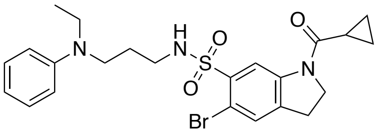	18

Inhibition potencies of starvation-induced autophagy are shown. Inhibition was measured in the phenotypic screen described in chapter 4.1.1.

Given the initial SAR with aliphatic sulfonamides described above, only the substitution on the aryl ring was analyzed for R^1 (Scheme 8) in detail. According to Erlenmeyer's definition of bioisosters, which is based on the similarity in the number of peripheral electrons, bromo- and chloro-substituents can be considered as bioisosteres.[101] In line with this rule, replacement of the *p*-chloro-substituent by its bioisosteric bromide had no significant effect on the activity of the compound class (Table 6, entry 1 vs. 3). This bioisosteric analogy does not apply to the replacement by methyl, another bioisostere of the chloro-substituent with a similar size and lipophilicity but a weaker inductive effect,[101] as **1d** is slightly less active than **1a** (entry 1 vs. 4). Trifluoromethyl aryl **1b** has a nearly identical activity as **1a** and **1c**, suggesting that a small-sized substituent in *para*-position to the sulfonamide is crucial for activity (entries 1–3). This finding is supported by the loss in potency upon replacement of the trifluoromethyl group by the considerably bigger methoxygroup (entry 4 vs. 8). Replacement of hydrogen by the fluoro-substituent causes a 2.5-fold loss in activity, despite their similarity in size and lipophilicity and could therefore arise from the substantial difference in electronics (entry 2 vs. 9). These results indicate that only a moderate to low inductive effect of the group in *p*-position to the sulfonamide is tolerated.

The importance of the trifluoromethyl group is showcased by the dramatic loss in activity upon its replacement to bioisosterically related groups. For example, replacement by the electronically similar nitrile (entry 2 vs. 20), carboxylic acid (entry 2 vs. 21), and chlorine (entry 8 vs. 13) groups[102-103] or by the much smaller hydrogen (entry 9 vs. 17) and fluorine groups (entries 2 vs. 16) renders the compounds considerably less active or even inactive. Judging by the similarity in electronics of many of these analogs, it is possible that the indispensability of the trifluoromethyl substituent is caused not only by its strong electronegativity, but also additional factors, including size, lipophilicity and direct interactions of the fluorine atoms.

Unlike the overall electronegativity of the aryl ring, the substitution pattern has a major impact on the activity of the compound class. Thus, the *m*- and *o*-chloro analogs **1e** and **1g** are 1.6 and 2.1-times less active than the *p*-chloro **1a** (entries 5 and 7 vs. 1). The position of the trifluoromethyl group affects the activity strongly: the *meta*-to-*para*- (entry 2 vs. 11) or *meta*-to-*ortho*-modification (entry 1 vs. 10) causes a 4.1 or 5.5-fold loss in activity, respectively. Generally, a negative effect on activity upon *ortho*-substitution was observed (entries 7, 10, and 22). Finally, the replacement of the aryl ring by heteroaromatic groups (entries 14, 23, and 24) did not increase the activity of **1a**.

*Table 6. Structures and activities for analogs of **1a** with varying aryl substitution (Scheme 8, R^1).*

Entry	R^1	IC_{50} (µM)	Entry	R^1	IC_{50} (µM)
1	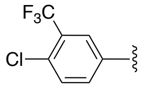 **(1a)**	0.52 ± 0.55	13	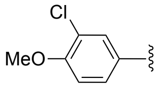 **(1m)**	4.30 ± 2.30
2	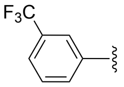 **(1b)**	0.56 ± 0.38	14	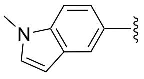 **(1n)**	5.90 ± 1.80
3	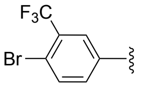 **(1c)**	0.56 ± 0.15	15	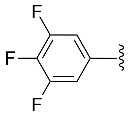 **(1o)**	9.20 ± 0.90
4	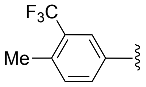 **(1d)**	0.81 ± 0.49	16	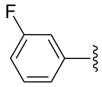 **(1p)**	inactive
5	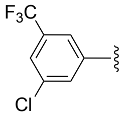 **(1e)**	0.84 ± 0.16	17	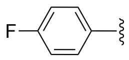 **(1q)**	inactive
6	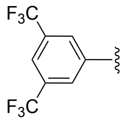 **(1f)**	1.00 ± 0.40	18	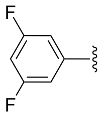 **(1r)**	inactive
7	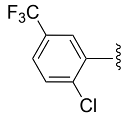 **(1g)**	1.10 ± 0.50	19	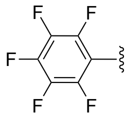 **(1s)**	inactive
8	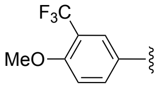 **(1h)**	1.30 ± 0.30	20	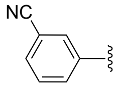 **(1t)**	inactive
9	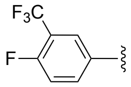 **(1i)**	1.40 ± 0.40	21	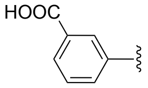 **(1u)**	inactive
10	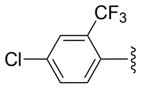 **(1j)**	2.40 ± 0.20	22	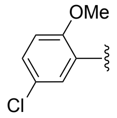 **(1v)**	inactive
11	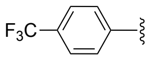 **(1k)**	3.10 ± 1.00	23	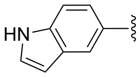 **(1w)**	inactive
12	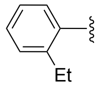 **(1l)**	4.30 ± 0.80	24	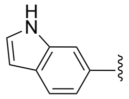 **(1x)**	inactive

Inhibition potencies of starvation-induced autophagy are shown. Inhibition was measured in the phenotypic screen described in chapter 4.1.1. Data shown are mean values ± SEM (N ≥ 3).

4.3.2. Biological Relevance of the Carboxamide Functionality

Given that **1a** and **1b** were the most active compounds of the series described in the previous chapter, the aryl moieties of these compounds were maintained constant in the SAR analysis of the carboxamide functionality (Scheme 8, R^2).

The cyclopropyl ring on the carbonyl (Table 7, entry 1) was replaced by a variety of structurally related alkyl analogs, such as isopropyl (entry 3), cyclobutyl (entry 4), cyclopentyl (entry 6), pivalyl (entry 8), methanecyclopropyl (entry 9), and ethyl (entry 13). The smaller substituents acetyl (entry 12) and ethyl (entry 14), as well as aromatic moieties (entries 2, 5, 7, and 10) and an oxetane analog **19** (entry 11) were also evaluated. In all cases, modifications of this substituent had a strong negative effect on the inhibition potency of the indoline compound class, making this site unsuitable for the attachment of a functional tag.

*Table 7. Structures and activities for **1a** analogs with varying* N-*indoline substitution.*

Entry	R^2	IC$_{50}$ (µM)	Entry	R^2	IC$_{50}$ (µM)
1	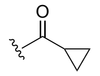 (**1a**, **13a**)	0.52 ± 0.55[a] 0.56 ± 0.38[b]	8	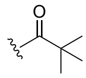 (**15h**)	4.10 ± 0.90[a]
2	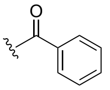 (**15b**)	2.40 ± 0.30[a]	9	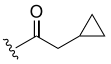 (**13i**, **15i**)	4.50 ± 0.50[a] inactive[b]
3	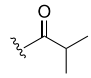 (**13c**; **15c**)	3.00 ± 0.70[a] 8.70 ± 0.80[b]	10	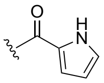 (**15j**)	5.00 ± 1.40[a]
4	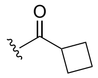 (**13d**; **15d**)	3.30 ± 0.60[a] 7.90 ± 0.00[b]	11	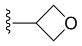 (**19**)	6.30 ± 1.60[a]
5	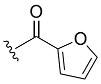 (**15e**)	3.50 ± 0.30[a]	12	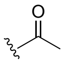 (**13k**, **9**)	6.90 ± 2.20[a] inactive[b]
6	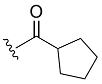 (**13f**; **15f**)	3.80 ± 0.60[a] 7.00 ± 1.50[b]	13	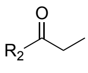 (**13l**)	7.00 ± 2.20[b]
7	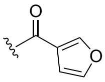 (**15g**)	4.10 ± 0.90[a]	14	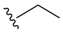 (**20**)	inactive[a]

*Inhibition potencies of starvation-induced autophagy are shown. Inhibition was measured in the phenotypic screen described in Chapter 4.1.1. [a] R^1 = Cl (**15**); [b]: R^1 = H (**13**). Data shown are mean values ± SEM (N ≥ 3).*

The cyclopropyl moiety is a frequent scaffold found in clinically approved drugs.[104] Compared to its alkyl isosteres methyl and isopropyl, it has proven to have enhanced metabolic stability in numerous cases caused by its C–H bond properties. On the other hand, its ring strain can lead to metabolic activation, which is in contradiction to the first statement.[105] These unique properties could be the origin of the steep SAR observed for R^2, which suggests that replacement of the cyclopropyl ring is not tolerated.

4.3.3. Biological Relevance of Additional Modifications

The biological activity of further analogs with single modifications was evaluated in the eGFP-LC3 phenotypic screen. Compounds with an *N*-alkylated sulfonamide (Table 8, entries 1 and 2) were inactive. C2-methylation of indoline resulted in a slightly more active inhibitor (**32**) than its demethylated analog **13k** (Table 8, entry 3 vs. Table 7, entry 12). Modification of the substitution pattern on the indoline ring to give C5-sulfonamide **7** resulted in an inactive compound (entry 5). The activity of C5-sulfonamide **33** is contradictory to the findings derived from the aryl sulfonamide series (Chapter 4.3.1), which suggested that the trifluoromethyl group is essential for activity. Hence, one would predict a higher activity for **7** than for **33**, which was not the case (entries 4 vs. 5). However, this unexpected behavior could be caused by an off-target effect. The C5-debrominated **18a** and **18b** and their alk(en)yl hydroxy analogs **34** and **35** showed a significant drop in activity (entries 6–9). Indoles **16a**, **16b**, and **17** were also less active (entries 10–12). Given its chemical accessibility, the indole-C3 position was explored on **16a**. Considering the importance of the cyclopropyl ring and the indoline moiety described in the previous chapters, the activities of indoles **37** and **38** (entries13 and 14) were, although still low, rather unexpected and render this position a potential site for linker attachment in the synthesis of a chemical probe.

*Table 8. SAR of further analogs of **1a**.*

Entry	Structure	IC_{50} (µM)	Entry	Structure	IC_{50} (µM)
1	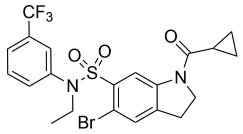 **(30)**	inactive	8	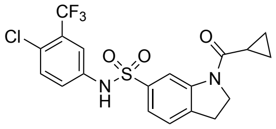 **(18a)**	6.6 ± 1.2
2	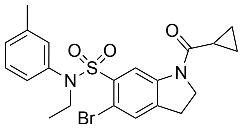 **(31)**	inactive	9	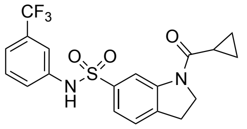 **(18b)**	inactive
3	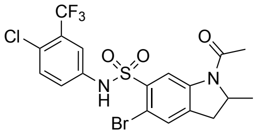 **(32)**	3.9 ± 0.5	10	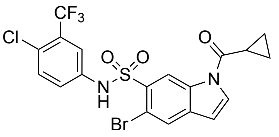 **(16a)**	2.2 ± 0.1
4	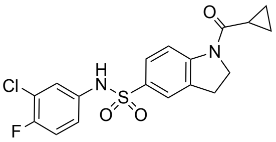 **(33)**	5.7 ± 0.5	11	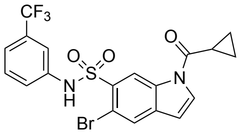 **(16b)**	4.6 ± 0.1
5	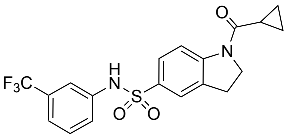 **(7)**	inactive	12	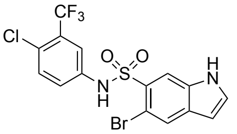 **(17)**	5.4 ± 1.5
6	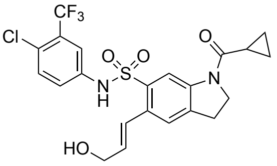 **(34)**	9.2 ± 0.9	13	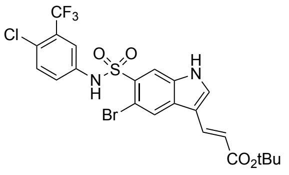 **(37)**	7.6 ± 2.3
7	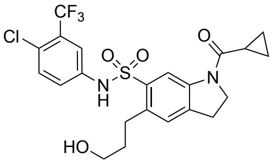 **(35)**	9.9 ± 0.4	14	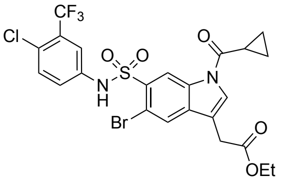 **(38)**	7.3 ± 2.6

Inhibition potencies of starvation-induced autophagy are shown. Inhibition was measured in the phenotypic screen described in Chapter 4.1.1. Data shown are mean values ± SEM (N ≥ 3).

4.3.4. Conclusion

From the SAR derived for analogs of **1a**, it was evident that all the functional groups in **1a** are indispensable for strong activity. Consequently, any site modification for the attachment of a tag could potentially affect the activity of the identified inhibitor and result in an inactive probe.

According to the activity of **38**, C3 was the most promising site for modification. Another possible modification site is C5, despite the 18-fold lower potency of **34**, when compared to the initial hit **1a**, as the loss in activity could arise from the properties of the hydroxyl group. Furthermore, unlike a C2-derived probe, both sites are chemically accessible either from **1a** or a precursor thereof, which would require late-stage ring closure to build the indoline moiety.

4.4. Target Identification by Affinity Chromatography

One of the methods utilized towards the determination of the target of **1a** consists in the most widely utilized technique in this field: affinity-based proteomics, or "pull-down" (Chapter 2.2.1). In this chapter, the design, synthesis, and biological evaluation of a pull-down probe based on the information obtained from the SAR will be discussed. Moreover, the results obtained in a pull-down experiment and the validation of the isolated proteins will be explained.

4.4.1. Design and Synthesis of Pull-Down Probes

As described in Chapter 2.2.1, a pull-down experiment requires the immobilization of the active compound on a matrix using a functional tag. Herein, an amine-tag was chosen for covalent attachment to NHS-activated magnetic sepharose beads. A spacer between the amine and the active compound should minimize steric hindrance between the target proteins and solid support. For this purpose, the hydrophilic 3-unit PEG linker was employed. PEG-based linkers are commonly used in affinity-based proteomics, as they improve the solubility of the probe and reduce non-specific binding due to their hydrophilicity (Chapter 2.2.1).[40]

Based on the derived SAR and because of their synthetic accessibility, two probes were designed which involved either C5-functionalization of indoline **1a** or C3-functionalization of indole **16a**. In order to evaluate their suitability for pull-down experiments, the probes were tested for their inhibitory activity in the GFP-based phenotypic screen for autophagy inhibition. Probes derived from an inactive analog of the compound collection served as negative controls. To increase the probability of binding to the sought-after target, pull-down probes should ideally retain the specific activity of the parent compound and be stable in aqueous media.

a) Synthesis of 1^st^ Generation Pull-Down Probes

Prior to the attachment of a linker at C5, the bromide needed to be replaced by a bifunctional group which could be then reacted with a linker. Boronic acid pinacol ester **50** was a suitable candidate, as it can be inserted via palladium-catalyzed cross-coupling and then deprotected to give an alcohol nucleophile. Indoline **1a** was coupled to **50** using standard Suzuki conditions to give protected **51** in moderate yield. Tetrabutylammonium fluoride (TBAF)-mediated *t*-butyldimethylsilyl (TBDMS) removal gave **34**. Subsequent S_N2 reaction with linker **52** using a reported procedure[106] afforded Boc-protected probe **53** (Scheme 9).

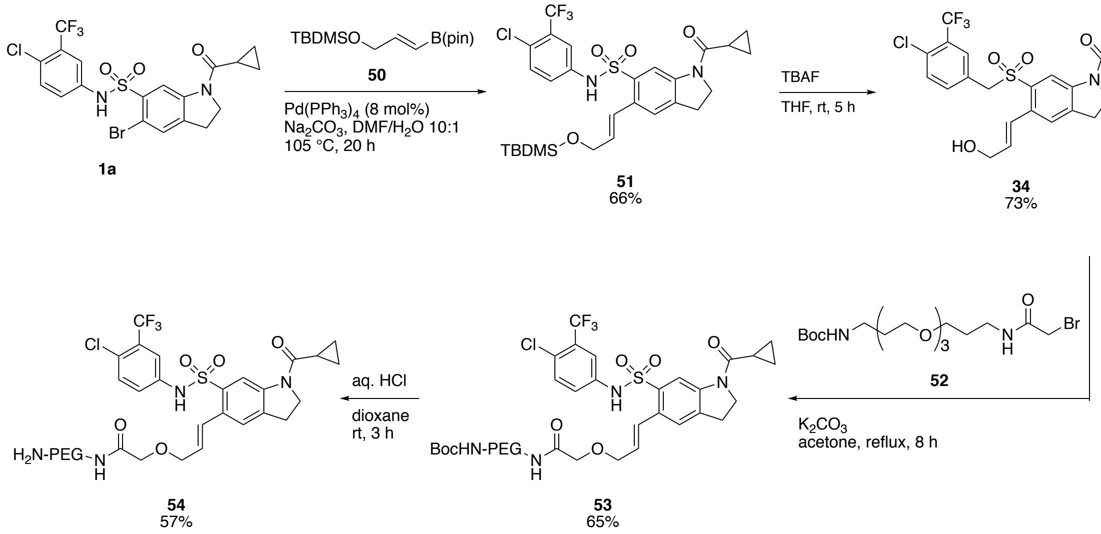
TBDMSO
B(pin)
50
Pd(PPh3)4 (8 mol%)
Na2CO3, DMF/H2O 10:1
105 °C, 20 h
1a
51
66%
TBAF
THF, rt, 5 h
34
73%
BocHN
3
52
K2CO3
acetone, reflux, 8 h
53
65%
aq. HCl
dioxane
rt, 3 h
H2N-PEG
BocHN-PEG
54
57%

Scheme 9. Route employed in the preparation of a pull-down probe for ***1a*** *with a linker attached at C5; pin = pinacol ester.*

Trifluoroacetic acid (TFA)-mediated deprotection of **53** in CH_2Cl_2 resulted in uncharacterized side products, which were observed even upon reduction of the TFA concentration (Table 9, entry 1). Use of TFA in toluene or a CH_2Cl_2/toluene mixture as solvent afforded only traces of the desired product **54** (entries 2 and 3). Therefore, a mixture of HCl in dioxane was employed, yielding probe **54** in an overall yield of 18% after purification by preparative high-performance liquid chromatography (HPLC) in the absence of TFA (entry 4).

*Table 9. Optimization of reaction conditions for the deprotection of **53**.*[a]

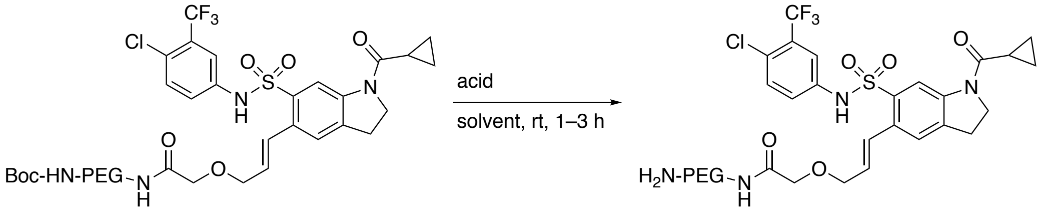

53 **54**

Entry	Acid	Solvent	Yield
1	TFA (7–50% v/v)	CH_2Cl_2	many side products[b]
2	TFA (20% v/v)	toluene	traces[b]
3	TFA (20% v/v)	toluene/CH_2Cl_2	traces[b]
4	HCl (20% v/v)	dioxane	59%

*[a] To a solution of **53** in the indicated solvent under an argon atmosphere, the acid was added dropwise. [b] Monitored by U-HPLC.*

For the synthesis of a control probe, the inactive analog **1p** was selected as a starting point. However, when the Suzuki conditions used for the conversion of **1a** were applied to **1p**, only the formation of sultam **55** was observed (Scheme 10). Generation of the 5-membered ring could occur via palladium-mediated activation of the alkene moiety in **56** and subsequent attack by the sulfonamide-N, followed by elimination of the TBDMSO group and final rearrangement to **55**. Given that this side product was not detected upon reaction with **1a**, this altered reactivity could be explained by an increased nucleophilicity of the sulfonamide-N, arising from the lower electronegativity on the aryl ring in **1p**. No consumption of starting material **1p** was observed upon reduction of the reaction temperature, whereas prolonged reaction time lead to formation of a second side product (uncharacterized) in addition to **55**. As an alternative starting material, an inactive analog with an additional fluoro-substituent at the sulfonamide aryl ring and hence increased electronegativity was chosen. As predicted, control probe **57** was prepared in a satisfactory overall yield of 8% from 3,5-difluoro analog **1r**.

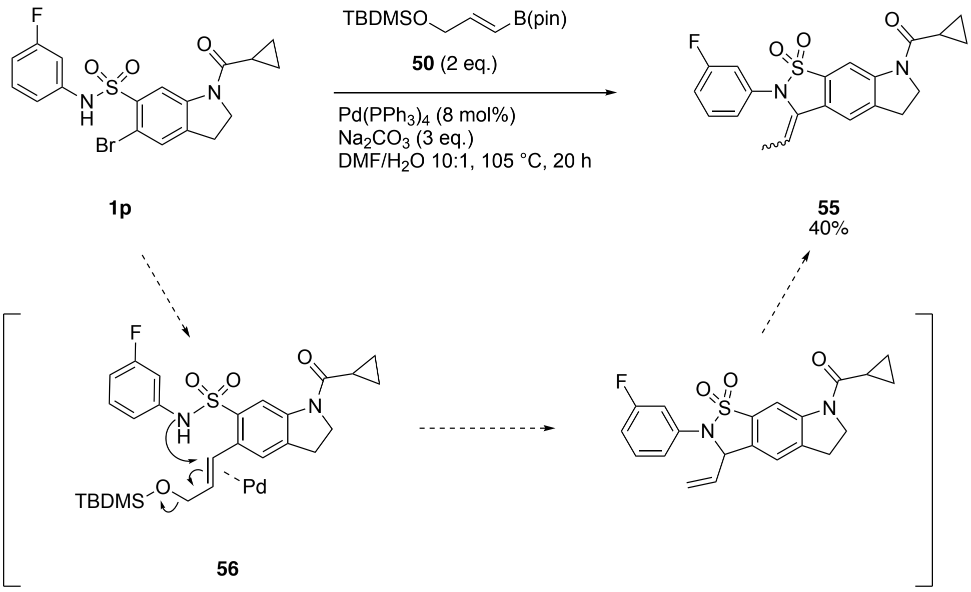

Scheme 10. Suzuki-cross coupling conditions employed successfully in the synthesis of positive probe ***54*** *lead to the formation of side product* ***56*** *when applied to the preparation of* ***55****. After prolonged time at lower temperatures, only the formation of a second product was observed.*

b) Synthesis of 2nd Generation Pull-Down Probes

Based on the SAR, which showed that C3 was a promising site for linker attachment (Chapter 4.3.3), a pull-down probe was designed consisting of indoline **1a** with a linker at C3. Probe **70** can be traced back to an indoline bearing a functional group R suitable for linker attachment (**71**). The C3-functionalized indoline can be obtained by reduction of the corresponding indole **72**. Given that C3 is the most nucleophilic position on indoles, **16a** can be reacted with a suitable electrophile to afford **72** (Scheme 11).

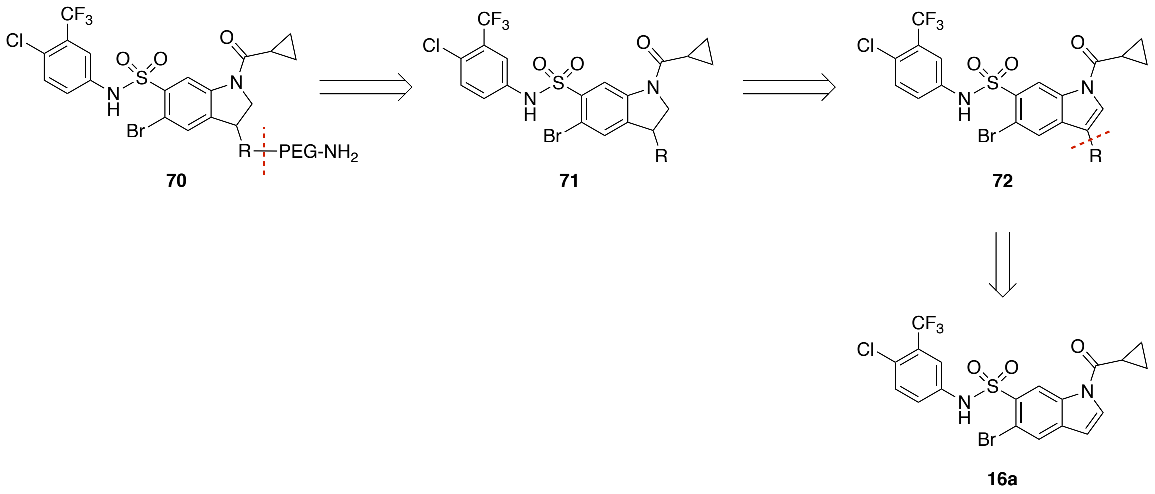

Scheme 11. Retrosynthetic analysis used in the design of a second pull-down probe for affinity chromatography.

i. C3-Functionalization of Indoles

In a first functionalization attempt, indole **16a** was planned to be converted to **73** by electrophilic aromatic substitution with oxalyl chloride and subsequent condensation with EtOH. Alternatively, direct reaction with ethyl chlorooxoacetate was pursued. However, reaction with oxalyl chloride and EtOH resulted in no conversion of the starting material (Table 10, entry 1). The same outcome was observed upon change of solvent and temperature increase (entries 2, 3). Using $AlCl_3$ as a catalyst in a Friedel-Crafts acylation reaction at room temperature or reflux, no conversion was detected (entries 4, 5). Furthermore, employment of ethyl chlorooxoacetate gave the same result as the previous conditions (entries 6–8).

Table 10. Reaction conditions tested for the oxalylation of indole ***16a***.

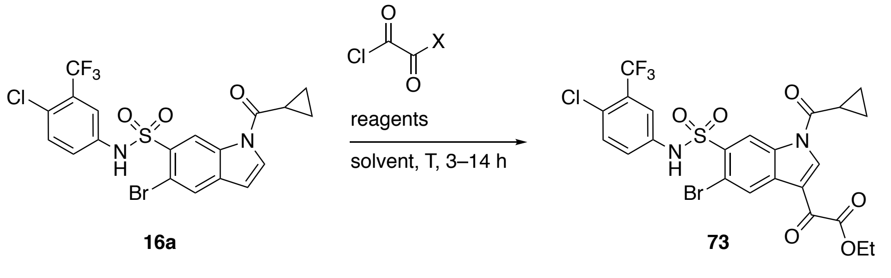
CF3
Cl
O O
N S
H
Br
O
N
16a
O
Cl X
O
reagents
solvent, T, 3–14 h
CF3
Cl
O O
N S
H
Br
O
N
O
73
O OEt

Entry	X	Eq. Oxalyl Reagent	Reagents	Solvent	T	Time	Product[c]
1[a]	Cl	2.0	2. EtOH	Et_2O	rt	3.5 h	no conversion
2[a]	Cl	2.0	2. EtOH	Et_2O/CH_2Cl_2 1:1	rt	4 h	no conversion
3[a]	Cl	2.0	2. EtOH	toluene	reflux	16 h	no conversion
4[a]	Cl	10.0	1. $AlCl_3$, 2. EtOH	CH_2Cl_2	rt	4 h	no conversion
5[a]	Cl	10.0	1. $AlCl_3$, 2. EtOH	CH_2Cl_2	reflux	4 h	no conversion
6[b]	Et	10.0	$AlCl_3$	CH_2Cl_2	rt	14 h	no conversion
7[b]	Et	10.0	$AlCl_3$	CH_2Cl_2	reflux	14 h	no conversion
8[a]	Et	10.0	1. $AlCl_3$, 2. EtOH	CH_2Cl_2	rt	14 h	no conversion

[a] To a solution of ***16a*** *in the indicated solvent, the oxalyl chloride source (and $AlCl_3$, if indicated) was added, and the mixture was stirred at the indicated temperature for 3 h. The mixture was concentrated under reduced pressure, EtOH was added, and the mixture was stirred for a further 2–14 h. [b] To a solution of* ***16a*** *in the indicated solvent, the ethyl oxalyl chloride and $AlCl_3$, were successively added, and the mixture was stirred at the indicated temperature for 14 h. [c] Conversion determined by ^1H NMR.*

In a second attempt to functionalize **16a**, reported conditions for the Heck cross-coupling of indoles with *t*-butyl acrylate[107] were applied with no success (Scheme 12).

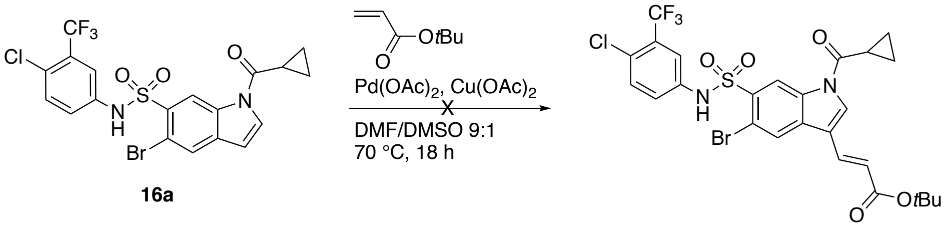
CF3
Cl
O O
N S
H
Br
O
N
16a
OtBu
O
Pd(OAc)2, Cu(OAc)2
X
DMF/DMSO 9:1
70 °C, 18 h
CF3
Cl
O O
N S
H
Br
O
N
OtBu
O

Scheme 12. Attempted C3-functionalization of indole ***16a*** *via Heck-coupling, following a reported procedure.*[108]

The lack of reactivity observed could originate in the low nucleophilicity of the indole-C3 due to the electron-withdrawing properties of the *N*-acyl moiety. Therefore, free indole **17** was submitted to the reaction conditions tested in the **16a** functionalization attempts, affording **74** and **75** in moderate and good yield, respectively (Scheme 13), thereby confirming our hypothesis.

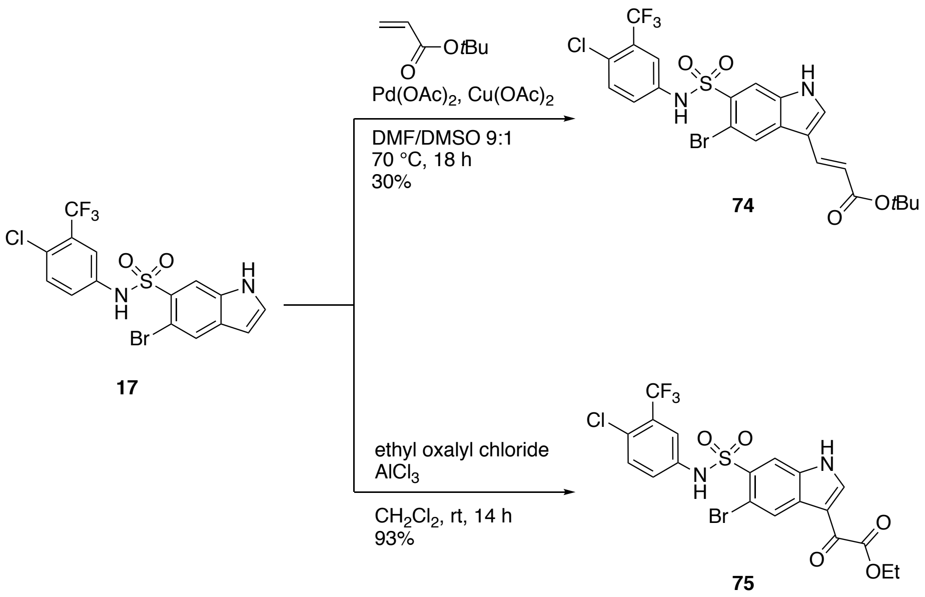
OtBu
Pd(OAc)2, Cu(OAc)2
DMF/DMSO 9:1
70 °C, 18 h
30%
CF3
Cl
O
S
N
H
Br
OtBu
17
74
ethyl oxalyl chloride
AlCl3
CH2Cl2, rt, 14 h
93%
OEt
75

*Scheme 13. C3-functionalization of indole **17** via Heck-coupling (74) and Friedel-Crafts acylation (75).*

ii. Reduction of C3-Functionalized Indoles

After successful C3-functionalization of **16a**, the next step towards a C3-functionalized derivative of **1a** consisted in reduction to its indoline analog, followed by *N*-acylation. For the reductive step, conditions were necessary that would not compromise the C5-bromide functionality, thereby excluding Pd-catalyzed hydrogenations. A widely-used method for the reduction of indoles is the acid-mediated hydrogenation, which proceeds, similarly to most electrophilic aromatic substitutions on indoles, via C3-protonation and subsequent hydride attack at C2 (Scheme 14).[109]

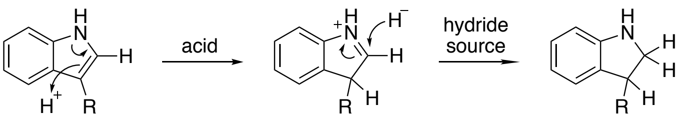
acid
hydride source
H
N
R
H+
H−

Scheme 14. Mechanism of the acid-mediated hydrogenation of indoles.

Treatment of **74** with $NaBH_3CN$ and acetic acid as a hydride source/acid pair resulted in no conversion of the starting material (Table 11, entry 1). Given that the first step in this reaction involves dearomatization of the indole, it is plausible that this is the rate-determining step and a stronger acid than AcOH is needed. Therefore, the broadly-used Et_3SiH/TFA pair[110-111] was employed in a test reaction to reduce C3-unsubstituted indole **17** and lead to full conversion to the corresponding indoline **10** (monitored by analytical HPLC and ^1H-NMR, data not shown). When applied to **74**, these conditions lead exclusively to reduction of the alkene while leaving the indole moiety intact (entry 2). No difference was observed when using CH_2Cl_2 as solvent or increasing the number of equivalents of the hydride/acid pair (entries 2–3).

*Table 11. Optimization conditions tested for the reduction of **74**.*

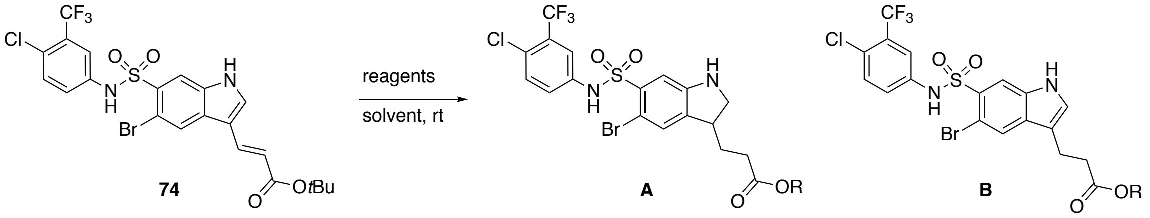

Entry	Hydride Source	Acid	Solvent	Product[c]
1[a]	$NaBH_3CN$ (5 eq.)	AcOH	–	starting material
2[a]	Et_3SiH (6 eq.)	TFA (37 eq.)	–	B (R = H)
3[b]	Et_3SiH (6 eq.)	TFA (6 eq.)	CH_2Cl_2	B (R = H)
4[a]	Et_3SiH (151 eq.)	TFA (316 eq.)	–	B (R = H)

*[a] To a solution of **74** in the indicated acid, the hydride source was added. [b] To a solution of **74** in the indicated solvent, the acid and the hydride source were added. [c] The reaction was monitored by U-HPLC after 2–48 h.*

Likewise, reduction of **75** using Et_3SiH and TFA yielded only the deoxygenation of the oxalyl moiety (Scheme 15). Given that a) reduction of indoles with similar functional groups at C3 as **75** has been reported before[112] and b) reduction of indole **17** was successful, the lack of reactivity could come from the cumulative effect of all the electron-withdrawing groups on the indole ring, which would render the C3 insufficiently nucleophilic. Therefore, a new strategy was attempted, in which the C3 group should be installed prior to C5- and C6-functionalization.

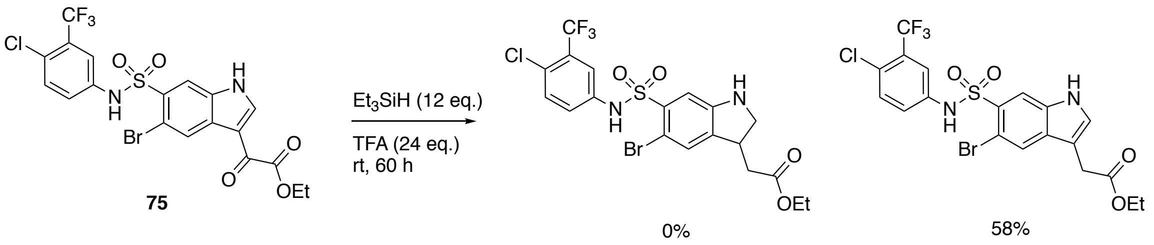

*Scheme 15. Indole-reduction attempt of **75** by acid-mediated hydrogenation.*

iii. Early Installation of C3-Functionality Strategy

An alternative strategy for the preparation of a probe with a linker at C3 consisted in the early installation of a C3 group. After reduction of the indole, the remaining functionalities of **1a** should be installed prior to linker attachment. Starting from 5-bromoindole (**76**) the same conditions used for C3-functionalization of **17** were employed to give Heck-product **77** and ethyl oxoacetate **78** in satisfactory yields (Scheme 16)

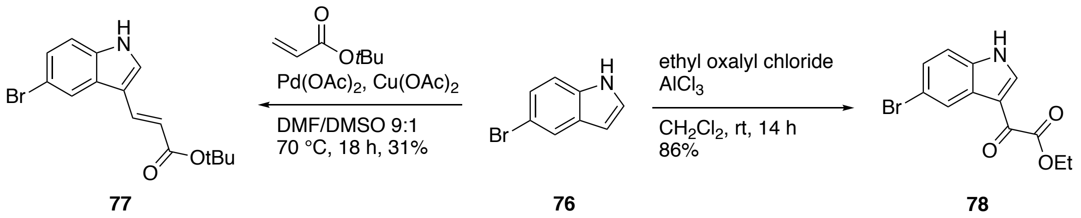

*Scheme 16. C3-Functionalization of 5-bromoindole (**76**) via Heck-cross coupling (**77**)[107] and Friedel Crafts acylation (**78**).*

In order to reduce the indole moiety, **77** was subjected to several conditions (Table 12). In neat $NaBH_3CN$/AcOH, only the alkene group was reduced (entry 1). Traces of the desired product were observed when $NaBH_3CN$ was used in excess (entry 2). No conversion of the starting material was detected when using MeOH or DMF as solvents (entries 3–4) or the stronger acid TFA (entry 5). Reaction with triethylsilane and TFA resulted in a number of uncharacterized side products (entry 6). Using the same hydride/acid system, traces of the indoline were detected when performing the reaction in CH_2Cl_2 (entry 7). However, increase of temperature or prolonged reaction time resulted again in several side products (not shown). Sodium borohydride in combination with TFA or acetic acid or in THF as a solvent resulted in either side products or starting material (entries 9–11).

Table 12. Reaction conditions tested for the reduction of 77.

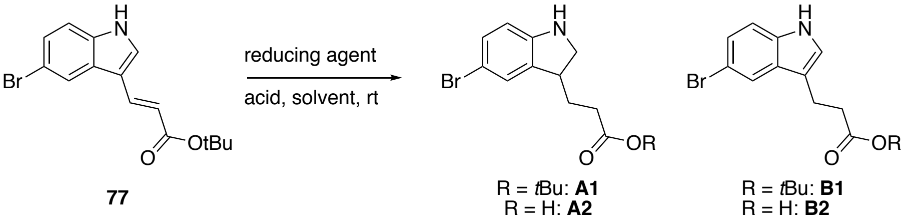
reducing agent
acid, solvent, rt
Br
OtBu
OR
77
R = *t*Bu: **A1**
R = H: **A2**
R = *t*Bu: **B1**
R = H: **B2**

Entry	Reducing Agent (eq.)	Acid	Solvent	Products[c]
1[a]	NaBH$_3$CN (2)	AcOH	–	starting material, **B1**
2[a]	NaBH$_3$CN (5–20)	AcOH	–	**B1**, traces of **A1**, side products
3[b]	NaBH$_3$CN (4)	AcOH	MeOH	starting material
4[b]	NaBH$_3$CN (4)	AcOH	DMF	starting material
5[a]	NaBH$_3$CN (6)	TFA	–	starting material
6[a]	Et$_3$SiH (6–12)	TFA	–	many side products
7[b]	Et$_3$SiH (6–12)	TFA	CH$_2$Cl$_2$	**B2**, traces of **A2**
8[a]	BH$_3$-THF (5)	TFA	–	many side products
9[a]	NaBH$_4$ (5)	TFA	–	many side products
10[a]	NaBH$_4$ (4)	AcOH	–	starting material, **B1**
11[a]	NaBH$_4$ (4)	THF	–	starting material

[a] To a solution of 77 in the indicated acid, the hydride source was added. [b] To a solution of 77 in the indicated solvent, the acid and the hydride source were added. [c] The reaction was monitored by U-HPLC after 2–48 h.

Alternatively, the reduction of **78** was performed with triethylsilane/TFA, yielding indoline **79** in excellent yield (Scheme 17). Acylated indoline **80** was obtained in good yield following the procedure employed in the synthesis of **1a**.

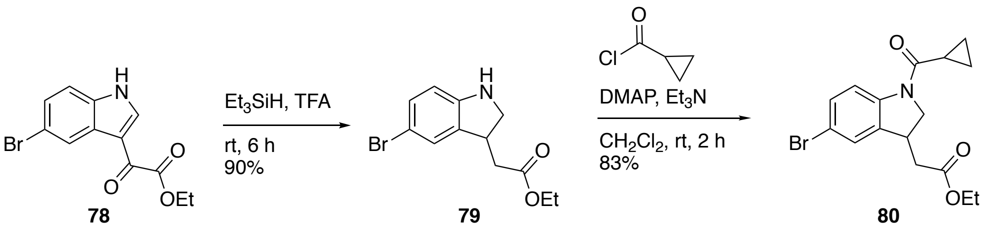
Et$_3$SiH, TFA
rt, 6 h
90%
Cl
DMAP, Et$_3$N
CH$_2$Cl$_2$, rt, 2 h
83%
Br
OEt
78
79
80

Scheme 17 Reduction and subsequent acylation of oxalyl indole ***78*** *leading to C3-functionalized acyl indoline* ***80****.*

Chlorosulfonylation of **80** was attempted using the general procedure employed in the generation of compound series **1**. However, whereas no conversion was observed at room temperature in neat conditions or using a solvent (Table 13, entries 1–3), numerous side products were obtained at higher temperatures (entries 4–6).

*Table 13. Reaction conditions tested for the chlorosulfonylation of **80**.*

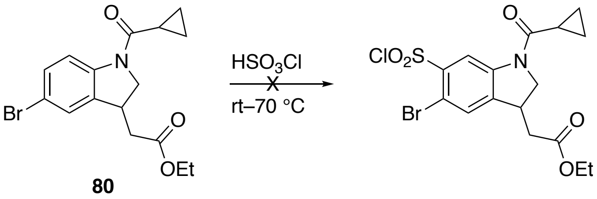

Entry	**Temperature**	**Time**	**Solvent**	**Product**[c]
1[a]	rt	3 h	–	no conversion
2[b]	rt	3 h	CH_2Cl_2	no conversion
3[b]	rt	3 h	CH_2Cl_2/EtOH	no conversion
4[a]	40–70 °C	1–3 h	–	side products
5[b]	40–70 °C	1–3 h	CH_2Cl_2	side products
6[b]	40–70 °C	1–3 h	CH_2Cl_2/EtOH	side products

*[a] To chlorosulfonic acid (≥ 12 eq.) at rt under an argon atmosphere, **80** was added and the mixture was stirred at the indicated temperature. [b] To a mixture of **80** in the indicated solvent at rt under an argon atmosphere, chlorosulfonic acid (1–12 eq.) was added dropwise, and the mixture was stirred at the indicated temperature. [c] Monitored by U-HPLC.*

A possible cause for the aberrant reactivity of **80** in contrast to bromoindoline **3** is the ester functionality, which can hydrolyze in acidic milieu and consequently interfere with the electrophilic aromatic substitution with chlorosulfonic acid. Therefore, a protecting group was chosen, which was more tolerant towards acidic conditions than an ester. For this purpose, the ester functionality in **80** was reduced selectively using lithium borohydride. The resulting alcohol **81** was reacted with a) TBDMSCl or b) acetic anhydride to give the corresponding TBDMS- and acetate-protected alcohols **82** and **83**, respectively. However, chlorosulfonylation leading to the desired products **84** and **85** was not successful (Scheme 18).

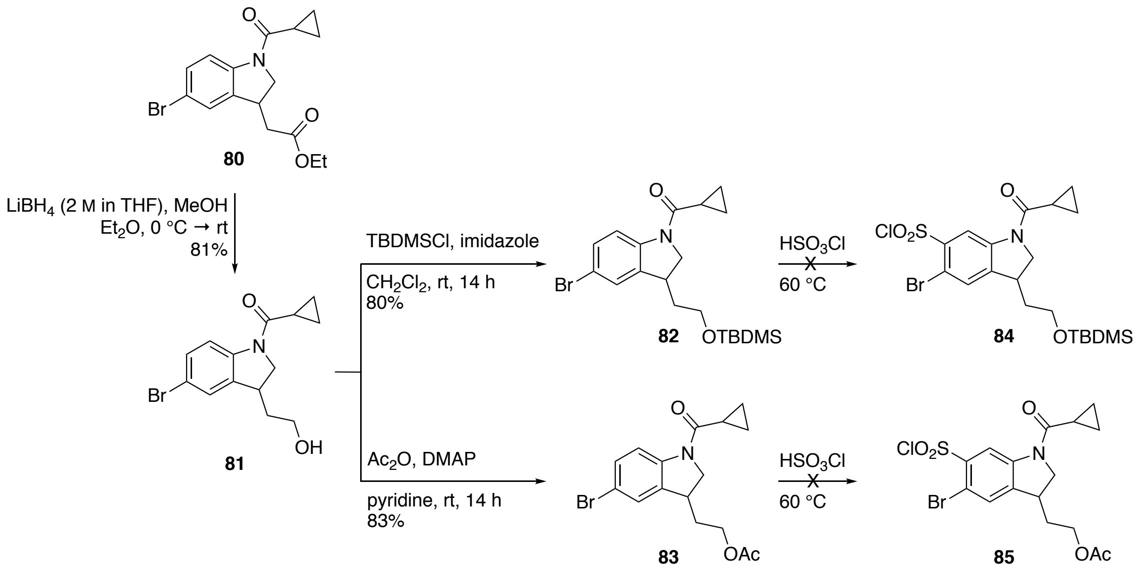

Scheme 18. Selective reduction of the ester acetate functionality at C3, protection of the generated alcohol, and subsequent chlorosulfonylation attempts for the synthesis of a C3-functionalized indoline derivative of ***1a****.*

Due to the poor reactivity of multifunctionalized indoles towards mild reduction agents and the low tolerance of acid-labile groups towards chlorosulfonylation, it was not possible to obtain a C3-functionalized indoline analog of **1a** from the precursors available. Late-stage ring closing of the indoline moiety might represent a better strategy to circumvent the above-mentioned issues. However, because of time limitations, a different synthetic strategy was not attempted in the course of this thesis. Nevertheless, a pull-down probe with an indole core provided a good alternative to the initially designed probe, as indole analogs of **1a** inhibited autophagy with low micromolar potencies (Chapter 4.3.3).

iv. Probe Synthesis

The second generation of pull-down probes was prepared starting from indole **17** (Scheme 19). Friedel-Crafts acylation followed by deoxygenation of the resulting oxoacetate moiety afforded **90** in good overall yield. Given that reaction with cyclopropane carboxylic acid gave a 1:1 mixture of the mono- and double-acylated products and hydrolysis of the ester was not chemoselective, i.e. also cleaved the previously installed acyl groups (not shown), the acyl group needed to be installed at a later stage. Thus, ester **90** was hydrolyzed and subsequently reacted with mono-Boc PEG linker **91** using standard amide coupling conditions to give **92**. Acylation and final Boc-deprotection afforded pull-down probe **93**, which was separated from the double-acylated product by preparative

HPLC. The **1r**-derived negative control **94** was synthesized analogously from indole **95** in 30% overall yield.

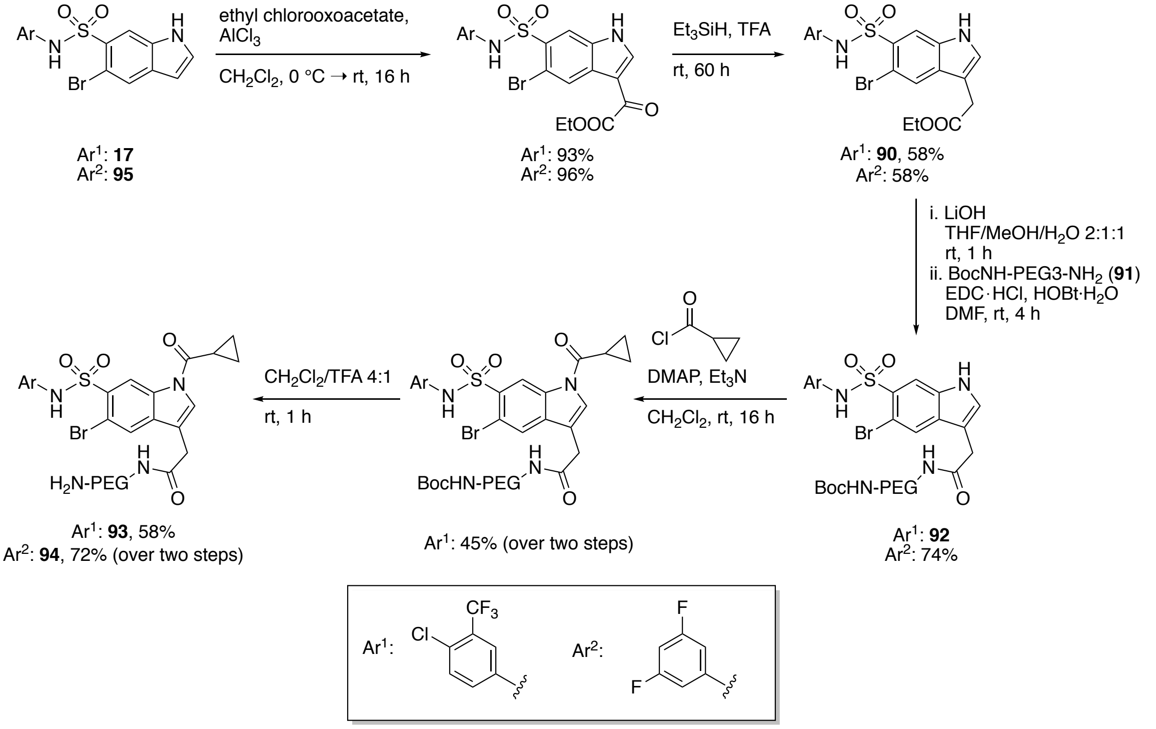

ethyl chlorooxoacetate, $AlCl_3$
CH_2Cl_2, 0 °C → rt, 16 h
Et_3SiH, TFA
rt, 60 h
i. LiOH THF/MeOH/H_2O 2:1:1 rt, 1 h
ii. BocNH-PEG3-NH_2 (**91**) EDC·HCl, HOBt·H_2O DMF, rt, 4 h
DMAP, Et_3N
CH_2Cl_2, rt, 16 h
CH_2Cl_2/TFA 4:1
rt, 1 h
Ar¹: **17**
Ar²: **95**
Ar¹: 93%
Ar²: 96%
Ar¹: **90**, 58%
Ar²: 58%
Ar¹: **92**
Ar²: 74%
Ar¹: 45% (over two steps)
Ar¹: **93**, 58%
Ar²: **94**, 72% (over two steps)
Ar¹:
Ar²:

*Scheme 19. Route employed in the preparation of a pull-down probe for **1a** with a linker attached at C3.*

4.4.2. Biological Activity and Stability of Pull-Down Probes

To avoid off-target binding during a pull-down experiment, a chemical probe should ideally retain the activity of the parent compound and be stable in assay conditions. To address these questions, the pull-down probes were tested by COMAS in the phenotypic screen for autophagy inhibition. Whereas pull-down probe **53** displayed no activity, **93** inhibited autophagy, although nearly 15-times less potently than **1a**, still in the low micromolar range (Scheme 20). Additionally, stability analysis by NMR and analytical HPLC revealed that probe **54** decomposed over time. Consequently, only probe **93** was evaluated further

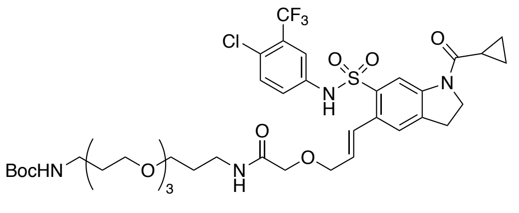

53
inactive

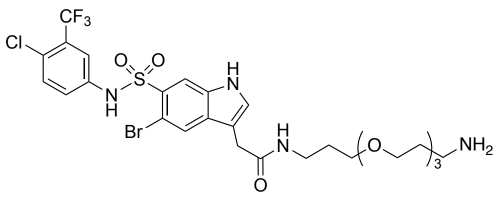

93
7.68 ± 2.26 μM

*Scheme 20. Inhibition potencies of starvation-induced autophagy are shown for the pull-down probes **53** and **93**. Inhibition was measured in the phenotypic screen described in Chapter 4.1.1. Data shown are mean values ± SEM (N ≥ 3).*

To determine whether the probe was stable under the conditions employed in a pull-down experiment, **93** was incubated in aqueous buffers and monitored by analytical HPLC. In coupling buffer (used for the immobilization of chemical probes to a solid support) at pH 8.4 and 4 °C, one main peak was visible in the chromatogram after incubation for 13 h (Figure 18). Analysis of this peak by MS revealed an m/z = 713.2, which was assigned to hydrolysis product **96**, and only traces of **93** were obtained. Partial conversion to **93** also occurred after a shorter incubation time, indicating that these conditions were not optimal for coupling. Therefore, the stability of **93** was monitored at lower pH. Whereas no hydrolysis of the probe was observed in water after 13 h, a 1:1 ratio of **93**/**96** was detected in coupling buffer at physiological pH. Nevertheless, the latter conditions were selected for the experiment, as slightly basic conditions are required for efficient coupling.

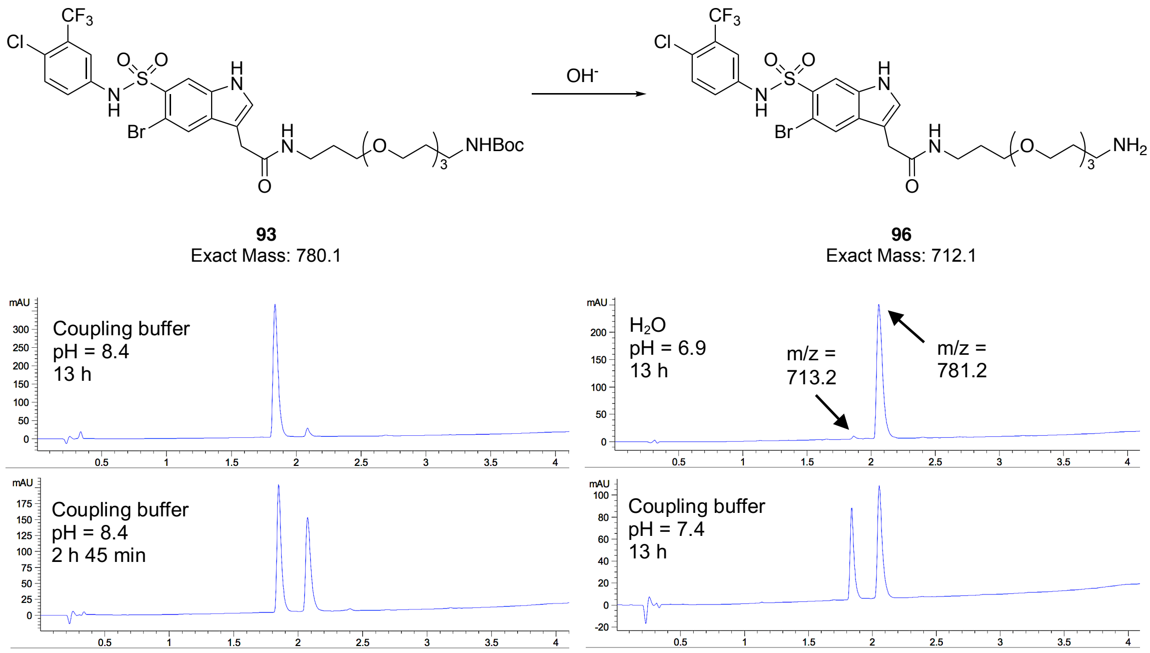

*Figure 18. Pull-down probe **93** hydrolyzes in aqueous solutions at pH > 7. Reaction was monitored by preparative MS-coupled HPLC. Coupling buffer: 0.15 M triethanolamine, 0.5 M NaCl.*

4.4.3. Affinity Chromatography and Subsequent SILAC-Based Quantitative Proteomics

To identify the target of **1a**, a label-free pull-down experiment was conducted using active probe **93** and control probe **94**. For this purpose, lysates were prepared from MCF7-eGFP-LC3, i.e. the cell line used in the phenotypic assay. Immobilization of the probes to NHS-magnetic sepharose beads was performed at pH 7.4 and 4 °C for 13 h due to the unstable character of the probes at higher pH (see previous chapter). According to the analysis of the samples by tandem MS/MS, none of the proteins quantified (ca. 800 in each sample) were enriched in the active probe sample compared to the control, hence no potential targets were determined. Therefore, SILAC (Chapter 2.2.1) was employed, which allows for quantitative analysis of the probes as a result of its higher sensitivity. For this experiment, two lysates were prepared from MCF7-eGFP-LC3 cells. The first contained proteins with natural amino acids ("light", L). For the second lysate, cells were utilized that had incorporated isotopically labeled arginine and lysine into their proteins ("heavy", H). This results in a characteristic mass shift for every protein. Each lysate was incubated with active probe **93** and control **94** separately, thereby generating the samples H_{active}, $H_{control}$, L_{active}, and $L_{control}$. The lysates were then combined as follows: L_{active} with $H_{control}$ and $L_{control}$ with H_{active}, and the tryptic peptides of the mixtures analyzed by tandem MS/MS. Proteins enriched by only by active probe **93** displayed peak pairs with an opposite H:L ratio for each sample (Figure 19) and were thus identified as potential targets of **1a**.

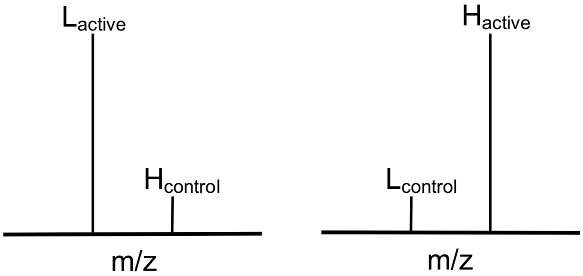

Figure 19. Mass shift and peak intensities observed by MS/MS for proteins enriched by the active pull-down probe in a SILAC-based proteomics experiment.

A total of three proteins were identified as target candidates for **1a**: glutamate dehydrogenase (GDH or GLUD), calpain-1, and histidine triad nucleotide binding protein 1 (HINT-1) (Table 14). Because of their cellular functions, GDH and calpain-1 were selected as high priority target candidates for **1a**, and the effect of **1a** on these enzymes was evaluated in biochemical and biophysical assays.

*Table 14. Proteins identified by SILAC-based quantitative pull-down as potential targets of **1a**, using 2nd generation pull-down probe **93**.*

Protein (Gene Name)	**H_{act} : L_{ctrl}**	**L_{act} : H_{ctrl}**
GDH	2.19 ± 0.18	3.23 ± 0.02
CAPN1	1.64 ± 0.27	1.75 ± 0.02
HINT-1	1.71 ± 0.18	2.63 ± 0.02

The active probe and the control (10 µM) were immobilized to NHS magnetic sepharose beads and incubated with "heavy" and "light" MCF7-eGFP-LC3 lysates separately for 2 h at 4 °C. Values shown are MS-intensity ratios for the enriched proteins in the pull-downs. H = heavy lysate; L = light lysate; act = active probe; ctrl = control probe.

4.4.4. Target Validation

The last step in a target identification approach consists in the validation of the identified hits in proteomics experiments as targets of the modulator in question. Confirmation of the pull-down results can be accomplished by means of a competitive pull-down. For this purpose, cell lysate is incubated with the probe together with the linker-free compound. The higher the concentration of the linker-free compound, the less amount of target protein will bind to the probe, as a result of a higher degree of saturation of the target by the free compound (Figure 20). Proteins bound to the solid support are then analyzed by western blotting.

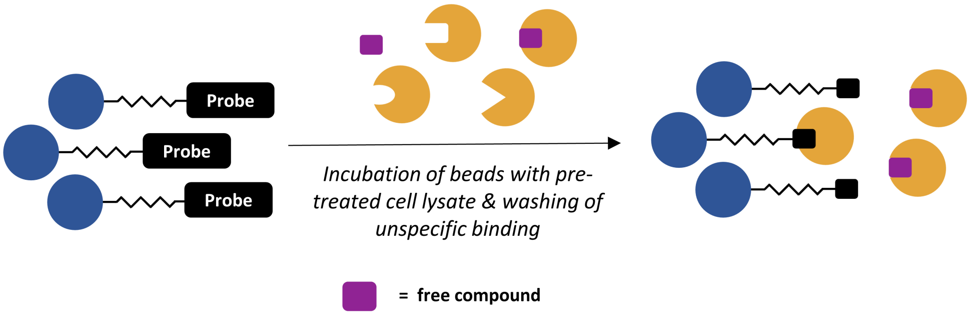
Probe
Probe
Probe
Incubation of beads with pre-treated cell lysate & washing of unspecific binding
= free compound

Figure 20. Schematic representation of the principle of a competitive pull-down experiment, employed to validate the results of a quantitative pull-down.

Other techniques to assess target engagement include DSF, ITC, FP, and microscale thermophoresis (Chapter 2.2.1). For the validation of targets for **1a**, biophysical assays that did not require labeling were prioritized because of the unstable nature and relatively low activity of the probe.

Potential enzymatic targets can be validated by determining the effect of the compound on their specific enzymatic activity. An additional tool is to study the effect of a genetic knockdown or overexpression of the target on the studied pathway. Once validated, the regulatory function of the target can be determined.

a) Evaluation of Glutamate Dehydrogenase as a Target of Indoline 1a

Glutaminolysis is the process responsible for the metabolism of the amino acid glutamine by converting it to α-ketoglutarate (α-KG). This metabolic pathway is activated by leucine and glutamine and thus involved in amino acid sensing. Furthermore, it has been proven to stimulate mTORC1 via the activation of prolyl hydroxylases (PHDs),[113] thereby regulating autophagy.[114] One of the key players of glutaminolysis is the enzyme GDH, which catalyzes the conversion of glutamate to α-KG upon activation by L-Leu, L-Ile, L-Val, or ADP. Recent studies by Blenis and coworkers showed that mTORC1 activates GDH via transcriptional repression of sirtuin

(SIRT4),[115] thereby establishing a possible connection to autophagy. Not much later, Lorin *et al.* reported the regulation of autophagy by GDH.[116] The authors describe an increase in LC3 puncta and LC3-II levels upon knock-down of GDH, which is consistent with autophagy activation. In addition, their results indicate that GDH is required for leucine-sensing in autophagy, as a GDH knock-down prevents the stimulation of mTOR by L-Leu and ultimately the inhibition of autophagy. These findings provide evidence for a negative regulation of autophagy by GDH via the activation of mTORC1, which, together with the findings of Blenis and coworkers, would suggest a feedback loop (Figure 21). Following the observations of Lorin *et al.*, an inhibitor of autophagy targeting GDH would be expected to act as an activator thereof. To test whether **1a** inhibits autophagy via modulation or binding of GDH, three independent assays were performed.

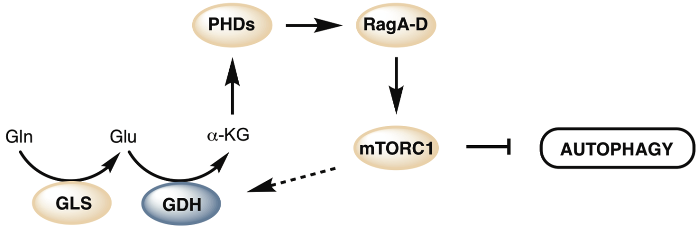

Figure 21. GDH negatively regulates autophagy via the activation of mTORC1.[113-114, 116]

i. Competitive Pull-Down

Whereas GLUD2 is enriched in Sertoli cells (testis) and astrocytes (brain), GLUD1 is expressed in all human tissues.[117] Moreover, both isozymes have a remarkably high sequence identity (96%). Therefore, validation studies focused on GLUD1. A competitive pull-down experiment confirmed that probes **93** and **94** bind to GDH in MCF7-eGFP-LC3 lysate (Figure 22). A slightly higher level of the protein was detected for the active probe by western blotting, which is consistent with the proteomics experiment. However, **1a** was not able to outcompete binding of the active probe **93**, suggesting that GDH is not a target of **1a**.

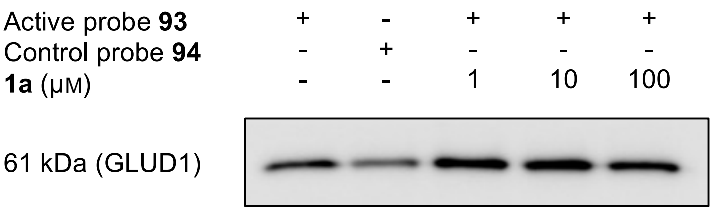

*Figure 22. Pull-down probes **93** and **94** bind to GDH in cell lysate, but free **1a** is not able to outcompete the positive probe. Competitive pull-down was performed with active pull-down probe **93** (10 µM) in presence of increasing concentrations of **1a** using MCF7-eGFP-LC3 cell lysate and NHS magnetic sepharose beads (GE Healthcare®, cat# 28951380) followed by SDS-PAGE and immunoblotting for detection of GDH using Anti-Glud1 (Merck Millipore, cat# ABN443). Control probe **94** was used as a control (n = 3).*

ii. Differential Scanning Fluorimetry

TSAs make use of the fact that protein thermostability can be enhanced by binding of a small molecule.[61] Hence, a shift in the melting temperature of a protein can be observed upon incubation with a small-molecule inhibitor. As a protein unfolds due to a gradual temperature increase, it exposes hydrophobic regions. By utilizing a dye whose fluorescence is enhanced when bound to these hydrophobic regions, protein denaturation can be monitored (Figure 23).[118] In a DSF assay, the fluorescence produced by Sypro Orange upon binding to a protein can be measured in a thermal cycler. One of the advantages of DSF is that no modification on the compound is required. However, as for most target engagement assays, large amounts of purified protein are needed.

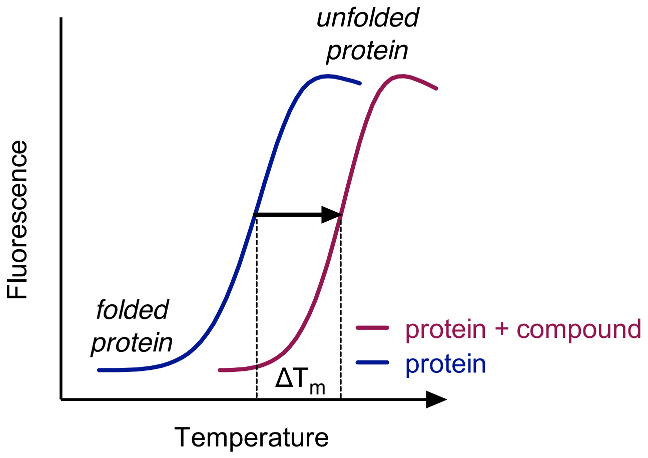

Figure 23. Principle of a TSA using DFS. A fluorescence increase of the dye Sypro Orange upon binding of a protein can be monitored in a real-time quantitative polymerase chain reaction (qPCR) cycler. A protein binder increases the melting point T_m.

Bovine GDH (bGDH) was used in the DSF assay because of its commercial availability, as it shares a high sequence homology with GDH1 (98%) and GDH2 (94%). Incubation of bGDH with its allosteric regulator L-leucine[119] resulted in a strong increase of the melting temperature only at concentrations > 1 mM (Figure 24 and Table 15, entries 4–6), suggesting that high concentrations are required for a measurable effect.

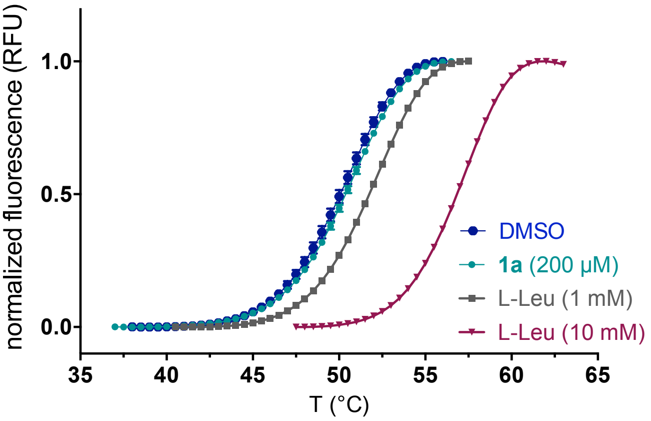

*Figure 24. Indoline **1a** has no effect on the thermostability of GDH. Melting curves of compound-treated bovine GDH (0.1 mg/mL) in phosphate buffer (pH = 8) determined by differential scanning fluorimetry using Sypro Orange). Lower concentrations omitted for clarity. Representative graph shown (n = 2–3, each in N = 3). RFU = Relative fluorescence units.*

Other compounds were tested only at lower maximal concentrations than L-Leu because of their low solubility in aqueous solutions. Only negligible melting temperature shifts ($dT_m < 0.5$ °C) were obtained for **1a** (Table 15, entries 1–3) and pull-down probes **93** (entries 8–10) and **94** (entries 11–13) at any of the concentrations assayed. Tested as additional controls, the known inhibitor epigallocatechin gallate (EGCG),[120] and the known activator 2-aminobicyclo[2.2.1]heptane-2-carboxylic acid (BCH)[119] displayed no effect on the thermostability of GDH (entries 7 and 14). The target engagement results for **1a** in this assay were therefore inconclusive, as no effect was observed for any of the controls tested at the concentrations accessible for **1a**.

Table 15. Melting temperature differences for bovine GDH upon incubation with different compounds compared to DMSO control, measured using differential scanning fluorimetry. Data shown are mean values ± SD (n = 2–3, each in N=3).

Entry	Compound	*c*	dT$_m$ (°C)	Entry	Compound	*c*	dT$_m$ (°C)
1	**1a**	10 µM	0.33 ± 0.24	**8**	**93**	10 µM	0.25 ± 0.35
2		50 µM	0.28 ± 0.19	**9**		50 µM	- 0.17 ± 0.24
3		200 µM	0.17 ± 0.29	**10**		200 µM	- 0.58 ± 0.35
4	L-Leu	200 µM	0.50 ± 0.24	**11**	**94**	10 µM	0.25 ± 0.12
5		1 mM	1.58 ± 0.35	**12**		50 µM	0.42 ± 0.35
6		10 mM	7.00 ± 0.33	**13**		200 µM	0.42 ± 0.12
7	BCH	200 µM	0.39 ± 0.19	**14**	EGCG	50 µM	0.56 ± 0.25

iii. Glutamate Dehydrogenase Activity

To determine whether **1a** affected the activity of GDH, a colorimetric assay was employed, which allowed the quantification of the generated NADH during the enzymatic reaction (Figure 25). The amount of NADH produced over a specific time range correlates with the enzymatic activity of GDH.

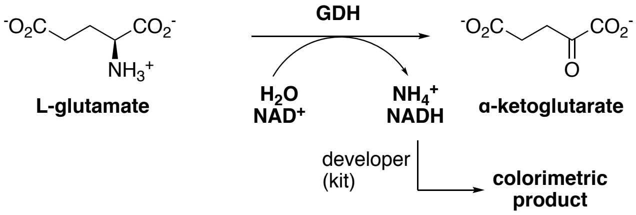

Figure 25. Principle of the enzymatic activity assay employed to test the modulating effect of ***1a*** *on GDH. GDH catalyzes the conversion of L-Glu to α-KG. The generated NADH is reacted with a developer to produce a colorimetric product. An NADH dilution series is employed to generate a standard curve, which is used to determine the specific activity of the enzyme.*

As for the DSF assay, bGDH was employed, with L-Leu and EGCG as controls. It could be demonstrated that EGCG inhibits GDH activity at 10 µM and L-Leucine only slightly activates GDH at 20 mM (109% activity), which is consistent with the literature.[120] Furthermore, a similar abrogative effect of L-Leu at on the inhibition of EGCG was observed (109%). No activation of GDH was measured when treated with **1a** alone (10 or 100 µM, 96 and 94%, respectively), as well as in the presence of EGCG (93%). Compared to EGCG, the inhibitory effect of **1a** was considered negligible (Figure 26).

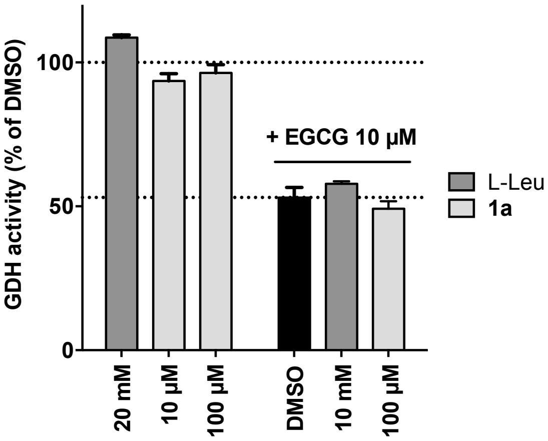

*Figure 26. Indoline **1a** has no effect on the enzymatic activity of GDH. GDH activity was determined in presence of **1a**, the endogenous allosteric activator L-Leu, and the inhibitor EGCG. The amount of glutamate consumed by GDH is measured by monitoring the amount of NADH generated per min in a colorimetric assay using bGDH at 2 µg/mL. Each data point represents a duplicate measurement of the activity normalized to the DMSO control. Further concentrations were omitted for clarity.*

To address the question whether a negative modulator of GDH activity had any effect on autophagy, the inhibitor EGCG was tested in the phenotypic assay for autophagy inhibition and was found to be inactive. Selective activators have unfortunately not yet been discovered, hence a positive control for GDH activation could not be tested for autophagy inhibition. In conclusion, whereas the thermostability studies were inconclusive, both the competitive pull-down and activity assay strongly suggest that GDH is not the target of **1a**. Therefore, further target validation studies were not pursued.

b) Evaluation of Calpain-1 as a Target of Indoline 1a

The second protein isolated by pull-down, CAPN1, is a subunit of calpain-1. The calpain family comprises over a dozen isoforms of calcium dependent cysteine proteases. The best-characterized calpains are the ubiquitously expressed calpain-1 and calpain-2. Both enzymes consist of a catalytic subunit (CAPN1 and CAPN2, respectively) and a common regulatory subunit (CAPNS1).[121] It has been reported that autophagy is impaired in calpain-deficient cells.[122] Moreover, studies prove that calpains are involved in the downregulation of the ATG5–ATG12 conjugate, which is required for autophagosome formation, by cleaving ATG5.[123] Therefore, as calpains are negative regulators of autophagy, an activator of these proteases would inhibit autophagy. To test this hypothesis regarding **1a** and validate the pull-down results, a competitive pull-down and activity assays were performed.

i. Competitive Pull-Down

A competitive pull-down was conducted under the same conditions as for the devalidation of GDH. Unlike for the first hit, no binding of the pull-down probe **93** or its control **94** was observed (Figure 27), thereby contradicting the initial finding. The low intensity observed in the input control indicates low levels of calpain-1 in the lysate, which could explain why enrichment by the active probe was only detected by the highly sensitive SILAC method. Therefore, an orthogonal assay was performed to address target engagement.

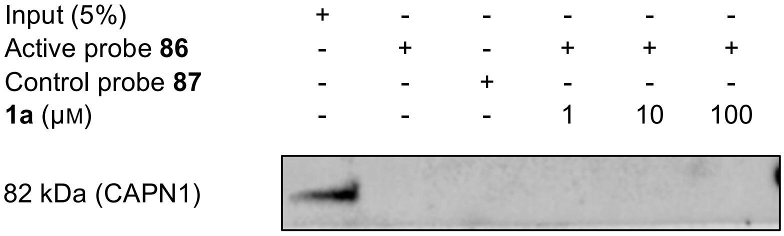
Input (5%) + - - - - -
Active probe **86** - + - + + +
Control probe **87** - - + - - -
1a (μM) - - - 1 10 100
82 kDa (CAPN1)

*Figure 27. Indoline-based probes do not bind to calpain-1 in cell lysate. Competitive pull-down of active pull-down probe **93** (10 μM) with increasing concentrations of **1a**, using MCF7-eGFP-LC3 cell lysate and NHS magnetic sepharose bead followed by SDS-PAGE and immunoblotting for detection of calpain-1 using Anti-CAPN1. Probe **94** was used as a negative control (n = 3).*

ii. Calpain-1 Activity

Calpain-1 activity was measured in a fluorescence-based assay, which utilizes Ac-LLY-7-amino-4-trifluoromethylcoumarin (AFC), a substrate for the protease (Figure 28). Generation of the fluorescent AFC upon cleavage by calpain-1 can be monitored over time. The calpain activator dibucaine[124] and the inhibitor MDL-28170[121, 125] were used as controls.

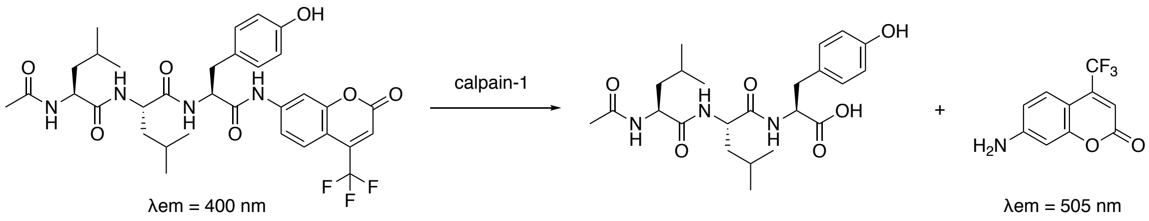

Figure 28. Calpain-1 activity can be determined by monitoring the calpain-1-mediated cleavage of Ac-LLY-AFC, which generates fluorescent AFC.

In agreement with the literature, MDL-28170 strongly inhibited calpain-1 at 500 nM (Table 16, entries 1–3), whereas only a slight activation was observed for the activator dibucaine (entries 4, 5). In contrast, **1a** had no effect on the activity of calpain (entries 6–8). Neither dibucaine nor **1a** were able to abrogate the inhibition of MDL-28170. Additionally, dibucaine and MDL-28170 were tested in the LC3-puncta assay and showed no inhibition of autophagy at 10 µM (Figure 29).

*Table 16. Effect of **1a** on the activity of calpain-1.*

Entry	Compound(s)	*c*	Inhibition (%)	Entry	Compound(s)	*c*	Inhibition (%)
1	MDL-28170	50 nM	23.3 ± 2.3	**6**	**1a**	10 µM	- 7.3 ± 3.7
2		100 nM	68.7 ± 5.5	**7**		5 µM	7.2 ± 6.5
3		500 nM	94.3 ± 4.7	**8**		3 µM	9.4 ± 7.2
4	dibucaine	2.5 µM	- 6.2 ± 8.5	**9**	dibucaine, MDL-28170	10 µM, 100 nM	78.0 ± 4.2
5		10 µM	- 7.5 ± 1.6	**10**	**1a**, MDL-28170	10 µM, 100 nM	80.0 ± 6.2

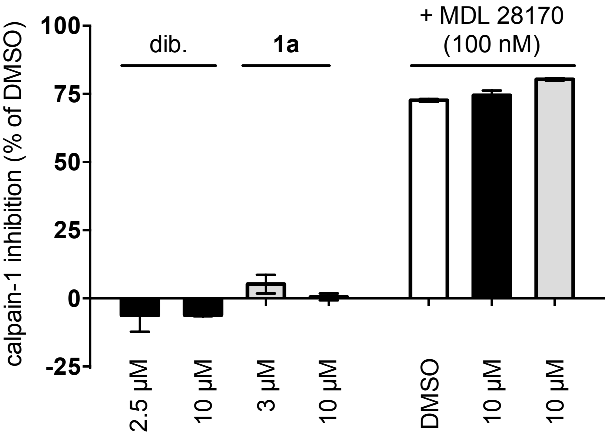

*Figure 29. Indoline **1a** does not inhibit the enzymatic activity of calpain-1. Calpain-1 activity was determined in a fluorescence-based assay using human calpain-1 inhibition screening kit, by monitoring the cleavage of Ac-LLY-AFC by the enzyme (i.e. the generation of the fluorescent AFC) after incubation with **1a**, the known activator dibucaine, or the known inhibitor MDL 28170 at 37 °C for 5 min. Each data point represents a duplicate measurement of the inhibition related to the DMSO control. Additional concentrations omitted for clarity (n = 2, each in N = 2).*

4.4.5. Conclusion

Two pull-down experiments were performed to identify the target of **1a**. To this end, two different pull-down probes were designed based on the SAR delineated for the autophagy inhibitor. Whereas no major difficulties were encountered when synthesizing a probe with a linker at the C5 of **1a** (**53**), all attempts to access a C3-functionalized derivative of indoline **1a** were unsuccessful. Given that the activities of indole analog **16a** and a C3-functionalized analog (**38**) were in the micromolar range, a pull-down probe was synthesized with an indole core instead (**93**). Stability tests revealed that Boc-protected **53** was highly unstable. The 2^nd^ generation probe **93** on the other hand, was stable only under neutral or acidic conditions, and hydrolyzed under standard pull-down coupling conditions. Therefore, the conditions for the pull-down experiments were optimized to minimize hydrolysis.

GDH, calpain-1, and HINT-1 were isolated in a quantitative pull-down. However, the validation studies indicate that neither GDH nor calpain-1 are targets of **1a**. HINT-1 was not pursued as a putative target due to the low ratios detected by MS/MS. The results taken together provide evidence that the probes designed, which suffered from stability and biological activity issues, were not suitable for a pull-down assay. Furthermore, the surprisingly low number of hits obtained in both pull-down experiments could arise from the structural similarity of the probes, as these only differ in the sulfonamide aryl ring. The short list in the SILAC-based pull-down experiment may also suggest that the target of **1a** is either of low abundance, a membrane protein, or both. Despite the high sensitivity of SILAC-based proteomics, low abundant proteins remain a significant hurdle. The identification of membrane proteins by affinity chromatography is another major challenge, as they are prone to aggregation in solution, and most detergents present in lysis buffers disrupt their secondary structure,[56] making them inaccessible for small molecule binders (Chapter 2.2.1). Considering all the obstacles faced by the target identification of **1a** using affinity chromatography, a different approach was necessary.

4.5. Target identification by Thermal Proteome Profiling

As described in the previous chapters, pull-down techniques are often hampered by modifications of the parent compound for the introduction of a linker, as it can interfere with binding to the target protein. TPP represents an attractive linker-free alternative to affinity-based proteomics. This method is based on the thermal stability of proteins, which can change upon binding of a small molecule (Chapter 2.2.1). Full cell lysates are incubated with either the studied compound in DMSO or DMSO alone in a thermal gradient and the soluble fractions analyzed by MS/MS. The peak intensities for each protein are then plotted against the temperature, thereby generating melting curves. A protein displaying a shift in its melting curve for the compound-treated sample in comparison to the DMSO-treated lysate represent potential targets of the compound.

4.5.1. Thermal Proteome Profiling with Indoline 1a

A TPP for **1a** was performed with MCF7-eGFP-LC3 cell lysate. A lysis buffer containing NP-40 alternative was used to enhance the solubility of membrane proteins and therefore increase their concentration in the lysate. To search for potential targets of **1a**, the results were filtered by the following criteria: 1) the protein is either stabilized or destabilized in all three replicates and 2) a strong (de)stabilization is observed with an average shift in melting temperature (dT_m) > 1.5 °C or an average final intensity difference (dInt) > 10%. A total of 96 proteins were identified as hits following the constraints set (Table 17).

*Table 17. Selected potential targets of **1a** identified in TPP experiment based on their melting temperature shift compared to DMSO (n = 3).*

Entry	**Gene Names**	**Protein names**	**dT$_m$ (°C)**	**dInt$_{T9}$**	**dInt$_{T10}$**
1	P2RX4	P2X purinoreceptor 4	3.27	0.14	0.08
2	SLC39A14	Zinc transporter ZIP14	2.71	0.08	0.08
3	RAB27A	Ras-related protein Rab-27A	2.64	0.19	0.18
4	CCS	Copper chaperone for superoxide dismutase	2.43	0.09	0.07
5	LAMTOR5	Ragulator complex protein LAMTOR5	2.39	0.12	0.05
6	ATRX	Transcriptional regulator ATRX	-4.04	0.10	0.10
7	FAM114A1	Protein NOXP20	-2.95	0.02	0.04
8	TSPYL5	Testis-specific Y-encoded-like protein 5	-2.58	0.08	0.09
9	RAB11FIP1	Rab11 family-interacting protein 1	-2.51	0.14	0.15
10	TBC1D5	TBC1 domain family member 5	-2.37	0.06	0.09
11	LTN1	E3 ubiquitin-protein ligase listerin	-2.30	0.08	0.04
12	CAMSAP3	Calmodulin-regulated spectrin-associated protein 3	-2.22	0.04	0.03
13	ARMC1	Armadillo repeat-containing protein 1	-2.18	0.08	0.07
14	TFG	Protein TFG	-2.14	0.06	0.02
15	EPB41	Protein 4.1	-2.12	0.09	0.06
16	POLR2I	DNA-directed RNA polymerase II subunit RPB9	-2.12	0.09	0.18
17	SUOX	Sulfite oxidase, mitochondrial	-2.09	0.02	0.03
18	VCPIP1	Deubiquitinating protein VCIP135	-2.07	0.12	0.09
19	RBM12B	RNA-binding protein 12B	-2.02	0.05	0.05
20	MRPS27	28S ribosomal protein S27, mitochondrial	-1.30	0.17	0.18
21	FOXK1	Forkhead box protein K1	0.30	0.13	0.15
22	FHOD1	FH1/FH2 domain-containing protein 1	-0.27	0.15	0.14
23	PPP1R13B	Apoptosis-stimulating of p53 protein 1	-0.27	0.16	0.13
24	ATXN2	Ataxin-2	1.07	0.13	0.13
25	SLC7A6OS	Probable RNA polymerase II nuclear localization protein SLC7A6OS	-1.90	0.13	0.13
26	PPP1R2 PPP1R2P3	Protein phosphatase inhibitor 2	0.37	0.10	0.11

*MCF7-eGFP-LC3 cell lysates were incubated with **1a** (2.5 µM) or DMSO (1 v/v%) for 30 min and aliquoted into ten samples, each of which was incubated at increasing temperatures. The soluble fraction of each sample was processed for MS-analysis. Proteins listed are stabilized or destabilized by **1a** with an average melting temperature shift of ≥ 2 °C or intensity shift of ≥ 10% at the highest temperature. dT$_m$ = difference in melting temperature between DMSO- and compound-treated samples; dInt = difference in signal intensity between DMSO- and compound-treated samples at 65 °C (T9) and 67 °C (T10) normalized to 1.*

4.5.2. Target Validation

As in every proteomics experiment, the hits identified by TPP needed to be confirmed as targets of **1a**. P2X4 and LAMTOR5 were selected as high priority candidates for further validation due to the strong stabilization displayed by these hits upon uncubation with **1a**. Depending on the protein class and function, different methods were employed for these putative targets.

a) Evaluation of P2X4 as a Target of Indoline 1a

The best hit in the TPP, P2X4, was stabilized in the presence of **1a** in all three biologically independent replicates. The melting point in the presence of **1a** was in average 3.3 °C higher than for the DMSO control, whereby a 14% stabilization was observed at 65 °C (Figure 30).

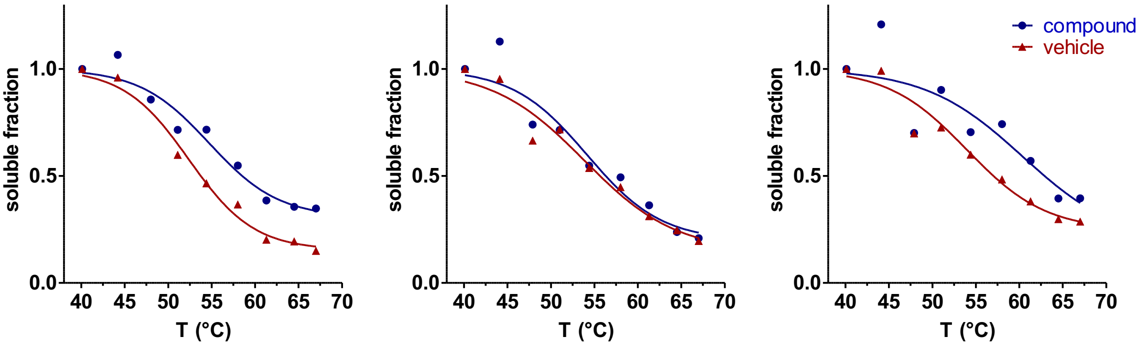

*Figure 30. Melting curves of P2X4 upon incubation with **1a** (compound, blue) or DMSO (vehicle, red) for each replicate.*

The ionotropic purinergic receptor P2X4 is an ATP-gated cation channel of the purinergic receptor family, with a strong affinity for Ca^{2+}. Though little is known about its function, it appears to regulate vascular tone and the development of neuropathic and inflammatory pain.[126] To date, only ATP and closely related analogs, such as 2-meSATP and α,β-meATP, have been identified as potent agonists. The macrolactone ivermectin, a glutamate-gated chloride channel (GluCl) and $GABA_A$ binder, can potentiate the currents evoked by ATP binding of P2X4.[126-127] The only antagonist known, benzodiazepine 5-BDBD, was developed over a decade ago.[128] This lack of potent, selective modulators is a major drawback in the study of this receptor and other subtypes of the P2X family.

Only recently it was shown that ivermectin induces autophagy in breast cancer cells.[129] However, a direct link between P2X channels and autophagy has not been demonstrated yet. Nevertheless, numerous calcium permeable channels have been reported to regulate autophagy,[130] which is consistent with the fact that Ca^{2+} plays a crucial role in the mTOR-independent inhibition of this pathway.[15] To confirm that **1a** acts via P2X4 to inhibit autophagy, different experiments were performed.

i. Cellular Thermal Shift Assay

CETSA is a complementary approach to TPP, which allows the visualization of protein melting by western blot. The samples utilized in both techniques may originate from the same experiment and are split after ultracentrifugation. For CETSA, the soluble fraction is processed for protein separation and immunostaining.

The findings of the TPP were confirmed for P2X4 by CETSA, as a substantial difference was observed between the compound- and DMSO-treated samples by immunoblotting (dT_m = 1.2 °C, Figure 31).

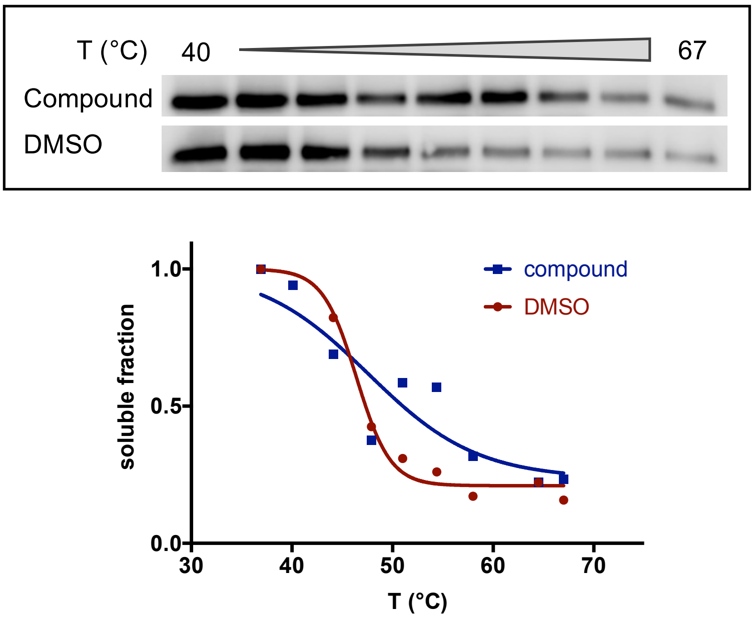

*Figure 31. The thermostability of P2X4 is enhanced by **1a**. Top: Visualization by immunoblotting; bottom: quantification of western bands strength using ImageStudio software. MCF7-eGFP-LC3 cell lysates were incubated with **1a** (2.5 µM) or DMSO (1 v/v%) for 30 min and aliquoted into 10 samples, each of which was incubated at a different temperature. Proteins in the soluble fraction were separated by SDS-PAGE and probed for P2X4 using anti-P2X4 (Alomone Labs, cat# APR-002) (n = 3).*

ii. Functional and Binding Assays

The role of Ca^{2+} in autophagy is not fully clear and still a matter of debate. It has been demonstrated that the divalent cation is involved in numerous pathways leading to both the induction and inhibition of autophagy.[131] For example, Ca^{2+}-release from the ER triggers autophagy through binding of calmodulin, which ultimately leads to the inhibition of mTOR.[132] Other studies suggest that extracellular influx of calcium activates calpain, which cleaves ATG5 thereby inhibiting the autophagosome formation.[123] Given the importance of calcium in the regulation of autophagy, modulation of the P2X4 receptor by an autophagy inhibitor could represent a possible relationship between the two.

As an initial study, the influence of **1a** on intracellular calcium levels was tested in MCF7 cells. Whereas the control ionomycin elicited a strong influx of calcium, no change was observed upon incubation with **1a** (Figure 32). Testing **1a** in antagonist mode was not possible in this setup, i.e. with cells expressing endogenous levels of P2X4, due to the lack of a selective agonist.

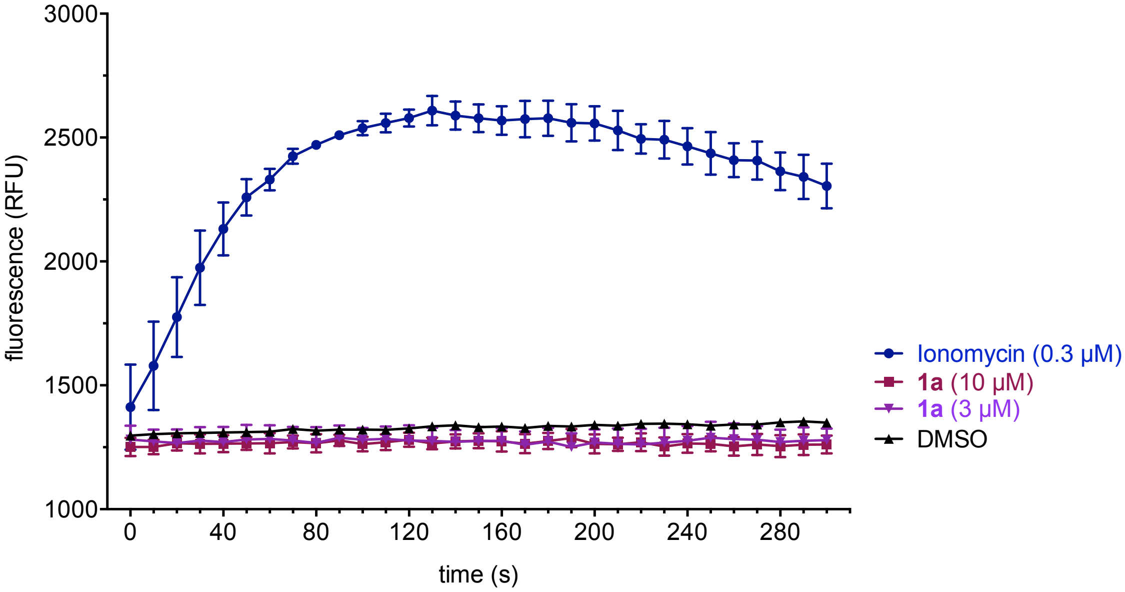

*Figure 32. Indoline **1a** does not increase intracellular calcium levels. Intracellular calcium levels in MCF7 cells were measured using the calcium-sensitive fluorescent dye Fluo-8NW and ionomycin as a positive control (n = 2, each in N = 3).*

The evaluation of ion receptor function in cell-based assays is generally not straightforward due to several issues: Although a high expression level of the studied receptor is necessary to detect a response in Ca^{2+}-based assays, overexpression of certain ion receptors can lead to cytotoxicity.[133-134] Unlike in the study of GPCRs, specific high-affinity receptor agonists are rare for certain channels or may not allow the detection of weak antagonists.[134-135] These are most likely the reasons why gating of P2X4 receptor is commonly studied using electrophysiological methods.[136-138] Electrophysiology is widely applied to the study of the functional characteristics of ion channels, as it provides high-quality functional information on channel–compound interaction.[133] Therefore, the effect of **1a** on P2X4 is currently being evaluated in a patch clamp assay.

A procedure to study binding of ion channels, consists in measuring the displacement of a labeled receptor binder by the studied compound, using membranes from a tissue with endogenously high levels of the studied receptor. Preliminary results showed only 5% [^{3}H]α,β-meATP displacement inhibition by **1a** for the P2X family, hence a negligible binding affinity. However, these results only prove that **1a** does not bind at the same site as ATP. It remains to be seen whether **1a** acts at a different allosteric site to ATP.

b) Evaluation of LAMTOR5 as a Target of Indoline 1a

The protein LAMTOR5 was identified as a putative target of **1a** because of its strong stabilization observed upon treatment with the compound. An average 2.4 °C melting point shift and a 12% intensity increase at 65 °C were detected with **1a** in contrast to the DMSO control (Figure 33).

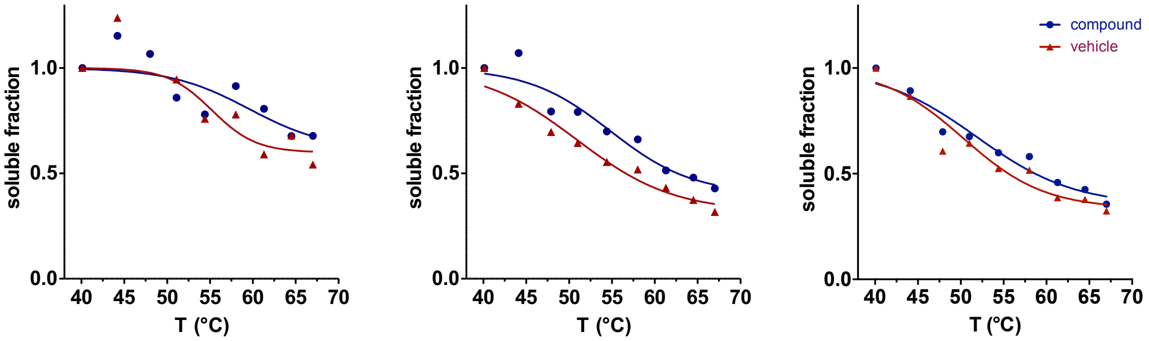

*Figure 33. Melting curves of LAMTOR5 upon incubation with **1a** (compound, blue) or DMSO (vehicle, red) for each replicate.*

LAMTOR5 constitutes part of the pentameric Ragulator complex and was only identified five years ago.[139] The Ragulator complex itself was found to exhibit binding affinity and a guanine nucleotide exchange factor (GEF) activity towards RagA and RagB upon activation by v-ATPase. The Rag heterodimer consists of a RagA/B and a RagC/D unit, both small GTPases. Upon activation, the dimer switches from RagA/B(GDP)-RagC/D(GTP) to RagA/B(GTP)-

RagC/D(GDP), which then recruits and activates mTORC1, leading to inhibition of autophagy.[139] No activity of individual Ragulator subunits has been reported to date. Thus, to examine whether **1a** inhibits autophagy by specific modulation of the complex, the activity of the downstream effector mTOR could be tested. In a more direct assay, the GEF activity of Ragulator towards RagA/B in the presence of **1a** could be evaluated by analyzing the displacement of GDP-γS from RagA/B-RagC^{D181N}, as described by Sabatini and coworkers.[139] To address binding affinity of LAMTOR5 towards **1a**, biophysical studies with the purified proteins could be performed.

As for the CETSA by immunoblotting, no change in the melting behavior of LAMTOR5 upon treatment with **1a** was observed (Figure 34). However, this result does not devalidate the findings in the TPP, as subtle differences in the amounts of soluble protein may necessarily be detected by immunoblotting, especially from poorly resolved bands, as was the case for the low-molecular-weight protein LAMTOR5. Therefore, the Ragulator subunit remains a valid candidate in the search for the target of **1a**. Evaluation of LAMTOR5 as a target of **1a** is currently under investigation in the group of Dr. Yaowen Wu.

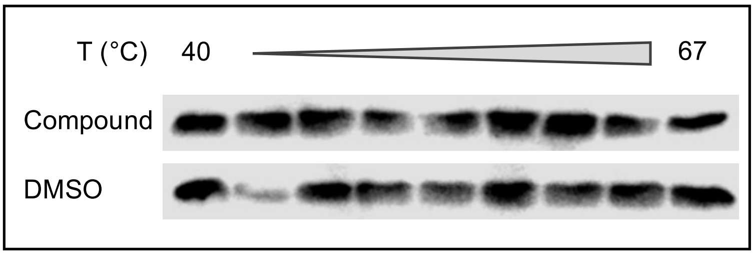

*Figure 34. The thermostability of LAMTOR5 is not enhanced by **1a** in immunoblotting. MCF7-eGFP-LC3 cell lysates were incubated with **1a** (2.5 μM) or DMSO (1 v/v%) for 30 min and aliquoted into 10 samples, each of which was incubated at a different temperature. Proteins in the soluble fraction were separated by SDS-PAGE and probed for LAMTOR5 using anti-LAMTOR5 (Cell Signaling, cat# 14633) (n = 3).*

4.5.3. Conclusion

In a TPP with MCF7-eGFP-LC3 cells, 96 proteins were (de)stabilized by **1a** and thus identified as potential targets of the autophagy inhibitor. The ion receptor P2X4 and the Ragulator member LAMTOR5 were selected as most promising candidates due to the strong stabilization observed upon incubation with **1a**. Preliminary results show no binding of **1a** to the P2X family. Because additional evidence is needed for a conclusive result, P2X4 is currently being tested in a patch clamp assay. As an upstream regulator of mTOR, LAMTOR5 plays an important role in autophagy and represents therefore an attractive candidate for the target of **1a**. Evaluation of this putative target will be performed by the group of Dr. Yaowen Wu.

4.6. Computational Target Prediction

Virtual target prediction is an alternative approach to proteomics in the identification of targets for small molecules (Chapter 2.2.1). Various computational tools, including SwissTargetPrediction,[65] SEA,[63] and a structure similarity/substructure search in SciFinder[140] were employed in order to predict a target for **1a** (Table 18). SwissTargetPrediction predicts targets by comparing shape and fingerprints with small molecules present in the ChEMBL that have an activity < 10 μM for a protein or protein complex.[65] SEA compares the query molecule to several databases based on fingerprints using the Tanimoto coefficient. As for the SciFinder similarity search, which searches through the Chemical Abstracts Service (CAS) database based on the Tanimoto similarity, references containing biological activities for similar molecules were selected and analyzed individually.

Table 18. Selected examples of predicted targets using SEA and SwissTargetPrediction.

Entry	Target	Gene Code	# Ligands	Probability	Most similar structure
A1	Urotensin II receptor	UR2R	71	0.42	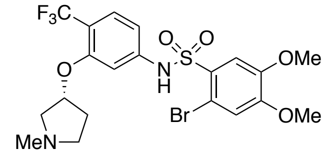
A2	Serine/threonine-protein kinase RAF	RAF1; BRAF	739	0.35	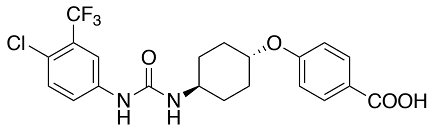
A3	Tyrosine-protein kinase ABL	ABL1	7	0.34	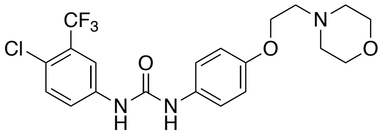
A4/ B1	Pyruvate kinase isozymes M1/M2	PKM	52	0.49	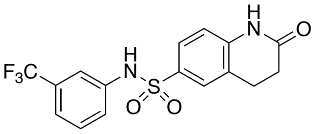
B2	5-hydroxytryptamine receptor 6	HTR6	58	0.29	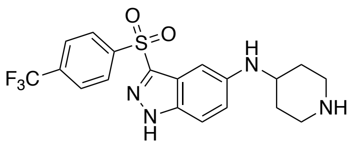
B3	Tyrosyl-DNA phosphodiesterase 1	TDP1	20	0.25	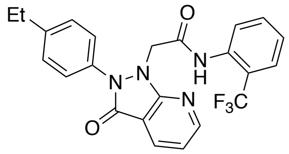
B4	RAF1; BRAF and ARAF kinases	RAF1; BRAF; ARAF	83	0.19	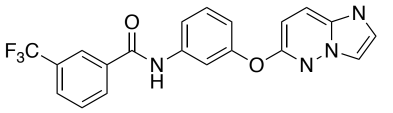

Entries A1–4 and B1–B4 correspond to search results of SEA and SwissTargetPrediction, respectively. Probability for A1–3 is the Tanimoto coefficient calculated for the most similar compound.

Within the numerous predictions obtained, pyruvate kinase (PK, entry A4/B4) and the serotonin GPCR family (5-HTR, entry B2) appeared as hits in both target prediction tools and the SciFinder similarity/substructure search results and represented therefore the most promising targets to pursue. Furthermore, the rapidly accelerated fibrosarcoma (RAF) kinase family was predicted as a target of **1a** by SEA (entry A3) and SwissTargetPrediction (entry B4).

4.6.1. Evaluation of Pyruvate Kinase as Target of Indoline 1a

Pyruvate kinase is a key glycolytic enzyme responsible for net energy production by catalyzing the conversion of phosphoenolpyruvate (PEP) and ADP to pyruvate and ATP.[141] This metabolic enzyme forms homotetramers and is ubiquitous in all organisms. Whereas the isozyme M1 is expressed in all tissues, PK-M2 is often found overexpressed in tumors.[142] Despite its importance in cancer, only one micromolar PK inhibitor has been identified to date.[143] Therefore, the discovery of selective small molecule regulators would largely contribute to the study of this enzyme and possibly provide a new druggable target. A possible relationship between the regulation of PK and autophagy was described by Chiavarina *et al.*, who demonstrate that PK-M2 overexpression leads to the activation of autophagy in stromal cells.[144] Given the important role of PK in glycolysis, it is possible the ATP production by the enzyme triggers the activation of autophagy via the glucose-sensing regulating proteins involved in this pathway.

To test the effect of **1a** on the activity of its predicted target PK, a fluorescence-based assay was employed. The method utilizes pyruvate oxidase to convert the produced pyruvate to acetyl phosphate, generating one molecule of H_2O_2, which can be quantified upon reaction with OxiRed^{TM} Probe (Scheme 21).

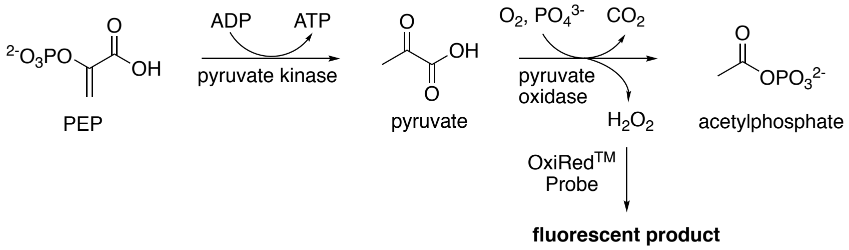

Scheme 21. Principle of the assay employed to determine the activity of PK.

No activity change was observed upon treatment of PK with **1a** at either of the concentrations tested (Figure 35). Due to the lack of a potent PK inhibitor, staurosporine was employed as an inhibition control, which inhibited PK by ca. 25%. Given these results, a different predicted target was pursued.

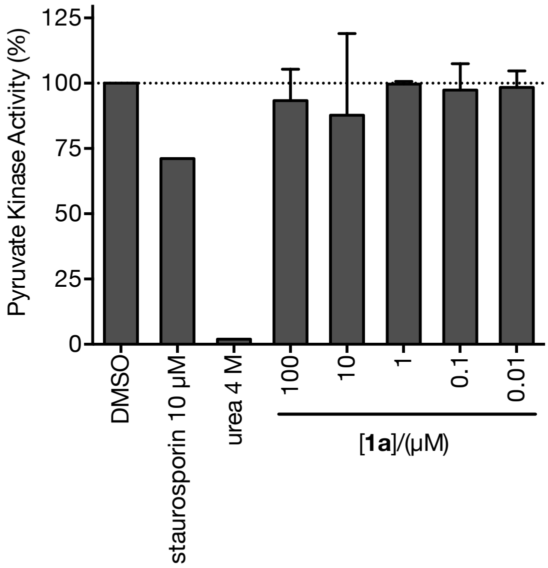

*Figure 35. Indoline **1a** has no effect on the enzymatic activity of PK. PK activity was determined in a fluorescence-based assay using Pyruvate Kinase Activity Colorimetric/Fluorometric Assay Kit, by monitoring the pyruvate kinase-catalyzed generation of pyruvate. Pyruvate is then oxidized by pyruvate oxidase, producing fluorescence. Each data point represents a duplicate measurement of the relative activity to the DMSO control. Data shown are mean values ± SEM (N = 2).*

4.6.2. Evaluation of RAF and ABL1 Kinases as Targets of Indoline 1a

RAF kinases are serine/threonine kinases involved in the mitogen activated protein kinase (MAPK) cascade. The signal transduction starts with an extracellular stimulus that binds to a receptor, leading to the activation of rat sarcoma (RAS). Activated RAS activates RAF kinases, which in turn activate mitogen-activated protein kinase kinase (MKK) by phosphorylation. MKK phosphorylates and activates mitogen-activated protein kinase (MAPK, also ERK), which can activate the cellular tumor antigen p53.[145] The MAPK pathway has been linked to autophagy through MAPK and p53. Moreover, modulation of RAF kinases has been associated with regulation of autophagy in numerous examples.[146-148]

The third kinase predicted, abelson murine leukemia viral oncogene homolog 1 (ABL1) is a proto-oncogenic tyrosine kinase implicated in numerous cancers, which is constitutively activated when fused to BCR. This chimera is caused by the Philadelphia translocation, an abnormal chromosomal defect, in which segments of chromosomes 9 and 22 are swapped, thereby juxtaposing the gene locus of BCR onto ABL.[149-150] Both ABL and BCR-ABL have been demonstrated to regulate autophagy at a downstream level.[151-152]

Given that RAF and ABL1 kinases represent attractive targets of **1a**, the compound was tested against RAF1, BRAF, and ABL1 in a functional assay. However, as the autophagy modulator did not affect the activity of any of the three kinases (-7, -15, and 18% inhibition, respectively), these were not pursued as targets of **1a**.

4.6.3. Evaluation of Serotonin Receptors as Targets of Indoline 1a

5-Hydroxytryptamine (5-HT, serotonin) GPCRs comprise 13 receptor subtypes and are thus the largest family of neurotransmitter receptors. Together with adrenergic, dopamine and histamine receptors, they are members of the Rhodopsin-like superfamily of GPCRs (type A).[153] Serotonin receptors are found both in the central and peripheral nervous systems and mediate a variety of physiological responses, including behavior, sensory perception, memory, and contraction of smooth muscle. Consequently, small molecules modulating their activity are used in clinics for various neurological disorders, such as anxiety, depression, Schizophrenia, and, more recently, Alzheimer's disease.[153-155]

The serotonin receptor subtypes 1, 2, 4–7 are not coupled to the same G protein and elicit thus different cellular responses. For instance, receptors of the subtype 2 are coupled to $G_{i/o}$, whose α-subunit, upon activation of the receptor, dissociates from the G protein and binds to PLCβ. Cleavage of PIP_2 to inositol 1,4,5-trisphosphate (IP_3) and diacyl glycerol (DAG) by PLCβ triggers the activation of protein kinase C (PKC) and the release of Ca^{2+} from the ER. The receptors 4, 6, and 7 are G_s-coupled and, as opposed to the $G_{i/o}$-coupled receptors 1 and 5, activate adenylyl cyclase. Active adenylyl cyclase catalyzes the formation of the secondary messenger cAMP, which in involved in numerous signaling pathways by activating ion channels, protein kinase A (PKA), cAMP response element-binding protein (CREB), and EPAC.[153] Despite the fact that most of the downstream effectors of serotonin receptors are involved in autophagy, no direct link between the two has been established yet.

To ascertain whether **1a** had a regulatory effect on serotonin receptors, the compound was tested in two cell-based assays using stable cell lines, each expressing one 5-HTR subtype. Depending on whether the receptor was $G_{q/11}$- or $G_s/G_{i/o}$-coupled, its activity was measured in a different readout, i.e. levels of IP_1 (a downstream metabolite of IP_3)[156] or impedance, respectively. Impedance-based biosensors rely on the observation that alterations in cAMP levels arising from $G_s/G_{i/o}$-coupled receptor modulation induce morphological changes, which result in varying extracellular and transcellular currents.[157-158]

In the first assay, **1a** was tested in agonist mode against nine receptor subtypes but had no effect on any of these. In the second assay, an antagonistic effect was determined by measuring the inhibition of the response triggered by an agonist. It could be shown that the autophagy inhibitor **1a** had a strong antagonistic effect on serotonin receptor 5-HT$_6$, and a moderate effect on receptors 5-HT$_{1B}$, 5-HT$_{2B}$, 4e, and 7 (Figure 36).

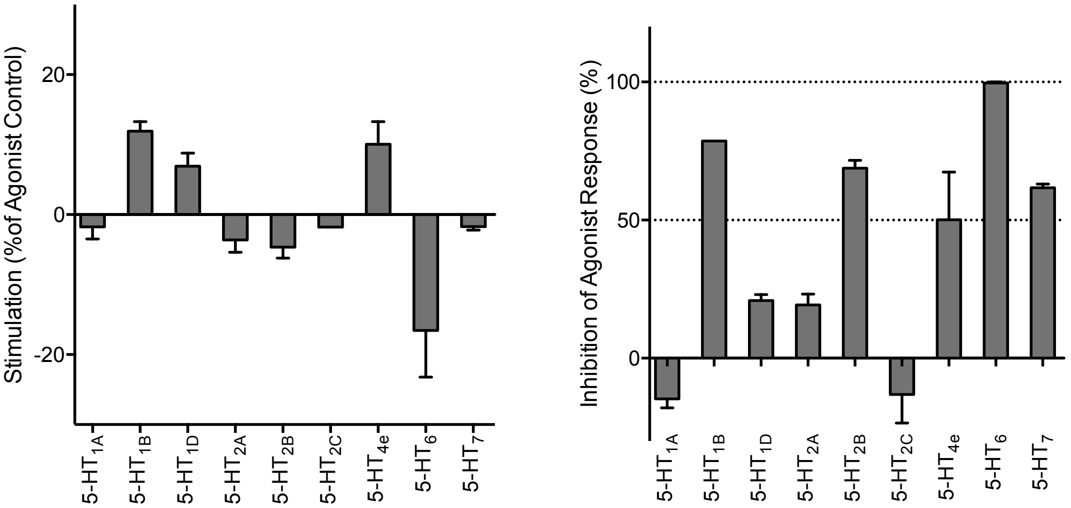

Figure 36. Left: Indoline ***1a*** *has no considerable agonistic effect on nine tested subtypes of the serotonin family of GPCRs. Agonistic effect of* ***1a*** *was measured at 10 µM using 7-(dipropylamino)-5,6,7,8-tetrahydronaphthalen-1-ol (8-OH-DPAT) for 5-HT*$_{1A}$ *and serotonin for the remaining receptors as agonist controls; right: indoline* ***1a*** *has a strong antagonistic effect on the serotonin GPCR subtypes 6 and a moderate effect on the subtypes 1B, 2B, 4e, and 7. Antagonist effect of* ***1a*** *was measured at 10 µM using 8-OH-DPAT (for 5-HT*$_{1A}$*) and serotonin (for the remaining receptors) to stimulate the receptor. Data shown are mean values ± SEM (N = 2).*

Moreover, dose-response analysis revealed a strong antagonistic effect for **1a** on 5-HT$_6$ with an IC$_{50}$ = 1.0 µM (Figure 37). Consequently, serotonin receptor 5-HT$_6$ was identified as a target of **1a** and was evaluated for its role in the inhibition of autophagy.

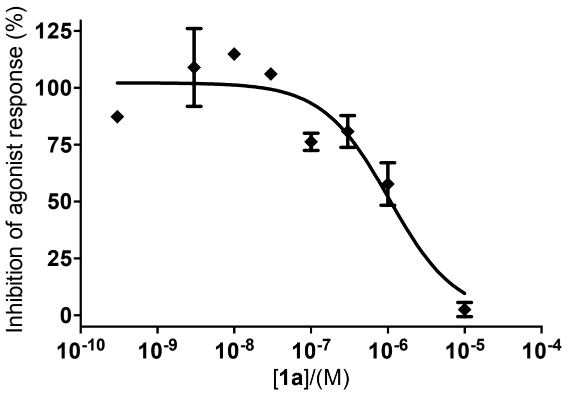

*Figure 37. Indoline **1a** is an antagonist of the serotonin GPCR 5-HT$_6$. Increase of intracellular cAMP levels upon treatment with **1a** was monitored in human CHO cells stably expressing 5-HT$_6$. by HTRF. Data shown are mean values ± SEM (N = 2).*

To test the hypothesis whether **1a** inhibits autophagy by antagonizing 5-HT$_6$, potent and selective antagonists of 5-HT$_6$ were tested for autophagy inhibition. Additionally, antagonists of the moderately inhibited receptors shown in Figure 36 were evaluated in the phenotypic screen. However, none of the antagonists inhibited autophagy (Table 19), indicating that serotonin receptors are most likely not responsible for the inhibitory effect of **1a** on autophagy.

Table 19. Selected examples of potent serotonin receptor antagonists against subtypes 1B, 2B, 4, 6, and 7 tested for autophagy inhibition in the LC3-phenotypic screen.

Entry	**Antagonist**	**Selectivity**	**Structure**	**Autophagy Inhibition (%)**
1	SB 216641	5-HT_{1B}	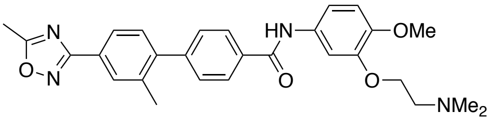	-10
2	SB 224289	5-HT_{1B}	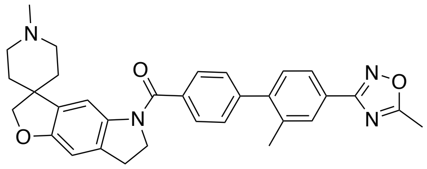	27
3	SB 215505	5-HT_{2B}	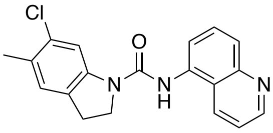	9
4	SB 204741	5-HT_{2B}	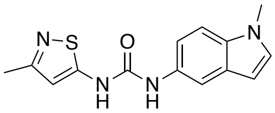	-3
5	SB 204070	5-HT_4	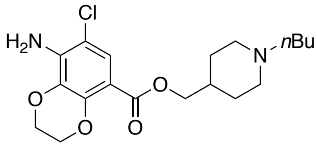	10
6	SB 203186	5-HT_4	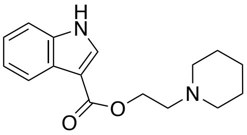	-5
7	GR 113808	5-HT_4	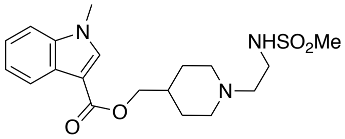	10
8	SDZ-205,557	5-HT_4	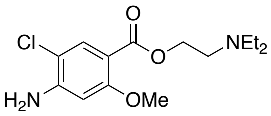	9
9	Ro 04-6790	5-HT_6	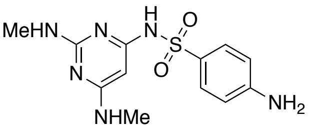	-14
10	SB 269970	5-HT_7	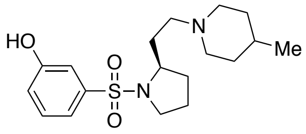	1

4.6.4. Evaluation of Different GPCR families as Targets of Indoline 1a

Given the low IC_{50} obtained for 5-HT_6, it was hypothesized that **1a** could inhibit autophagy by targeting a different GPCR of the same family as serotonin receptors, as these share a high sequence homology. Moreover, numerous GPCRs play an important role in autophagy via different mechanisms, making them likely targets of autophagy modulators.[159] However, as the identification of integral membrane proteins by proteomics has major obstacles, alternative strategies are necessary. Therefore, **1a** was tested against a small, unselective panel of consisting of a subset of GPCR families from rat (Figure 6). The binding assay uses whole membranes with endogenously high levels of the corresponding receptor and measures the compound-induced displacement of a specific radiolabeled ligand, which is selective for each receptor family. Indoline **1a** inhibited binding of the purinergic GPCR family (P2Y) to a radiolabeled analog of its native ligand ([^{35}S]-ATP-αS) by 42% (Figure 38).

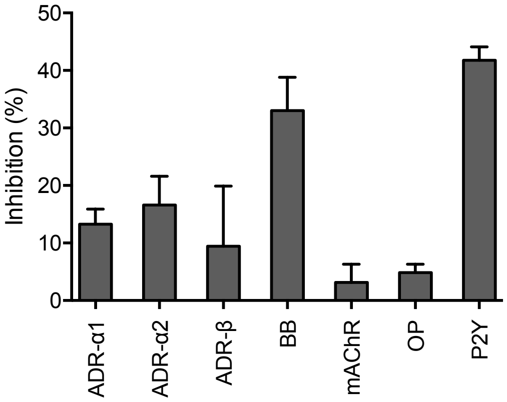

*Figure 38. Indoline **1a** moderately inhibits bombesin and purinergic GPCR families in a non-selective radioligand binding assay. Radioligand displacement by **1a** (10 µM) was measured using rat brain tissue and potent radioligands specific for each receptor family. Data shown are mean values ± SEM (N = 2).*

Considering the unselective nature of the assay, it is possible that the moderate inhibition measured arises from the strong inhibition of a single receptor subtype. Hence, **1a** was tested against five P2Y subtypes (1, 2, 4, 6, and 11) but neither an agonistic nor an antagonistic effect on any of these receptors could be detected (Figure 39). Interestingly, the P2Y12 antagonist PSB-0739, developed by Müller and coworkers,[160] strongly inhibits starvation-induced autophagy (IC_{50} = 64 ± 17 nM). Moreover, P2Y13 has been demonstrated to positively regulate autophagy.[161] Since **1a** was not tested against P2Y12 or P2Y13 initially, due to the inaccessibility of the receptors, P2Y receptors remain a potential target, and the remaining subtypes need to be evaluated in further detail.

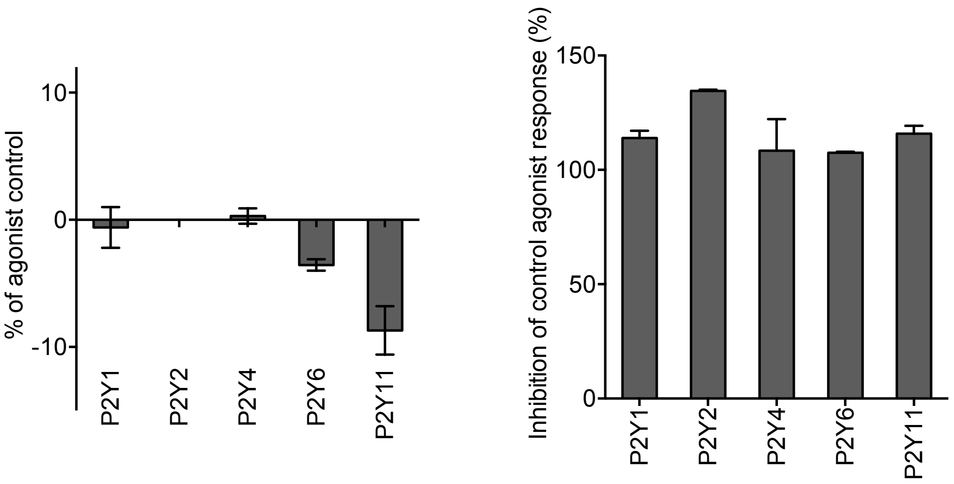

*Figure 39. Indoline **1a** has no considerable agonistic (left) or antagonistic effect (right) on five tested subtypes of the purinergic family of GPCRs. The effect of **1a** was measured at 10 µM using human recombinant 1321N1 cells and 2-MeSATP (for P2Y1), UTP (for P2Y2 and P2Y4), UDP (for P2Y6), and ATP (for P2Y11) as a positive control or stimulus. Data shown are mean values ± SEM (N = 2).*

4.6.5. Conclusion

Computational target prediction is a powerful tool in the identification of the biological targets of a small molecule. By utilizing various tools and performing database searches, pyruvate kinase, serotonin receptors, ABL, and RAF1 and related kinases were predicted. Of all hits, only 5-HT$_6$ was validated as a target of **1a**. However, no evidence was found for a regulatory role of serotonin receptors on autophagy. Nevertheless, the strong potency obtained for 5-HT$_6$ is a possible clue to the identification of a different GPCR as the target of **1a**, as these membrane receptors share a high structural similarity. Therefore, **1a** was tested against a small panel of GPCRs, which revealed that **1a** binds moderately to the purinergic family P2Y. Despite the preliminary results, P2Y remains a putative target of **1a** and will be evaluated through a collaboration with the group of Prof. Dr. Christa Müller.

5. SUMMARY

Autophagy is a highly conserved cellular process found in eukaryotes that mediates the degradation of cytosolic components. This dynamic process is regulated by upstream signaling and can compensate shortly for the lack of nutrients. Furthermore, autophagy is involved in the clearance of long-lived proteins and dysfunctional organelles,[15] and, at basal levels, it is necessary for maintaining cellular homeostasis.[16] Autophagy is therefore an essential catabolic process in the development, differentiation, and survival of cells.[15, 17-19]

Recent studies have revealed a crucial role of autophagy in the degradation of the protein aggregates responsible for Alzheimer's, Huntington's, and Parkinson's disease.[15, 34] These aggregate-prone proteins accumulate when autophagy is inhibited at various stages, and their clearance is enhanced by autophagy stimulators.[31-33] Moreover, evidence reveals that autophagy is involved in both the prevention of cancer initiation, by degrading toxic cellular waste, and the promotion of tumor cell survival.[15] Consequently, whereas autophagy upregulation might serve as a preventive strategy against cancer, autophagy inhibition is a potential approach for cancer therapy.

As many questions remain open regarding the function of autophagy in disease, there is a strong need for a deeper understanding of the mechanisms underlying this cellular process. By discovering novel autophagy small molecule activators and inhibitors, new tools for the modulation of this pathway can be developed. On the other hand, by determining the specific targets of autophagy modulators, new key players in the regulation of autophagy can be identified, which will allow a deeper understanding of autophagy and provide new targets for drug discovery. The goal of this thesis was to identify an autophagy inhibitor and the target thereof by means of forward chemical genetics.

In a fluorescence-based medium throughput screen that monitors the localization of the autophagy marker LC3, indoline **1a** was identified as a potent inhibitor of starvation-induced autophagy (IC_{50} = 520 nM, Figure 40). Furthermore, its inability to inhibit rapamycin-induced autophagy indicates that **1a** presumably acts upstream of mTOR. The inhibitor was validated in a tandem mCherry-GFP-LC3 assay and by immunoblotting. Additionally, cell viability assays show that its cytotoxicity is selective for starved cells, which is consistent with inhibition of autophagy.

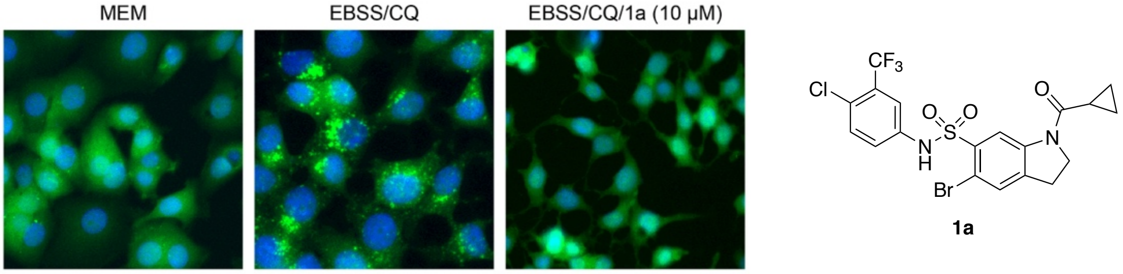
MEM
EBSS/CQ
EBSS/CQ/1a (10 μM)
CF3
Cl
O
O
O
N
S
N
H
Br
1a

*Figure 40. Left: Phenotypic assay employed to identify autophagy inhibitors. MCF7 cells stably expressing eGFP-LC3 were starved of amino acids with EBSS, simultaneously treated with compound, and incubated for 3 h. Blue = Hoechst (nuclei), green = eGFP-LC3 (n = 4, representative images shown). All data shown are mean values ± SEM. MEM = minimal essential medium; EBSS = Earle's balanced salt solution; CQ = chloroquine. Right: structure of indoline **1a**.*

A compound collection of structural analogs of **1a** was successfully synthesized using divergent synthetic routes (Scheme 22). To this end, indoline (**4**) was reacted with an acyl chloride to give the corresponding acyl indoline **100**. After C5-bromination, the sulfonamide moiety was introduced at C6 by treatment with chlorosulfonic acid and subsequent aminolysis. Alkyl groups (R^1) other than cyclopropyl were introduced by saponification of the acetyl group in **101** and subsequent acylation using amide coupling conditions. Further derivatives were obtained by oxidation of the indoline ring in **102** or dehalogenation via palladium-catalyzed hydrogenolysis.

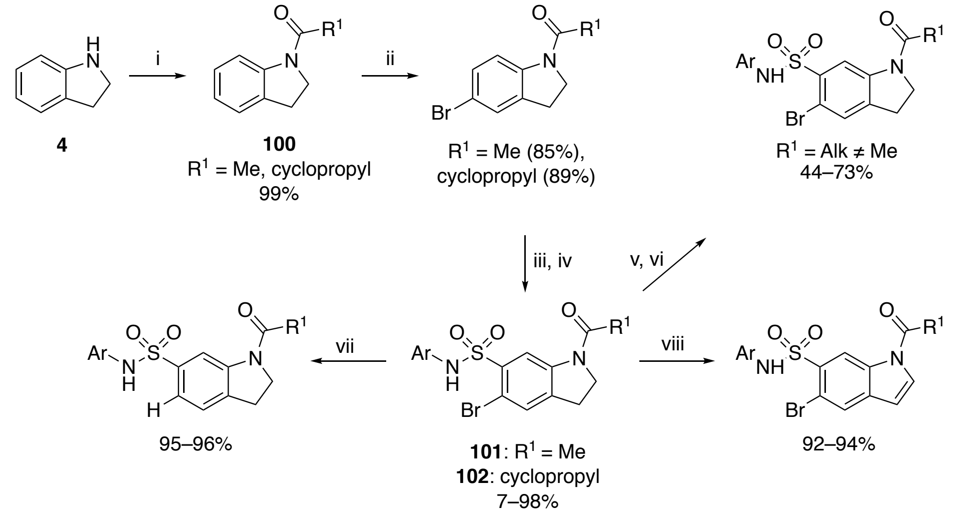
4
i
100
R1 = Me, cyclopropyl
99%
ii
Br
R1 = Me (85%),
cyclopropyl (89%)
Ar NH
R1 = Alk ≠ Me
44–73%
iii, iv
v, vi
vii
95–96%
101: R1 = Me
102: cyclopropyl
7–98%
viii
92–94%

*Scheme 22. Synthetic route for the preparation of aryl sulfonamide indolines and indoles. i) R^1COCl, Et_3N, DMAP, CH_2Cl_2, rt, 2 h; ii) NBS, CH_2Cl_2, rt, 2 h; iii) $ClSO_3H$ (neat), 70 °C, 5 h; iv) Ar-NH_2, pyridine, 70 °C, 16 h; v) (from **101**) aq. NaOH (40% w/v)/MeOH 1:1, reflux, 8 h; vi) R^1-COOH, T3P, EtOAc, rt, 16 h; vii) H_2, Pd/C, rt, 16 h; viii) MnO_2, toluene, reflux, 5 h.*

The compound collection was evaluated in the initial phenotypic screen and a structure–activity relationship (SAR) could be delineated (Scheme 23). Replacement of the trifluoromethyl- and chloro-substituents on the aryl ring (R^1) had a negative impact on the potency, whereby only few bioisosteres were tolerated. The substitution pattern of these substituents was also crucial, as compounds with an *ortho*-substituent to the sulfonamide were less active. Replacement of the cyclopropane carbonyl (R^2) by similarly sized groups decreased the activity of the inhibitor strongly. Further replacements such as N-alkylation of the sulfonamide moiety or C5- and C6-modifications resulted in less potent inhibitors as well. For the design of a chemical probe, C3 was explored as a potential site for modification. For this purpose, the *H*-indole analog of **1a** was derivatized at its most nucleophilic position C3. The resulting indole-based analogs displayed weaker activities but nevertheless in the low-micromolar range. Therefore, C3 was identified as a suitable site for the attachment of a linker for pull-down experiments.

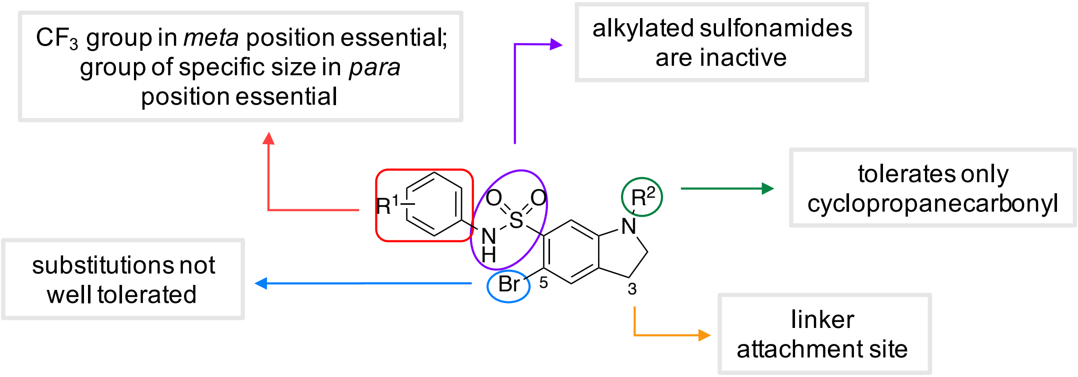
CF3 group in meta position essential; group of specific size in para position essential
alkylated sulfonamides are inactive
tolerates only cyclopropanecarbonyl
substitutions not well tolerated
linker attachment site
R1
O
O
S
N
H
R2
N
Br
5
3

Scheme 23. SAR for an indoline ***1a****-derived compound collection, based on the activities measured in the eGFP-LC3 puncta phenotypic screen.*

Based on the delineated SAR, two pull-down probes were designed for affinity-based proteomics. The first probe consisted of **1a** with a linker attached at either C5 and was prepared from **1a** in 18% overall yield. In contrast, the synthesis of an indoline-based probe with a linker at C3 was unsuccessful despite numerous efforts. Therefore, a pull-down probe with an indole core instead was obtained from the NH-indole analog in 12% overall yield (Scheme 24).

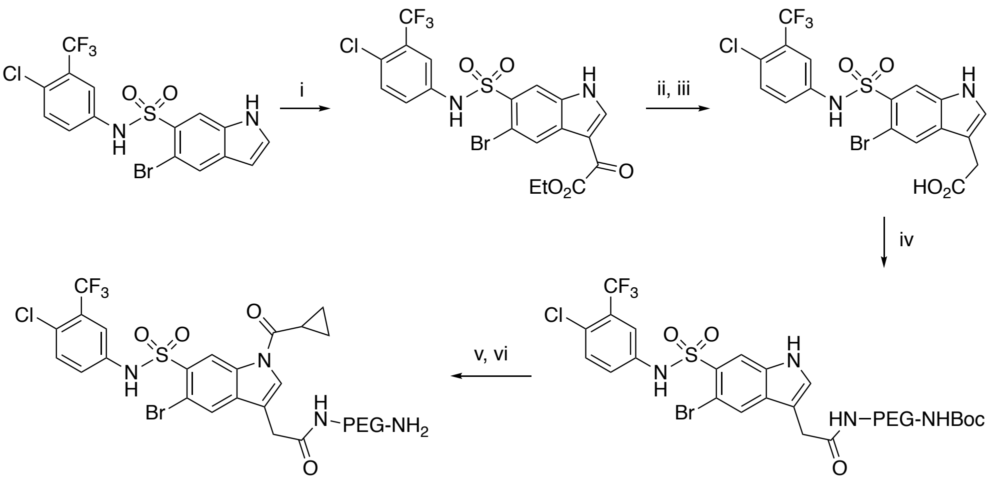

Scheme 24. Synthesis of a chemical probe for affinity proteomics. i) ethyl chlorooxoacetate, $AlCl_3$, CH_2Cl_2, 0 °C → rt, 16 h, 90%; ii) Et_3SiH, TFA, rt, 60 h, 58%; iii) LiOH, THF/MeOH/H_2O 2:1:1, rt, 1 h, quant.; iv) BocNH-PEG3-NH_2, EDC·HCl, HOBt·H_2O, DMF, rt, 4 h; v) cyclopropane carboxylic acid chloride, DMAP, Et_3N, CH_2Cl_2, 0 °C → rt; vi) CH_2Cl_2/TFA 4:1, rt, 1 h.

Numerous tests revealed both probes had stability issues. Whereas the C5-derived probe readily decomposed under various conditions, the indole-based probe only hydrolyzed under basic conditions. Because of the higher potency of the C3-derived probe (7.7 ± 2.3 µM), the conditions for the pull-down experiments were optimized for this probe to minimize hydrolysis. Using the active probe and a negative control probe derived from an inactive analog, a quantitative pull-down was conducted, which led to the identification of glutamate dehydrogenase (GDH), calpain-1, and histidine triad nucleotide binding protein 1 (HINT-1) as putative targets of **1a**.

GDH is involved in glutaminolysis and amino acid sensing as it catalyzes L-Glu to α-ketoglutarate (α-KG) upon activation by L-Leu, L-Ile, L-Val, or ADP. This metabolic enzyme has been proven to negatively regulate autophagy via the activation of the mammalian target of rapamycin complex (mTORC).[116] To test whether **1a** inhibits autophagy via modulation or binding of GDH, three independent assays were performed. A competitive pull-down experiment showed that **1a** was not able to outcompete binding of the active probe. Furthermore, **1a** had no effect on the thermostability or enzymatic activity of GDH. Therefore, we concluded that GDH is not the target of **1a**.

The second protein isolated by pull-down, CAPN1, is the catalytic subunit of calpain-1—a cysteine protease required for autophagy[122] involved in the cleavage of autophagy-related protein ATG5.[123] In a competitive pull-down, no binding of the active probe was detected and thus no competition could be observed, thereby devalidating the initial finding. Similarly as for GDH, **1a** had no effect on the activity of calpain-1, and the enzyme was discarded as putative target.

HINT-1 was not pursued as a putative target because of the low ratios detected by tandem mass spectrometry. The results taken together suggest that the probes designed, which suffered from stability and biological activity issues, were not suitable for a pull-down assay. Pull-down techniques are often hampered by modifications of the parent compound for the introduction of a linker, which can interfere with binding to the target protein. Furthermore, the target of **1a** may be either of low abundance, a membrane protein, or both and therefore difficult to identify by means of proteomics. Considering all the obstacles faced by the target identification of **1a** using affinity chromatography, a different approach was applied.

Thermal proteome profiling (TPP) represents an attractive linker-free alternative to affinity-based proteomics. Using **1a** and DMSO as control, a TPP was conducted with MCF7-eGFP-LC3 cell lysate. A total of 96 proteins were found to be thermally (de)stabilized by the inhibitor and thus identified as potential targets thereof. The ATP-gated ionotropic receptor P2X4 and the Ragulator member LAMTOR5 were selected as most promising candidates because of their strong thermostabilization upon incubation with **1a**. Preliminary results showed no binding of **1a** to the P2X family. As additional evidence is needed for a conclusive result, P2X4 is currently being tested in a patch clamp assay. LAMTOR5 is a member of the Ragulator complex and represents therefore an attractive putative target of **1a**. Evaluation of LAMTOR5 as target of **1a** will be performed by the group of Dr. Yaowen Wu.

In a different approach, various computational tools, including SwissTargetPrediction,[65] SEA,[63] and a structure similarity search in SciFinder[140] were employed in order to predict a target for **1a**. Within the numerous potential targets found, pyruvate kinase (PK), abelson murine leukemia viral oncogene homolog 1 (ABL1), rapidly accelerated fibrosarcoma (RAF) kinases, and the G-protein-coupled serotonin receptor family (5-HTR) were the most promising targets to pursue and hence selected for further investigation. Whereas no change in PK, ABL, or RAF activity was observed upon treatment with **1a**, the autophagy inhibitor had a strong antagonistic effect on serotonin receptors 5-HT$_{1B}$, 5-HT$_{2B}$, and 5-HT$_6$, with an IC$_{50}$ = 1.0 µM for the latter (Figure 41). However, none of the tested selective antagonists for the corresponding receptors inhibited autophagy, indicating that serotonin receptors may not be responsible for the inhibitory effect of **1a** on autophagy.

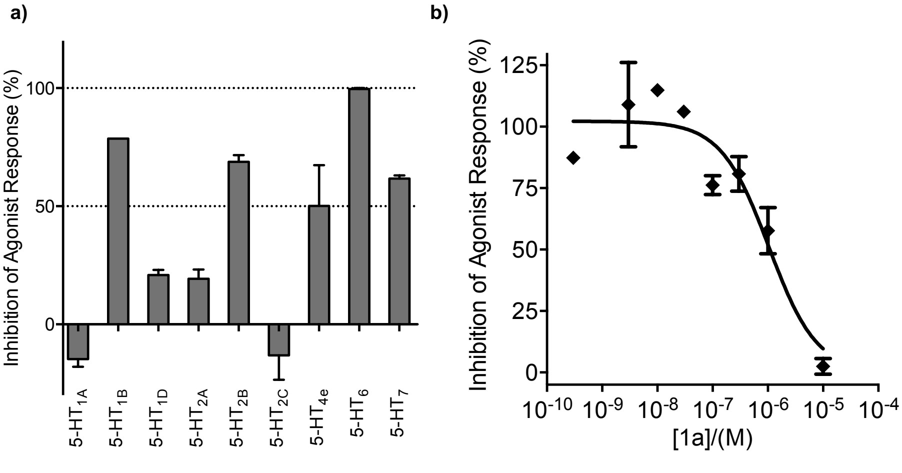

Figure 41. ***a)*** *Indoline* ***1a*** *has a strong antagonistic effect on the serotonin GPCR subtypes 1B, 2B, and 6 and a moderate effect on the subtypes 4e and 7. Antagonist effect of* ***1a*** *was measured at 10 µm using 8-OH-DPAT (for 5-HT*$_{1A}$*) and serotonin (for the remaining receptors) to stimulate the receptor. Data shown are mean values ± SEM, N = 2);* ***b)*** *Indoline* ***1a*** *has a dose-dependent antagonistic effect on serotonin GPCR 5-HT*$_6$*. Increase of intracellular cAMP levels upon treatment with* ***1a*** *were monitored in human CHO cells stably expressing 5-HT*$_6$*. by HTRF. Data shown are mean values ± SEM (N = 2). 5-HT = 5-hydroxytryptamine.*

The low IC$_{50}$ obtained for 5-HT$_6$ indicates that **1a** could target a different G-protein-coupled receptor (GPCR) of the same family as 5-HTRs. Therefore, **1a** was tested against a small, unselective panel of GPCRs and was found to inhibit binding of the purinergic GPCR family (P2Y) to a radiolabeled analog of its native ligand ([^{35}S]-ATP-αS) by 42%. In a follow-up study, **1a** was assayed against five P2Y subtypes (1, 2, 4, 6, and 11) but neither an agonistic nor an antagonistic effect was observed for any of these receptors. Interestingly, the P2Y12 antagonist PSB-0739, developed by Müller and coworkers,[160] strongly inhibits starvation-induced autophagy (IC$_{50}$ = 64 ± 17 nM). Since **1a** was not tested against P2Y12 initially, due to the inaccessibility of the receptor, P2Y receptors remain a potential target, and the remaining subtypes will be evaluated in further detail through a collaboration. Additionally, more powerful computational tools, as well as alternative genetic target identification strategies, such as haploinsufficiency profiling (HIP), could be employed to predict the cellular target of this potent autophagy inhibitor.[40]

Despite its hurdles and challenges, forward chemical genetics represents a powerful tool in the study of cellular pathways and processes. Of the numerous proteins identified as potential targets of **1a**, only receptor 5-HT$_6$ could be confirmed so far, although only as an off-target. The results combined highlight the need for the further evaluation of GPCRs and other receptors as targets of **1a**. The successful target identification of this potent inhibitor could help untangle the complex mechanisms of autophagy.

6. EXPERIMENTAL PART

6.1. Materials used in Biological Experiments

6.1.1. Buffers and Solutions

PBS	137 mM NaCl, 2.7 mM KCl, 10 mM Na_2HPO_4, 2.0 mM KH_2PO_4, pH 7.4
TBS	10 mM Tris/HCl, 150 mM NaCl, pH 7.4
TBS-T	10 mM Tris/HCl, 150 mM NaCl, 0.1% v/v Triton X-100, pH 7.4
Lysis buffer	50 mM PIPES, 50 mM NaCl, 5 mM $MgCl_2$, 5 mM EGTA, 0.1% v/v NP40, 0.1% v/v Triton X-100, 0.1% v/v Tween 20, Protease Inhibitor Cocktail, pH 7.4
Fixation buffer	3.7% Formaldehyde in PBS
Blocking buffer	10 mM Tris, 150 mM NaCl, 0.05% v/v Tween-20, pH 7.5 (supplemented with blocking substances)
Blocking substances	1-5% w/v Dry milk powder or BSA in TBS-T
Coomassie destaining solution	30% v/v MeOH, 10% v/v acetic acid
Coomassie staining solution	0.25% w/v Coomassie brilliant blue G-250, 45% v/v MeOH, 10% v/v acetic acid
Laemmli buffer (2x)	20% v/v Glycerol, 120 mM Tris (pH 6.8), 4% w/v SDS
SDS loading buffer (5x)	50% v/v Glycerol, 250 mM Tris (pH 6.8), 10% w/v SDS, 500 mM DTE, 360 μM bromophenol blue
SDS sample buffer	10% v/v Glycerol, 50 mM Tris (pH 6.8), 2% w/v SDS, 500 mM DTE, 360 μM bromophenol blue
SDS running buffer (10x)	2.5 M Glycine, 250 mM Tris, 35 mM SDS
SDS gels	According to Harlow and Lane, 1988[162]
Transfer buffer	14.41 g/L glycine, 3.03 g/L Tris, 20% v/v MeOH
Coupling buffer	0.15 M triethanolamine, 0.5 M NaCl, pH 7.0
Block A solution	0.5 M ethanolamine, 0.5 M NaCl, pH 8.3
Block B solution	0.1 M sodium acetate, 0.5 M NaCl, pH 4.0
Reducing/denaturing buffer	8 M urea in 50 mM Tris, pH 7.9
OBD alkylation buffer	50 mM chloroacetamide in reducing/denaturing buffer
Lys-C digestion solution	0.25 μg/μL Lys-C in H_2O

Trypsin digestion solution	0.01 µg/mL trypsin (proteomic grade) in 25 mM NH_4HCO_3
STAGE elution buffer	0.1% v/v formic acid, 80% v/v acetonitrile in H_2O
STAGE equilibration buffer	0.1% v/v formic acid in H_2O
IGD washing solution 1	25 mM NH_4HCO_3/acetonitrile (3:1)
IGD washing solution 2	25 mM NH_4HCO_3/acetonitrile (1:1)
IGD reducing solution	50 mM DTT in 25 mM NH_4HCO_3
IGD alkylation solution	55 mM iodoacetamide in 25 mM NH_4HCO_3
CETSA reducing buffer	200 mM TCEP, 0.2 mM triethylammonium bicarbonate (TEAB)
CETSA alkylation solution	375 mM iodoacetamide in CETSA reducing buffer
CETSA digestion solution	0.4 µg/mL trypsin in 10 mM HCl

6.1.2. Antibodies for Western blotting

Target	Host	Cat#	Manufacturer	Dilution	Incubation Conditions
Anti-rabbit-HRP	goat	31460	Pierce	1:10,000	5% w/v milk in TBS-T
β-actin	rabbit	ab8227	Abcam	1:1,000	5% w/v milk in TBS-T
CAPN2 (M-type)	rabbit	2539	Cell Signaling	1:1,000	2% w/v milk in TBS-T
Glud1 (GDH)	rabbit	ABN443	Merck Millipore	1:1,000	5% w/v milk in TBS-T
LAMTOR5	rabbit	14633	Cell Signaling	1:1,000	5% w/v BSA in TBS-T
LC3-B	rabbit	2775	Cell Signaling	1:1,000	5% w/v milk in TBS-T
P2X4	rabbit	APR-002	Alomone Labs	1:1,000	5% w/v milk in TBS-T

6.1.3. Software

- EnsoChemLab Version 5.0.8 Enso Software GmbH, Erbach, Germany
- Image Studio™ Version 5.2 LI-COR Biosciences GmbH, Bad Homburg vor der Höhe, Germany
- IncuCyte® ZOOM Version 2016A, Essen BioScience, Ann Arbor, USA
- Maestro Version 10.5, Schrödinger LLC, New York, USA
- MaxQuant Version 1.4.1.2 MaxQuant; Cox & Mann, 2008[163]

- MestReNova Version 6.0.3-5604, Mestrelab Research, Santiago de Compostela, Spain
- MetaMorph Offline Version 7.7.0.0 Molecular Devices, Biberach, Germany
- MetaXpress Version 5.0.0.26 Molecular Devices, Biberach, Germany
- Tecan i-control Version 3.4.2.0 Tecan AG, Männedorf, CH

6.1.4. Laboratory Equipment

- AxioVert 200M fluorescence microscope, Carl Zeiss Microscopy GmbH, Oberkochen, Germany
- Centrifuge 5415R, Eppendorf, Hamburg, Germany
- Centrifuge, Minispin, Eppendorf, Hamburg, Germany
- CFX96 Touch™ Real-Time PCR Detection System, BioRad, Munich, Germany
- Concentrator Plus SpeedVac, Eppendorf, Hamburg, Germany
- ImageXpress Micro XLS Widefield High Content, Molecular Devices, California, USA
- Incubator Nuaire DHD Autoflow NU 5510 E, IBS Tecnomara, Fernwald, Germany
- IncuCyte® S3, Essen BioScience, Ann Arbor, USA
- Infinite M200 Plate Reader, Tecan, Männedorf, CH
- Invitrogen™ Countess™ II Automated Cell Counter, Life Technologies™, Darmstadt, Germany
- MagRack 6, GE Healtcare Life Sciences, Chicago, USA
- Mastercycler ep gradient S, Eppendorf, Hamburg, Germany
- Mini-PROTEAN® Tetracell Electrophoresis System, Bio-Rad, Munich, Germany
- NanoDrop 2000c UV-Vis Spectrophotometer, Thermo Fisher Scientific, Waltham, USA
- Odyssey® Fc imaging System, LI-COR Biosciences, Bad Homburg, Germany
- pH-Meter, Mettler Toledo, Giessen, Germany
- Q Exactive™ Plus Hybrid Quadrupole-Orbitrap Mass Spectrometer, Thermo Fisher Scientific, Waltham, USA
- Sterile Bench Microflow, NuncNalge, Rochester, USA
- Sterile Bench Nuaire, IBS tecnomara, Fernwald, Germany
- UltiMateTM 3000 RSLCnano system, Thermo Fisher Scientific, Waltham, USA
- Ultracentrifuge Optima™ MAX-XP, Beckman Coulter, Brea, USA
- Vortex Genie 2, Roth, Karlsruhe, Germany
- Waterbath (Memmert), Hettich AG, Bäch, Germany

6.2. Methods used for Biological Experiments

6.2.1. Methods in Mammalian Cell Culture

a) General Methods in Mammalian Cell Culture

All the work involving living mammalian cells was performed with sterile equipment, media, and solutions in cell culture-approved benches. The generated waste was collected and sterilized by autoclaving at 134 °C for 15 min.

Human breast cancer MCF7 cells (Sigma-Aldrich, cat# 800021) stably transfected with eGFP-LC3 (MCF7-eGFP-LC3) were cultured at 37 °C with 5% CO_2 using Eagle's DMEM (PAN Biotech, cat# P04-03550) or MEM (PAN Biotech, cat# P04-08500) containing 10% FBS (Invitrogen, cat# 10500-084), 1% sodium pyruvate (PAN Biotech, cat# P04-43100), 1% non-essential amino acids (PAN Biotech, cat# P08-32100), 0.01 mg/mL bovine insulin (Sigma Aldrich, cat# I9278), and 200 µg/mL G418 as the medium. Untransfected MCF7 cells were incubated in Eagle's MEM with the same additives as used for transfected cells but without G418.

i. Thawing and Freezing of Cryo-Conserved Cells

Aliquots of mammalian cells stored in liquid nitrogen were thawed by transferring the vial containing the cells into a 37 °C water bath. The cell suspension was diluted in 10 mL of the respective medium and the resulting suspension transferred into a 75 cm^2 tissue culture flask. The cells were incubated overnight. The DMSO-containing medium was replaced by fresh DMSO-free medium.

For cryo-conservation, mammalian cells were grown until reaching 80–95% confluence and then detached by trypsinization. The detached cells were suspended in the corresponding cell medium to inactivate the trypsin, and the cell number was determined. The suspension was centrifuged (rt, 150 *x g*, 5 min) and the medium replaced by an appropriate volume of DMSO-containing medium (5% v/v) to reach a final concentration of ca. 1×10^6 per cryo-vial. The vials were frozen in a cell freezing container (CoolCell® LX) at -80 °C overnight, to ensure a temperature decrease of 1 °C/min, and then stored in liquid nitrogen for long-term storage.

ii. Passaging Mammalian Cells

MCF7 cells were grown until reaching a confluence of 80–90%. The medium was removed, the cells were washed with PBS (5 mL for 75 cm^2, 10 mL for 175 cm^2 tissue culture flasks) and then detached from the flasks by trypsinization (Trypsin/EDTA, 1 mL for 75 cm^2, 3 mL for 175 cm^2 tissue culture flasks, 1–5 min incubation at 37 °C and 5% CO_2). After full detachment, fresh medium was added to inactivate trypsin. 1/6 of the cell suspension was transferred into a new flask, containing 10 mL of pre-warmed (37 °C) fresh medium.

iii. Determination of Cell Number

The cell number was determined using a Neubauer Counting Slide. The cell suspension was diluted with Trypan blue in a 1:1 ratio to distinguish between living and dead cells. The glass cover was moistened and placed on the Neubauer chamber's central area and 10 µL of the cell suspension prepared as described above were inserted into the chamber carefully. Cells in 4–5 quadrants were counted using a microscope, averaged and multiplied with the respective chamber factor (here 1×10^4) and dilution factor (here 2).

Alternatively, the Invitrogen™ Countess™ II Automated Cell Counter (Thermo Fisher Scientific, cat# AMQAX1000) together with Countess® Cell Counting Chamber Slides (Thermo Fisher Scientific, cat# C10228) was used according to the manufacturer's instructions. The sample was prepared as for the Neubauer chamber.

iv. Routine Check for Mycoplasma Contaminations in Cell Culture

Cultured cells were routinely checked for mycoplasma contamination using the MycoAlert™ Mycoplasma Detection Kit (Lonza) according to manufacturer's instructions.

v. Cell Treatment with Compounds

Compounds were dissolved in DMSO (Bioreagent, Sigma Aldrich, cat# D8418). Cells were plated into vessels in a cell number that allows 75–90% confluence at the end of the experiment. After 14–

24 h incubation, the cells were treated with compounds pre-diluted in the given medium. The final DMSO concentration did not exceed 0.5% v/v.

6.2.2. Autophagy-Related Assays

a) High-Content Screening for Autophagy Inhibitors

The phenotypic autophagy screen utilizes MCF7-eGFP-LC3 cells. A total of 10,000 cells per well were seeded in 100 µL medium in 96-well Corning® CellBIND® plates (cat# 3340) and incubated overnight. Additional preincubation of cells (optional) was carried out by adding 20 µL of compound solution in MEM at multiple concentrations (10 µM to 4.6 nM in 1:3 steps) to cells followed by incubation for one hour. Cells were washed with 50 µL PBS followed by a final aspiration of the washing buffer. Autophagy was induced by addition of 100 µL compound solution at multiple concentrations (10 µM to 4.6 nM in 1:3 dilution steps) in chloroquine-containing EBSS medium (50 µM). Alternatively, EBSS (100 µL) was added to the cells prior to compound addition (20 µL, diluted in EBSS). After incubation for 3 h cells were fixed by addition of 25 µL 4% formaldehyde in PBS + 1:500 Hoechst (stock: 1 mg/mL, Sigma Aldrich, cat# B2261-25mg) and incubation for 20 min at room temperature. Cells were then washed twice with and stored in 100 µL PBS. Four images per well were taken with an automated AxioVert 200M fluorescence microscope (Zeiss) at 20x. Automated image analysis was performed using a modified configuration of the granularity assay (approx. granule min. and max. width: 0.4 and 5 µm resp.; approx. nuclei min. and max. width: 6 and 20 µm resp.; intensity of granules and nuclei above background: 300 and 40 gray levels resp.) of MetaXpress Cell Analysis Software (Molecular Devices). Inhibition of autophagy was quantified by calculating the number of granules per nucleus and normalized to the compound-free controls.

b) Medium-Throughput High-Content Screening for Autophagy Inhibitors

This screening was performed by the Compound Management and Screening Center (COMAS).

The phenotypic autophagy screen utilizes MCF7-eGFP-LC3 cells. 4,000 cells per well were seeded in 25 µL medium in a 384-well Greiner µclear plate (cat# 781080, lid cat# 656191) and incubated overnight. Cells were then washed using a plate washer (Biotek, ELx405) three times with PBS followed by a final aspiration of the washing buffer. The addition of 25 nL of compound solution (10 mM stock solution in DMSO) was then carried out with an echo dispenser (Labcyte, Echo 520 dispenser). Addition of medium to induce autophagy was carried out with a Multidrop Combi (Thermo Scientific). 25 µL EBSS (Sigma Aldrich, cat# E3024-500mL) containing 50 µM chloroquine (Sigma Aldrich, cat# C6628-25g) was used for starvation-induced autophagy and 25 µL MEM containing 50 µL chloroquine and 100 nM rapamycin (Biomol, cat# Cay13346-1) was used for rapamycin-induced autophagy screening. After incubation for 3 h, cells were fixed by addition of 25 µL 1:4 formaldehyde in PBS + 1:500 Hoechst (stock: 1 mg/mL, Sigma Aldrich cat# B2261) and incubation for 20 min at room temperature. Cells were then washed three times with PBS. Four images per well were taken with ImageXpress Micro XL (Molecular Devices) at 20x. Automated image analysis was performed using the granularity setting of MetaXpress Software (Molecular Devices). The most significant analysis parameter was granule area, with resulting signal-to-background ratios around 40 and Z' values around 0.7.

c) Confocal Live-Cell Imaging of MCF7-mCherry-eGFP-LC3 Cells

This experiment was performed by Dr. Georgios Konstantinidis

After seeding of 400,000 MCF7-mCherry-eGFP-LC3 (kind gift of Sharon Tooze) cells in glass bottom dishes (MatTek, Ashland) and overnight incubation, media was removed and replaced with 2 mL of the indicated treatment media containing appropriate compounds. After incubation for 3 h, live cell imaging was performed in MEM without phenol red (Invitrogen) or EBSS (Sigma) by using an inverted confocal microscope Leica SP5 AOBS equipped with a 63x/1.4 HCX Plan Apo oil immersion lens and a temperature-controlled hood at 37 °C and 5% CO_2. Green and Red Puncta Colocalization macro was used to analyze mCherry-eGFP-LC3 puncta (Ruben K. Dagda, University of Nevada School of Medicine, Pharmacology Department; Daniel Shiwarski, Carneggie Mellon University; Charleen T Chu, University of Pittsburgh).

d) Immunoblotting for Autophagy Inhibition

MCF7-eGFP-LC3 cells (2 mL for 6-well, 1 mL for 12-well plates; 100,000 cells/mL) were seeded in 6- or 12-well plates and incubated overnight. The medium was replaced by fresh MEM, EBSS, or the respective compounds MEM or EBSS. The cells were then incubated for 3 h, the medium was removed, and the cells washed with PBS (1 mL for 6-well plates, 0.5 mL for 12-well plates). Cell lysis was performed by adding Laemmli buffer (1X), followed by stringent scraping with Cell Scrapers. The mixture was collected and homogenized by sonification. The protein concentration was determined using the DC assay (Chapter 6.2.5), and all samples were diluted to the same concentration. SDS sample buffer was added (20% v/v), and the proteins were denatured by heating at 95 °C for 5 min. The samples were snap-frozen and stored at -80 °C until further use. The proteins were then separated by SDS-PAGE and the LC3-B and p62 levels analyzed by western blot using β-actin as a loading control.

e) Selective Viability Assay

This experiment was performed by Dr. Luca Laraia

For fed conditions, 4,000 MCF7-eGFP-LC3 cells in 100 µL medium were seeded in a clear flat-bottom 96-well plate and incubated overnight. For starved conditions, 7,000 cells in 100 µL medium were used. The media was removed gently, and cells were washed with PBS (100 µL). The PBS was replaced with 100 µL of normal media (fed conditions) or EBSS (starved). Test compounds at a concentration of 6x the desired final concentration in 20 µL of the appropriate medium were added. Cells were incubated for 48 h. At this point 10 µL of WST-1 reagent (Roche) was added to each well. The absorbance was measured with a Beckman DTX-880 (Beckman Coulter, Germany) plate reader at 450/690 nm. Absorbance measurements were performed after 20, 30, 40, 50, 60 min of addition of **1a**. Good measurements are considered when absorbance of the DMSO control is around 1.00. IC_{50} values were calculated using GraphPad Prism using DMSO (negative) and nocodazole (10 µM, positive) as controls.

f) Induction of Apoptosis

MCF7 cells in 100 µL medium (3,000 for fed conditions or 10,000 for starved conditions) were seeded in a clear flat-bottom 96-well plate and incubated overnight. The media was removed carefully, and cells were washed with PBS (50 µL), and 100 µL of medium (DMEM for fed, EBSS for starved conditions) containing 1.2 v/v% IncuCyte® Kinetic Caspase-3/7 Apoptosis Assay Reagent. Test compounds in a DMSO stock solution were prediluted in the appropriate medium (MEM or EBSS) at a concentration of 6x the desired final concentration, while keeping the DMSO content constant. Of this solution, 20 µL were added to the cells, and the cells were incubated for 72 h in the IncuCyte® ZOOM. Images were acquired at 10X magnification in both the phase and green channel every hour. Images were analyzed using automated image analysis with the

IncuCyte® ZOOM Control Software. The key parameter was green fluorescence confluence as a percentage of phase contrast confluence (%). Data was normalized to the DMSO control.

6.2.3. Affinity-Based Proteomics

i. Cell Lysate Preparation

MCF7-eGFP-LC3 cells were grown until reaching ca. 90% confluence in growing medium (Eagle's MEM). After washing with PBS and trypsinization for 5 min at 37 °C, they were resuspended in PBS. The cell suspension was centrifuged (150 *x g*, 5 min, 4 °C) and the supernatant discarded. The cell pellet was washed twice by resuspension into PBS, followed by centrifugation (150 g, 5 min, 4 °C) and resuspension in lysis buffer (prepared according to a standard procedure[164]). The suspension was incubated for 30 min at 4 °C, with gentle vortexing every 10 min. The lysate was homogenized by passing it 10 times through a 20 G needle and centrifuged for 20 °C at 18,500 *x g* and 4 °C. The supernatant was collected, the protein concentration determined, and the lysate stored at -80 °C.

ii. Generation of MCF7-eGFP-LC3-SILAC Cell Line

In order to label MCF7-eGFP-LC3 cells with heavy amino acids for SILAC, the cells were grown in two different MEM SILAC media. Each medium was supplied with amino acids consisting of either light ($^{12}C_6$-L-lysine and $^{12}C_6{}^{14}N_4$-L-arginine) or heavy isotopes ($^{13}C_6$-L-lysine and $^{13}C_6{}^{15}N_4$-L-arginine). Both media contained dialyzed FBS, and were else prepared as normal MEM medium (Chapter 6.2.1). To verify the incorporation efficiency, samples of light, heavy, and a 1:1 (protein ratio) mixture of light and heavy lysates, together with a BSA control (5 pmol) were subjected to in-gel digest and subsequently analyzed by MS/MS.

iii. Pull-Down

NHS Mag Sepharose beads (GE Healthcare®, cat# 28951380, 25 µL) were equilibrated with ice-cold aq. HCl solution (1 mM) and incubated with the amines **93** or **94** in coupling buffer (0.15 M triethanolamine, 0.5 M NaCl, pH 7.4, 500 µL; compound concentration: 10 µM) overnight at 4 °C in a rotation wheel. Residual active groups were quenched in an alternating blocking and alkylation sequence with block A (0.5 M ethanolamine, 0.5 M NaCl, pH 7.4) and B solutions (0.5 M NaOAc, 0.5 M NaCl, pH 4) three times respectively (500 µL, rt, 15 min the second time with A, else 2 min, in a rotation wheel). The beads were equilibrated with lysis buffer (500 µL, 2 min), and bulk protein lysate was added (500 µL, protein concentration = 6 mg/mL, for competitive pull-down, the lysate was pre-treated with 10 µM compound), and the suspension incubated at 4 °C for 2 h in a rotation wheel. The supernatant was removed and the beads washed with lysis buffer with increasing $MgCl_2$ concentrations in order to remove unspecific binding (5 min, 4 °C). The beads were washed with PBS (3 x 500 µL, 5 min, 4 °C). For SILAC-based pull-down, the beads were combined as follows: heavy/active with light/control and heavy/control with light/active. The samples were further processed by for on-bead digest or SDS-PAGE.

iv. SILAC Incorporation Test: In-Gel Digest

SDS loading buffer (5 µL, 5X) was added to each SILAC-lysate (20 µL) and the BSA control (20 µL, 5 pmol). Denaturation of the proteins was achieved by heating the samples at 95 °C for 5 min. The samples were loaded onto a 4–20% mini-PROTEAN® TGX precast protein gel and the proteins allowed to come into the gel by applying 120 V for 10 min.

The protein gel bands were cut out and cut into 1–2 mm squares. The gel slices were incubated with fixation solution (H_2O/EtOH/AcOH = 5:4:1, 500 µL, 350 rpm, rt) for 5 min, and the solution replaced by fresh fixation solution. The samples were incubated overnight at 25 °C and 350 rpm. The fixation solution was replaced by washing solution 1 (200 µL, 25 mM NH_4HCO_3/acetonitrile [3:1] at 37 °C and 600 rpm for 30 min), then washing solution 2 (200 µL, 25 mM NH_4HCO_3/ACN [1:1] at 37 °C and 600 rpm for 15 min), then reducing solution (200 µL, 50 mM DTT in 25 mM NH_4HCO_3 at 37 °C and 600 rpm for 45 min), and finally alkylation solution (200 µL, 55 mM iodoacetamide in 25 mM NH_4HCO_3 at 25 °C and 600 for 1 h in the dark). The gels were washed with washing solution 2 (200 µL, 25 °C and at 600 rpm for 15 min). The supernatant was removed and the gel dehydrated by washing with acetonitrile (100 µL). The gels were left to air-dry for 30 min at room temperature, and incubated with digest solution (75 µL, 10 µg/mL trypsin in 25 mM NH_4HCO_3 at 25 °C and 600 rpm for 15 min). A NH_4HCO_3 solution (25 mM, 75 µL) was added and the mixture incubated overnight for the digestion reaction to take place (30 °C, 350 rpm).

TFA (10%, 10 µL) was added to stop the digestion, the mixture was centrifuged shortly and the tryptic peptides mobilized by sonification (30 min, 0 °C, max. amplitude). The supernatant was collected, and the gels were incubated with ACN (75 µL, 15 min, 25 °C, 350 rpm). The supernatants were combined and this step was repeated once more. The samples were concentrated by vacuum centrifugation (30 °C, 3 h, max. speed) and analyzed by MS/MS.

v. On-Bead Digest

Proteins immobilized to the beads through affinity purification were denatured and reduced by incubation in reducing/denaturing buffer (8 M urea, 1 mM DTT in 50 mM Tris, pH 7.9, rt, 350 rpm, 30 min). Cysteine side chains were alkylated by incubation in alkylation solution (5 µL, 50 mM chloroacetamide in reducing/denaturing buffer, rt, 350 rpm, 30 min). The proteins were digested using Lys-C (4 µL, 0.25 µg/µL in H_2O, 37 °C, 350 rpm, 1 h) and the supernatant transferred into a new vessel. Additional tryptic digest was accomplished by incubation with trypsin (1 µg in 150 µL Tris [50 mM, pH 7.5] at 37 °C and 350 rpm for 1 h). The supernatants from both digestion steps were combined, trypsin was added (2 µg in 5 µL H_2O), and the samples were incubated overnight (37 °C, 350 rpm). The digest was stopped by addition of TFA (2 µL, conc.).

vi. Stop and Go Extraction Tip (STAGE)-Based Peptide Purification

To purify the soluble on-bead-digested peptides, self-packed micro-columns in pipet tips with 3M Empore™ SPE Extraction Disks (2215-C18) were used according to a known procedure.[165] The C18 material was activated by washing with MeOH (100 µL) and equilibrated with elution buffer (100 µL, H_2O/acetonitrile (1:4) + 0.1% v/v HCOOH) and equilibration buffer (2 x 100 µL, H_2O + 0.1% v/v HCOOH). The samples were loaded onto the tips and after 1 min filtered through the C18 material by centrifugation (rt, 2500 rpm, 3 min). Salts and detergents were washed off using equilibration buffer (100 µL), and the peptides were eluted with elution buffer (2 x 20 µL, 1 min incubation) by centrifugation (rt, 2500 rpm, 30 s) into a new reaction vessel. The samples were concentrated by vacuum centrifugation (30 °C, 1.5 h) and submitted to nano-LC-MS/MS analysis.

vii. Peptide Identification by Nano-LC-MS/MS

This part of the experiment was performed by the mass spectrometry group.

The resulting peptides from the tryptic digest were separated by nano-HPLC and subsequently identified by MS and MS/MS.

The dried peptides were re-suspended in 20 µL TFA and dissolved by sonication (15 min, max. amplitude). Insoluble particles were separated by centrifugation (15000x g, 1min). A fraction (10 µL) was desalted and concentrated in a nano-(U)HPLC system suitable for flow-rates of 300 nL/min using the UltiMate^{TM} 3000 RSLCnano system (Dionex) equipped with a nano-HPLC Acclaim PepMap RSLC C18 (2 µm, 100 Å, 75 µm ID × 25 cm, nanoViper, Dionex), a pre-column cartridges (Acclaim PepMap100 C18, 5 µm, 100 Å, 300 µm ID × 5 mm, Dionex), and a nano-spray emitter (Standard Coated SilicaTip^{TM} Emitter, 360 µm OD, 20 µm ID, 10 µm Tip ID, 10.5 cm, New Objective, USA) in a linear gradient (start: 96.8% formic acid (0.1%), 3.2% formic acid (0.1%) in acetonitrile, end: 62% formic acid (0.1%), 38% formic acid (0.1%) in acetonitrile) at a constant flow rate of 300 nL/ min at a column temperature of 40°C.

The MS and MS/MS experiments were carried out on a Q Exactive™ Plus Hybrid Quadrupole-Orbitrap Mass Spectrometer equipped with a nanospray source (Nanospray Flex Ion Source, Thermo Scientific). All solvents were LC-MS grade. The lyophilized tryptic peptides were dissolved in 20 mL 0.1% v/v TFA in water. 3 mL of sample were injected onto a pre-column cartridge (5 mm, 100 Å, 300 mm ID * 5 mm, Dionex, Germany) using 0.1% v/v TFA in water as eluent at a flow rate of 30 mL/min. Desalting was performed for 5 min with eluent flow to waste followed by back-flushing of the sample during the whole analysis from the pre-column to the PepMap100 RSLC C18 nano-HPLC column (2 mm, 100 Å, 75 mm ID × 50 cm, nanoViper, Dionex, Germany) using a linear gradient of water/ACN (containing 0.1% v/v HCOOH) 95:5 → 70:30 during 95 min using a flow rate of 300 nL/min.

The nano-HPLC was coupled online to the Quadrupole-Orbitrap Mass Spectrometer using a standard coated SilicaTip (ID 20 µm, Tip-ID 10 µM, New Objective, Woburn, MA, USA). Mass range of m/z = 300–1650 was acquired with a resolution of 70,000 for full scan, followed by up to ten high energy collision dissociation (HCD) MS/MS scans of the most intense at least doubly charged ion peaks.

viii. MS-Data Evaluation

This part of the experiment was performed by the mass spectrometry group.

Data evaluation was performed using MaxQuant software[42] (v.1.5.3.30) including the Andromeda search algorithm and searching the human reference proteome of the Uniprot database. The search was performed for full enzymatic trypsin cleavages allowing two miscleavages. For protein modifications, carbamidomethylation was chosen as fixed and oxidation of methionine and acetylation of the N-terminus as variable modifications. The mass accuracy for full mass spectra was set to 4.5 ppm and for MS/MS spectra 20 ppm. The false discovery rates for peptide and protein identification were set to 1%. Only proteins for which at least two peptides were quantified were chosen for further validation. Relative quantification of proteins was carried out using the label-free quantification algorithm implemented in MaxQuant. All experiments were performed in technical triplicates. Label-free quantification (LFQ) intensities were logarithmized (log2) and proteins which were not three times quantified in at least one of the groups were filtered off. Missing values were imputed using small normal distributed values and a t-test was performed. Proteins which were statistically significant outliers in at least one of the three experiments were considered as hits.

6.2.4. Cellular Thermal Shift and Thermal Proteome Profiling

i. Lysate Preparation

For CETSA and TPP experiments, MCF7-eGFP-LC3 cells were cultured according to the procedures described in Chapter 6.2.1. For one T175 flask, the cells were tripsinized with 3 mL trypsin/EDTA, resuspended in MEM medium (10 mL), and centrifuged at 150 *x g* and 4 °C for 5 min. The medium was removed and the cell pellet washed with ice-cold PBS (2 x 25 mL and 1 x 10 mL, centrifugation at 150 *x g* and 4 °C for 5 min each time). The pellet was resuspended in PBS containing the nonylphenyl polyethylene glycol (NP-40 alternative, 1.5 mL, 0.4% v/v), used to enhance membrane protein solubilization. The cells were lysed via a freeze-thaw cycle (4 x). The insoluble components were separated by centrifugation for 20 min 4 °C and 100,000 *x g* using polycarbonate tubes in an ultra-centrifuge. Protein concentration was determined using the Bradford method[166] with the Bradford reagent (Bio-Rad laboratories). After dilution to 2 mg/mL, the lysate was snap-frozen and stored at -80 °C until further use.

ii. Thermal Shift Assay

The cell lysate was thawed and split into two vials (1.4 mL each). One sample was treated with **1a** in DMSO and the other only with DMSO, resulting in a final concentration of 2.5 µM and 1% v/v DMSO. The samples were incubated at rt for 30 min, each split into 10 aliquots of 120 µL and subjected to heating at different temperatures in a gradient PCR cycler (Eppendorf Mastercycler ep gradient S) for 3 min. The temperature gradient ranged from 37–67 °C, while one vehicle sample was always heated in parallel with one compound sample. The samples were then cooled to 4 °C, centrifuged for 20 min at 4 °C and 100,000 *x g*. The supernatant (100 µL) was transferred into low-binding Eppendorf tubes.

iii. Trypsin Digest

After the thermal shift assay, 75 µL of each aliquot were treated with freshly prepared TEAB buffer (75 µL, 100 mM) and reducing buffer (200 mM TCEP, 0.2 mM TEAB, 7.5 µL) and incubated for 1 h at 55 °C and 350 rpm. The remaining 25 µL were snap-frozen, stored at -80 °C for immunoblotting. A freshly prepared alkylation solution (iodoacetamide in reducing buffer, 375 mM, 7.5 µL) was added to each sample, and incubation was continued for 30 min in darkness. Afterwards, pre-chilled acetone (ca. 900 µL) was added, and the proteins were allowed to precipitate overnight at -20 °C. The samples were centrifuged for 10 min at 4 °C and 8,000 *x g*, and the supernatant was removed carefully. The pellets were air-dried for 45 min and resuspended in TEAB buffer (100 µL, 100 mM) and digestion solution (0.4 µg/mL trypsin in 10 mM HCl, 7.5 µL). The digestion was performed at 37 °C overnight.

iv. TMT-labeling

This part of the experiment was performed by the mass spectrometry group.

The tryptic peptide solution was centrifuged and labeled with TMT according to the manufacturer's description, but using half the amount of labeling reagent. Briefly, 82 µL of anhydrous acetonitrile were added to each 0.8 mg of TMT label reagent aliquot (TMT10plex, Thermo Fisher Scientific, cat# 90110). Of the respective TMT reagent solution, 41 µL were transferred to the peptide sample of the respective DMSO control (V1-10). Directly after addition, samples were briefly vortexed. For the compound-treated samples, 100 µL were transferred to the respective remaining TMT reagent. Directly after addition, samples are briefly vortexed. Samples were incubated for 2 h at rt Afterwards, 8 µL of 5% hydroxylamine were added to the samples, and the reaction was quenched by incubating the samples for 15 min. Of each compound-treated, labeled sample, 120 µL were combined into one sample, and 120 µL of each DMSO-treated, labeled sample were combined to a second one. Both samples were concentrated by vacuum centrifugation (30 °C, max. speed) until a dry white pellet was visible.

v. Peptide Identification by Nano-LC-MS/MS

This part of the experiment was performed by the mass spectrometry group.

Prior to nanoHPLC-MS/MS analysis, samples were divided into 10 fractions on a C18 column using high pH conditions to reduce the complexity of the samples and thereby increase the number of quantified proteins. For this purpose, both samples were dissolved in 120 µL 20 mM NH_4HCO_2 solution at pH 11, followed by incubation in an ultra-sonicator for ca. 2 min, vortexing for 1 min, and centrifugation at 13,000 rpm and rt for 3 min. Subsequently, 50 µL of supernatant were injected onto an XBridge C18 column (130 Å, 3.5 µm, 1 mm x 150 mm) using a U3000 capHPLC- System (Thermo Fisher Scientific, Germany). Separation was performed at a flow rate of 50 µL/min using 20 mM aq. NH_4HCO_2 solution (pH 11) as solvent A and a mixture of aq. 20 mM NH_4HCO_2 solution (pH 11) with acetonitrile (2:3) as solvent B. Separation conditions were 95% solvent A / 5% solvent B for 15 min, to desalt the samples, followed by a linear gradient up to 25% for 5 min and a second linear gradient up to 100% solvent B for 60 min. Afterwards, the column was washed with 100% solvent B for 20 min and re-equilibrated to the starting conditions. Detection was carried out at a valve length of 214 nm. The eluate between 10 and 80 min was fractionated into 10 (1st fraction 20 min, 2nd fraction 10 min, 3rd–8th fraction 5 min each, 9th fraction 10 min, 10th fraction 25 min). Each fraction was concentrated by vacuum centrifugation (30 °C, max. speed) until complete dryness and subsequently subjected to nanoHPLC-MS/MS analysis.

For nanoHPLC-MS/MS analysis, samples were dissolved in 10 µL of 0.1% aq. TFA. Of this solution, 4 µL were injected into a UltiMate™ 3000 RSLCnano system (Thermo Fisher Scientific, Germany) online-coupled to a Q Exactive™ Plus Hybrid Quadrupole-Orbitrap Mass Spectrometer, which was equipped with a nanospray source (Nanospray Flex Ion Source, Thermo Fisher Scientific), using a standard coated SilicaTip (ID 20 µm, Tip-ID 10 µM, New Objective, Woburn, MA, USA). All solvents were LC-MS grade. For desalting, samples were injected into a pre-column cartridge (5 µm, 100 Å, 300 µm ID * 5 mm, Dionex, Germany) using 0.1% TFA in water as eluent at a flow rate of 30 µL/min. Desalting was performed for 5 min with eluent flow to waste followed by back-flushing of the sample during the whole analysis from the pre-column to the PepMap100 RSLC C18 nano-HPLC column (2 mm, 100 Å, 75 mm ID × 50 cm, nanoViper, Dionex, Germany) using a linear gradient of water/ACN (containing 0.1% v/v HCOOH) 95:5 → 60:40 during 125 min using a flow rate of 300 nL/min. Afterwards, the column was washed (95% solvent B) and re-equilibrated to starting conditions.

Mass range of m/z = 300–1650 was acquired with a resolution of 70,000 for full scan, followed by up to ten high energy collision dissociation (HCD) MS/MS scans of the most intense at least doubly charged ion peaks using a resolution of 35,000 and a NCE energy of 35%.

vi. MS-Data Evaluation

This part of the experiment was performed by the mass spectrometry group.

Data evaluation was performed using MaxQuant software[163] (v.1.5.3.30) including the Andromeda search algorithm and searching the human reference proteome of the Uniprot database. The search was performed for full enzymatic trypsin cleavages allowing two miscleavages. For protein modifications carbamidomethylation was chosen as fixed and oxidation of methionine and acetylation of the N-terminus as variable modifications. For relative quantification, the type "reporter ion MS2" was chosen and for all lysines and peptide N-termini 10plex TMT labels were defined. The mass accuracy for first and second search of full mass spectra was set to 20 ppm and 4.5 ppm, respectively and to 20 ppm for MS/MS spectra. The false discovery rates for peptide and protein identification were set to 1%. Only proteins for which at least two peptides were quantified were chosen for further validation. Relative quantification of proteins was carried out using the reporter ion MS2 algorithm implemented in MaxQuant. All experiments were performed in biological triplicates.

vii. Melting Curve Calculation

This part of the experiment was performed by the mass spectrometry group.

To determine the melting point shifts between compound- and DMSO-treated samples of each protein, an in-house developed Excel-Macro was used. Briefly, denaturation changes at different temperatures were tracked using the reporter ion intensity and observed in relation to the lowest temperature; the reporter ion intensity for lowest temperature was normalized to 1.

The relative fold changes of melting temperatures were calculated as a function of temperature using the Boltzmann equation:

$$y = \text{bottom plateau} + \frac{\text{top plateau} - \text{bottom plateau}}{1 + e^{-\left(\frac{a}{T}\right) - b}}$$

Equation 1. The sigmoidal trend of the measured intensities was fitted with the following equation using an iterative working macro in Microsoft Excel. Top plateau is fixed to one; bottom plateau is a protein specific constant that defines the maximal denaturation; a and b are constants which describe the curve progression.

The melting point of a protein is defined as the temperature at which half of the protein has been denatured. This point corresponds to the inflection point of the curve, the highest slope of the curve which is defined as the value of the first derivative.

For hit identification, following requirements were defined and had to be fulfilled for all replicates: (1) the protein is identified with at least two unique peptides, (2) the average shift of the melting point is at least 2 °C, while displaying either a stabilization of destabilization for all replicates, and/or (3) the relative difference in the peak intensities of the two highest temperatures between the DMSO control and the compound-treated sample is at least 10% of the maximum intensity.

6.2.5. Methods in Protein Biochemistry

a) Protein Concentration Determination

Routine determination of protein concentration was performed using the Bradford method[166] with the Bradford reagent (Bio-Rad laboratories) in the linear range of a BSA control (0.3–10 mg/mL). The absorbance was measured at 595 nm using a BioPhotometer (Eppendorf).

For a large number of samples or low protein concentrations, a DC protein assay (Bio-Rad laboratories) was performed in 96-well plates according to the manufacturer's instructions. The absorbance was measured at 650–750 nm using a Tecan microplate reader and the concentration calculated using a BSA standard curve.

b) SDS-Polyacrylamide Gel Electrophoresis (SDS-PAGE)

Protein separation was performed by SDS-PAGE according to a standard procedure[167] using the Mini-PROTEAN® Tetracell Electrophoresis System (Bio-Rad). SDS loading buffer was added to the protein mixtures, reaching a final DTT concentration of 100 mM in each sample. The proteins were denatured by heating the samples at 95 °C for 5 min prior to loading. Separation was performed in running buffer at 80 V for 15 min, then 120 V at rt and stopped when the desired separation was observed in the protein marker. Protein size was estimated by comparison to the marker PageRuler™ Plus Prestained Protein Ladder (Thermo Fisher Scientific, cat# 26619). For in-gel digestion during proteomics experiments, Mini-PROTEAN®TGXTM Gels (4–20%) were used.

c) Coomassie Protein Staining

The SDS gel was incubated in fixing solution for 15 min, transferred into Coomassie staining solution, and stained for 2 h. Destaining of the gel was performed in destaining solution until the background was clear. The gel was then imaged using the Gellogic 200 Imaging System (KODAK) and KODAK-Mi software.

d) Electrophoretic Transfer of Proteins (Western Blot)

Proteins separated in SDS-PAGE were transferred to a PVDF membrane using an electrical field. All components of the sandwich were presoaked in freshly prepared transfer buffer, whereas the membrane was equilibrated in MeOH and then with miliQ H_2O prior to soaking in transfer buffer.

Wet transfer was performed in a Mini Trans-Blot® Cell (Bio-Rad). A sandwich containing the gel and the membrane was assembled according to the manufacturer's instructions. The transfer was conducted at 0 °C and 100 V for 1 h. Alternatively, a semi-dry transfer was performed in a Trans-Blot® SD Semi-Dry Transfer Cell (Bio-Rad) according to the manufacturer's instructions. Transfer was conducted at rt and 25 V for 1 h.

e) Immunodetection of Immobilized Proteins

The PVDF membrane was blocked for 1 h at rt with blocking buffer. The primary antibody was added at the concentration and in the buffer described by the manufacturers (Chapter 6.1.2). The membrane was then incubated overnight at 4 °C and constant agitation. Unbound antibody was removed and the membrane washed thrice with TBS-T for 5 min at rt and constant agitation. Then, the second antibody was added at the concentration and in the buffer described by the manufacturer. The membrane was incubated for 1 h at rt and constant agitation and washed thrice with TBS-T.

The enzymatic HRP signal was detected using SuperSignal West Pico/Femto Chemiluminescent Substrate (Pierce) according to the manufacturer's instructions. The resulting chemiluminescence was quantified using the Odyssey® Fc Imaging System (Li-COR® Bioscience) with adequate exposure times.

6.2.6. Methods to Study Small Molecule–Target Binding

a) Thermal Shift Assay

Protein thermostability was measured in a DSF assay using the fluorescent dye SYPRO® Orange Protein Gel Stain (5,000X, Thermo Fischer Scientific, cat# S6651). In a 96-well PCR plate (Hard-Shell®, Bio-Rad, cat# HSP960), protein melt buffer (phosphate buffer, 100 mM, pH 8, 8.5 µL) was added to each well, followed by a bGDH solution (5X in protein melt buffer, 4 µL, Sigma Aldrich, cat# G2626), a solution of compound in protein melt buffer (4X, 5 µL), and a solution of the dye in protein melt buffer (40X) sequentially. The plate was centrifuged shortly and subjected to a thermal gradient scan (20–90 °C) in a CFX96 Touch™ Real-Time PCR Detection System. The fluorescence was measured after each increment of 0.5 °C at excitation and emission wavelengths of 490 and 575 nm resp. Melting temperatures were derived using the CFX Manager^{TM} software.

b) Pyruvate Kinase Assay

Pyruvate kinase activity was measured in a fluorescence-based assay using the Pyruvate Kinase Activity Colorimetric/Fluorometric Assay Kit (BioVision, cat# K709-100) according to the manufacturer's instructions. Briefly, a solution containing an enzyme mix, a substrate mix, and OxiRed™ Probe in assay buffer was added to a solution of the compound or DMSO control in assay buffer. The absorbance was monitored using a Tecan microplate reader. The amount of pyruvate generated in the presence of compound was calculated using a standard curve.

c) Glutamate Dehydrogenase Assay

The activity of glutamate dehydrogenase was measured in a colorimetric assay using the GDH Assay Kit (Sigma-Aldrich, cat# MAK099) and bGDH (Sigma Aldrich, cat# G2626) according to the manufacturer's instructions. Briefly, a solution of glutamate and GDH developer in assay buffer was added to a solution of compound or controls in assay buffer, and the samples were incubated at 37 °C for 3 min. The absorbance was measured in a Tecan microplate reader at 450 nm and 37 °C every 5 min. The amount of NADH generated in the presence of compound was calculated using a standard curve. To be able to observe a potential increase in activity, the concentration was chosen so that the reaction rate was lower than the one of the control provided. Hence, the assay was performed at [bGDH] = 2–4 µg/mL and the measurement time adjusted accordingly.

d) Calpain Assay

Calpain-1 activity was measured in a fluorescence-based assay using the Human Calpain 1 Inhibitor Screening Kit (Sigma-Aldrich, cat# MAK210) according to the manufacturer's instructions. Briefly, a solution of calpain-1 in assay buffer was added to the compound and DMSO control in assay buffer and the mixture was incubated at 37 °C for 5 min. A solution of substrate in assay buffer was added to the mixture prepared above, and the fluorescence ($\lambda_{ex} = 400/\lambda_{em} = 505$ nm) was measured at 37 °C every minute in a Tecan microplate reader. The enzymatic activity was defined as the percentage of the control provided in the kit.

6.2.7. Profiling Services

a) Functional Assay Against AMPK

This experiment was performed by SignalChem.

Briefly, to a mixture of AMPKα1β1γ1 or AMPKα2β1γ1 (10–50 nM), kinase substrate, and compound (10 μM) in assay buffer, ^{33}P-ATP (10 μM) was added, and the reaction was incubated for 20–30 min. A volume of the mixture was spotted onto a Multiscreen phosphocellulose P81 plate and the plate washed in a 1% phosphoric acid solution. The radioactivity was measured in the presence of scintillation fluid in a Trilux scintillation counter.

b) Functional Assay Against Phosphatase Targets

This experiment was performed by SignalChem.

For DUSP22, PTPN1, PTPN2, PTPN7, PTPRC, PTPN13, PTPRS, and PTPRA, a mixture of the phosphatase, pNPP substrate (5 mM), and compound (10 μM) in assay buffer was incubated at 37 °C for 15 min. The reaction as stopped by adding an aq. NaOH solution and the absorbance measured at 405 nm.

For PTPN6, PTPN12, PTPRF, and PTPN11, a mixture of the phosphatase, tyrosine phosphopeptide-2 substrate (89 μM), and compound (10 μM) in assay buffer was incubated at 37 °C for 15 min. The reaction as stopped by adding Biomol Green reagent and the absorbance measured at 650 nm.

c) Functional Assay Against RAF1, BRAF, and ABL Kinases

This experiment was performed by Eurofins, Cerep®.

Briefly, a mixture of human recombinant kinase, kinase substrate (U*Light*™-Histone H3 (Thr3/Ser10) Peptide (50 nM), inactive MEK1 (15 nM), and U*Light*™-TK peptide (100 nM) for RAF1, BRAF, and ABL, respectively), ATP, and compound (10 µM) was incubated at rt for 60, 30, or 180 min, resp. The phosphorylated substrate was detected by LANCE® *Ultra* time-resolved fluorescence resonance energy transfer (TR-FRET).

d) Measurement of Agonist and Antagonist Effects on Serotonin Receptors

This experiment was performed by Cerep®.

Briefly, human recombinant cells or cells endogenously overexpressing the receptor of interest were treated with compound. To determine an antagonistic effect, the receptors were simultaneously stimulated with a known agonist. Depending on the receptor subtype, either impedance, IP_1, or cAMP levels were measured (Table 20).

*Table 20. Functional assays employed to determine a possible agonist/antagonist effect of indoline **1a** on serotonin receptors.*

Receptor	Cell line	Effect	Stimulus	Measured Component	Detection Method
5-HT$_{1A}$	human recombinant (HEK-293 cells)	agonist	none	impedance	CDS
		antagonist	8-OH-DPAT (100 nM)	impedance	CDS
5-HT$_{1B}$	CHO cells (endogenous)	agonist	none	impedance	CDS
		antagonist	serotonin (10 nM)	impedance	CDS
5-HT$_{1D}$	rat recombinant (CHO cells)	agonist	none	impedance	CDS
		antagonist	serotonin (3 nM)	impedance	CDS
5-HT$_{2A}$	human recombinant (HEK-293 cells)	agonist	none	IP$_1$	HTRF
		antagonist	serotonin (100 nM)	IP$_1$	HTRF
5-HT$_{2B}$	human recombinant (CHO cells)	agonist	none	IP$_1$	HTRF
		antagonist	serotonin (30 nM)	IP$_1$	HTRF
5-HT$_{2C}$	human recombinant (HEK-293 cells)	agonist	none	IP$_1$	HTRF
		antagonist	serotonin (10 nM)	IP$_1$	HTRF
5-HT$_{4e}$	human recombinant (CHO cells)	agonist	none	cAMP	HTRF
		antagonist	serotonin (30 nM)	cAMP	HTRF
5-HT$_6$	human recombinant (CHO cells)	agonist	none	cAMP	HTRF
		antagonist	serotonin (300 nM)	cAMP	HTRF
5-HT$_7$	human recombinant (CHO cells)	agonist	none	cAMP	HTRF
		antagonist	serotonin (300 nM)	cAMP	HTRF

CDS: Cellular dielectric spectroscopy; HTRF: Homogeneous Time Resolved Fluorescence

e) Unselective Binding Assay Against Rat GPCRs

This experiment was performed by Eurofins, Panlabs ®.

The assays were performed in whole Wistar Rat brain membranes using radiolabeled ligands, which are specific for each receptor family (Table 21). Non-specific binding was determined by measuring displacement of the respective radioligand.

Table 21. Radioligands used for each binding assay.

Receptor	Radioligand
Adrenergic α1	[^{3}H] Prazosin (0.25 nM)
Adrenergic α2	[^{3}H] Rauwolscine (0.70 nM)
Adrenergic β	[^{3}H] Dihydroalprenolol (0.25 nM)
Bombesin	[^{125}I] (Tyr^4)-Bombesin (10 pM)
Muscarinic	[^{3}H] Quinuclidinyl benzilate (0.15 nM)
Opiate	[^{3}H] Naloxone (1.0 nM)
Purinergic	[^{35}S] ATP-αS (0.10 nM)

f) Functional Assay Against on Purinergic Receptors

This experiment was performed by Eurofins, Cerep ®.

Briefly, human recombinant 1321N1 cells or cells endogenously overexpressing the receptor of interest were treated with compound. To determine an antagonistic effect, the receptors were simultaneously stimulated with a known agonist. Intracellular calcium levels were measured and detected by fluorimetry (Table 22).

Table 22. Stimuli used in functional assays to determine a possible agonist/antagonist effect of indoline ***1a*** *on P2Y receptors.*

Receptor	Effect	Stimulus
P2Y1	agonist	none
	antagonist	2MeSATP (1 nM)
P2Y2	agonist	none
	antagonist	UTP (300 nM)
P2Y4	agonist	none
	antagonist	UTP (10 nM)
P2Y6	agonist	none
	antagonist	UDP (10 nM)
P2Y11	agonist	none
	antagonist	ATP (60 µM)

g) Binding Assay against P2X

This experiment was performed by Eurofins, Panlabs®.

The assay was performed in whole membranes of New Zealand-derived albino rabbit urinary bladder using the P2X-specific radiolabeled ligand [^{3}H] α,β-methylene-ATP (8 mM). Non-specific binding was determined by measuring displacement of the radioligand.

6.3. Materials in Chemical Synthesis

All reactions involving air or moisture sensitive reagents or intermediates were carried out under an argon atmosphere, and all the glassware was dried by heat gun under high vacuum prior to use. Commercial reagents were used without further purification. Dry solvents were received from Acros in anhydrous quality and used without any further purification. All other solvents or reagents were purified according to standard procedures or were used as received from Sigma Aldrich, Alfa Aesar, Acros, Activate Scientific, Matrix Scientific, Combi Blocks, Fisher Scientific, Merck and TCI.

Analytical thin-layer chromatography (TLC) was performed on Merck silica gel aluminium plates with F-254 indicator. Detection of compounds was performed by UV254 light or staining with a solution of $KMnO_4$ (1.5 g in 400 mL H_2O, 5 g $NaHCO_3$) followed by heating with a heat gun. Flash column chromatography was performed using silica gel from Acros Organics (40–65 µm, 230–400 mesh). Flash master chromatography was performed using a Reveleris® X2 Flash System (Büchi) and GraceResolve^{TM} cartridges.

Preparative HPLC-MS: Separations were carried out using a preparative mass-directed HPLC (Agilent Series, 1100/LC/MSD VL, Agilent Series) with a reversed-phase C18 column (RP C4, flow 20.0 mL/min, solvent A: 0.1% TFA in water, solvent B: 0.1% TFA in acetonitrile).

^{1}H NMR and ^{13}C NMR were recorded on spectrometers from Bruker (AMX 400, AMX 500 MHz, AMX 600 MHz, Avance DRX 400, and Avance DRX 500) and Varian (Mercury 400 MHz or Unity Inova 600) using $CDCl_3$, DMSO-d_6, or CD_3OD as solvent. The NMR spectra are reported as follows: chemical shift (δ) in ppm relative to TMS (δ = 0 ppm), multiplicity, coupling constant (J) in Hertz (Hz), number of protons. Chemical shift values are reported with the solvent resonance as internal standard ($CDCl_3$: δ_H = 7.26 ppm, δ_C = 77.16 ppm; DMSO-d_6: δ_H = 2.50 ppm, δ_C = 39.52 ppm; CD_3OD: δ_H = 3.31 ppm, δ_C = 49.00 ppm). Multiplicities are indicated as br. (broad signal), s (singlet), d (doublet), t (triplet), q (quartet), sept (septet), combinations thereof, or m (multiplet). Unless stated otherwise all NMRs were measured at room temperature. Where possible, structural assignments were attempted using standard 2-D NMR techniques (gCOSY, gHSQC, gHMBC).

HR-MS spectra were recorded on a LTQ Orbitrap (Thermo Fisher) mass spectrometer coupled to an Accela HPLC-System (HPLC column: Hypersyl GOLD, 50 mm x 1 mm, particle size 1.9 µm), ionization method: electron spray ionization (ESI).

6.4. Synthesis of Indoline-Based Analogs

*Analogs of indoline **1a** that are not described in this section were purchased from ChemDiv.*

Cyclopropyl(indolin-1-yl)methanone (3)

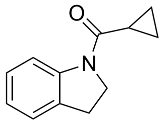

To a solution of indoline (**4**, 1.50 mL, 13.4 mmol) and Et_3N (7.18 mL, 40.1 mmol, 3.0 eq.) in CH_2Cl_2 (25 mL) under an argon atmosphere, DMAP (33 mg, 0.3 mmol, 0.02 eq.) was added. The solution was cooled to 0 °C, and cyclopropanecarbonyl chloride (1.37 mL, 14.7 mmol, 1.1 eq.) was added dropwise. The mixture was stirred for 10 min at 0 °C and 2 h at rt, EtOAc was added (30 mL), and the organic phase was washed with an aq. 1 M HCl solution (2 x 10 mL), sat. aq. $NaHCO_3$ solution (1 x 10 mL), and brine (1 x 10 mL). The organic layer was dried over $MgSO_4$ and concentrated under reduced pressure. The crude product was purified by flash chromatography (SiO_2; cyclohexane/EtOAc 1:0 → 9:1) to afford **3** (2.479 g, 99%) as an off-white amorphous solid.

^{1}H NMR (400 MHz, $CDCl_3$): $\delta = 8.17$ (s, 1H), 7.24–7.11 (m, 2H), 6.99 (t, $J = 7.4$ Hz, 1H), 4.26 (t, $J = 8.7$ Hz, 2H), 3.21 (t, $J = 8.7$ Hz, 2H), 1.88–1.65 (m, 1H), 1.19–1.07 (m, 2H), 0.96–0.79 (m, 2H); **HR-ESI-MS**: $m/z = 188.1069$ ($[M + H]^+$, calcd. for $C_{12}H_{14}NO^+$: 188.1070).

General Procedure I – C5-Bromination of N-Acylated Indolines

To a solution of the acyl indoline (9.3 mmol) in CH_2Cl_2 (40 mL) at rt under an argon atmosphere, NBS (1.1 eq.) was added. The mixture was stirred at rt for 2–16 h and poured into sat. aq. $NaHCO_3$ (20 mL). The layers were separated, and the aq. layer was extracted with EtOAc (3 x 10 mL). The combined organic layers were washed with brine (1 x 50 mL), dried over $MgSO_4$, filtered, and concentrated under reduced pressure. The crude product was purified by flash chromatography (SiO_2; cyclohexane/EtOAc mixture).

1-(5-Bromoindolin-1-yl)ethan-1-one (SI-1)

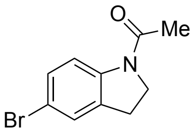

Bromoindoline **SI-1** was synthesized according to GP I, using 1-(indolin-1-yl)ethan-1-one (1.500 g, 9.3 mmol), which was reacted for 2 h. Purification of the product by flash chromatography (SiO_2; cyclohexane/EtOAc 4:1 → 3:2) afforded **SI-1** (2.123 g, 85%) as a white amorphous solid.

^{1}H NMR (500 MHz, DMSO-d_6): δ = 7.95 (d, J = 8.6 Hz, 1H), 7.40 (s, 1H), 7.30 (d, J = 8.5 Hz, 1H), 4.09 (t, J = 8.6 Hz, 2H), 3.14 (t, J = 8.5 Hz, 2H), 2.14 ppm (s, 3H); **^{13}C NMR** (126 MHz, DMSO-d_6): δ = 168.8, 142.3, 134.8, 129.6, 127.6, 117.3, 114.4, 48.3, 27.1, 23.9 ppm; **HR-ESI-MS**: m/z = 240.00166 ($[M + H]^+$, calcd. for $C_{10}H_{11}{}^{79}BrNO^+$: 240.0019), 241.99886 ($[M + H]^+$, calcd. for $C_{10}H_{11}{}^{81}BrNO^+$: 241.9998).

(5-Bromoindolin-1-yl)(cyclopropyl)methanone (6)

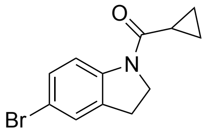

Bromoindoline **6** was synthesized according to GP I, using **3** (300 mg, 1.6 mmol), which was reacted for 2 h. Purification of the product by flash chromatography (SiO_2; cyclohexane/EtOAc 1:0 → 9:1) afforded **6** (379 mg, 89%) as an off-white amorphous solid.

^{1}H NMR (400 MHz, $CDCl_3$): δ = 8.05 (s, 1H), 7.29 (s, 1H), 7.28–7.26 (m, 1H), 4.28 (t, J = 8.2 Hz, 2H), 3.21 (t, J = 8.1 Hz, 2H), 1.74 (s, 1H), 1.13 (m, 2H), 0.98–0.81 ppm (m, 2H); **^{13}C NMR** (126 MHz, DMSO-d_6): δ = 142.6, 135.0, 129.5, 127.6, 117.4, 114.4, 47.9, 27.1, 13.1, 7.9 ppm; **HR-ESI-MS**: m/z = 266.0173 ($[M + H]^+$, calcd. for $C_{12}H_{13}{}^{79}BrNO^+$: 266.0175), 268.0145 ($[M + H]^+$, calcd. for $C_{12}H_{13}{}^{81}BrNO^+$: 268.0155).

General Procedure II – Chlorosulfonylation of N-Acylindolines

To chlorosulfonic acid (12.0 eq.), the *N*-acylindoline (0.9 mmol) was added slowly at 0 °C under an argon atmosphere. The mixture was stirred at 0 °C for 20 min, and at 70 °C for 5 h. The mixture was quenched by pipetting it carefully onto ice (10 mL) under vigorous stirring. The precipitated crude product was extracted with EtOAc (5 x 20 mL). The combined organic layers were dried over $MgSO_4$, filtered, and concentrated under reduced pressure. The crude product was used without purification in the next step. Due to its poor stability in water, no ESI-MS data could be obtained.

5-Bromo-1-(cyclopropanecarbonyl)indoline-6-sulfonyl chloride (SI-2)

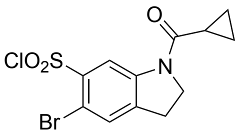

Chlorosulfonyl **SI-2** was synthesized according to GP II using **6** (100 mg, 0.4 mmol).

^{1}H NMR (400 MHz, $CDCl_3$): δ = 9.11–8.90 (m, 1H), 7.61 (s, 1H), 4.38 (t, J = 8.8 Hz, 2H), 3.33 (t, J = 8.3 Hz, 2H), 1.80–1.70 (m, 1H), 1.21–1.14 (m, 2H), 1.02–0.90 ppm (m, 2H).

1-(Cyclopropanecarbonyl)indoline-5-sulfonyl Chloride (SI-3)

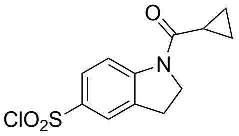

Chlorosulfonyl **SI-3** was synthesized according to GP II using **3** (100 mg, 0.5 mmol).

^{1}H NMR (400 MHz, $CDCl_3$): δ = 8.42–8.20 (m, 1H), 7.88 (dd, J = 8.8, 2.1 Hz, 1H), 7.82 (s, 1H), 4.40 (t, J = 8.7 Hz, 2H), 3.33 (t, J = 8.7 Hz, 2H), 1.86–1.68 (m, 1H), 1.21–1.15 (m, 2H), 1.01–0.94 ppm (m, 2H).

1-Acetyl-5-bromoindoline-6-sulfonyl Chloride (SI-4)[108]

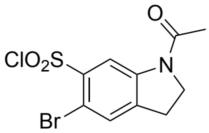

Chlorosulfonyl **SI-4** was synthesized according to GP II using **SI-1** (500 mg, 2.1 mmol).

^{1}H NMR (400 MHz, $CDCl_3$): δ = 9.01 (s, 1H), 7.60 (s, 1H), 4.17 (t, *J* = 8.6 Hz, 2H), 3.30 (s, 2H), 2.25 ppm (s, 3H).

General Procedure III – Synthesis of Sulfonamides

A mixture of the sulfonyl chloride (82 µmol) and the aniline (1.0–1.1 eq.) in pyridine (2 mL) was heated to 60 °C under an argon atmosphere for 16 h. The solution was concentrated under reduced pressure, and the residue dissolved in EtOAc, and washed with an aq. 1 M HCl solution (1 x). The aq. phase was extracted with EtOAc, and the combined organic layers were dried over $MgSO_4$, filtered, and concentrated under reduced pressure. The product was purified by flash chromatography (SiO_2; cyclohexane/EtOAc mixture). Yields are reported over two steps.

5-Bromo-*N*-(4-chloro-3-(trifluoromethyl)phenyl)-1-(cyclopropanecarbonyl)indoline-6-sulfonamide (1a)

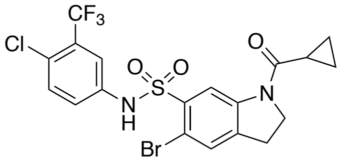

Sulfonamide **1a** was synthesized according to GP III using **SI-2** (300 mg, 823 µmol) and 4-chloro-3-(trifluoromethyl)aniline (169 mg, 864 µmol, 1.1 eq.). Purification of the product by flash column chromatography (SiO_2; cyclohexane/EtOAc 4:1 → 2:1) afforded **1a** (329 mg, 76%) as an off-white amorphous solid.

^{1}H NMR (500 MHz, DMSO-*d$_6$*): δ = 11.13 (s, 1H), 8.80 (s, 1H), 7.66 (s, 1H), 7.60 (d, *J* = 8.8 Hz, 1H), 7.55 (d, *J* = 2.6 Hz, 1H), 7.34 (dd, *J* = 8.8, 2.6 Hz, 1H), 4.32 (t, *J* = 8.5 Hz, 2H), 3.22 (t, *J* = 8.6 Hz, 2H), 1.93 (tt, *J* = 7.2, 5.4 Hz, 1H), 0.95–0.84 ppm (m, 4H); **^{13}C NMR** (126 MHz, DMSO-

d_6): δ = 172.0, 142.9, 140.0, 136.8, 136.1, 132.7, 131.4, 127.2 (q, J = 30.8 Hz), 124.8 (q, J = 1.9 Hz), 123.3, 122.3 (q, J = 273.3 Hz), 117.8, 117.6 (q, J = 5.8 Hz), 111.9, 48.1, 27.0, 13.1, 8.3 ppm; **^{19}F NMR** (377 MHz, DMSO-d_6): δ = -61.77 ppm; **HR-ESI-MS**: m/z = 522.9708 ([M + H]$^+$, calcd. for $C_{19}H_{16}{}^{79}BrClF_3N_2O_3S^+$: 522.9700), 524.9682 ([$M$ + H]$^+$, calcd. for $C_{19}H_{16}{}^{81}BrClF_3N_2O_3S^+$: 524.9680), 526.9652 ([$M$ + H]$^+$, calcd. for $C_{19}H_{16}{}^{81}Br^{37}ClF_3N_2O_3S^+$: 526.9650).

5-Bromo-1-(cyclopropanecarbonyl)-*N*-(3-(trifluoromethyl)phenyl)indoline-6-sulfonamide (1b)

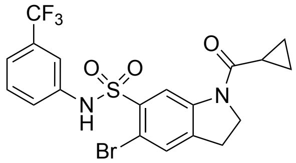

Sulfonamide **1b** was synthesized according to GP III using **SI-2** (50 mg, 137 µmol) and 3-(trifluoromethyl)aniline (17 µL, 137 µmol, 1.0 eq.). Purification of the product by flash column chromatography (SiO_2; cyclohexane/EtOAc 4:1 → 2:1) afforded **1b** (61 mg, 90%) as an off-white amorphous solid.

^{1}H NMR (600 MHz, DMSO-d_6): δ = 11.00 (s, 1H), 8.81 (s, 1H), 7.65 (s, 1H), 7.47 (t, J = 8.0 Hz, 1H), 7.41 (s, 1H), 7.37–7.31 (m, J = 8.0, 1.6 Hz, 2H), 4.32 (t, J = 8.2 Hz, 2H), 3.21 (t, J = 8.5 Hz, 2H), 1.93 (tt, J = 7.2, 5.4 Hz, 1H), 0.94–0.84 ppm (m, 4H); **^{13}C NMR** (151 MHz, DMSO-d_6): δ = 142.9, 139.9, 138.1, 136.2, 131.4, 130.6, 129.9 (q, J = 31.8 Hz), 123.7 (q, J = 272.4 Hz), 122.1, 120.0, 118.1, 115.0, 112.0, 48.1, 27.0, 13.2, 8.3 ppm; **^{19}F NMR** (565 MHz, DMSO-d_6): δ = -61.51 ppm; **HR-ESI-MS**: m/z = 489.0093 ([M + H]$^+$, calcd. for $C_{19}H_{17}{}^{79}BrF_3N_2O_3S^+$: 489.0090), 491.0069 ([$M$ + H]$^+$, calcd. for $C_{19}H_{17}{}^{81}BrF_3N_2O_3S^+$: 491.0069).

5-Bromo-*N*-(4-bromo-3-(trifluoromethyl)phenyl)-1-(cyclopropanecarbonyl)indoline-6-sulfonamide (1c)

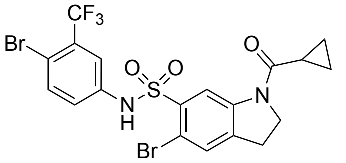

Sulfonamide **1c** was synthesized according to GP III using **SI-2** (30 mg, 82 μmol) and 4-bromo-3-(trifluoromethyl)aniline (20 mg, 82 μmol, 1.0 eq.). Purification of the product by flash column chromatography (SiO_2; cyclohexane/EtOAc 4:1 → 2:1) afforded **1c** (43 mg, 91%) as an off-white amorphous solid.

^{1}H NMR (600 MHz, DMSO-*d$_6$*): δ = 11.16 (s, 1H), 8.80 (s, 1H), 7.75 (d, J = 8.7 Hz, 1H), 7.66 (s, 1H), 7.54 (d, J = 2.6 Hz, 1H), 7.25 (dd, J = 8.7, 2.5 Hz, 1H), 4.32 (t, J = 8.3 Hz, 2H), 3.22 (t, J = 8.5 Hz, 2H), 1.99–1.88 (m, 1H), 0.95–0.84 ppm (m, 4H); **^{13}C NMR** (151 MHz, DMSO-*d$_6$*): δ = 172.1, 142.9, 140.1, 136.1, 136.1, 131.5, 129.0 (q, J = 30.8 Hz), 123.3, 122.5 (q, J = 273.4 Hz), 118.2–117.7 (m); 117.9, 117.8, 112.4, 111.9, 48.2, 27.1, 13.1, 8.3 ppm; **^{19}F NMR** (565 MHz, DMSO-*d$_6$*): δ = -61.84 ppm; **HR-ESI-MS**: m/z = 566.9206 ($[M + H]^+$, calcd. for $C_{19}H_{16}{}^{79}Br_2F_3N_2O_3S^+$: 566.9195), 568.9181 ($[M + H]^+$, calcd. for $C_{19}H_{16}{}^{79}Br^{81}BrF_3N_2O_3S^+$: 568.9175), 570.9158 ($[M + H]^+$, calcd. for $C_{19}H_{16}{}^{81}Br_2F_3N_2O_3S^+$: 570.9154).

5-Bromo-1-(cyclopropanecarbonyl)-*N*-(4-methyl-3-(trifluoromethyl)phenyl)indoline-6-sulfonamide (1d)

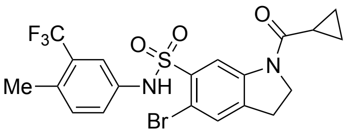

Sulfonamide **1d** was synthesized according to GP III using **SI-2** (36 mg, 96 μmol) and 4-methyl-3-(trifluoromethyl)aniline (15 μL, 108 μmol, 1.1 eq.). Purification of the product by flash column chromatography (SiO_2; cyclohexane/EtOAc 4:1 → 2:1) afforded **1d** (45 mg, 92%) as an off-white amorphous solid.

^{1}H NMR (700 MHz, DMSO-*d$_6$*): δ = 10.79 (br. s, 1H), 8.78 (br. s, 1H), 7.64 (s, 1H), 7.40 (s, 1H), 7.29 (d, J = 8.4 Hz, 1H), 7.24 (d, J = 8.5 Hz, 1H), 4.32 (t, J = 8.0 Hz, 2H), 3.21 (t, J = 8.5 Hz, 2H), 2.29 (s, 3H), 1.97–1.87 (m, 1H), 0.99–0.77 ppm (m, 4H); **^{13}C NMR** (176 MHz, DMSO-*d$_6$*): δ =

172.0, 142.8, 139.7, 136.4, 135.4, 133.2, 131.3, 131.0, 127.9 (q, *J* = 29.5 Hz), 124.0 (q, *J* = 273.8 Hz), 122.4, 118.0, 116.4 (d, *J* = 5.3 Hz), 111.9, 48.1, 27.0, 18.0, 17.9, 13.1, 8.3 ppm; **^{19}F NMR** (377 MHz, DMSO-d_6): δ = -60.76 ppm; **HR-ESI-MS**: *m*/*z* = 503.0261 ([*M* + H]$^+$, calcd. for $C_{20}H_{19}{}^{79}BrF_3N_2O_3S^+$: 503.0246), 505.0235 ([*M* + H]$^+$, calcd. for $C_{20}H_{19}{}^{81}BrF_3N_2O_3S^+$: 505.0226).

5-Bromo-*N*-(3-chloro-5-(trifluoromethyl)phenyl)-1-(cyclopropanecarbonyl)indoline-6-sulfonamide (1e)

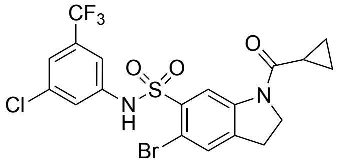

Sulfonamide **1e** was synthesized according to GP III using **SI-2** (35 mg, 96 µmol) and 3-chloro-5-(trifluoromethyl)aniline (21 mg, 106 µmol, 1.1 eq.). Purification of the product by flash column chromatography (SiO_2; cyclohexane/EtOAc 4:1 → 2:1) afforded **1e** (28 mg, 56%) as an off-white amorphous solid.

^{1}H NMR (600 MHz, DMSO-d_6): δ = 11.33 (s, 1H), 8.82 (s, 1H), 7.67 (s, 1H), 7.48 (s, 1H), 7.37 (dd, *J* = 3.1, 1.4 Hz, 2H), 4.32 (t, *J* = 8.2 Hz, 2H), 3.22 (t, *J* = 8.5 Hz, 2H), 1.93 (dq, *J* = 7.0, 5.6 Hz, 1H), 0.89 ppm (dd, *J* = 10.8, 5.9 Hz, 4H); **^{13}C NMR** (151 MHz, DMSO-d_6): δ = 172.1, 143.0, 140.2, 139.7, 135.8, 134.7, 131.6, 131.5 (q, *J* = 32.7 Hz), 122.9 (q, *J* = 273.0 Hz), 121.4, 119.9, 117.9, 113.3, 111.9, 48.1, 27.1, 13.1, 8.4 ppm; **^{19}F NMR** (565 MHz, DMSO-d_6): δ = -61.82 ppm; **HR-ESI-MS**: *m*/*z* = 522.9707 ([*M* + H]$^+$, calcd. for $C_{19}H_{16}{}^{79}BrClF_3N_2O_3S^+$: 522.9700), 524.9680 ([*M* + H]$^+$, calcd. for $C_{19}H_{16}{}^{81}BrClF_3N_2O_3S^+$: 524.9680), 526.9652 ([M + H]$^+$, calcd. for $C_{19}H_{16}{}^{81}Br^{37}ClF_3N_2O_3S^+$: 526.9650).

N-(3,5-Bis(trifluoromethyl)phenyl)-5-bromo-1-(cyclopropanecarbonyl)indoline-6-sulfonamide (1f)

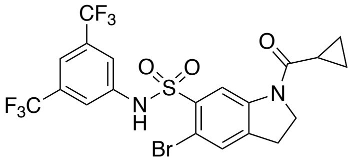

Sulfonamide **1f** was synthesized according to GP III using **SI-2** (30 mg, 83 µmol) and 3,5-bis(trifluoromethyl)aniline (19.3 µL, 123 µmol, 1.5 eq.). Purification of the product by flash column chromatography (SiO_2; cyclohexane/EtOAc 2:1→ 1:0) afforded **1f** (24 mg, 52%) as an off-white amorphous solid.

^{1}H NMR (400 MHz, CD_3OD): δ = 8.94 (s, 1H), 7.67 (s, 2H), 7.57 (s, 1H), 7.54 (s, 1H), 4.36 (t, J = 8.6 Hz, 2H), 3.25 (t, J = 8.6 Hz, 2H), 1.97–1.88 (m, 1H), 1.08–1.00 (m, 2H), 1.01–0.93 ppm (m, 2H); **HR-ESI-MS**: m/z = 556.9973 ([M + H]$^+$, calcd. for $C_{20}H_{16}{}^{79}BrF_6N_2O_3S^+$: 556.9964), 558.9949 ([$M$ + H]$^+$, calcd. for $C_{20}H_{16}{}^{81}BrF_6N_2O_3S^+$: 558.9943).

5-Bromo-1-(cyclopropanecarbonyl)-*N*-(4-methoxy-3-(trifluoromethyl)phenyl)indoline-6-sulfonamide (1h)

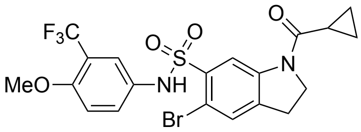

Sulfonamide **1h** was synthesized according to GP III using **SI-2** (34 mg, 93 µmol) and 4-methoxy-3-(trifluoromethyl)aniline (19 mg, 98 µmol, 1.1 eq.). Purification of the product by flash column chromatography (SiO_2; cyclohexane/EtOAc 4:1 → 2:1) afforded **1h** (37 mg, 77%) as an off-white amorphous solid.

^{1}H NMR (600 MHz, DMSO-d_6): δ = 10.50 (s, 1H), 8.71 (s, 1H), 7.66 (s, 1H), 7.37–7.30 (m, 2H), 7.17 (d, J = 8.9 Hz, 1H), 4.32 (t, J = 8.3 Hz, 2H), 3.79 (s, 3H), 3.21 (t, J = 8.5 Hz, 2H), 1.96–1.87 (m, 1H), 0.95-0.76 ppm (m, 4H); **^{13}C NMR** (151 MHz, DMSO-d_6): δ = 172.0, 153.8, 142.8, 139.6, 136.6, 131.3, 129.5, 126.1, 123.2 (q, J = 272.4 Hz), 119.4 (q, J = 5.2 Hz), 117.9, 117.1 (q, J = 30.4 Hz), 113.9, 112.0, 56.3, 48.1, 27.0, 13.1, 8.3 ppm; **^{19}F NMR** (565 MHz, DMSO-d_6): δ = -61.23 ppm; **HR-ESI-MS**: m/z = 519.0211 ([M + H]$^+$, calcd. for $C_{20}H_{19}{}^{79}BrF_3N_2O_4S^+$: 519.0196), 521.0187 ([$M$ + H]$^+$, calcd. for $C_{20}H_{19}{}^{81}BrF_3N_2O_4S^+$: 521.0175).

5-Bromo-1-(cyclopropanecarbonyl)-*N*-(4-fluoro-3-(trifluoromethyl)phenyl)indoline-6-sulfonamide (1i)

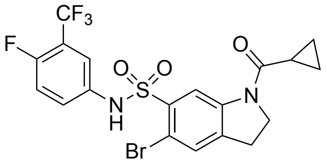

Sulfonamide **1i** was synthesized according to GP III using **SI-2** (35 mg, 96 µmol) and 4-fluoro-3-(trifluoromethyl)aniline (12 µL, 96 µmol, 1.0 eq.). Purification of the product by flash column chromatography (SiO_2; cyclohexane/EtOAc 4:1 → 2:1) afforded **1i** (32 mg, 66%) as an off-white amorphous solid.

^{1}H NMR (600 MHz, DMSO-d_6): δ = 10.95 (s, 1H), 8.77 (s, 1H), 7.66 (s, 1H), 7.50–7.34 (m, 3H), 4.32 (t, J = 8.4 Hz, 2H), 3.22 (t, J = 8.6 Hz, 2H), 1.95–1.86 (m, 1H), 0.88 ppm (dd, J = 10.5, 6.4 Hz, 4H); **^{13}C NMR** (151 MHz, DMSO-d_6): δ = 172.0, 155.1 (d, J = 250.6 Hz), 142.9, 139.9, 136.2, 134.0 (d, J = 2.8 Hz), 131.4, 125.3 (d, J = 8.6 Hz), 122.1 (q, J = 272.2 Hz), 118.4 (d, J = 21.8 Hz), 117.8, 117.6 (d, J = 4.4 Hz), 117.0 (qd, J = 32.5, 13.5 Hz), 111.9, 48.1, 27.0, 13.1, 8.3 ppm; **^{19}F NMR** (565 MHz, DMSO-d_6): δ = -60.52 (d, J = 12.4 Hz), -121.98–-122.12 ppm (m); **HR-ESI-MS**: m/z = 507.0001 ([M + H]$^+$, calcd. for $C_{19}H_{16}{}^{79}BrF_4N_2O_3S^+$: 506.9996), 508.9975 ([$M$ + H]$^+$, calcd. for $C_{19}H_{16}{}^{81}BrF_4N_2O_3S^+$: 508.9975).

5-Bromo-*N*-(4-chloro-2-(trifluoromethyl)phenyl)-1-(cyclopropanecarbonyl)indoline-6-sulfonamide (1j)

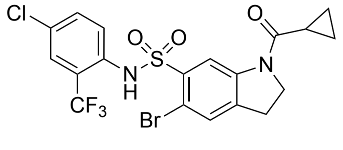

Sulfonamide **1j** was synthesized according to GP III using **SI-2** (35 mg, 96 µmol) and 4-chloro-2-(trifluoromethyl)aniline (15 µL, 106 µmol, 1.0 eq.). Purification of the product by flash column chromatography (SiO_2; cyclohexane/EtOAc 1:0 → 9:1) afforded **1j** (4 mg, 7%) as an off-white amorphous solid.

^{1}H NMR (400 MHz, $CDCl_3$): δ = 9.08–8.81 (m, 1H), 7.64–7.56 (m, 1H), 7.50 (s, 1H), 7.43–7.36 (m, 2H), 4.34 (t, J = 8.3 Hz, 2H), 3.26 (t, J = 8.8 Hz, 2H), 1.88–1.65 (m, 1H), 1.00–0.79 ppm (m, 4H); **ESI-MS**: m/z = 522.8 ([M + H]$^+$, calcd. for $C_{19}H_{16}{}^{79}BrClF_3N_2O_3S^+$: 523.0), 524.8 ([$M$ + H]$^+$, calcd. for $C_{19}H_{15}{}^{81}BrClF_3N_2O_3S^+$: 525.0), 526.8 ([M + H]$^+$, calcd. for $C_{19}H_{15}{}^{81}Br^{37}ClF_3N_2O_3S^+$: 527.0).

5-Bromo-1-(cyclopropanecarbonyl)-*N*-(1-methyl-1*H*-indol-5-yl)indoline-6-sulfonamide (1n)

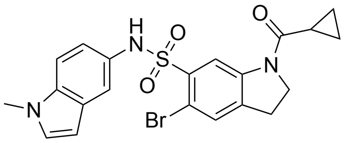

Sulfonamide **1n** was synthesized according to GP III using **SI-2** (37 mg, 101 µmol) and 1-methyl-1*H*-indol-5-amine (16 mg, 111 µmol, 1.1 eq.). Purification of the product by flash column chromatography (SiO_2; cyclohexane/EtOAc 4:1 → 2:1) afforded **1n** (32 mg, 67%) as an off-white amorphous solid.

^{1}H NMR (700 MHz, DMSO-d_6): δ = 9.98 (br. s, 1H), 8.63 (s, 1H), 7.63 (d, J = 16.0 Hz, 1H), 7.30–7.25 (m, 3H), 6.96 (d, J = 8.9 Hz, 1H), 6.31 (d, J = 2.9 Hz, 1H), 4.25 (t, J = 7.9 Hz, 2H), 3.69 (s, 3H), 3.16 (t, J = 8.5 Hz, 2H), 1.92–1.82 (m, J = 32.5 Hz, 1H), 0.89–0.78 ppm (m, 4H); **^{13}C NMR** (176 MHz, DMSO-d_6): δ = 171.8, 142.6, 139.0, 137.0, 134.1, 130.9, 130.5, 128.3, 127.9, 118.3, 116.9, 114.0, 112.2, 110.0, 100.2, 48.0, 32.5, 26.9, 13.1, 8.2 ppm; **HR-ESI-MS**: m/z = 474.0502 ([M + H]$^+$, calcd. for $C_{21}H_{21}{}^{79}BrN_3O_3S^+$: 474.0482), 476.0479 ([$M$ + H]$^+$, calcd. for $C_{21}H_{21}{}^{81}BrN_3O_3S^+$: 476.0461).

5-Bromo-1-(cyclopropanecarbonyl)-*N*-(3,4,5-trifluorophenyl)indoline-6-sulfonamide (1o)

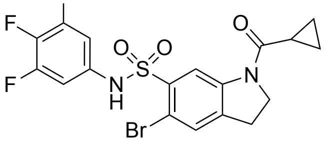

Sulfonamide **1o** was synthesized according to GP III using **SI-2** (33 mg, 91 µmol) and 3,4,5-trifluoroaniline (13 mg, 91 µmol, 1.0 eq.). Purification of the product by flash column chromatography (SiO_2; cyclohexane/EtOAc 4:1 → 2:1) afforded **1o** (25 mg, 58%) as an off-white amorphous solid.

^{1}H NMR (600 MHz, DMSO-*d$_6$*): δ = 11.09 (s, 1H), 8.78 (s, 1H), 7.68 (s, 1H), 6.90 (dd, *J* = 9.4, 6.1 Hz, 2H), 4.34 (t, *J* = 8.5 Hz, 2H), 3.23 (t, *J* = 8.6 Hz, 2H), 1.94 (ddt, *J* = 14.5, 12.0, 5.9 Hz, 1H), 0.99–0.81 ppm (m, 4H); **^{13}C NMR** (151 MHz, DMSO-*d$_6$*): δ = 172.2, 150.3 (ddd, *J* = 246.4, 10.1, 5.2 Hz), 142.9, 140.2, 135.9, 135.3 (dt, *J* = 245.5, 15.6 Hz), 133.7 (td, *J* = 11.3, 3.2 Hz), 131.5, 117.9, 112.0, 103.3 (dd, *J* = 19.9, 5.1 Hz), 48.2, 27.1, 13.2, 8.4 ppm; **^{19}F NMR** (565 MHz, DMSO-*d$_6$*): δ = -133.42 (dd, *J* = 22.4, 9.6 Hz), -167.50 ppm (t, *J* = 22.2 Hz); **HR-ESI-MS**: *m*/*z* = 474.9937 ([*M* + H]$^+$, calcd. for $C_{18}H_{15}{}^{79}BrF_3N_2O_3S^+$: 474.9933), 476.9909 ([*M* + H]$^+$, calcd. for $C_{18}H_{15}{}^{81}BrF_3N_2O_3S^+$: 476.9913).

5-Bromo-1-(cyclopropanecarbonyl)-*N*-(3-fluorophenyl)indoline-6-sulfonamide (1p)

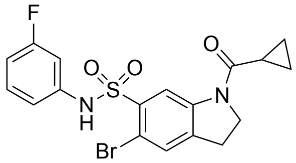

Sulfonamide **1p** was synthesized according to GP III using **SI-2** (30 mg, 82 µmol) and 3-fluoroaniline (8 µL, 82 µmol, 1.0 eq.). Purification of the product by flash column chromatography (SiO$_2$; cyclohexane/EtOAc 4:1 → 2:1) afforded **1p** (35 mg, 98%) as an off-white amorphous solid.

^{1}H NMR (600 MHz, DMSO-*d$_6$*): δ = 10.85 (s, 1H), 8.81 (s, 1H), 7.65 (s, 1H), 7.26 (td, *J* = 8.2, 6.9 Hz, 1H), 6.91 (dd, *J* = 8.2, 0.7 Hz, 1H), 6.87 (dt, *J* = 11.0, 2.2 Hz, 1H), 6.82 (td, *J* = 8.3, 2.0 Hz, 1H), 4.33 (t, *J* = 8.4 Hz, 2H), 3.22 (t, *J* = 8.5 Hz, 2H), 1.98–1.88 (m, 1H), 0.96–0.83 ppm (m, 4H); **^{13}C NMR** (151 MHz, DMSO-*d$_6$*): δ = 172.1, 162.2 (d, *J* = 243.0 Hz), 142.9, 139.9, 139.0 (d, *J* = 10.7 Hz), 136.3, 131.4, 131.0 (d, *J* = 9.6 Hz), 118.1, 114.5 (d, *J* = 2.4 Hz), 112.0, 110.2 (d, *J* = 20.9 Hz), 105.5 (d, *J* = 25.6 Hz), 48.2, 27.0, 13.2, 8.3 ppm; **^{19}F NMR** (565 MHz, DMSO-*d$_6$*): δ = -111.49 ppm; **HR-ESI-MS**: *m*/*z* = 439.0125 ([*M* + H]$^+$, calcd. for $C_{18}H_{17}{}^{79}BrFN_2O_3S^+$: 439.0122), 441.0098 ([*M* + H]$^+$, calcd. for $C_{18}H_{17}{}^{81}BrFN_2O_3S^+$: 441.0101).

5-Bromo-1-(cyclopropanecarbonyl)-*N*-(4-fluorophenyl)indoline-6-sulfonamide (1q)

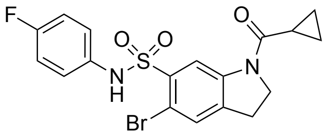

Sulfonamide **1q** was synthesized according to GP III using **SI-2** (30 mg, 82 µmol) and 4-fluoroaniline (8 µL, 82 µmol, 1.0 eq.). Purification of the product by flash column chromatography (SiO_2; cyclohexane/EtOAc 4:1 → 2:1) afforded **1q** (7 mg, 20%) as an off-white amorphous solid.

^{1}H NMR (600 MHz, DMSO-*d$_6$*): δ = 10.47 (s, 1H), 8.72 (s, 1H), 7.64 (s, 1H), 7.18–7.00 (m, 4H), 4.32 (t, J = 8.4 Hz, 2H), 3.21 (t, J = 8.5 Hz, 2H), 1.99–1.87 (m, 1H), 0.93–0.83 ppm (m, 4H); **^{13}C NMR** (151 MHz, DMSO-*d$_6$*): δ = 172.0, 158.8 (d, J = 240.6 Hz), 142.8, 139.6, 136.6, 133.3, 131.2, 121.9 (d, J = 8.3 Hz), 118.1, 115.9 (d, J = 22.7 Hz), 112.0, 48.1, 27.0, 13.2, 8.3 ppm; **^{19}F NMR** (565 MHz, DMSO-*d$_6$*): δ = -118.72 ppm; **HR-ESI-MS**: m/z = 439.0121 ([M + H]$^+$, calcd. for $C_{18}H_{17}{}^{79}BrFN_2O_3S^+$: 439.0122), 441.0099 ([$M$ + H]$^+$, calcd. for $C_{18}H_{17}{}^{81}BrFN_2O_3S^+$: 441.0101).

5-Bromo-1-(cyclopropanecarbonyl)-*N*-(3,5-difluorophenyl)indoline-6-sulfonamide (1r)

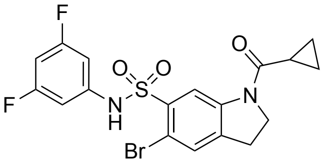

Sulfonamide **1r** was synthesized according to GP III using **SI-2** (30 mg, 82 µmol) and 3,5-difluoroaniline (11 mg, 82 µmol, 1.0 eq.). Purification of the product by flash column chromatography (SiO_2; cyclohexane/EtOAc 4:1 → 2:1) afforded **1r** (30 mg, 79%) as an off-white amorphous solid.

^{1}H NMR (600 MHz, DMSO-*d$_6$*): δ = 11.17 (s, 1H), 8.81 (s, 1H), 7.67 (s, 1H), 6.86 (tt, J = 9.3, 2.1 Hz, 1H), 6.81–6.66 (m, 2H), 4.34 (t, J = 8.4 Hz, 2H), 3.23 (t, J = 8.6 Hz, 2H), 1.99–1.89 (m, 1H), 0.98–0.84 ppm (m, 4H); **^{13}C NMR** (151 MHz, DMSO-*d$_6$*): δ = 172.2, 163.4 (dd, J = 17.0, 6.4 Hz), 142.9, 140.2, 140.1, 136.0, 131.5, 118.0, 112.0, 101.6–101.1 (m), 98.7 (t, J = 26.0 Hz), 48.2, 27.1, 13.2, 8.4 ppm; **^{19}F NMR** (565 MHz, DMSO-*d$_6$*): δ = -108.26 ppm; **HR-ESI-MS**: m/z = 457.0031 ([M + H]$^+$, calcd. for $C_{18}H_{16}{}^{79}BrF_2N_2O_3S^+$: 457.0028), 459.0004 ([$M$ + H]$^+$, calcd. for $C_{18}H_{16}N_2{}^{81}BrF_2O_3S^+$: 459.0007).

5-Bromo-1-(cyclopropanecarbonyl)-*N*-(perfluorophenyl)indoline-6-sulfonamide (1s)

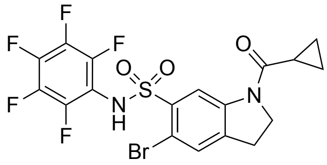

Sulfonamide **1s** was synthesized according to GP III using **SI-2** (35 mg, 96 µmol) and 2,3,4,5,6-pentafluoroaniline (19 mg, 101 µmol, 1.0 eq.). Purification of the product by flash column chromatography (SiO_2; cyclohexane/EtOAc 4:1 → 2:1) afforded **1s** (8 mg, 16%) as an off-white amorphous solid.

^{1}H NMR (400 MHz, CD_3OD): δ = 8.68 (s, 1H), 7.68 (s, 1H), 4.40 (t, J = 8.5 Hz, 2H), 3.34 (t, J = 8.5 Hz, 2H), 1.98–1.88 (m, 1H), 1.03–0.97 (m, 2H), 0.97–0.91 ppm (m, 2H); **HR-ESI-MS**: m/z = 510.9745 ([M + H]$^+$, calcd. for $C_{18}H_{13}{}^{79}BrF_5N_2O_3S^+$: 510.9745), 512.9723 ([$M$ + H]$^+$, calcd. for $C_{18}H_{13}{}^{81}BrF_5N_2O_3S^+$: 512.9725).

5-Bromo-*N*-(3-cyanophenyl)-1-(cyclopropanecarbonyl)indoline-6-sulfonamide (1t)

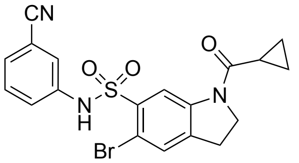

Sulfonamide **1t** was synthesized according to GP III using **SI-2** (30 mg, 82 µmol) and 3-aminobenzonitrile (10 mg, 82 µmol, 1.0 eq.). Purification of the product by flash column chromatography (SiO_2; cyclohexane/EtOAc 4:1 → 2:1) afforded **1t** (34 mg, 93%) as an off-white amorphous solid.

^{1}H NMR (600 MHz, DMSO-d_6): δ = 11.05 (s, 1H), 8.80 (s, 1H), 7.65 (s, 1H), 7.51–7.43 (m, 2H), 7.43–7.40 (m, 1H), 7.40–7.35 (m, 1H), 4.33 (t, J = 8.3 Hz, 2H), 3.22 (t, J = 8.5 Hz, 2H), 1.96–1.88 (m, 1H), 0.99–0.81 ppm (m, 4H); **^{13}C NMR** (151 MHz, DMSO-d_6): δ = 172.1, 142.9, 140.0, 138.2, 136.2, 131.5, 130.8, 127.3, 123.2, 121.5, 118.2, 117.9, 112.0, 112.0, 48.2, 27.0, 13.2, 8.4 ppm; **HR-ESI-MS**: m/z = 446.0173 ([M + H]$^+$, calcd. for $C_{19}H_{17}{}^{79}BrN_3O_3S^+$: 446.0169), 448.0145 ([$M$ + H]$^+$, calcd. for $C_{19}H_{17}{}^{81}BrN_3O_3S^+$: 448.0148).

3-((5-Bromo-1-(cyclopropanecarbonyl)indoline)-6-sulfonamido)benzoic Acid (1u)

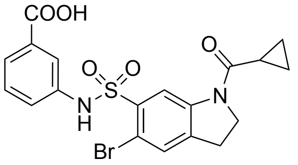

Sulfonamide **1u** was synthesized according to GP III using **SI-2** (32 mg, 88 µmol) and 3-aminobenzoic acid (12 µL, 88 µmol, 1.0 eq.). Purification of the product by flash column chromatography (SiO_2; cyclohexane/EtOAc/HOAc 1:1:0 → 49.5:49.5:1) afforded **1u** as an off-white amorphous solid (38 mg, 92%).

^{1}H NMR (600 MHz, DMSO-d_6): δ = 13.00 (s, 1H), 10.75 (s, 1H), 8.77 (s, 1H), 7.71 (d, J = 1.6 Hz, 1H), 7.63 (s, 1H), 7.56 (dt, J = 7.5, 1.4 Hz, 1H), 7.33 (tt, J = 4.7, 3.5 Hz, 2H), 4.30 (t, J = 7.6 Hz, 2H), 3.19 (t, J = 8.5 Hz, 2H), 1.96–1.84 (m, 1H), 0.95–0.80 ppm (m, 4H); **^{13}C NMR** (151 MHz, DMSO-d_6): δ = 172.0, 166.7, 142.8, 139.7, 137.4, 136.6, 131.8, 131.3, 129.5, 124.6, 123.1, 120.1, 118.1, 112.0, 48.1, 27.0, 13.2, 8.3 ppm; **HR-ESI-MS**: m/z = 465.0117 ([M + H]$^+$, calcd. for $C_{19}H_{18}{}^{79}BrN_2O_5S^+$: 465.0114), 467.0092 ([$M$ + H]$^+$, calcd. for $C_{19}H_{18}{}^{81}BrN_2O_5S^+$: 467.0094).

5-Bromo-1-(cyclopropanecarbonyl)-*N*-(1*H*-indol-5-yl)indoline-6-sulfonamide (1w)

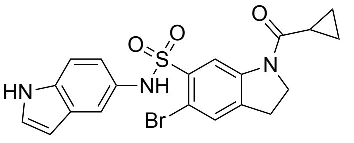

Sulfonamide **1w** was synthesized according to GP III using **SI-2** (35 mg, 96 µmol) and 1*H*-indol-5-amine (13 mg, 101 µmol, 1.1 eq.). Purification of the product by flash column chromatography (SiO_2; cyclohexane/EtOAc 4:1 → 2:1) afforded **1w** (44 mg, 99%) as an off-white amorphous solid.

^{1}H NMR (700 MHz, DMSO-d_6): δ = 11.06 (s, 1H), 9.93 (s, 1H), 8.68–8.58 (m, 1H), 7.62 (s, 1H), 7.28 (s, 1H), 7.22 (d, J = 8.6 Hz, 1H), 6.94–6.87 (m, 1H), 6.31 (s, 1H), 4.26 (s, 2H), 3.17 (t, J = 8.3 Hz, 2H), 3.11–3.01 (m, 1H), 1.91–1.83 (m, 1H), 0.90–0.78 ppm (m, 4H); **^{13}C NMR** (176 MHz, DMSO-d_6): δ = 171.8, 142.6, 139.0, 137.1, 133.6, 130.9, 128.0, 127.5, 126.3, 118.3, 117.0, 113.8, 112.2, 111.6, 101.1, 48.0, 26.9, 13.1, 8.2 ppm; **HR-ESI-MS**: m/z = 460.0337 ([M + H]$^+$, calcd. for $C_{20}H_{19}{}^{79}BrO_3N_3S^+$: 460.0325), 462.0315 ([$M$ + H]$^+$, calcd. for $C_{20}H_{19}{}^{81}BrO_3N_3S^+$: 462.0305).

5-Bromo-1-(cyclopropanecarbonyl)-*N*-(1*H*-indol-6-yl)indoline-6-sulfonamide (1x)

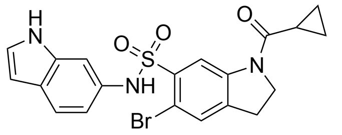

Sulfonamide **1x** was synthesized according to GP III using **SI-2** (35 mg, 96 µmol) and 1*H*-indol-6-amine (13 mg, 101 µmol, 1.1 eq.). Purification of the product by flash column chromatography (SiO_2; cyclohexane/EtOAc 4:1 → 2:1) afforded **1x** (44 mg, 99%) as an off-white amorphous solid.

^{1}H NMR (600 MHz, DMSO-d_6): δ = 11.02 (s, 1H), 10.12 (s, 1H), 8.69 (s, 1H), 7.61 (s, 1H), 7.34 (d, J = 8.5 Hz, 1H), 7.23 (t, J = 2.8 Hz, 1H), 7.20 (t, J = 0.8 Hz, 1H), 6.82 (dd, J = 8.5, 1.9 Hz, 1H), 6.29 (t, J = 2.0 Hz, 1H), 4.25 (t, J = 8.2 Hz, 2H), 3.16 (t, J = 8.5 Hz, 2H), 1.89 (m, 1H), 0.92–0.76 ppm (m, 4H); **^{13}C NMR** (151 MHz, DMSO- d_6): δ = 171.8, 142.7, 139.1, 137.0, 135.7, 131.0, 130.4, 125.5, 124.9, 120.2, 118.4, 114.0, 112.1, 104.1, 100.9, 48.1, 26.9, 13.1, 8.2 ppm; **HR-ESI-MS**: m/z = 460.0334 ($[M + H]^+$, calcd. for $C_{20}H_{19}{}^{79}BrN_3O_3S^+$: 460.0325), 462.0312 ($[M + H]^+$, calcd. for $C_{20}H_{19}{}^{81}BrN_3O_3S^+$: 462.0305).

1-(Cyclopropanecarbonyl)-*N*-(3-(trifluoromethyl)phenyl)indoline-5-sulfonamide (7)

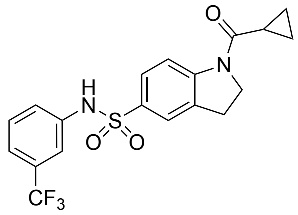

Sulfonamide **7** was synthesized according to GP III using **SI-3** (50 mg, 137 µmol) and 3-(trifluoromethyl)aniline (22 µL, 137 µmol, 1.0 eq.). Purification of the product by flash column chromatography (SiO_2; cyclohexane/EtOAc 4:1 → 2:1) afforded **7** (53 mg, 74%) as an off-white amorphous solid.

^{1}H NMR (600 MHz, DMSO-d_6): δ = 10.62 (s, 1H), 8.07 (d, J = 5.9 Hz, 1H), 7.64–7.57 (m, 2H), 7.47 (t, J = 7.9 Hz, 1H), 7.40–7.33 (m, 3H), 4.31 (t, J = 7.5 Hz, 2H), 3.19 (t, J = 8.5 Hz, 2H), 1.93 (dq, J = 12.5, 6.2 Hz, 1H), 0.86 ppm (t, J = 8.5 Hz, 4H); **^{13}C NMR** (151 MHz, DMSO-d_6): δ = 172.21, 146.9, 138.9, 133.5, 132.6, 130.6, 129.8 (q, J = 31.8 Hz), 127.1, 123.8 (q, J = 272.4 Hz), 123.3, 122.8, 120.1, 115.3, 115.2 (q, J = 3.8 Hz); 48.3, 26.8, 13.4, 8.3 ppm; **^{19}F NMR** (565 MHz, DMSO-d_6): δ = -61.47 ppm; **HR-ESI-MS**: m/z = 411.0982 ([M + H]$^+$, calcd. for $C_{19}H_{18}F_3N_2O_3S^+$: 411.0985).

1-Acetyl-5-bromo-*N*-(4-chloro-3-(trifluoromethyl)phenyl)indoline-6-sulfonamide (9)

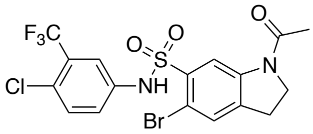

Sulfonamide **15k** was synthesized according to GP III using **SI-4** (750 mg, 2.2 mmol) and 4-chloro-3-(trifluoromethyl)aniline (455 mg, 2.3 mmol, 1.1 eq.). Purification of the product by flash column chromatography (SiO_2; cyclohexane/EtOAc 4:1 → 1:4) afforded **15k** (1.046 g, 95%) as an off-white amorphous solid.

^{1}H NMR (400 MHz, DMSO-d_6): δ = 11.17 (s, 1H), 8.79 (s, 1H), 7.66 (s, 1H), 7.62 (d, J = 8.8 Hz, 1H), 7.55 (d, J = 2.6 Hz, 1H), 7.34 (dd, J = 8.8, 2.5 Hz, 1H), 4.13 (t, J = 8.6 Hz, 2H), 3.18 (t, J = 8.6 Hz, 2H), 2.16 ppm (s, 3H); **^{13}C NMR** (126 MHz, DMSO-d_6): δ = 169.3, 142.8, 139.9, 136.8, 136.1, 132.7, 131.5, 127.20 (q, J = 30.8 Hz), 124.7, 123.2, 122.32 (q, J = 273.1 Hz), 117.6, 117.4 (q, J = 5.3 Hz), 112.0, 48.5, 27.1, 23.8 ppm; **^{19}F NMR** (377 MHz, DMSO-d_6): δ = -61.76 ppm; **HR-ESI-MS**: m/z = 496.9549 ([M + H]$^+$, calcd. for $C_{17}H_{14}{}^{79}BrClF_3N_2O_3S^+$: 496.9544), 498.9524 ([$M$ + H]$^+$, calcd. for $C_{17}H_{14}{}^{81}BrClF_3N_2O_3S^+$: 498.9523), 500.9493 ([$M$ + H]$^+$, calcd. for $C_{17}H_{14}{}^{81}BrClF_3N_2O_3S^+$: 500.9494).

1-Acetyl-5-bromo-*N*-(3-(trifluoromethyl)phenyl)indoline-6-sulfonamide (13k)

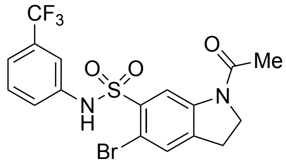

Sulfonamide **13k** was synthesized according to GP III using **SI-4** (70 mg, 206 µmol) and 3-(trifluoromethyl)aniline (26 µL, 206 µmol, 1.0 eq.). Purification of the product by flash column chromatography (SiO_2; cyclohexane/EtOAc 4:1 → 2:1) afforded **13k** (83 mg, 83%) as an off-white amorphous solid.

^{1}H NMR (600 MHz, DMSO-*d$_6$*): *δ* = 11.02 (s, 1H), 8.80 (s, 1H), 7.65 (s, 1H), 7.64–7.57 (m, 1H), 7.47 (dd, *J* = 10.8, 5.2 Hz, 2H), 7.42 (s, 1H), 7.36 (dd, *J* = 15.0, 8.3 Hz, 4H), 4.12 (t, *J* = 8.6 Hz, 2H), 3.17 (t, *J* = 8.7 Hz, 2H), 2.16 ppm (s, 3H); **^{13}C NMR** (151 MHz, DMSO-*d$_6$*): *δ* = 169.4, 142.8, 139.9, 138.8, 138.1, 136.3, 132.6, 131.4, 130.6, 130.0, 129.7, 127.1, 124.6, 123.3, 122.8, 122.1, 120.1, 117.8, 114.9, 112.0, 48.5, 27.1, 23.9 ppm; **^{19}F NMR** (565 MHz, DMSO-*d$_6$*): *δ* = -61.49 ppm; **HR-ESI-MS**: *m*/*z* = 462.9936 ([*M* + H]$^+$, calcd. for $C_{17}H_{15}{}^{79}BrF_3N_2O_3S^+$: 462.9933), 464.9911 ([*M* + H]$^+$, calcd. for $C_{17}H_{15}{}^{81}BrF_3N_2O_3S^+$: 464.9913).

1-Acetyl-5-bromo-*N*-(3,5-difluorophenyl)indoline-6-sulfonamide (SI-5)

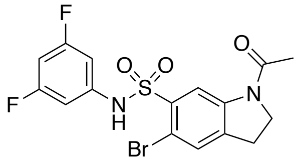

Sulfonamide **SI-5** was synthesized according to GP III using **SI-4** (500 mg, 1.5 mmol) and 3,5-difluoroaniline (286 mg, 2.2 mmol, 1.5 eq.). Purification of the product by flash column chromatography (SiO_2; cyclohexane/EtOAc 4:1 → 1:4) afforded **SI-5** (450 g, 71%) as an off-white amorphous solid.

^{1}H NMR (600 MHz, DMSO-*d$_6$*) δ 11.20 (s, 1H), 8.80 (s, 1H), 7.66 (s, 1H), 6.86 (tt, *J* = 9.2, 2.1 Hz, 1H), 6.73 (dd, *J* = 7.7, 6.0 Hz, 2H), 4.13 (t, *J* = 8.6 Hz, 2H), 3.18 (t, *J* = 8.6 Hz, 2H), 2.16 ppm (s, 3H); **^{13}C NMR** (151 MHz, DMSO-*d$_6$*): *δ* = 169.5, 162.6 (dd, *J* = 244.9, 15.4 Hz), 142.8, 140.1, 140.0 (t, *J* = 13.5 Hz), 136.0, 131.6, 117.7, 112.1, 101.6–100.9 (m), 98.7 (t, *J* = 26.1 Hz), 48.5, 27.1, 23.9 ppm; **^{19}F NMR** (565 MHz, DMSO-*d$_6$*) δ -108.21 ppm (t, *J* = 8.9 Hz); **HR-ESI-MS**: *m*/*z* = 430.9862 ([*M* + H]$^+$, calcd. for $C_{16}H_{14}{}^{79}BrF_2N_2O_3S^+$: 430.9871), 432.9838 ([*M* + H]$^+$, calcd. for $C_{16}H_{14}{}^{81}BrF_2N_2O_3S^+$: 432.9851).

General Procedure IV – Saponification of N-Acetylated Indolines

To a solution of the *N*-acetylindoline (2 mmol) in MeOH (10 mL) under an argon atmosphere, a 40% w/v aq. NaOH solution (10 mL) was added. The mixture was heated to reflux for 8 h and the organic solvent evaporated. The resulting solution was neutralized with an aq. 1 M HCl solution and extracted with EtOAc (5 x 30 mL). The combined organic layers were dried over $MgSO_4$, filtered, and concentrated under reduced pressure. The crude product was either used in the next step without further purification of purified by flash column chromatography (SiO_2; cyclohexane/EtOAc mixture).

5-Bromo-*N*-(4-chloro-3-(trifluoromethyl)phenyl)indoline-6-sulfonamide (11)

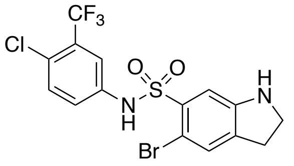

Indoline **11** was prepared according to GP IV using **15k** (1.000 g, 2.0 mmol). Purification by flash column chromatography (SiO_2; EtOAc in cyclohexane 14%) afforded **11** (803 mg, 88%) as an off-white amorphous solid.

^{1}H NMR (600 MHz, DMSO-*d*$_6$) δ 10.97 (br. s, 1H), 7.61 (d, J = 8.8 Hz, 1H), 7.52 (d, J = 2.6 Hz, 1H), 7.36–7.29 (m, 2H), 7.13 (s, 1H), 6.17 (br. s, 1H), 3.48 (t, J = 8.8 Hz, 2H), 2.96 ppm (t, J = 8.7 Hz, 2H); **^{13}C NMR** (151 MHz, DMSO-*d*$_6$): δ = 152.5, 137.1, 136.9, 135.9, 132.7, 130.5, 127.14 (q, J = 30.8 Hz), 124.4, 123.0, 122.41 (q, J = 273.2 Hz), 117.08 (q, J = 5.5 Hz), 109.2, 103.7, 46.5, 28.6 ppm; **^{19}F NMR** (565 MHz, DMSO-*d*$_6$) δ -61.73 ppm; **HR-ESI-MS**: m/z = 454.9437 ([M + H]$^+$, calcd. for $C_{15}H_{12}{}^{79}BrClF_3N_2O_2S^+$: 454.9438), 456.9411 ([$M$ + H]$^+$, calcd. for $C_{15}H_{12}{}^{81}BrClF_3N_2O_2S^+$: 456.9409), 458.9381 ([$M$ + H]$^+$, calcd. for $C_{15}H_{12}{}^{81}Br^{37}ClF_3N_2O_2S^+$: 458.9388).

5-Bromo-*N*-(3-(trifluoromethyl)phenyl)indoline-6-sulfonamide (12)

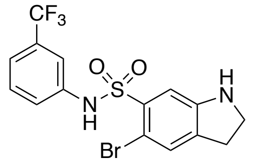

Indoline **12** was prepared according to GP IV using **13k** (200 mg, 432 µmol), and used in the next step without further purification.

^{1}H NMR (400 MHz, $CDCl_3$): δ = 7.37–7.31 (m, J = 1.5 Hz, 5H), 7.30 (s, 1H), 3.64 (t, J = 8.6 Hz, 2H), 3.05 ppm (t, J = 8.5 Hz, 2H); **HR-ESI-MS**: m/z = 419.9750 ([M + H]$^+$, calcd. for $C_{15}H_{12}{}^{79}BrF_3N_2O_2S^+$: 419.9750), 422.9801 ([$M$ + H]$^+$, calcd. for $C_{15}H_{12}{}^{81}BrF_3N_2O_2S^+$: 422.9807).

5-Bromo-*N*-(3,5-difluorophenyl)indoline-6-sulfonamide (SI-6)

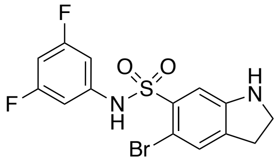

Indoline **SI-6** was prepared according to GP IV using **SI-5** (200 mg, 464 µmol). Purification by flash column chromatography (SiO_2; EtOAc in cyclohexane 14%) afforded **SI-6** (177 mg, 98%) as an off-white amorphous solid.

^{1}**H NMR** (400 MHz, DMSO-d_6): δ = 10.97 (br. s, 1H), 7.34 (s, 1H), 7.17 (s, 1H), 6.85 (tt, J = 9.4, 2.3 Hz, 1H), 6.77–6.66 (m, 2H), 6.16 (br. s, 1H), 3.49 (t, J = 8.7 Hz, 2H), 2.97 ppm (t, J = 8.7 Hz, 2H); ^{13}**C NMR** (101 MHz, DMSO-d_6): δ = 161.4, 152.5, 136.9, 135.9, 130.5, 109.3, 103.8, 101.1, 100.9, 98.7, 98.4, 46.5, 28.6 ppm; **ESI-MS**: m/z = 389.0 ([M + H]$^+$, calcd. for $C_{14}H_{12}{}^{79}BrF_2N_2O_2S^+$: 389.0); 391.0 ([$M$ + H]$^+$, calcd. for $C_{14}H_{12}{}^{81}BrF_2N_2O_2S^+$: 391.0).

General Procedure V-A – *N*-Acylation of Sulfonamido Indolines

To a solution of the indoline (0.66 µmol), the acid (1.5–3.0 eq.), and DIPEA (2–5 eq.) in EtOAc (1 mL) at 0 °C under an argon atmosphere, a solution of T3P in EtOAc (50% v/v, 1.5–3.0 eq.) was added. The solution was allowed to warm to rt and stirred for 16 h. The mixture was diluted with EtOAc (15 mL) and washed with sat. aq. $NaHCO_3$ (1 x 15 mL), an aq. 1 M HCl solution (1 x 15 mL), and brine (2 x 15 mL). The organic layer was dried over $MgSO_4$, filtered, and concentrated under reduced pressure. The product was purified by flash column chromatography (SiO_2; cyclohexane/EtOAc mixture).

General Procedure V-B – *N*-Acylation of Sulfonamido Indolines

To a solution of the acid (4.0 eq.) in DMF (1 mL), PyBOP (2.2 eq.), DMAP (2.2 eq.) and DIPEA (8.0 eq.) were successively added. After 10 min preactivation, the mixture was added to a solution of the indoline (59 µmol) in DMF (1 mL). The mixture was stirred at rt for 16 h. The mixture was concentrated to a minimum volume *in vacuo*, diluted in EtOAc (15 mL), and washed with sat. aq. $NaHCO_3$ (1 x 15 mL), an aq. 1 M HCl solution (1 x 15 mL), and brine (2 x 15 mL). The organic layer was dried over $MgSO_4$, concentrated, and the product was purified by flash column chromatography or preparative HPLC.

5-Bromo-1-isobutyryl-*N*-(3-(trifluoromethyl)phenyl)indoline-6-sulfonamide (13c)

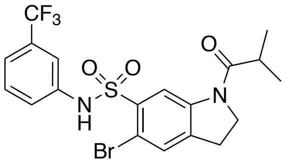

Acyl indoline **13c** was prepared according to GP V-B using **12** (10 mg, 24 µmol) and isobutyric acid (9 µL, 95 µmol, 4.0 eq.). Purification of the product by preparative HPLC afforded **13c** (7 mg, 57%) as an off-white amorphous solid.

^{1}H NMR (600 MHz, DMSO-*d$_6$*): δ = 11.01 (s, 1H), 8.90 (s, 1H), 7.65 (s, 1H), 7.48 (t, J = 8.0 Hz, 1H), 7.42 (s, 1H), 7.36 (t, J = 8.7 Hz, 2H), 4.20 (t, J = 8.5 Hz, 2H), 3.18 (t, J = 8.5 Hz, 2H), 2.85–2.76 (m, 1H), 1.09 ppm (d, J = 6.7 Hz, 6H); **^{13}C NMR** (151 MHz, DMSO-*d$_6$*): δ = 175.8, 143.1, 140.0, 138.1, 136.2, 131.3, 130.6, 129.8 (q, J = 31.9 Hz), 123.7 (q, J = 272.4 Hz), 122.2, 120.0 (q, J = 3.5 Hz), 118.3, 115.0, 112.1, 47.8, 32.5, 27.2, 18.8 ppm; **^{19}F NMR** (565 MHz, DMSO-*d$_6$*): δ = -61.53 ppm; **HR-ESI-MS**: m/z = 491.0254 ($[M + H]^+$, calcd. for $C_{19}H_{19}{}^{79}BrF_3N_2O_3S^+$: 491.0246), 493.0229 ($[M + H]^+$, calcd. for $C_{19}H_{19}{}^{81}BrF_3N_2O_3S^+$: 493.0226).

5-Bromo-1-(cyclobutanecarbonyl)-*N*-(3-(trifluoromethyl)phenyl)indoline-6-sulfonamide (13d)

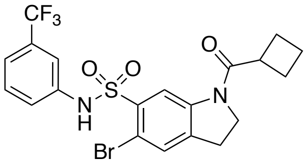

Acyl indoline **13d** was prepared according to GP V-A using **12** (25 mg, 59 µmol), cyclobutane carboxylic acid (9 µL, 89 µmol, 1.5 eq.), DIPEA (21 µL, 119 µmol, 2.0 eq.), and T3P (53 µL, 89 µmol, 1.5 eq.). Purification by preparative HPLC afforded **13d** (14 mg, 44%) as an off-white amorphous solid.

^{1}H NMR (600 MHz, DMSO-d_6): δ = 11.01 (s, 1H), 8.87 (s, 1H), 7.64 (s, 1H), 7.48 (t, J = 8.0 Hz, 1H), 7.42 (s, 1H), 7.35 (t, J = 9.1 Hz, 2H), 4.02 (t, J = 8.6 Hz, 2H), 3.43 (p, J = 8.4 Hz, 1H), 3.16 (t, J = 8.5 Hz, 2H), 2.30–2.21 (m, 2H), 2.20–2.12 (m, 2H), 2.00–1.90 (m, 1H), 1.85–1.75 ppm (m, 1H); **^{13}C NMR** (151 MHz, DMSO-d_6): δ = 173.0, 143.0, 139.8, 138.1, 136.3, 131.4, 130.6, 129.8 (q, J = 31.8 Hz), 123.8 (q, J = 272.4 Hz), 122.1, 120.0, 118.0, 115.0 (q, J = 3.8 Hz), 112.0, 47.2, 38.4, 27.2, 23.9, 17.3 ppm; **^{19}F NMR** (565 MHz, DMSO-d_6): δ = -61.50 ppm; **HR-ESI-MS**: m/z = 503.0249 ([M + H]$^+$, calcd. for $C_{20}H_{19}{}^{79}BrF_3N_2O_3S^+$: 503.0247), 505.0223 ([$M$ + H]$^+$, calcd. for $C_{20}H_{19}{}^{81}BrF_3N_2O_3S^+$: 505.0226).

5-Bromo-1-(cyclopentanecarbonyl)-*N*-(3-(trifluoromethyl)phenyl)indoline-6-sulfonamide (13f)

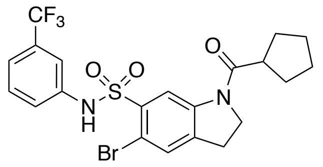

Acyl indoline **13f** was prepared according to GP V-A using **12** (25 mg, 59 µmol), cyclopentane carboxylic acid (19 µL, 178 µmol, 3.0 eq.), DIPEA (52 µL, 297 µmol, 5.0 eq.), and T3P (106 µL, 178 µmol, 3.0 eq.). Purification by preparative HPLC afforded **13f** (14 mg, 45%) as an off-white amorphous solid.

^{1}H NMR (600 MHz, DMSO-d_6): δ = 11.00 (s, 1H), 8.88 (s, 1H), 7.64 (s, 1H), 7.47 (t, J = 8.0 Hz, 1H), 7.41 (d, J = 14.8 Hz, 1H), 7.35 (t, J = 8.3 Hz, 2H), 4.19 (t, J = 8.5 Hz, 2H), 3.18 (t, J = 8.5 Hz, 2H), 3.00 (p, J = 7.8 Hz, 1H), 1.87 (td, J = 12.0, 7.5 Hz, 2H), 1.79–1.71 (m, 2H), 1.70–1.62 (m, 2H), 1.61–1.52 ppm (m, 2H); **^{13}C NMR** (151 MHz, DMSO-d_6): δ = 174.9, 143.1, 140.0, 138.1, 136.2, 131.3, 130.6, 129.8 (q, J = 31.8 Hz), 123.7 (q, J = 272.4 Hz), 122.2, 120.0 (q, J = 3.7 Hz), 118.2, 115.0 (q, J = 3.8 Hz), 112.0, 48.0, 43.1, 29.3, 27.1, 25.7 ppm; **^{19}F NMR** (565 MHz, DMSO-d_6): δ = -64.66 ppm; **HR-ESI-MS**: m/z = 517.0404 ([M + H]$^+$, calcd. for $C_{21}H_{21}{}^{79}BrF_3N_2O_3S^+$: 517.0403), 519.0383 ([$M$ + H]$^+$, calcd. for $C_{21}H_{21}{}^{81}BrF_3N_2O_3S^+$: 519.0382).

5-Bromo-1-(2-cyclopropylacetyl)-*N*-(3-(trifluoromethyl)phenyl)indoline-6-sulfonamide (13i)

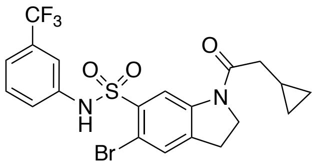

Acyl indoline **13i** was prepared according to GP V-B using **12** (25 mg, 59 µmol) and 2-cyclopropylacetic acid (44 µL, 474 µmol, 4.0 eq.). After 16 h, only partial conversion was observed, hence a further 4.0 eq of 2-cyclopropylacetic acid, 2.2 eq. of PyBOP, 2.2 eq. of DMAP, and 8 eq. of DIPEA were added, and the mixture was stirred for a further 24 h. Purification of the product by preparative HPLC afforded **13i** (13 mg, 42%) as an off-white amorphous solid.

^{1}H NMR (600 MHz, DMSO-d_6): δ = 11.01 (s, 1H), 8.87 (s, 1H), 7.64 (s, 1H), 7.48 (t, J = 8.0 Hz, 1H), 7.43 (s, 1H), 7.36 (t, J = 8.6 Hz, 2H), 4.08 (t, J = 8.6 Hz, 2H), 3.16 (t, J = 8.5 Hz, 2H), 2.40 (d, J = 6.7 Hz, 2H), 1.11–0.97 (m, 1H), 0.54–0.44 (m, 2H), 0.21–0.09 ppm (m, 2H); **^{13}C NMR** (151 MHz, DMSO-d_6): δ = 171.5, 142.9, 139.8, 138.1, 136.3, 131.4, 130.6, 129.9 (q, J = 31.8 Hz), 123.7 (q, J = 272.4 Hz), 122.1, 120.0 (q, J = 3.6 Hz), 117.9, 115.0, 111.9, 47.8, 39.9, 27.1, 6.3, 4.2 ppm; **^{19}F NMR** (565 MHz, DMSO-d_6): δ = -61.49 ppm; **HR-ESI-MS**: m/z = 503.0235 ($[M + H]^+$, calcd. for $C_{20}H_{19}{}^{79}BrF_3N_2O_3S^+$: 503.0246), 505.0211 ($[M + H]^+$, calcd. for $C_{20}H_{19}{}^{81}BrF_3N_2O_3S^+$: 505.0226).

5-Bromo-1-propionyl-*N*-(3-(trifluoromethyl)phenyl)indoline-6-sulfonamide (13l)

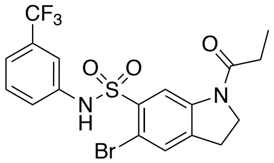

To a solution of **12** (25 mg, 59 µmol) and Et_3N (43 µL, 237 µmol, 4.0 eq.) in CH_2Cl_2 (1.5 mL) under an argon atmosphere, DMAP (1 mg, 7 µmol, 0.1 eq.) was added. The solution was cooled to 0 °C and propionic acid anhydride (15 µL, 0.1 mmol, 2.0 eq.) was added. After stirring for 10 min at 0 °C and 16 h at rt, EtOAc was added (30 mL), and the mixture was washed with sat. aq. $NaHCO_3$ (1 x 15 mL), an aq. 1 M HCl solution (1 x 15 mL) and brine (2 x 15 mL). The organic layer was dried over $MgSO_4$, filtered, and concentrated under reduced pressure. Purification of the product by flash column chromatography (SiO_2; cyclohexane/EtOAc 4:1 → 2:1) afforded **13l** (6 mg, 20%) as an off-white amorphous solid.

^{1}H NMR (400 MHz, CD_3OD): δ = 8.96 (s, 1H), 7.57 (s, 1H), 7.46–7.39 (m, 2H), 7.37 (t, *J* = 7.7 Hz, 1H), 7.27 (d, *J* = 7.3 Hz, 1H), 4.14 (t, *J* = 8.6 Hz, 2H), 3.22 (t, *J* = 8.6 Hz, 2H), 2.51 (q, *J* = 7.2 Hz, 2H), 1.18 ppm (t, *J* = 7.4 Hz, 3H); **HR-ESI-MS**: *m*/*z* = 477.0093 ([*M* + H]$^+$, calcd. for $C_{18}H_{17}{}^{79}BrF_3N_2O_3S^+$: 477.0090), 479.0072 ([*M* + H]$^+$, calcd. for $C_{18}H_{17}{}^{81}BrF_3N_2O_3S^+$: 479.0069).

1-Benzoyl-5-bromo-*N*-(4-chloro-3-(trifluoromethyl)phenyl)indoline-6-sulfonamide (15b)

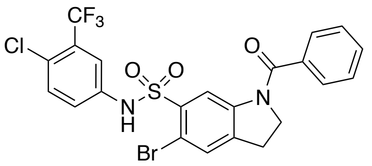

Acyl indoline **15b** was prepared according to GP V-A using **11**, (30 mg, 66 µmol), benzoic acid (12 mg, 99 µmol, 1.5 eq.), DIPEA (23 µL, 132 µmol, 2.0 eq.), and T3P (59 µL, 99 µmol, 1.5 eq.). Purification by flash column chromatography (SiO_2; EtOAc in cyclohexane 15.0 → 17.5%) afforded **15b** (24 mg, 65%) as an off-white amorphous solid.

^{1}H NMR (600 MHz, DMSO-*d*$_6$): δ = 11.19 (s, 1H), 7.74 (s, 1H), 7.65 (d, *J* = 8.8 Hz, 1H), 7.64–7.45 (m, 7H), 7.44– 7.24 (m, 1H), 4.05 (t, *J* = 8.4 Hz, 2H), 3.14 ppm (t, *J* = 8.3 Hz, 2H); **^{19}F NMR** (565 MHz, DMSO-*d*$_6$): δ = -61.75 ppm; **HR-ESI-MS**: *m*/*z* = 558.9717 ([*M* + H]$^+$, calcd. for $C_{22}H_{16}{}^{79}BrClF_3N_2O_3S^+$: 558.9700), 560.9693 ([*M* + H]$^+$, calcd. for $C_{22}H_{16}{}^{81}BrClF_3N_2O_3S^+$: 560.9680), 562.9657 ([*M* + H]$^+$, calcd. for $C_{22}H_{16}{}^{81}Br^{37}ClF_3N_2O_3S^+$: 562.9650).

5-Bromo-*N*-(4-chloro-3-(trifluoromethyl)phenyl)-1-isobutyrylindoline-6-sulfonamide (15c)

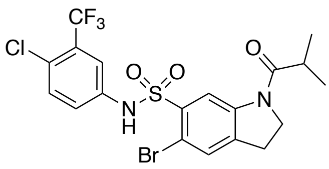

Acyl indoline **15c** was prepared according to GP V-A using **11**, (30 mg, 66 µmol), isobutyric acid (9 µL, 99 µmol, 1.5 eq.), DIPEA (23 µL, 132 µmol, 2.0 eq.), and T3P (59 µL, 99 µmol, 1.5 eq.). Purification by flash column chromatography (SiO_2; cyclohexane/EtOAc 4:1 → 2:1) afforded **15c** (13 mg, 39%) as an amorphous off-white solid.

^{1}H NMR (400 MHz, DMSO-*d$_6$*): δ = 11.15 (br. s, 1H), 8.88 (br. s, 1H), 7.67 (s, 1H), 7.62 (d, *J* = 8.8 Hz, 1H), 7.56 (d, *J* = 2.6 Hz, 1H), 7.35 (dd, *J* = 8.8, 2.6 Hz, 1H), 4.21 (t, *J* = 8.5 Hz, 2H), 3.19 (t, *J* = 8.5 Hz, 2H), 2.80 (sep, *J* = 6.7 Hz, 1H), 1.10 ppm (d, *J* = 6.7 Hz, 6H); **^{13}C NMR** (101 MHz, DMSO-*d$_6$*): δ = 175.8, 143.1, 140.2, 136.9, 136.1, 132.8, 131.4, 127.4, 127.1, 124.8, 123.4, 118.1, 117.6, 117.6, 112.0, 47.8, 32.5, 27.2, 18.8 ppm; ^{19}F NMR (377 MHz, DMSO-*d$_6$*) : δ = -61.79 ppm; **HR-ESI-MS**: *m*/*z* = 524.98652 ([*M* + H]$^+$, calcd. for $C_{19}H_{18}{}^{79}BrClF_3N_2O_3S^+$: 524.98566), 526.9838 ([*M* + H]$^+$, calcd. for $C_{19}H_{18}{}^{81}BrClF_3N_2O_3S^+$: 526.9836), 528.9808 ([*M* + H]$^+$, calcd. for $C_{19}H_{18}{}^{81}Br^{37}ClF_3N_2O_3S^+$: 528.9807).

5-Bromo-*N*-(4-chloro-3-(trifluoromethyl)phenyl)-1-(cyclobutanecarbonyl)indoline-6-sulfonamide (15d)

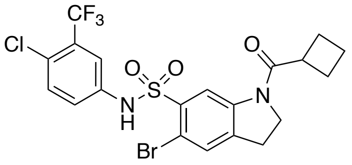

Acyl indoline **15d** was prepared according to GP V-A using **11** (30 mg, 66 µmol), cyclobutane carboxylic acid (9 µL, 99 µmol, 1.5 eq.), DIPEA (23 µL, 132 µmol, 2.0 eq.), and T3P (59 µL, 99 µmol, 1.5 eq.). After 16 h, only partial conversion was observed, so a further 1.5 eq. of cyclobutane carboxylic acid, 4.0 eq. of DIPEA, and 1.5 eq. of T3P were added, and the mixture was stirred for a further 24 h. Purification by preparative HPLC afforded **15d** (25 mg, 72%) as an off-white amorphous solid.

^{1}H NMR (600 MHz, DMSO-*d$_6$*): δ = 11.16 (s, 1H), 8.85 (s, 1H), 7.65 (s, 1H), 7.62 (d, *J* = 8.8 Hz, 1H), 7.56 (d, *J* = 2.6 Hz, 1H), 7.36 (dd, *J* = 8.8, 2.6 Hz, 1H), 4.02 (t, *J* = 8.6 Hz, 2H), 3.43 (p, *J* = 8.3 Hz, 1H), 3.17 (t, *J* = 8.5 Hz, 2H), 2.25 (qd, *J* = 9.1, 2.1 Hz, 2H), 2.21–2.12 (m, 2H), 2.03–1.89 (m, 1H), 1.86–1.75 ppm (m, 1H); **^{13}C NMR** (151 MHz, DMSO-*d$_6$*): δ = 173.1, 143.1, 140.0, 136.9, 136.1, 132.8, 131.5, 127.9-126.6 (q, *J* = 30.9 Hz), 124.8, 123.3, 122.4 (q, *J* = 272.9 Hz), 117.8, 117.6 (q, *J* = 5.3 Hz), 112.0, 47.2, 38.4, 27.2, 23.9, 17.3 ppm; **^{19}F NMR** (565 MHz, DMSO-*d$_6$*): δ = -61.78 ppm; **HR-ESI-MS**: *m*/*z* = 536.9865 ([*M* + H]$^+$, calcd. for $C_{20}H_{18}{}^{79}BrClF_3N_2O_3S^+$: 536.9857), 538.9841 ([*M* + H]$^+$, calcd. for $C_{20}H_{18}{}^{81}BrClF_3N_2O_3S^+$: 538.9836), 540.9807 ([*M* + H]$^+$, calcd. for $C_{20}H_{18}{}^{81}Br^{37}ClF_3N_2O_3S^+$: 540.9807).

5-Bromo-*N*-(4-chloro-3-(trifluoromethyl)phenyl)-1-(furan-2-carbonyl)indoline-6-sulfonamide (15e)

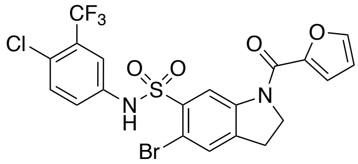

Acyl indoline **15e** was prepared according to GP V-A using **11**, (30 mg, 66 μmol), furan-2-carboxylic acid (11 mg, 99 μmol, 1.5 eq.), DIPEA (23 μL, 132 μmol, 2.0 eq.), and T3P (59 μL, 99 μmol, 1.5 eq.). Purification by flash column chromatography (SiO_2; EtOAc in cyclohexane 15 → 30%) afforded **15e** (26 mg, 73%) as a brown amorphous solid.

^{1}H NMR (600 MHz, DMSO- *d*$_6$): δ = 11.22 (br. s, 1H), 8.89 (s, 1H), 8.00 (dd, *J* = 1.6, 0.6 Hz, 1H), 7.74 (s, 1H), 7.62 (d, *J* = 8.8 Hz, 1H), 7.57 (d, *J* = 2.6 Hz, 1H), 7.36 (dd, *J* = 8.8, 2.6 Hz, 1H), 7.33 (dd, *J* = 3.6, 0.5 Hz, 1H), 6.74 (dd, *J* = 3.6, 1.7 Hz, 1H), 4.48 (t, *J* = 8.5 Hz, 2H), 3.26 (t, *J* = 8.4 Hz, 2H); **^{13}C NMR** (151 MHz, DMSO- *d*$_6$): δ = 157.0, 146.8, 146.4, 143.2, 140.4, 136.9, 136.1, 132.8, 131.6, 127.2 (q, *J* = 30.8 Hz), 124.7, 123.2, 122.4 (q, *J* = 273.2 Hz), 118.9, 117.9, 117.5 (q, *J* = 5.4 Hz), 112.9, 112.1, 49.5, 27.8 ppm; **^{19}F NMR** (565 MHz, DMSO- *d*$_6$): δ = -61.76 ppm; **HR-ESI-MS**: *m*/*z* = 548.9508 ([*M* + H]$^+$, calcd. for $C_{20}H_{14}O_4N_2{}^{79}BrClF_3S^+$: 548.9493), 550.9483 ([*M* + H]$^+$, calcd. for $C_{20}H_{14}O_4N_2{}^{81}BrClF_3S^+$: 550.9472), 552.9454 ([*M* + H]$^+$, calcd. for $C_{20}H_{14}O_4N_2{}^{81}Br^{37}ClF_3S^+$: 552.9443).

5-Bromo-*N*-(4-chloro-3-(trifluoromethyl)phenyl)-1-(cyclopentanecarbonyl)indoline-6-sulfonamide (15f)

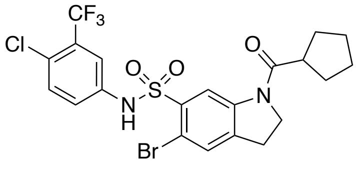

Acyl indoline **15f** was prepared according to GP V-A using **11**, (30 mg, 66 μmol), cyclopentane carboxylic acid (11 μL, 99 μmol, 1.5 eq.), DIPEA (23 μL, 132 μmol, 2.0 eq.), and T3P (59 μL, 99 μmol, 1.5 eq.). After 16 h, only partial conversion was observed, hence a further 1.5 eq. of cyclopentane carboxylic acid, 2.0 eq. of DIPEA, and 1.5 eq. of T3P were added, and the mixture was stirred for a further 24 h. Purification by flash column chromatography (SiO_2; cyclohexane/EtOAc 4:1 → 2:1) afforded **15f** (18 mg, 50%) as an off-white amorphous solid.

^{1}H NMR (400 MHz, DMSO-*d_6*): δ = 11.15 (s, 1H), 8.86 (s, 1H), 7.66 (s, 1H), 7.61 (d, *J* = 8.8 Hz, 1H), 7.55 (d, *J* = 2.6 Hz, 1H), 7.35 (dd, *J* = 8.8, 2.6 Hz, 1H), 4.20 (t, *J* = 8.5 Hz, 2H), 3.19 (t, *J* = 8.5 Hz, 2H), 3.09–2.94 (m, 1H), 1.95–1.83 (m, 2H), 1.81–1.63 (m, 4H), 1.63–1.51 ppm (m, 2H); **^{13}C NMR** (101 MHz, DMSO-*d_6*): δ = 175.0, 143.2, 140.1, 136.9, 136.1, 132.8, 131.4, 127.2 (q, *J* = 31.0 Hz), 124.7, 123.4, 122.4 (q, *J* = 273.1 Hz), 118.0, 117.6 (q, *J* = 6.0 Hz), 112.0, 48.0, 43.1, 29.3, 27.2, 25.7 ppm; **^{19}F NMR** (377 MHz, DMSO-*d_6*): δ = -61.79 ppm; **HR-ESI-MS**: *m*/*z* = 520.9540 ($[M + H]^+$, calcd. for $C_{19}H_{14}{}^{79}BrClF_3N_2O_3S^+$: 520.9544), 522.9517 ($[M + H]^+$, calcd. for $C_{19}H_{14}{}^{81}BrClF_3N_2O_3S^+$: 522.9514), 524.9487 ($[M + H]^+$, calcd. for $C_{19}H_{14}{}^{81}Br^{37}ClF_3N_2O_3S^+$: 524.9494).

5-Bromo-*N*-(4-chloro-3-(trifluoromethyl)phenyl)-1-(furan-3-carbonyl)indoline-6-sulfonamide (15g)

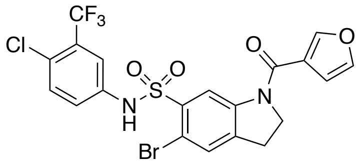

Acyl indoline **15g** was prepared according to GP V-A using **11**, (30 mg, 66 µmol), 1*H*-pyrrole-2-carboxylic acid (11 mg, 99 µmol, 1.5 eq.), DIPEA (23 µL, 132 µmol, 2.0 eq.), and T3P (59 µL, 99 µmol, 1.5 eq.). Purification by flash column chromatography (SiO_2; EtOAc in cyclohexane 15 → 30%) afforded **15g** (25 mg, 70%) as a brown amorphous solid.

^{1}H NMR (600 MHz, DMSO-*d_6*): δ = 11.20 (br. s, 1H), 8.89 (br. s, *J* = 34.1 Hz, 1H), 8.35 (s, 1H), 7.83 (t, *J* = 1.6 Hz, 1H), 7.72 (s, 1H), 7.63 (d, *J* = 8.8 Hz, 1H), 7.57 (d, *J* = 2.6 Hz, 1H), 7.37 (dd, *J* = 8.8, 2.6 Hz, 1H), 6.89 (d, *J* = 1.1 Hz, 1H), 4.34 (t, *J* = 8.5 Hz, 2H), 3.24 ppm (t, *J* = 8.4 Hz, 2H); **^{13}C NMR** (151 MHz, DMSO-*d_6*): δ = 161.7, 145.7, 143.8, 143.1, 140.5, 136.9, 136.1, 132.8, 131.6, 127.3 (q, *J* = 30.9 Hz), 124.8, 122.4 (q, *J* = 273.2 Hz), 123.2, 121.9, 118.6, 117.6 (q, *J* = 5.4 Hz), 112.7, 110.8, 49.5, 27.6 ppm; **^{19}F NMR** (565 MHz, DMSO-*d_6*): δ = -61.76 ppm; **HR-ESI-MS**: *m*/*z* = 548.9510 ($[M + H]^+$, calcd. for $C_{20}H_{14}O_4N_2{}^{79}BrClF_3S^+$: 548.9493), 550.9486 ($[M + H]^+$, calcd. for $C_{20}H_{14}O_4N_2{}^{81}BrClF_3S^+$: 550.9472), 552.9455 ($[M + H]^+$, calcd. for $C_{20}H_{14}O_4N_2{}^{81}Br^{37}ClF_3S^+$: 552.9443)

5-Bromo-*N*-(4-chloro-3-(trifluoromethyl)phenyl)-1-(2-cyclopropylacetyl)indoline-6-sulfonamide (15i)

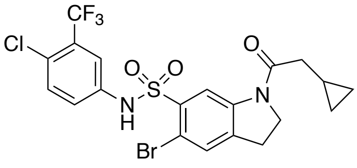

Acyl indoline **15i** was prepared according to GP V-A using **11**, (30 mg, 66 µmol), 2-cyclopropylacetic acid (9 µL, 99 µmol, 1.5 eq.), DIPEA (23 µL, 132 µmol, 2.0 eq.), and T3P (59 µL, 99 µmol, 1.5 eq.). Purification by flash column chromatography (SiO_2; cyclohexane/EtOAc 4:1 → 2:1) afforded **15i** (22 mg, 63%) as an off-white amorphous solid.

^{1}H NMR (400 MHz, DMSO-d_6): δ = 11.16 (s, 1H), 8.86 (s, 1H), 7.66 (s, 1H), 7.62 (d, J = 8.8 Hz, 1H), 7.56 (d, J = 2.6 Hz, 1H), 7.35 (dd, J = 8.8, 2.6 Hz, 1H), 4.09 (t, J = 8.6 Hz, 2H), 3.17 (t, J = 8.5 Hz, 2H), 2.40 (d, J = 6.7 Hz, 2H), 1.12–0.97 (m, 1H), 0.60–0.42 (m, 2H), 0.24–0.07 ppm (m, 2H); **^{13}C NMR** (101 MHz, DMSO-d_6): δ = 171.5, 143.0, 139.9, 136.9, 136.1, 132.8, 131.5, 127.2 (q, J = 31.0 Hz), 124.8, 123.3, 122.4 (q, J = 273.2 Hz), 117.7, 117.6 (q, J = 5.4 Hz), 111.9, 47.8, 39.9, 27.1, 6.3, 4.1 ppm; **^{19}F NMR** (377 MHz, DMSO-d_6): δ = -61.76 ppm; **HR-ESI-MS**: m/z = 536.98667 ($[M + H]^+$, calcd. for $C_{20}H_{18}{}^{79}BrClF_3N_2O_3S^+$: 536.9857), 538.9840 ($[M + H]^+$, calcd. for $C_{20}H_{18}{}^{81}BrClF_3N_2O_3S^+$: 538.9836), 540.9810 ($[M + H]^+$, calcd. for $C_{20}H_{18}{}^{81}Br^{37}ClF_3N_2O_3S^+$: 540.9807).

5-Bromo-*N*-(4-chloro-3-(trifluoromethyl)phenyl)-1-(1*H*-pyrrole-2-carbonyl)indoline-6-sulfonamide (15j)

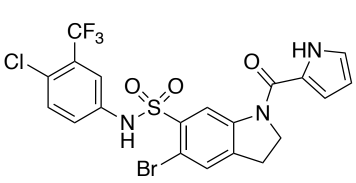

Acyl indoline **15j** was prepared according to GP V-A using **11**, (30 mg, 66 µmol), 1*H*-pyrrole-2-carboxylic acid (11 mg, 99 µmol, 1.5 eq.), DIPEA (23 µL, 132 µmol, 2.0 eq.), and T3P (59 µL, 99 µmol, 1.5 eq.). Purification by flash column chromatography (SiO_2; EtOAc in cyclohexane 14 → 25%) afforded **15j** (21 mg, 58%) as a brown amorphous solid.

^{1}H NMR (600 MHz, DMSO- *d$_6$*): δ = 11.76 (br. s, 1H), 11.19 (br. s, 1H), 8.98 (s, 1H), 7.70 (s, 1H), 7.61 (d, *J* = 8.8 Hz, 1H), 7.55 (d, *J* = 2.5 Hz, 1H), 7.35 (dd, *J* = 8.8, 2.5 Hz, 1H), 7.10–7.04 (m, 1H), 6.86–6.80 (m, 1H), 6.24 (dt, *J* = 3.7, 2.4 Hz, 1H), 4.43 (t, *J* = 8.5 Hz, 2H), 3.27 ppm (t, *J* = 8.4 Hz, 2H); **^{13}C NMR** (151 MHz, DMSO- *d$_6$*): δ = 159.8, 143.9, 140.2, 136.9, 136.0, 132.8, 131.4, 127.2 (q, *J* = 30.9 Hz), 124.7, 124.6, 123.5, 123.1, 122.4 (q, *J* = 273.1 Hz), 118.8, 117.3 (q, *J* = 5.3 Hz), 113.9, 112.0, 109.7, 49.6, 27.9 ppm; **^{19}F NMR** (565 MHz, DMSO- *d$_6$*): δ = -61.74 ppm; **HR-ESI-MS**: *m*/*z* = 547.9674 ([*M* + H]$^+$, calcd. for $C_{20}H_{15}O_3N_3{}^{79}BrClF_3S^+$: 547.9653), 549.9648 ([*M* + H]$^+$, calcd. for $C_{20}H_{15}O_3N_3{}^{81}BrClF_3S^+$: 549.96322), 551.9618 ([*M* + H]$^+$, calcd. for $C_{20}H_{15}O_3N_3{}^{81}Br^{37}ClF_3S^+$: 551.9603).

General Procedure VI – Oxidation of Sulfonamidylindolines

A suspension of the indoline (100 µmol) and MnO_2 (10.0 eq.) in CH_2Cl_2 or toluene (5 mL) was heated to reflux and stirred for 4 h. The crude mixture was concentrated and the product purified by flash column chromatography (SiO_2; CH_2Cl_2/MeOH mixture).

5-Bromo-*N*-(4-chloro-3-(trifluoromethyl)phenyl)-1-(cyclopropanecarbonyl)-1*H*-indole-6-sulfonamide (16a)

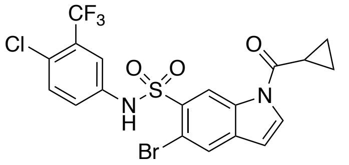

Indole **16a** was prepared according to GP VI using **1a** (50 mg, 96 µmol) in toluene (5 mL). Purification by flash column chromatography (SiO_2; pentane/CH_2Cl_2 2:3 → 0:1) afforded **16a** (46 mg, 92%) as an off-white amorphous solid.

^{1}H NMR (400 MHz, DMSO-*d$_6$*): δ = 11.18 (s, 1H), 9.18 (s, 1H), 8.53 (d, *J* = 3.8 Hz, 1H), 8.11 (s, 1H), 7.56 (t, *J* = 5.9 Hz, 2H), 7.35 (dd, *J* = 8.8, 2.6 Hz, 1H), 6.85 (d, *J* = 3.7 Hz, 1H), 2.81–2.70 (m, 1H), 1.23–1.07 ppm (m, 4H); **^{13}C NMR** (151 MHz, DMSO-*d$_6$*): δ = 172.8, 136.9, 135.0, 132.7, 132.6, 132.4, 131.9, 127.3, 127.2 (q, J = 30.9 Hz), 124.7, 123.2, 122.3 (q, J = 273.2 Hz), 119.8, 117.4 (q, J = 5.5 Hz), 112.2, 107.3, 13.4, 10.4 ppm; **^{19}F NMR** (377 MHz, DMSO-*d$_6$*): δ = -61.87 ppm; **HR-ESI-MS**: *m*/*z* = 520.9540 ([*M* + H]$^+$, calcd. for $C_{19}H_{14}{}^{79}BrClF_3N_2O_3S^+$:

520.9544), 522.9517 ([*M* + H]$^+$, calcd. for $C_{19}H_{14}{}^{81}BrClF_3N_2O_3S^+$: 522.9514), 524.9487 ([*M* + H]$^+$, calcd. for $C_{19}H_{14}{}^{81}Br^{37}ClF_3N_2O_3S^+$: 524.9494).

5-Bromo-1-(cyclopropanecarbonyl)-*N*-(3-(trifluoromethyl)phenyl)-1*H*-indole-6-sulfonamide (16b)

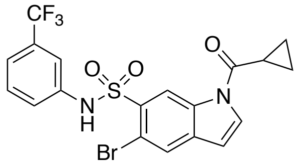

Indole **16b** was prepared according to GP VI using **1b** (10 mg, 10 µmol) in toluene (2 mL). Purification by flash column chromatography afforded **16b** (9 mg, 94%) as an off-white amorphous solid.

^{1}**H NMR** (600 MHz, DMSO-d_6): δ = 11.04 (s, 1H), 9.19 (s, 1H), 8.52 (d, *J* = 3.8 Hz, 1H), 8.10 (s, 1H), 7.46–7.40 (m, 2H), 7.36 (d, *J* = 8.1 Hz, 1H), 7.30 (d, *J* = 7.7 Hz, 1H), 6.85 (d, *J* = 3.7 Hz, 1H), 2.81–2.68 (m, 1H), 1.20–1.08 ppm (m, 4H); ^{13}**C NMR** (151 MHz, DMSO-d_6): δ = 172.8, 138.2, 134.9, 132.6, 131.8, 130.6, 130.1, 129.8 (q, *J* = 31.8 Hz), 127.2, 123.7 (q, *J* = 272.4 Hz), 122.2, 119.9, 119.9, 114.8 (q, *J* = 4.0 Hz), 112.3, 107.3, 13.4, 10.4 ppm; ^{19}**F NMR** (565 MHz, DMSO-d_6): δ = -61.61 ppm; **HR-ESI-MS**: *m/z* = 486.9937 ([*M* + H]$^+$, calcd. for $C_{19}H_{15}{}^{79}BrF_3N_2O_3S^+$: 486.9933), 488.9916 ([*M* + H]$^+$, calcd. for $C_{19}H_{15}{}^{81}BrF_3N_2O_3S^+$: 488.9913).

5-Bromo-*N*-(4-chloro-3-(trifluoromethyl)phenyl)-1*H*-indole-6-sulfonamide (17)

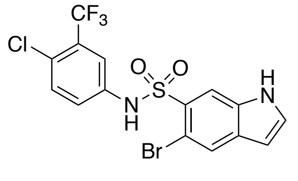

Indole **17** was prepared according to GP VI using **11** (50 mg, 110 µmol) in CH_2Cl_2 (5 mL). Purification by flash column chromatography (SiO_2; EtOAc in cyclohexane 15%) afforded **17** (27 mg, 54%) as an off-white amorphous solid.

^{1}**H NMR** (600 MHz, DMSO): δ = 11.80 (s, 1H), 11.01 (s, 1H), 8.28 (s, 1H), 7.97 (s, 1H), 7.71 (t, *J* = 2.8 Hz, 1H), 7.58–7.53 (m, 2H), 7.35 (dd, *J* = 8.8, 2.6 Hz, 1H), 6.56–6.50 ppm (m, 1H);

^{13}C NMR (151 MHz, DMSO): δ = 137.2, 133.2, 132.7, 132.2, 131.6, 128.2, 127.1 (q, J = 30.7 Hz), 126.2, 124.3, 122.9, 122.4 (q, J = 273.1 Hz), 116.8 (q, J = 5.6 Hz), 116.4, 107.0, 101.4 ppm; **^{19}F NMR** (565 MHz, DMSO): δ = -61.79 ppm; **HR-ESI-MS**: m/z = 452.9277 ([M + H]$^+$, calcd. for $C_{15}H_{10}{}^{79}BrClF_3N_2O_2S^+$: 452.92815), 454.9256 ([M + H]$^+$, calcd. for $C_{15}H_{10}{}^{81}BrClF_3N_2O_2S^+$: 454.9252), 456.9230 ([$M$ + H]$^+$, calcd. for $C_{15}H_{10}{}^{81}Br^{37}ClF_3N_2O_2S^+$: 456.9232).

5-Bromo-*N*-(3,5-difluorophenyl)-1*H*-indole-6-sulfonamide (95)

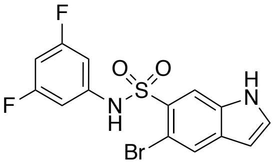

Indole **95** was prepared according to GP VI using **SI-6** (174 mg, 447 µmol) in CH_2Cl_2 (20 mL). Purification by flash column chromatography (SiO_2; EtOAc in cyclohexane 15%) afforded **95** (148 mg, 85%) as an off-white amorphous solid.

^{1}H NMR (600 MHz, DMSO-d_6): δ = 11.76 (br. s, 1H), 11.02 (br. s, 1H), 8.31 (s, 1H), 7.98 (s, 1H), 7.72 (t, J = 2.8 Hz, 1H), 6.79 (tt, J = 9.3, 2.2 Hz, 1H), 6.77–6.72 (m, 2H), 6.53 ppm (t, J = 2.0 Hz, 1H); **^{13}C NMR** (151 MHz, DMSO-d_6): δ = 162.6 (dd, J = 244.5, 15.4 Hz), 140.4 (t, J = 13.5 Hz), 133.2, 132.2, 131.6, 128.3, 126.2, 116.4, 107.1, 101.4, 101.2–100.6 (m), 98.3 ppm (t, J = 26.1 Hz); **^{19}F NMR** (565 MHz, DMSO d_6): δ = -108.51 ppm (t, J = 8.9 Hz); **HR-ESI-MS**: m/z = 386.9612 ([M + H]$^+$, calcd. for $C_{14}H_{10}{}^{79}BrF_2N_2O_2S^+$: 386.9609), 388.9590 ([$M$ + H]$^+$, calcd. for $C_{14}H_{10}{}^{81}BrF_2N_2O_2S^+$: 388.9589).

General Procedure VII – Dehalogenation of Bromoindolines

To a solution of the bromoindoline (61 µmol) in DMF (1 mL), Et_3N (1.2 eq.) and Pd/C (10% w/w loading, 2 mol%) were added, and the resulting suspension was stirred under a H_2 atmosphere for 16 h. The mixture was filtered through a pad of Celite® and concentrated under reduced pressure. The product was purified by flash column chromatography.

N-(4-Chloro-3-(trifluoromethyl)phenyl)-1-(cyclopropanecarbonyl)indoline-6-sulfonamide (18a)

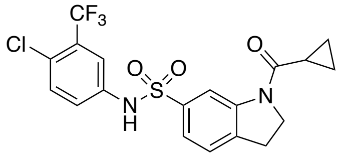

Indoline **18a** was prepared according to GP VII using **1a** (30 mg, 57 µmol). Purification by flash column chromatography (SiO_2; cyclohexane/EtOAc 4:1 → 2:1) afforded **18a** (25 mg, 96%) as an off-white amorphous solid.

^{1}H NMR (600 MHz, DMSO-*d$_6$*): δ = 10.85 (s, 1H), 8.49 (s, 1H), 7.59 (dd, *J* = 10.3, 7.0 Hz, 1H), 7.51 (d, *J* = 2.6 Hz, 1H), 7.42–7.31 (m, 3H), 4.31 (t, *J* = 8.3 Hz, 2H), 3.21 (t, *J* = 8.5 Hz, 2H), 2.00–1.86 (m, 1H), 0.97–0.79 ppm (m, 4H); **^{13}C NMR** (151 MHz, DMSO-*d$_6$*): δ = 172.0, 143.0, 138.2, 137.5 (q, *J* = 3.7 Hz), 132.7, 127.2 (q, *J* = 30.9 Hz), 125.4, 124.9, 123.97, 122.8, 122.4 (q, *J* = 273.2 Hz), 121.8, 117.8 (q, *J* = 5.3 Hz), 113.5, 48.0, 27.3, 13.2, 8.2 ppm; **^{19}F NMR** (565 MHz, DMSO-*d$_6$*): δ = -61.78 ppm; **HR-ESI-MS**: *m*/*z* = 445.0603 ([*M* + H]$^+$, calcd. for $C_{19}H_{17}ClF_3N_2O_3S^+$: 445.0595), 447.0571 ([*M* + H]$^+$, calcd. for $C_{19}H_{17}{}^{37}ClF_3N_2O_3S^+$: 447.0566).

1-(Cyclopropanecarbonyl)-*N*-(3-(trifluoromethyl)phenyl)indoline-6-sulfonamide (18b)

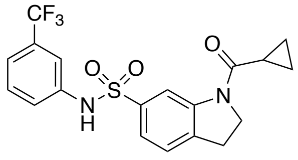

Indoline **18b** was prepared according to GP VII using **1b** (30 mg, 61 µmol). Purification by flash column chromatography (SiO_2; cyclohexane/EtOAc 4:1 → 2:1) afforded **18b** (24 mg, 95%) as an off-white amorphous solid.

^{1}H NMR (600 MHz, DMSO-*d$_6$*): δ = 10.73 (s, 1H), 8.51 (s, 1H), 7.47 (t, *J* = 7.9 Hz, 1H), 7.42–7.31 (m, 5H), 4.30 (t, *J* = 8.2 Hz, 2H), 3.27–3.10 (m, 2H), 1.97–1.82 (m, 1H), 0.95–0.78 ppm (m, 4H); **^{13}C NMR** (151 MHz, DMSO-*d$_6$*): δ = 171.9, 143.8, 138.8, 138.0, 137.8, 130.6, 129.8 (q, *J* = 31.8 Hz), 125.3, 123.8 (q, *J* = 272.4 Hz), 122.8, 121.9, 120.1 (q, *J* = 3.3 Hz) 115.2, 113.6, 48.0, 27.3, 13.2, 8.2 ppm; **^{19}F NMR** (565 MHz, DMSO-*d$_6$*): δ = -61.49 ppm; **HR-ESI-MS**: *m*/*z* = 411.0992 ([*M* + H]$^+$, calcd. for $C_{19}H_{18}F_3N_2O_3S$+: 411.0985).

Preparation of Further Analogs of Indoline 1a

5-Bromo-*N*-(4-chloro-3-(trifluoromethyl)phenyl)-1-pivaloylindoline-6-sulfonamide (15h)

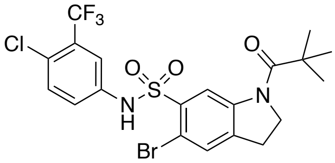

To a solution of **11**, (30 mg, 66 µmol), DMAP (1 mg, 8 µmol, 0.1 eq.), and Et_3N (35 µL, 198 µmol, 3.0 eq.) in pyridine (1 mL) under an argon atmosphere at 0 °C, pivalic acid chloride (9 µL, 72 µmol, 1.1 eq.) was added. The solution was heated to 60 °C. Only partial conversion was observed after 16 h, hence a further 10.0 eq. of pivalic acid chloride were added, and the solution was stirred for a further 8 h at 60 °C and for 16 h at 100 °C. The mixture was concentrated under reduced pressure, diluted with EtOAc (20 mL), and washed with an aq. 1 M HCl solution (1 x 20 mL). The aq. phase was extracted with EtOAc (2 x 20 mL). The combined organic layers were dried over $MgSO_4$, filtered, and concentrated under reduced pressure. Purification by flash column chromatography (EtOAc in cyclohexane 10% → 20%) afforded **15h** (23 mg, 65%) as an off-white amorphous solid.

^{1}H NMR (600 MHz, DMSO-*d$_6$*): δ = 11.13 (br. s, 1H), 8.89 (s, 1H), 7.67 (s, 1H), 7.62 (d, *J* = 8.8 Hz, 1H), 7.56 (d, *J* = 2.6 Hz, 1H), 7.36 (dd, *J* = 8.8, 2.6 Hz, 1H), 4.29 (t, *J* = 8.4 Hz, 2H), 3.18 (t, *J* = 8.2 Hz, 2H), 1.28 ppm (s, 9H); **^{13}C NMR** (151 MHz, DMSO-*d$_6$*): δ = 176.5, 144.6, 139.6, 136.9, 135.9, 132.8, 131.1, 127.2 (q, *J* = 30.9 Hz), 124.8, 123.4, 122.4 (q, *J* = 273.1 Hz), 119.5, 117.7 (q, *J* = 5.4 Hz), 112.2, 49.5, 40.0, 28.4, 27.2 ppm; **^{19}F NMR** (565 MHz, DMSO-*d$_6$*): δ = -61.80 ppm; **HR-ESI-MS**: *m*/*z* = 539.0020 ([*M* + H]$^+$, calcd. for $C_{20}H_{20}O_3N_2{}^{79}BrClF_3S^+$: 539.0013), 540.9996 ([*M* + H]$^+$, calcd. for $C_{20}H_{20}O_3N_2{}^{81}BrClF_3S^+$: 540.9993), 542.9967 ([*M* + H]$^+$, calcd. for $C_{20}H_{20}O_3N_2{}^{81}Br^{37}ClF_3S^+$: 542.9963).

5-Bromo-*N*-(4-chloro-3-(trifluoromethyl)phenyl)-1-(oxetan-3-yl)indoline-6-sulfonamide (19) and 5-Bromo-*N*-(4-chloro-3-(trifluoromethyl)phenyl)-1-ethylindoline-6-sulfonamide (20)

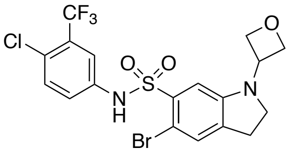

19

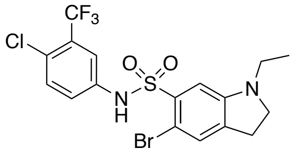

20

To a solution of **11** (50 mg, 110 μmol) in CH_2Cl_2 (2 mL) under an argon atmosphere, 3-oxetanone (40 mg, 549 μmol, 5.0 eq.) was added, and the solution was stirred at reflux for 10 min. $NaB(OAc)_3H$ (75 mg, 351 μmol, 3.2 eq.) was added, and the mixture was stirred for a further 90 min. The mixture was cooled to rt and quenched by adding H_2O (2 mL), followed by sat. aq. $NaHCO_3$ (2 mL). The aqueous phase was extracted with CH_2Cl_2, (3 x 20 mL) and the combined organic layers were dried over $MgSO_4$, filtered, and concentrated under reduced pressure. Purification by flash column chromatography (SiO_2; cyclohexane/EtOAc 9:1 → 4:1) afforded **19** (47 mg, 84%) and **20** (6 mg, 12%) as colorless oils.

19:

^{1}H NMR (500 MHz, DMSO-*d*$_6$): δ = 11.05 (s, 1H), 7.60 (d, *J* = 8.8 Hz, 1H), 7.51 (d, *J* = 2.4 Hz, 1H), 7.40 (s, 1H), 7.35 (dd, *J* = 8.8, 2.4 Hz, 1H), 7.00 (s, 1H), 4.81–4.64 (m, 5H), 3.63 (t, *J* = 8.5 Hz, 2H), 2.99 ppm (t, *J* = 8.4 Hz, 2H); **^{13}C NMR** (126 MHz, DMSO-*d*$_6$): δ = 150.3, 138.3, 137.0, 136.0, 132.7, 130.8, 127.1 (d, *J* = 30.8 Hz), 124.4, 123.1, 122.4 (q, *J* = 273.2 Hz), 116.7 (q, *J* = 5.5 Hz), 108.2, 105.9, 73.6, 50.8, 48.6, 27.2 ppm; **HR-ESI-MS**: *m*/*z* = 510.9697 ([*M* + H]$^+$, calcd. for $C_{18}H_{16}O_3N_2{}^{79}BrClF_3S^+$: 510.97001), 512.9673 ([*M* + H]$^+$, calcd. for $C_{18}H_{16}O_3N_2{}^{81}BrClF_3S^+$: 512.9671), 514.9643 ([*M* + H]$^+$, calcd. for $C_{18}H_{16}O_3N_2{}^{81}Br^{37}ClF_3S^+$: 514.9650).

20:

^{1}H NMR (500 MHz, DMSO-*d*$_6$): δ = 11.01 (s, 1H), 7.60 (d, *J* = 8.8 Hz, 1H), 7.53 (d, *J* = 2.7 Hz, 1H), 7.36 (dd, *J* = 8.8, 2.7 Hz, 1H), 7.33 (t, *J* = 1.1 Hz, 1H), 7.01 (s, 1H), 3.42 (t, *J* = 8.6 Hz, 2H), 3.15 (q, *J* = 7.1 Hz, 2H), 2.94 (t, *J* = 8.3 Hz, 2H), 1.04 ppm (t, *J* = 7.2 Hz, 3H); **HR-ESI-MS**: *m*/*z* = 482.9747 ([*M* + H]$^+$, calcd. for $C_{17}H_{16}O_2N_2{}^{79}BrClF_3S^+$: 482.9751), 484.9723 ([*M* + H]$^+$, calcd. for $C_{17}H_{16}O_2N_2{}^{81}BrClF_3S^+$: 484.9722), 486.9694 ([*M* + H]$^+$, calcd. for $C_{17}H_{16}O_2N_2{}^{81}Br^{37}ClF_3S^+$: 486.9701).

6.5. Synthesis of Pull-Down Probes

i. Linker Synthesis

***tert*-Butyl (3-(2-(2-(3-aminopropoxy)ethoxy)ethoxy)propyl)carbamate (91)[168]**

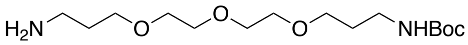

To a vigorously stirred solution of 3,3'-((oxybis(ethane-2,1-diyl))bis(oxy))bis(propan-1-amine) (9.837 mL, 44 mmol, 1.9 eq.) in CH_2Cl_2 (200 mL) at rt, a solution of Boc_2O (5.000 g, 23 mmol) in CH_2Cl_2 (100 mL) was added using a dropping funnel over a period of 1 h. The solution was stirred at rt for 16 h and washed with an aq. 0.1 M HCl solution (2 x 100 mL). The aqueous layer was extracted with CH_2Cl_2 (5 x 50 mL). The combined organic layers were dried over Na_2SO_4, concentrated under reduced pressure and dried *in vacuo*. The crude, containing the desired product in 62% purity with bis-Boc-protected diamino-PEG as side product, was used without further purification (5 g).

***tert*-Butyl (1-bromo-2-oxo-7,10,13-trioxa-3-azahexadecan-16-yl)carbamate (52)**

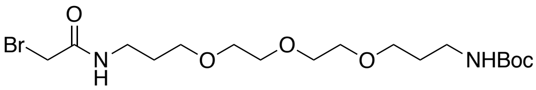

To a solution of bromoacetylbromide (668 µL, 3.9 mmol, 1.0 eq.) in THF (50 mL) at 0 °C, a solution of Boc-NH-PEG3-NH_2 (**91** [62% purity], 2.000 g, 3.9 mmol) and DIPEA (687 µL, 3.9 mmol, 1.0 eq.) in THF (20 mL) was added over 1 h. The solution was stirred for 1 h at rt and diluted with EtOAc (50 mL). The organic layer was washed with a NH_4Cl solution (50 mL sat. aq. NH_4Cl_2 + 50 mL water, 1 x), a $NaHCO_3$ solution (50 mL sat. aq. $NaHCO_3$ + 50 mL water, 1 x), and brine (2 x 50 mL). The organic layer was dried over $MgSO_4$, and concentrated under reduced pressure. Purification by flash chromatography (SiO_2; EtOAc/cyclohexane 1:1 → 1:0) afforded **52** (1.471 g, 86%) as a colorless oil.

^{1}H NMR (400 MHz, $CDCl_3$): δ = 7.17 (br. s, 1H), 4.91 (br. s, 1H), 3.82 (s, 2H), 3.67–3.53 (m, 10H), 3.51 (t, J = 6.0 Hz, 2H), 3.39 (dd, J = 12.1, 5.8 Hz, 2H), 3.24–3.13 (m, J = 4.8 Hz, 2H), 1.79 (dt, J = 11.7, 5.9 Hz, 2H), 1.76–1.67 (m, 2H), 1.41 ppm (s, 9H); **HR-ESI-MS**: m/z = 441.1604 ($[M + H]^+$, calcd. for $C_{17}H_{34}{}^{79}BrN_2O_6{}^+$: 441.1600), 443.1579 ($[M + H]^+$, calcd. for $C_{17}H_{34}{}^{81}BrN_2O_6{}^+$: 443.1580).

ii. Synthesis of 1st Generation Active Probe for Pull-Down

(*E*)-5-(3-((*tert*-Butyldimethylsilyl)oxy)prop-1-en-1-yl)-*N*-(4-chloro-3-(trifluoromethyl)phenyl)-1-(cyclopropanecarbonyl)indoline-6-sulfonamide (51)

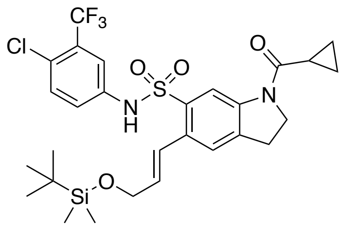

To a solution of **1a** (70 mg, 134 µmol) in DMF (1 mL) under an argon atmosphere, (*E*)-3-(tert-butyldimethylsilyloxy)propene-1-yl-boronic acid pinacol ester (**50**, 88 µL, 267 µmol, 2.0 eq.), Na_2CO_3 (43 mg, 401 µmol, 3.0 eq.) and water (100 µL) were added. The mixture was bubbled with argon for 10 min, $Pd(PPh_3)_4$ (6 mg, 5 µmol, 4 mol%) was added, and the mixture was heated to 105 °C for 20 h. The mixture was concentrated *in vacuo*, and the crude product was diluted in EtOAc (20 mL) and washed with brine (1 x 20 mL). The aq. phase was extracted with EtOAc (3 x 20 mL), and the combined organic layers were dried over $MgSO_4$, filtered, and concentrated under reduced pressure. Purification by flash column chromatography (SiO_2; CH_2Cl_2/pentane 9:1 → cyclohexane/EtOAc 4:1) afforded **51** (55 mg, 66%) as an off-white amorphous solid.

^{1}H NMR (400 MHz, $CDCl_3$): δ = 8.72 (br. s, 1H), 7.42 (d, , *J* = 15.7 Hz, 1H), 7.39–7.31 (m, 1H), 7.29 (d, *J* = 8.5 Hz, 2H), 7.22 (s, 1H), 7.09 (s, 1H), 6.08 (dt, *J* = 15.4, 4.8 Hz, 1H), 4.37 (dd, *J* = 4.8, 1.7 Hz, 2H), 4.29 (t, *J* = 8.3 Hz, 2H), 3.22 (t, *J* = 8.2 Hz, 2H), 1.77–1.69 (m, 1H), 1.25 (d, *J* = 4.7 Hz, 2H), 1.17–1.09 (m, 2H), 0.97–0.95 (m, 9H), 0.17–0.12 ppm (m, 6H); **HR-ESI-MS**: *m*/*z* = 615.1736 ([*M* + H]$^+$, calcd. for $C_{28}H_{35}ClF_3N_2O_4SSi^+$: 615.1722), 617.1712 ([*M* + H]$^+$, calcd. for $C_{28}H_{35}{}^{37}ClF_3N_2O_4SSi^+$: 617.1692).

(*E*)-*N*-(4-Chloro-3-(trifluoromethyl)phenyl)-1-(cyclopropanecarbonyl)-5-(3-hydroxyprop-1-en-1-yl)indoline-6-sulfonamide (34)

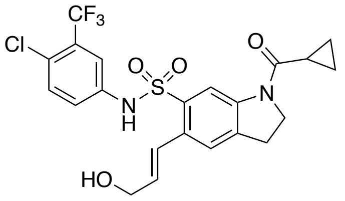

To a solution of **51** (40 mg, 65 µmol) in THF (1.5 mL) under an argon atmosphere, a solution of TBAF in THF (1 M, 195 µL, 3.0 eq.) was added and the mixture was stirred for 5 h at rt. The solution was concentrated under reduced pressure and re-dissolved in EtOAc (25 mL). The organic layer was washed with an aq. 1 M HCl solution (1 x 25 mL) and brine (1 x 10 mL), dried over $MgSO_4$, filtered, and concentrated under reduced pressure. Purification by flash column chromatography (SiO_2; cyclohexane/EtOAc (1% AcOH) 2:1 → 2:3) afforded **34** (24 mg, 73%) as a thick colorless oil.

^{1}H NMR (400 MHz, CD_3OD): δ = 8.73 (br. s, 1H), 7.48 (s, 1H), 7.41–7.38 (m, 1H), 7.36 (s, 2H), 7.26 (dd, *J* = 8.8, 2.3 Hz, 1H), 6.21 (dt, *J* = 15.9, 5.0 Hz, 1H), 4.35 (t, *J* = 8.6 Hz, 2H), 4.28 (d, *J* = 5.2 Hz, 2H), 3.26 (t, *J* = 8.1 Hz, 2H), 1.96–1.89 (m, 1H), 1.10–1.00 (m, 2H), 1.00–0.92 ppm (m, 2H); **HR-ESI-MS**: *m*/*z* = 501.0862 ([*M* + H]$^+$, calcd. for $C_{22}H_{21}ClF_3N_2O_4S^+$: 501.0863), 503.0832 ([*M* + H]$^+$, calcd. for $C_{22}H_{21}{}^{37}ClF_3N_2O_4S^+$: 503.0833).

N-(4-Chloro-3-(trifluoromethyl)phenyl)-1-(cyclopropanecarbonyl)-5-(3-hydroxypropyl)indoline-6-sulfonamide (35)

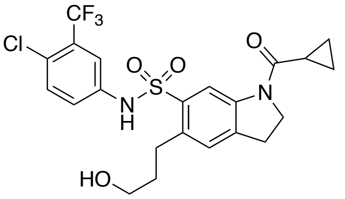

A suspension of TBDMS-alkenyl indoline **51** (15 mg, 24 µmol) and Pd/C (1 mg, 1.2 µmol, 10% loading, 5 mol%) in MeOH (1 mL) under a H_2 atmosphere (balloon) was stirred for 24 h. The mixture was filtered through a pad of Celite®, concentrated under reduced pressure, and the product purified by flash column chromatography to afford **35** (5 mg, 44%) as a thick colorless oil.

^{1}H NMR (400 MHz, CD_3OD): δ = 8.79–8.62 (m, 1H), 7.48–7.44 (m, 1H), 7.44–7.39 (m, 1H), 7.34–7.29 (m, 1H), 7.30–7.25 (m, 1H), 4.35 (t, *J* = 8.1 Hz, 2H), 3.63 (t, *J* = 6.1 Hz, 2H), 3.25 (t, *J* = 8.3 Hz, 2H), 3.08–2.97 (m, 2H), 1.98–1.88 (m, 1H), 1.88–1.78 (m, 2H), 1.08–0.99 (m, 2H), 0.99–0.89 ppm (m, 2H); **HR-ESI-MS**: *m*/*z* = 503.1020 ([*M* + H]$^+$, calcd. for $C_{22}H_{23}ClF_3N_2O_4S^+$: 503.1019), 505.0990 ([*M* + H]$^+$, calcd. for $C_{22}H_{23}{}^{37}ClF_3N_2O_4S^+$: 505.0990).

***tert*-Butyl (*E*)-(20-(6-(*N*-(4-Chloro-3-(trifluoromethyl)phenyl)sulfamoyl)-1-(cyclopropanecarbonyl)indolin-5-yl)-15-oxo-4,7,10,17-tetraoxa-14-azaicos-19-en-1-yl)carbamate (53)**

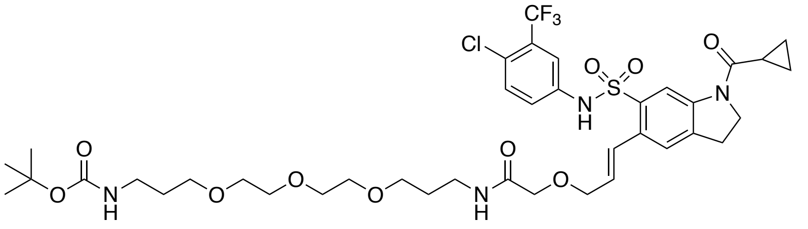

A mixture of the alcohol **34** (10 mg, 19 µmol), linker **52** (13 mg, 29 µmol, 1.5 eq.), and K_2CO_3 (4 mg, 29 µmol, 1.5 eq.) in acetone (2 mL) under an argon atmosphere was heated to reflux for 8 h. The solvent was evaporated under reduced pressure and the product purified by flash column chromatography (SiO_2; CH_2Cl_2/MeOH 99:1 → 97.5:2.5 → 95:5) to afford **53** (11 mg, 65%) as a thick colorless oil.

^{1}H NMR (400 MHz, CD_3OD): δ = 8.52 (br. s, 1H), 7.64–7.59 (m, 1H), 7.55 (s, 1H), 7.54–7.47 (m, 2H), 7.07 (d, *J* = 15.7 Hz, 1H), 6.14 (dt, *J* = 11.0, 5.7 Hz, 1H), 4.39 (t, *J* = 9.0 Hz, 2H), 4.31 (s, 2H), 4.07 (d, *J* = 4.6 Hz, 2H), 3.66–3.45 (m, 12H), 3.39 (s, 2H), 3.22 (s, 2H), 3.12 (dd, *J* = 12.0, 6.5 Hz, 2H), 2.00–1.91 (m, 1H), 1.71 (s, 2H), 1.69–1.57 (m, 2H), 1.42 (s, 9H), 1.05–0.99 (m, 2H), 0.99–0.93 ppm (m, 2H); **HR-ESI-MS**: *m*/*z* = 861.3147 ([*M* + H]$^+$, calcd. for $C_{39}H_{53}O_{10}N_4ClF_3S^+$: 861.3118), 863.3131 ([*M* + H]$^+$, calcd. for $C_{39}H_{53}O_{10}N_4{}^{37}ClF_3S^+$: 863.3088).

(*E*)-*N*-(3-(2-(2-(3-Aminopropoxy)ethoxy)ethoxy)propyl)-2-((3-(6-(*N*-(4-chloro-3-(trifluoromethyl)phenyl)sulfamoyl)-1-(cyclopropanecarbonyl)indolin-5-yl)allyl)oxy)acetamide (54)

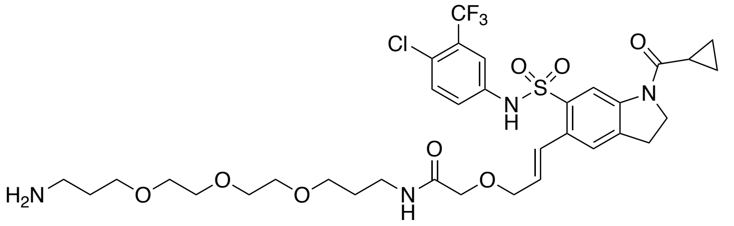

Boc-protected positive probe **53** (20 mg, 23 μmol) was dissolved in dioxane (200 μL) and a drop of conc. HCl was added. The mixture was stirred for 3 h at rt and freeze-dried *in vacuo*. Purification by preparative HPLC (in the absence of TFA) afforded **54** (10 mg, 57%) as a thick colorless oil.

^{1}H NMR (400 MHz, CD_3OD) δ 8.52 (br. s, 1H), 7.61 (d, *J* = 1.7 Hz, 1H), 7.58–7.43 (m, 3H), 7.07 (d, *J* = 15.5 Hz, 1H), 6.15 (dt, *J* = 15.7, 5.2 Hz, 1H), 4.39 (t, *J* = 8.0 Hz, 2H), 4.34 (s, 2H), 4.09 (d, *J* = 4.8 Hz, 2H), 3.67 (t, *J* = 5.5 Hz, 2H), 3.66–3.61 (m, 6H), 3.57–3.52 (m, 2H), 3.42 (s, 2H), 3.32–3.30 (m, 2H), 3.25 (s, 2H), 3.11 (s, 2H), 1.92 (s, 3H), 1.74–1.62 (m, 2H), 1.09–0.77 ppm (m, 4H); **ESI-MS**: *m*/*z* = 761.2 ($[M + H]^+$, calcd. for $C_{34}H_{45}O_8N_4ClF_3S^+$: 761.2).

iii. Synthesis of 1st Generation Control Probe for Pull-Down

(*E*)-5-(3-((*tert*-Butyldimethylsilyl)oxy)prop-1-en-1-yl)-1-(cyclopropanecarbonyl)-*N*-(3,5-difluorophenyl)indoline-6-sulfonamide (SI-7)

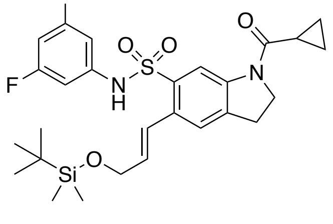

Silyl ester **SI-7** was prepared following the procedure employed in the synthesis of **51**, using **1r** (65 mg, 142 μmol), **50** (93 μL, 284 μmol, 2.0 eq.), Na_2CO_3 (45, 426 μmol, 3.0 eq.), and $Pd(PPh_3)_4$ (13 mg, 11 μmol, 8 mol%). Purification by flash column chromatography (SiO2; EtOAc in cyclohexane 20 → 25 → 30%) afforded **SI-7** (25 mg, 33%) as thick colorless oil.

^{1}H NMR (400 MHz, $CDCl_3$): *δ* = 8.73 (br. s, 1H), 7.40 (d, *J* = 15.9 Hz, 1H), 7.10 (s, 1H), 6.68–6.56 (m, 2H), 6.43 (tt, *J* = 8.8, 2.0 Hz, 1H), 6.11 (dt, *J* = 15.7, 5.1 Hz, 1H), 4.37 (dd, *J* = 5.0, 1.7 Hz, 2H), 4.34–4.21 (m, 2H), 3.31–3.10 (m, 2H), 1.84–1.59 (m, 1H), 1.19–1.07 (m, 2H), 0.96 (s, 9H), 0.95–0.88 (m, 2H), 0.15 ppm (s, 6H); **ESI-MS**: *m*/*z* = 571.0 ([*M* + Na]$^+$, calcd. for $C_{27}H_{34}F_2N_2NaO_4SSi^+$: 571.2).

(*E*)-1-(Cyclopropanecarbonyl)-*N*-(3,5-difluorophenyl)-5-(3-hydroxyprop-1-en-1-yl)indoline-6-sulfonamide (SI-8)

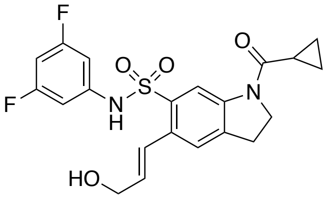

Alcohol **SI-8**was prepared following the procedure employed in the synthesis of **34**, using **SI-7** (24 mg, 44 μmol). Purification by flash column chromatography (SiO_2; cyclohexane/EtOAc (1% AcOH) 2:1 → 1:1) afforded **SI-8** (17 mg, 89%) as a thick colorless oil.

^{1}H NMR (400 MHz, CD_3OD): *δ* = 8.76 (br. s, 1H), 7.49 (s, 1H), 7.38 (d, *J* = 15.7 Hz, 1H), 6.67–6.55 (m, 2H), 6.50 (tt, *J* = 9.1, 2.2 Hz, 1H), 6.23 (dt, *J* = 16.0, 5.2 Hz, 1H), 4.36 (s, 2H), 4.30 (dd, *J* = 5.1, 1.8 Hz, 2H), 3.26 (t, *J* = 8.5 Hz, 2H), 1.97–1.89 (m, 1H), 1.08–1.01 (m, 2H), 0.96 ppm (d, *J* = 7.9 Hz, 2H); **HR-ESI-MS**: *m*/*z* = 435.1182 ([*M* + H]$^+$, calcd. for $C_{21}H_{21}F_2N_2O_4S^+$: 435.1185).

tert-Butyl (*E*)-(20-(1-(Cyclopropanecarbonyl)-6-(*N*-(3,5-difluorophenyl)sulfamoyl)indolin-5-yl)-15-oxo-4,7,10,17-tetraoxa-14-azaicos-19-en-1-yl)carbamate (SI-9)

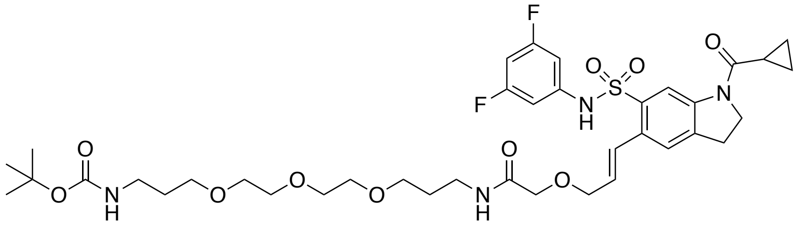

The Boc-protected negative probe **SI-9** was prepared following the procedure employed in the synthesis of **53**, using **SI-8** (13 mg, 29 μmol). Purification by flash column chromatography (SiO_2; CH_2Cl_2/MeOH 99:1 → 97.5:2.5 → 95:5) afforded **SI-9** (11 mg, 47%) as a thick colorless oil.

^{1}H NMR (400 MHz, CD_3OD): δ = 8.57 (s, 1H), 7.55 (s, 1H), 7.09 (d, J = 15.7 Hz, 1H), 7.00–6.91 (m, 2H), 6.86 (tt, J = 9.1, 2.4 Hz, 1H), 6.18 (dt, J = 15.5, 5.4 Hz, 1H), 4.39 (t, J = 8.0 Hz, 2H), 4.32 (s, 2H), 4.12 (dd, J = 5.3, 1.4 Hz, 2H), 3.63 (dd, J = 5.1, 3.7 Hz, 4H), 3.60–3.53 (m, 4H), 3.50 (t, J = 6.2 Hz, 2H), 3.41 (t, J = 6.1 Hz, 2H), 3.30–3.27 (m, 2H), 3.27–3.18 (m, 2H), 3.11 (t, J = 6.8 Hz, 2H), 1.93 (d, J = 4.5 Hz, 1H), 1.69 (dp, J = 19.2, 6.4 Hz, 4H), 1.43 (s, 9H), 1.06–0.92 ppm (m, 4H); **HR-ESI-MS**: m/z = 795.3450 ($[M + H]^+$, calcd. for $C_{38}H_{53}F_2N_4O_{10}S^+$: 795.3445).

(*E*)-*N*-(3-(2-(2-(3-Aminopropoxy)ethoxy)ethoxy)propyl)-2-((3-(1-(cyclopropanecarbonyl)-6-(*N*-(3,5-difluorophenyl)sulfamoyl)indolin-5-yl)allyl)oxy)acetamide (57)

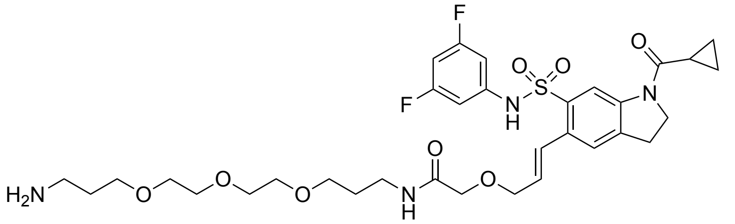

Negative probe **57** was prepared following the procedure employed in the synthesis of **54**, using **SI-9** (22 mg, 27 µmol) and 2 drops of conc. HCl in dioxane (400 µL). Purification by preparative HPLC (in the absence of TFA) afforded **57** (11 mg, 59%) as a thick colorless oil.

^{1}H NMR (500 MHz, $CDCl_3$): δ = 8.59 (d, J = 5.5 Hz, 1H), 7.56 (s, 1H), 7.08 (s, 1H), 6.93 (d, J = 5.7 Hz, 2H), 6.90–6.81 (m, 1H), 6.27–6.13 (m, 1H), 4.40 (s, 2H), 4.37 (s, 2H), 4.13 (dd, J = 28.0, 5.8 Hz, 2H), 3.68 (t, J = 5.4 Hz, 2H), 3.64 (s, 6H), 3.56 (d, J = 2.4 Hz, 2H), 3.43 (t, J = 5.9 Hz, 2H), 3.26 (d, J = 6.8 Hz, 4H), 3.12 (t, J = 6.2 Hz, 2H), 1.98–1.88 (m, 3H), 1.74–1.65 (m, 2H), 1.00 ppm (m, 4H); **HR-ESI-MS**: m/z = 695.2936 ($[M + H]^+$, calcd. for $C_{33}H_{45}F_2N_4O_8S^+$: 695.2921).

iv. Synthesis of 2nd Generation Active Probe for Pull-Down

Ethyl 2-(5-Bromo-6-(*N*-(4-chloro-3-(trifluoromethyl)phenyl)sulfamoyl)-1*H*-indol-3-yl)-2-oxoacetate (75)

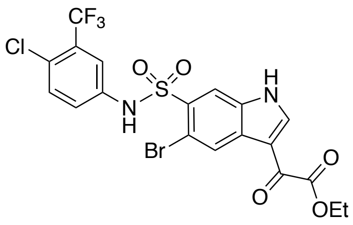

To a solution of **17** (100 mg, 220 µmol) in CH_2Cl_2 (1 mL) at 0 °C under an argon atmosphere, ethyl chlorooxoacetate (238 µL, 2.2 mmol, 10.0 eq.) and $AlCl_3$ (88 mg, 661 µmol, 3.0 eq.) were successively added. The resulting yellow suspension was stirred for 14 h at rt, and the excess of reagents were quenched with water (10 mL). The mixture was extracted with EtOAc (3 x 15 mL), and the combined organic layers were washed with brine (1 x 20 mL), dried over Na_2SO_4, and concentrated under reduced pressure. Purification by flash column chromatography (SiO_2; cyclohexane/EtOAc 4:1 → 2:3) afforded **75** (126 mg, 93%, 90% pure according to NMR) as an off-white amorphous solid.

^{1}H NMR (400 MHz, DMSO-*d₆*): δ = 12.94–12.70 (m, 1H), 11.34–11.07 (m, 1H), 8.73 (s, 1H), 8.46 (s, 1H), 8.39 (s, 1H), 7.62–7.49 (m, 2H), 7.40–7.31 (m, 1H), 4.36 (q, J = 7.2 Hz, 2H), 1.33 ppm (t, J = 7.1 Hz, 3H); **^{13}C NMR** (101 MHz, DMSO-d_6): δ = 178.6, 162.3, 142.2, 142.0, 136.8, 134.4, 132.7, 131.7, 130.1, 127.0, 124.7, 123.3, 117.3, 117.1, 111.8, 111.6, 62.0, 13.8 ppm; **HR-ESI-MS**: *m*/*z* = 552.9437 ([*M* + H]$^+$, calcd. for $C_{19}H_{14}{}^{79}BrClF_3N_2O_5S^+$: 552.9442), 554.9413 ([*M* + H]$^+$, calcd. for $C_{19}H_{14}{}^{81}BrClF_3N_2O_5S^+$: 554.9412), 556.9384 ([*M* + H]$^+$, calcd. for $C_{19}H_{14}{}^{81}Br^{37}ClF_3N_2O_5S^+$: 556.9392).

Ethyl 2-(5-Bromo-6-(*N*-(4-chloro-3-(trifluoromethyl)phenyl)sulfamoyl)-1*H*-indol-3-yl)acetate (SI-10)

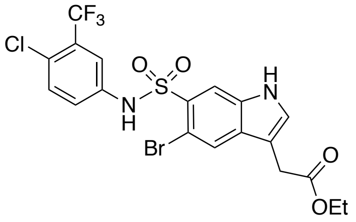

To a suspension of **75** (100 mg, 181 µmol) in TFA (332 µL, 4.3 mmol, 24.0 eq.) at 0 °C, triethylsilane (346 µL, 2.2 mmol, 12.0 eq.) was added. The mixture was stirred at rt for 6 h, and the TFA was co-evaporated with toluene (5 mL). Purification by flash column chromatography (SiO_2; cyclohexane/EtOAc 5:1) afforded **SI-10** (56 mg, 58%) as an off-white amorphous solid.

^{1}H NMR (400 MHz, CD_3OD): δ = 8.26 (s, 1H), 7.91 (s, 1H), 7.55 (d, J = 2.0 Hz, 1H), 7.47 (s, 1H), 7.39–7.30 (m, 2H), 4.12 (q, J = 7.2 Hz, 2H), 3.74 (s, 2H), 1.21 ppm (t, J = 7.1 Hz, 3H); **^{13}C NMR** (151 MHz, DMSO-d_6): δ = 171.1, 137.1, 133.4, 132.7, 131.5, 130.5, 128.3, 127.1 (q, J = 30.8 Hz), 125.2, 124.3, 122.8, 122.4 (q, J = 273.1 Hz), 116.8 (q, J = 5.5 Hz), 116.5, 107.9, 106.8, 60.2, 30.2, 14.0 ppm; **^{19}F NMR** (565 MHz, DMSO) δ -61.77 ppm; **HR-ESI-MS**: m/z = 538.9656 ([M + H]$^+$, calcd. for $C_{19}H_{16}{}^{79}BrClF_3N_2O_4S^+$: 538.9649).

Ethyl 2-(5-Bromo-6-(*N*-(4-chloro-3-(trifluoromethyl)phenyl)-*N*-(cyclopropanecarbonyl)sulfamoyl)-1-(cyclopropanecarbonyl)-1*H*-indol-3-yl)-2-oxoacetate (SI-11)

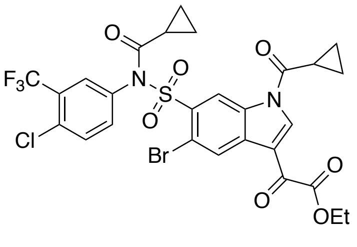

To a solution of **75** (20 mg, 36 µmol) and Et_3N (19 µL, 108 µmol, 1.2 eq.) in CH_2Cl_2 (1 mL) under an argon atmosphere, DMAP (0.1 mg, 2 mol%) was added. The solution was cooled to 0 °C and cyclopropyl acyl chloride (4 µL, 43 µmol, 1.2 eq.) was added. After stirring for 10 min at 0 °C and 16 h at rt, only partial conversion was observed, so a further 3.0 eq. of Et_3N and 10.0 eq. of cyclopropyl acyl chloride were added, and the mixture was stirred for a further 8 h. EtOAc was added (10 mL), and the mixture was washed with brine (1 x 5 mL). The organic layer was dried over $MgSO_4$, filtered, and concentrated under reduced pressure. Purification by flash master chromatography (SiO_2; EtOAc in cyclohexane 0 → 50%) afforded **SI-11** (13 mg).

^{1}H NMR (400 MHz, $CDCl_3$): δ = 9.37 (s, 1H), 9.24 (s, 1H), 8.80 (s, 1H), 7.93 (d, J = 2.5 Hz, 1H), 7.76 (dd, J = 8.5, 2.5 Hz, 1H), 7.63 (d, J = 8.5 Hz, 1H), 4.46 (q, J = 7.1 Hz, 2H), 2.41–2.31 (m, 1H), 1.52–1.41 (m, 4H), 1.35–1.21 (m, 4H), 1.09–1.01 (m, 2H), 0.88–0.78 (m, 2H) ppm; **ESI-MS**: m/z = 689.0 ([M + H]$^+$, calcd. for $C_{27}H_{22}N_2O_7{}^{79}BrClF_3S^+$: 689.0), 691.0 ([$M$ + H]$^+$, calcd. for $C_{27}H_{22}N_2O_7{}^{81}BrClF_3S^+$: 691.0), 693.0 ([M + H]$^+$, calcd. for $C_{27}H_{22}N_2O_7{}^{81}Br^{37}ClF_3S^+$: 693.0).

Ethyl 2-(5-Bromo-6-(*N*-(4-chloro-3-(trifluoromethyl)phenyl)-*N*-(cyclopropanecarbonyl)sulfamoyl)-1-(cyclopropanecarbonyl)-1*H*-indol-3-yl)acetate (SI-12)

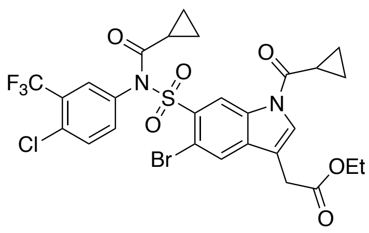

To a suspension of **SI-11** (20 mg, 32 µmol) in TFA (59 µL, 772 µmol, 24.0 eq.) at 0 °C, triethylsilane (62 µL, 386 µmol, 12.0 eq.) was added. The mixture was stirred at rt for 6 h, and the TFA was co-evaporated with toluene (5 mL). Purification by flash master chromatography (SiO_2; EtOAc in cyclohexane 0 → 90%) afforded **SI-12** (3 mg, 14%) as an off-white amorphous solid.

^{1}H NMR (400 MHz, $CDCl_3$): δ = 8.77 (br. s, 1H), 8.34 (s, 1H), 7.93 (d, J = 2.7 Hz, 2H), 7.73 (dd, J = 8.4, 2.3 Hz, 1H), 7.60 (d, J = 8.4 Hz, 1H), 7.37 (s, 1H), 4.20 (q, J = 7.1 Hz, 2H), 3.73 (s, 2H), 1.58–1.50 (m, 1H), 1.29 (t, J = 7.1 Hz, 3H), 1.09–0.99 (m, 2H), 0.87–0.78 ppm (m, 2H); **ESI-MS**: m/z = 675.0 ([M + H]$^+$, calcd. for $C_{27}H_{24}N_2O_6{}^{79}BrClF_3S^+$: 675.0), 677.0 ([$M$ + H]$^+$, calcd. for $C_{27}H_{24}N_2O_6{}^{81}BrClF_3S^+$: 677.0), 679.0 ([M + H]$^+$, calcd. for $C_{27}H_{24}N_2O_6{}^{81}Br^{37}ClF_3S^+$: 679.0).

tert-Butyl (1-(5-Bromo-6-(*N*-(4-chloro-3-(trifluoromethyl)phenyl)sulfamoyl)-1-(cyclopropanecarbonyl)-1*H*-indol-3-yl)-2-oxo-7,10,13-trioxa-3-azahexadecan-16-yl)carbamate (SI-13)

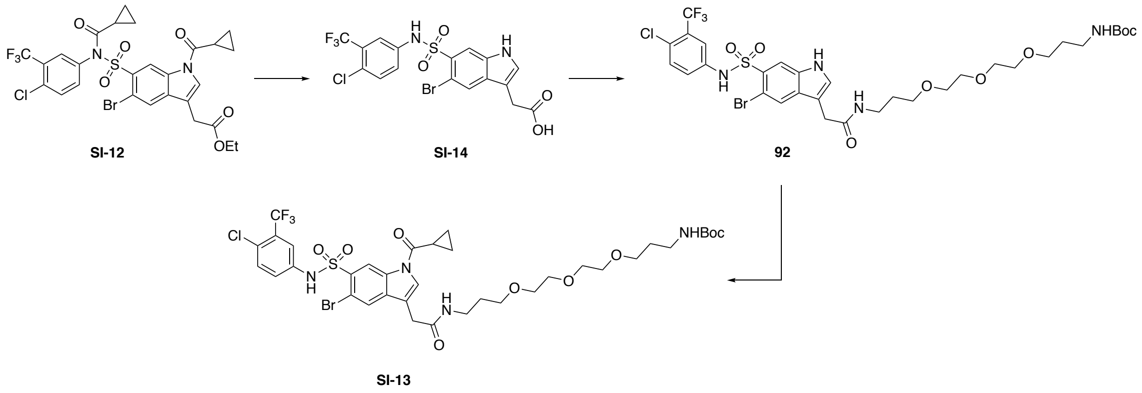

To a solution of **SI-12** (15 mg, 25 µmol, but **SI-10** should have been used instead) in THF/MeOH/H_2O 2:1:1 (1 mL), LiOH (3 mg, 74 µmol, 3.0 eq.) was added. The mixture was stirred at rt for 4 h, concentrated under reduced pressure, and dried *in vacuo*. The hydrolysis product **SI-14** was used in the next step without further purification.

To a solution of crude acid **SI-14** in CH_2Cl_2 (1 mL), EDC·H_2O (10 mg, 59 µmol, 1.5 eq.) and HOBt·H_2O (1.5 mg, 10 µmol, 0.3 eq.) were successively added. After 10 min pre-activation of the acid, a solution of **91** (14 mg, 43 µmol, 1.1 eq.) in CH_2Cl_2 (500 µL) was added, followed by DIPEA (14 µL, 79 µmol, 2.0 eq.). The solution was stirred at rt for 16 h and diluted with EtOAc (5 mL). The organic layer was washed with $NaHCO_3$ (1 x 2 mL), an aq. 1 M HCl solution (1 x 2 mL), and brine (1 x 2 mL). The organic layer was dried over $MgSO_4$, filtered, and concentrated under reduced pressure and dried *in vacuo*. The crude product was used in the next step without further purification.

To a solution of crude **92** and DIPEA (14 µL, 77 µmol, 2.0 eq.) in CH_2Cl_2 (1 mL) under an argon atmosphere, DMAP (0.1 mg, 2 mol%) was added. The solution was cooled to 0 °C, and a solution of cyclopropyl acyl chloride (4 µL, 43 µmol, 1.1 eq.) in CH_2Cl_2 (500 µmol) was added slowly. After stirring for 10 min at 0 °C and 2 h at rt, EtOAc was added (5 mL), and the organic layer was washed with an aq. 1 M HCl solution (1 x 2 mL), sat. aq. $NaHCO_3$ (1 x 2 mL), and brine (1 x 2 mL). The organic layer was dried over $MgSO_4$, filtered, and concentrated. Purification preparative HPLC afforded the TFA salt of **SI-13** (17 mg, 45%) as a white powder.

^{1}H NMR (400 MHz, CD_3OD): δ = 9.24 (s, 1H), 8.18 (s, 1H), 8.00 (s, 1H), 7.54 (d, J = 2.1 Hz, 1H), 7.39–7.35 (m, 2H), 3.66–3.61 (m, 4H), 3.61–3.40 (m, 10H), 3.16–3.06 (m, 4H), 2.56–2.48 (m, 1H), 1.80–1.63 (m, 4H), 1.41 (s, 9H), 1.27–1.24 (m, 2H), 1.22–1.13 ppm (m, 2H); **HR-ESI-MS**: m/z =

881.1795 ([*M* + H]$^+$, calcd. for $C_{36}H_{46}{}^{79}Br^{35}ClF_3N_4O_9S^+$: 881.1804), 883.1768 ([*M* + H]$^+$, calcd. for $C_{36}H_{46}{}^{79}Br^{37}ClF_3N_4O_9S^+$: 883.1775), 885.2 ([*M* + H]$^+$, calcd. for $C_{36}H_{46}{}^{81}Br^{37}ClF_3N_4O_9S^+$: 885.2).

N-(3-(2-(2-(3-Aminopropoxy)ethoxy)ethoxy)propyl)-2-(5-bromo-6-(*N*-(4-chloro-3-(trifluoromethyl)phenyl)sulfamoyl)-1-(cyclopropanecarbonyl)-1*H*-indol-3-yl)acetamide (93)

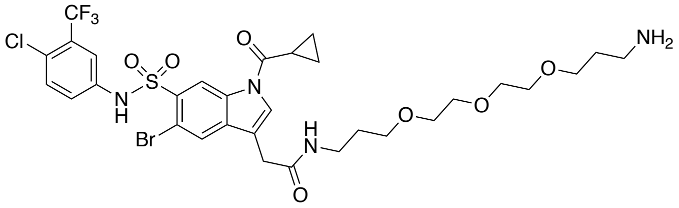

To a solution of **SI-13** (17 mg, 19 μmol) in CH_2Cl_2 (1 mL), TFA (7 μL, 96 μmol, 5.0 eq.) was added. The solution was stirred for 1 h at rt and the solvent co-evaporated with toluene. Purification by preparative HPLC afforded the TFA salt of **93** (10 mg, 58%) as a white amorphous solid.

^{1}H NMR (500 MHz, CD_3OD): δ = 9.26 (s, 1H), 8.20 (s, 1H), 8.02 (s, 1H), 7.55 (d, *J* = 2.0 Hz, 1H), 7.42–7.36 (m, 2H), 3.65 (s, 2H), 3.59 (t, *J* = 5.5 Hz, 2H), 3.57–3.53 (m, 6H), 3.50–3.46 (m, 2H), 3.43 (t, *J* = 6.0 Hz, 2H), 3.27 (t, *J* = 6.9 Hz, 2H), 3.02 (t, *J* = 6.3 Hz, 2H), 2.54 (ddd, *J* = 12.3, 8.0, 4.5 Hz, 1H), 1.83 (dt, *J* = 11.9, 6.0 Hz, 2H), 1.73 (dt, *J* = 12.9, 6.4 Hz, 2H), 1.30–1.24 (m, 2H), 1.18 ppm (dt, *J* = 11.4, 3.7 Hz, 2H); **HR-ESI-MS**: *m*/*z* = 781.1291 ([*M* + H]$^+$, calcd. for $C_{31}H_{38}{}^{79}BrClF_3N_4O_7S^+$: 781.1280), 783.1257 ([*M* + H]$^+$, calcd. for $C_{31}H_{38}{}^{81}BrClF_3N_4O_7S^+$: 783.1259), 785.1237 ([*M* + H]$^+$, calcd. for $C_{31}H_{38}{}^{81}Br^{37}ClF_3N_4O_7S^+$: 785.1230).

v. Synthesis of 2nd Generation Control Probe for Pull-Down

Ethyl 2-(5-Bromo-6-(*N*-(3,5-difluorophenyl)sulfamoyl)-1*H*-indol-3-yl)-2-oxoacetate (SI-15)

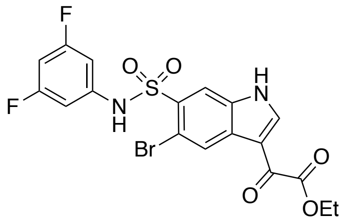

Oxoacetate **SI-15** was prepared following the procedure employed in the synthesis of **75**, using **95** (140 mg, 361 µmol). Purification by flash column chromatography (SiO_2; cyclohexane/EtOAc 4:1 → 2:3) afforded **SI-15** (126 mg, 72%) as an off-white amorphous solid.

^{1}H NMR (600 MHz, DMSO-d_6): δ = 12.80 (d, J = 2.9 Hz, 1H), 11.23 (s, 1H), 8.73 (d, J = 3.3 Hz, 1H), 8.46 (s, 1H), 8.43 (s, 1H), 6.83 (tt, J = 9.2, 2.2 Hz, 1H), 6.78–6.71 (m, 2H), 4.35 (q, J = 7.1 Hz, 2H), 1.33 ppm (t, J = 7.1 Hz, 3H); **^{13}C NMR** (151 MHz, DMSO-d_6): δ = 178.7, 162.7 (dd, J = 245.0, 15.5 Hz), 162.5, 142.3, 140.1 (t, J = 13.5 Hz), 134.4, 131.8, 130.2, 127.1, 117.5, 111.9, 111.8, 101.6–101.1 (m), 98.83 (t, J = 26.1 Hz), 62.1, 13.9 ppm; **^{19}F NMR** (565 MHz, DMSO-d_6): δ = -108.22 ppm; **HR-ESI-MS**: m/z = 486.9767 ($[M + H]^+$, calcd. for $C_{18}H_{14}{}^{79}BrF_2N_2O_5S^+$: 486.97694); 488.97455 ($[M + H]^+$, calcd. for $C_{18}H_{14}{}^{81}BrF_2N_2O_5S^+$: 488.97489).

Ethyl 2-(5-Bromo-1-(cyclopropanecarbonyl)-6-(*N*-(3,5-difluorophenyl)sulfamoyl)-1*H*-indol-3-yl)acetate (SI-16)

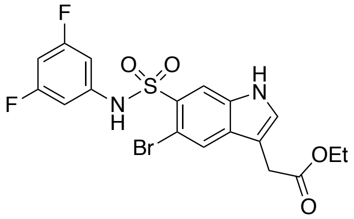

Indole ethyl acetate **SI-16** was prepared following the procedure employed in the synthesis of **90**, using **SI-15** (185 mg, 380 µmol). Purification by flash master chromatography (SiO_2; MeOH in CH_2Cl_2 0 → 17.5%) afforded **SI-16** (105 mg, 58%) as an off-white amorphous solid.

^{1}H NMR (500 MHz, DMSO-*d*$_6$): δ = 11.64 (d, *J* = 1.9 Hz, 1H), 11.02 (s, 1H), 8.28 (s, 1H), 7.94 (s, 1H), 7.62 (d, *J* = 2.5 Hz, 1H), 6.91–6.68 (m, 3H), 4.06 (q, *J* = 7.1 Hz, 2H), 3.77 (s, 2H), 1.17 ppm (t, *J* = 7.1 Hz, 3H); **ESI-MS**: *m*/*z* = 475.0130 ([*M* + H]$^+$, calcd. for $C_{18}H_{18}BrF_2N_2O_4S^+$: 475.0139).

tert-Butyl (1-(5-Bromo-6-(*N*-(3,5-difluorophenyl)sulfamoyl)-1*H*-indol-3-yl)-2-oxo-7,10,13-trioxa-3-azahexadecan-16-yl)carbamate (SI-17)

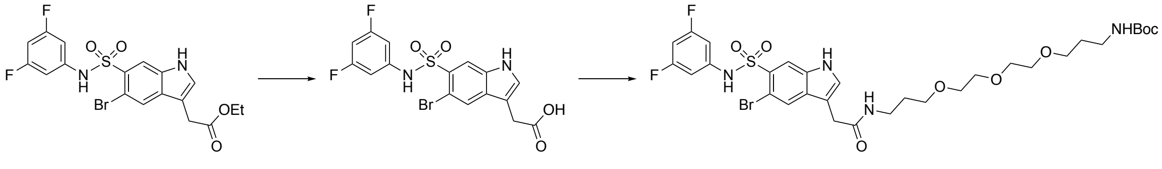

Acid **SI-18** was prepared following the procedure employed in the synthesis of **SI-14** using **SI-16** (48 mg, 101 µmol). The crude product was used in the next step without further purification.

To a solution of crude **SI-18** (29 mg, 39 µmol) in DMF (1 mL), EDC·H_2O (18 mg, 96 µmol, 1.5 eq.) and HOBt·H_2O (3 mg, 16 µmol, 0.3 eq.) were successively added. After 10 min pre-activation of the acid, a solution of **91** (23 mg, 70 µmol, 1.1 eq.) in CH_2Cl_2 (500 µL) was added, followed by DIPEA (28 µL, 160 µmol, 2.0 eq.). The solution was stirred at rt for 4 h, concentrated *in vacuo*, and diluted with EtOAc (5 mL). The organic layer was washed with $NaHCO_3$ (1 x 2 mL), an aq. 1 M HCl solution (1 x 2 mL), and brine (1 x 2 mL). The organic layer was dried over $MgSO_4$, filtered, concentrated under reduced pressure, and dried *in vacuo*. Crude product **SI-17** was used in the next step without further purification.

^{1}H NMR (600 MHz, $CDCl_3$): δ = 8.21 (s, 1H), 7.86 (s, 1H), 7.37 (s, 1H), 6.74 (dd, *J* = 7.9, 1.8 Hz, 2H), 6.42 (t, *J* = 8.8 Hz, 1H), 3.63 (s, 2H), 3.61–3.18 (m, 16H), 1.81–1.71 (m, 2H), 1.71–1.62 (m, 2H), 1.44 ppm (s, 9H); **^{19}F NMR** (565 MHz, $CDCl_3$): δ = -108.05 ppm; **HR-ESI-MS**: *m*/*z* = 747.1869 ([*M* + H]$^+$, calcd. for $C_{31}H_{42}{}^{79}BrF_2N_4O_8S^+$: 747.1869), 749.1847 ([*M* + H]$^+$, calcd. for $C_{31}H_{42}{}^{81}BrF_2N_4O_8S^+$: 749.1849).

N-(3-(2-(2-(3-aminopropoxy)ethoxy)ethoxy)propyl)-2-(5-bromo-1-(cyclopropanecarbonyl)-6-(*N*-(3,5-difluorophenyl)sulfamoyl)-1*H*-indol-3-yl)acetamide (94)

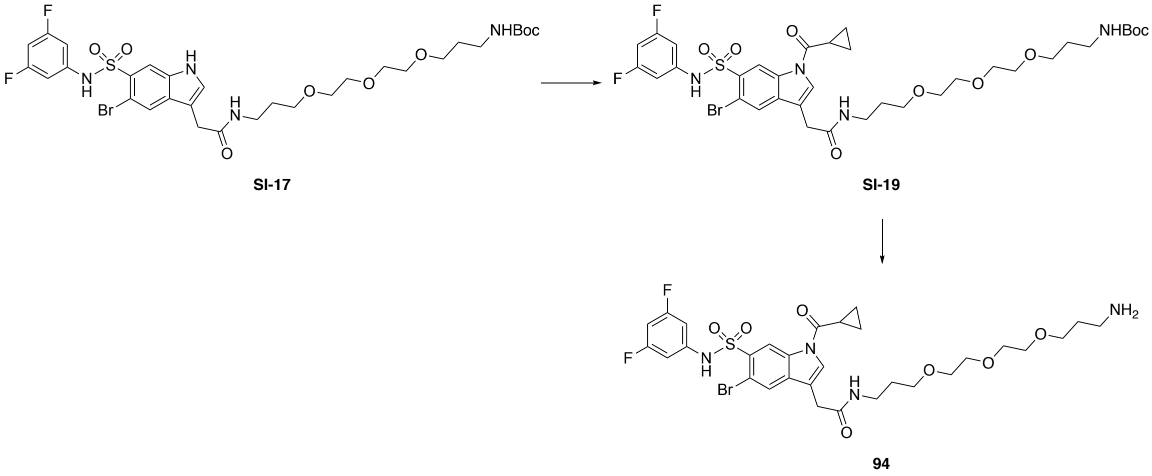

Cyclopropyl amide **SI-19** was prepared following the procedure employed in the synthesis of **SI-13**, using **SI-17** (30 mg, 40 µmol). The crude product was used without further purification in the next step.

Boc-deprotection of **SI-19** was accomplished following the procedure employed in the synthesis of **93**. Purification by preparative HPLC afforded the TFA salt of **94** (10 mg, 72%) as a white amorphous solid.

^{1}H NMR (500 MHz, CD_3OD): δ = 9.27 (s, 1H), 8.20 (s, 1H), 8.02 (s, 1H), 6.79–6.70 (m, 2H), 6.52 (tt, J = 9.1, 2.3 Hz, 1H), 3.66 (s, 2H), 3.59 (t, J = 5.5 Hz, 2H), 3.58–3.53 (m, 5H), 3.50–3.46 (m, 2H), 3.43 (t, J = 6.0 Hz, 2H), 3.27 (t, J = 6.9 Hz, 2H), 3.02 (t, J = 6.3 Hz, 2H), 2.59–2.50 (m, 1H), 1.87–1.80 (m, 2H), 1.79–1.71 (m, 2H), 1.31–1.25 (m, 3H), 1.22–1.14 ppm (m, 2H); **HR-ESI-MS**: m/z = 715.1609 ($[M + H]^+$, calcd. for $C_{30}H_{38}{}^{79}BrF_2N_4O_7S^+$: 715.1607), 717.1585 ($[M + H]^+$, calcd. for $C_{30}H_{38}{}^{81}BrF_2N_4O_7S^+$: 717.1587).

vi. C3-Functionalization of Indoles

tert-Butyl (_E_)-3-(5-Bromo-6-(_N_-(4-chloro-3-(trifluoromethyl)phenyl)sulfamoyl)-1_H_-indol-3-yl)acrylate (74)

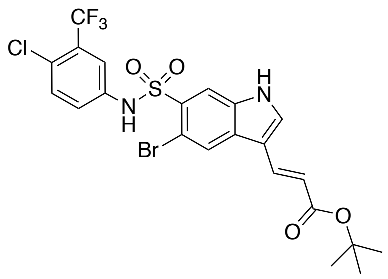

To a mixture of **17** (50 mg, 110 µmol), *tert*-butyl acrylate (32 µL, 200 µmol, 2.0 eq.), and Cu(OAc)$_2$ (36 mg, 198 µmol, 1.8 eq.) in DMF/DMSO (1.5 mL, 9:1) under an argon atmosphere, Pd(OAc)$_2$ (2.5 mg, 11 µmol, 10 mol%) was added. The mixture was stirred at 70 °C for 18 h, cooled to rt, partitioned between water and EtOAc (10 mL, 1:1), and filtered through a pad of Celite®. The organic layer was washed with brine (1 x 5 mL), dried over MgSO$_4$, filtered, and concentrated under reduced pressure. Purification by flash column chromatography (SiO$_2$; CH$_2$Cl$_2$/MeOH 100:0 → 99.5:0.5 → 99:1) afforded **74** (20 mg, 31%) as an off-white amorphous solid.

^{1}H NMR (400 MHz, CDCl$_3$): δ = 8.97 (s, 1H), 8.19 (d, J = 5.8 Hz, 2H), 7.70 (d, J = 16.1 Hz, 1H), 7.65 (d, J = 2.8 Hz, 1H), 7.53 (d, J = 2.4 Hz, 1H), 7.44 (s, 1H), 7.32–7.26 (m, 2H), 6.33 (d, J = 16.1 Hz, 1H), 1.55 ppm (s, 9H); **HR-ESI-MS**: m/z = 578.9962 ([M + H]$^+$, calcd. for $C_{22}H_{20}BrClF_3N_2O_4S^+$: 578.9962).

tert-Butyl (_E_)-3-(5-Bromo-1_H_-indol-3-yl)acrylate (77)[107]

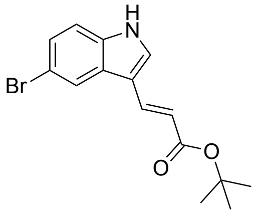

Indole acrylate **77** was prepared following the procedure employed in the synthesis of **74**, using 5-bromoindole (**76**, 1.000 g, 5.1 mmol) in DMF/DMSO (12 mL, 9:1). Purification by flash column chromatography (SiO$_2$; cyclohexane/EtOAc 95:5→ 9:1) afforded **77** (882 mg, 54%) as an off-white amorphous solid.

^{1}H NMR (600 MHz, $CDCl_3$): δ = 8.55 (br. s, 1H), 8.04 (s, 1H), 7.75 (d, J = 16.0 Hz, 1H), 7.45 (s, 1H), 7.36 (d, J = 8.6 Hz, 1H), 7.28 (d, J = 8.6 Hz, 1H), 6.34 (d, J = 16.0 Hz, 1H), 1.56 ppm (s, 9H); **^{13}C NMR** (151 MHz, $CDCl_3$): δ = 167.5, 136.4, 135.8, 129.1, 127.1, 126.3, 123.3, 116.4, 114.9, 113.5, 113.2, 80.3, 28.5 ppm; **HR-ESI-MS**: m/z = 322.0433 ([M + H]$^+$, calcd. for $C_{15}H_{17}{}^{79}BrNO_2{}^+$: 322.0437), 324.0413 ([$M$ + H]$^+$, calcd. for $C_{15}H_{17}{}^{81}BrNO_2{}^+$: 324.04167).

Ethyl 2-(5-Bromo-1*H*-indol-3-yl)-2-oxoacetate (78)[169]

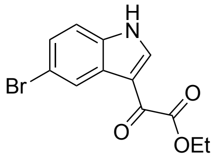

To a solution of 5-bromoindole (1.000 g, 5.1 mmol) in Et_2O (7.5 mL) at 0 °C under an argon atmosphere, oxalyl chloride (878 µL, 10.2 mmol, 2.0 eq.) was added. The mixture was stirred at rt for 4 h concentrated and concentrated under reduced pressure. EtOH (7.5 mL) was added and the mixture was stirred for a further 1 h and concentrated under reduced pressure. The residue was dissolved in EtOAc (100 mL), washed with brine (100 mL), dried over $MgSO_4$, and concentrated under reduced pressure. Purification by flash chromatography (SiO_2; cyclohexane/EtOAc 4:1 → 2:3) afforded **78** (1.300 g, 86%) as a light-brown amorphous solid

^{1}H NMR (400 MHz, CD_3OD): δ = 8.45 (s, 1H), 8.43–8.40 (m, 1H), 7.44–7.41 (m, 2H), 4.41 (q, J = 7.1 Hz, 2H), 1.42 ppm (t, J = 7.1 Hz, 3H); **^{13}C NMR** (151 MHz, CD_3OD): δ = 173.0, 141.0, 140.0, 132.9, 129.5, 119.5, 108.5, 62.0, 52.9, 39.5, 38.6, 14.5 ppm; **HR-ESI-MS**: m/z = 295.9926 ([M + H]$^+$, calcd. for $C_{12}H_{11}{}^{79}BrNO_3{}^+$: 295.9917), 297.9905 ([$M$ + H]$^+$, calcd. for $C_{12}H_{11}{}^{81}BrNO_3{}^+$: 297.9896).

Ethyl 2-(5-Bromoindolin-3-yl)acetate (79)

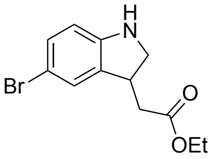

To a suspension of **78** (1.044 g, 3.5 mmol) in TFA (6.5 mL, 85 µmol, 24.0 eq.) at 0 °C, Et_3SiH (6.8 mL, 42 mmol, 12.0 eq.) was added. The mixture was stirred for 6 h and the TFA co-evaporated with toluene. The product was purified by flash column chromatography (SiO_2; cyclohexane/EtOAc 9:1 → 5:1) to afford **79** (900 mg, 90%) as a thick brownish oil.

^{1}H NMR (600 MHz, MeOD): δ = 7.57 (s, 1H), 7.48 (dd, J = 8.4, 1.6 Hz, 1H), 7.17 (d, J = 8.4 Hz, 1H), 4.21–4.11 (m, 2H), 4.00 (dd, J = 11.0, 8.7 Hz, 1H), 3.94–3.86 (m, 1H), 3.56 (dd, J = 11.0, 6.5 Hz, 1H), 2.92 (dd, J = 16.9, 5.4 Hz, 1H), 2.73 (dd, J = 16.9, 8.1 Hz, 1H), 1.25 ppm (t, J = 7.1 Hz, 3H); **^{13}C NMR** (151 MHz, MeOD): δ = 173.0, 141.0, 140.0, 132.9, 129.5, 119.5, 108.5, 62.0, 52.9, 39.5, 38.6, 14.5 ppm; **ESI-MS**: m/z = 284.0 ($[M + H]^+$, calcd. for $C_{12}H_{15}{}^{79}BrNO_2^+$: 284.0), 286.0 ($[M + H]^+$, calcd. for $C_{12}H_{15}{}^{81}BrNO_2^+$: 286.0).

Ethyl 2-(5-Bromo-1-(cyclopropanecarbonyl)indolin-3-yl)acetate (80)

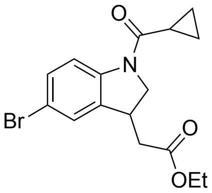

To a solution of **79** (900 mg, 3.2 mmol) and Et_3N (1.7 mL, 9.5 mmol, 3.0 eq.) in CH_2Cl_2 (7 mL) under an argon atmosphere, DMAP (7.7 mg, 63 µmol, 2 mol%) was added. The solution was cooled to 0 °C, and cyclopropyl acyl chloride (323 µL, 3.5 mmol, 1.1 eq.) was added. The mixture was stirred at 0 °C for 10 min and at rt for 2 h. EtOAc was added (50 mL), and the mixture was washed with brine (1 x 30 mL). The organic layer was dried over Na_2SO_4, filtered, and concentrated under reduced pressure. Purification by flash column chromatography (SiO_2; pentane/CH_2Cl_2 1:1 → 9:1) afforded **80** (775 mg, 70%) as an off-white amorphous solid.

^{1}H NMR (400 MHz, $CDCl_3$): δ = 8.05 (br. s, 1H), 7.31 (dd, J = 8.6, 2.0 Hz, 1H), 7.27 (s, 1H), 4.62–4.46 (m, 1H), 4.27–4.13 (m, 2H), 3.98 (dd, J = 10.3, 6.1 Hz, 1H), 3.90–3.75 (m, 1H), 2.81 (dd, J = 16.6, 4.6 Hz, 1H), 2.59 (dd, J = 16.6, 9.8 Hz, 1H), 1.82–1.66 (m, 1H), 1.28 (t, J = 7.1 Hz, 3H), 1.15–1.07 (m, 2H), 0.94–0.86 ppm (m, 2H); **^{13}C NMR** (101 MHz, $CDCl_3$): δ = 172.06, 171.64, 142.32, 135.48, 131.34, 126.96, 118.58, 115.88, 61.13, 54.77, 39.97, 36.40, 14.36, 13.74, 8.70, 8.62 ppm; **HR-ESI-MS**: m/z = 352.0551 ($[M + H]^+$, calcd. for $C_{16}H_{19}{}^{79}BrNO_3^+$: 352.0543), 354.0530 ($[M + H]^+$, calcd. for $C_{16}H_{19}{}^{81}BrNO_3^+$: 354.0522).

(5-Bromo-3-(2-hydroxyethyl)indolin-1-yl)(cyclopropyl)methanone (81)

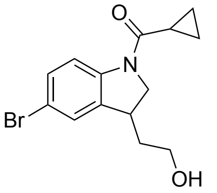

To a solution of **80** (111 mg, 315 µmol) in anhydrous Et_2O (1 mL) at 0 °C under an argon atmosphere, MeOH (2 drops) and $LiBH_4$ (2 M in THF, 630 µL, 1.3 mmol, 4.0 eq) were added dropwise. The mixture was stirred for 2 h at rt, cooled to 0 °C, and quenched via slow addition of MeOH (1.6 mL), followed by careful addition of solid NH_4Cl (157 mg) in small portions. The resulting mixture was stirred for 1 h at rt, and the solvent was removed under reduced pressure. The mixture was re-suspended in EtOAc (30 mL) and washed with brine (1 x 20 mL). The organic layer was dried over $MgSO_4$, filtered, concentrated under reduced pressure, and dried *in vacuo*. The crude product was used without further purification in the next step.

(5-Bromo-3-(2-((*tert*-butyldimethylsilyl)oxy)ethyl)indolin-1-yl)(cyclopropyl)methanone (82)

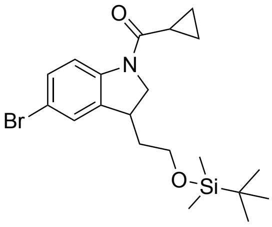

To a solution of **81** (39 mg, 126 µmol) in DMF (1 mL) at 0 °C under an argon atmosphere, TBDMSCl (41 mg, 264 µmol, 2.1 eq.) and imidazole (18 mg, 264 mmol, 2.1 eq.) were added. The mixture was warmed to rt and stirred for 2 h. EtOAc (20 mL) was added, and the organic phase was washed with brine (2 x 10 mL). Purification by flash master chromatography (SiO_2; EtOAc in cyclohexane 0 → 100%) afforded **82** (42 mg, 80%) as an off-white amorphous solid.

^{1}H NMR (400 MHz, $CDCl_3$): δ = 8.06 (br. s, 1H), 7.32–7.23 (m, 2H), 4.39 (t, J = 9.6 Hz, 1H), 4.12–3.94 (m, 1H), 3.76 (t, J = 5.9 Hz, 2H), 3.63–3.44 (m, 1H), 2.08–1.93 (m, 1H), 1.88–1.60 (m, 2H), 1.14–1.07 (m, 2H), 0.90 (s, 9H), 0.88–0.83 (m, 2H), 0.07 ppm (d, J = 4.8 Hz, 6H); **ESI-MS**: m/z = 424.0 ($[M + H]^+$, calcd. for $C_{20}H_{31}{}^{79}BrNO_2Si^+$: 424.1), 426.0 ($[M + H]^+$, calcd. for $C_{20}H_{31}{}^{81}BrNO_2Si^+$: 426.1).

2-(5-Bromo-1-(cyclopropanecarbonyl)indolin-3-yl)ethyl Acetate (83)

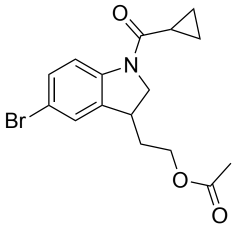

A solution of **81** (40 mg, 129 µmol), Ac_2O (14 µL, 142 µmol, 1.1 eq.), and DMAP (0.1 mg, 2 mol%) in pyridine (2 mL) under an argon atmosphere was stirred at rt for 16 h. The mixture was concentrated under reduced pressure, re-suspended in EtOAc (20 mL), and washed with an aq. 1 M HCl solution (10 mL). The organic layer was dried over $MgSO_4$, filtered, and concentrated under reduced pressure. Purification by flash master chromatography (SiO_2; EtOAc in cyclohexane 0 → 40%) afforded **83** (38 mg, 83%) as an off-white amorphous solid.

^{1}H NMR (400 MHz, $CDCl_3$): δ = 8.12–7.92 (m, 1H), 7.29–7.20 (m, 2H), 4.38 (t, J = 9.0 Hz, 1H), 4.25–4.07 (m, 2H), 3.95 (dd, J = 9.5, 6.0 Hz, 1H), 3.56–3.40 (m, 1H), 2.21–2.08 (m, 1H), 2.05 (s, 3H), 1.95–1.81 (m, 1H), 1.79–1.62 (m, 1H), 1.16–1.02 (m, 2H), 0.95–0.81 ppm (m, 2H); **ESI-MS**: m/z = 352.0 ($[M + H]^+$, calcd. for $C_{16}H_{19}{}^{79}BrNO_3^+$: 352.1), 354.0 ($[M + H]^+$, calcd. for $C_{16}H_{19}{}^{81}BrNO_3^+$: 354.1).

7. LIST OF ABBREVIATIONS

°C	degrees Celsius
4EPB1	eukaryotic initiation factor 4E-binding protein 1
ABL1	abelson murine leukemia viral oncogene homolog 1
AC	adenylate cyclase
Ac	acyl
AFC	Ac-LLY-7-amino-4-trifluoromethylcoumarin
AMBRA	activating molecule in BECN1-regulated autophagy protein 1
AMPK	5'-AMP-activated protein kinase
aq.	aqueous
Ar	aryl
ATG	autophagy-related
Bcl-2	B cell lymphoma 2
Boc	t-butyloxycarbonyl
BSA	bovine serum albumin
calcd.	calculated
CAPN1	catalytic subunit of calpain-1
CAS	Chemical Abstracts Service
cat.	catalytic
CETSA	cellular thermal shift assay
COMAS	Compound Management and Screening Center
COMU	(1-cyano-2-ethoxy-2-oxoethylidenaminooxy)dimethylamino-
morpholino-	carbenium hexafluorophosphate
CQ	chloroquine
CREB	cAMP response element-binding protein
DAG	diacyl glycerol
DARTS	drug affinity responsive target stability
DCC	dicyclohexyl-carbodiimide
DDQ	,3-dichloro-5,6-dicyano-1,4-benzoquinone
DIPEA	*N*,*N*-diisopropylethylamine
DMAP	4-dimethylamino pyridine
DMF	dimethyl formamide
DMSO	dimethyl sulfoxide
DSF	differential scanning fluorimetry
EDC	1-ethyl-3-(3-dimethylaminopropyl)carbodiimide

eGFP	enhanced green fluorescent protein
EPAC	exchange protein directly activated by cAMP
equiv.	equivalents
ER	endoplasmic reticulum
FCG	forward chemical genetics
FDA	Food and Drug Administration
FP	fluorescence polarization
GABARAP	gamma-aminobutyric acid receptor-associated protein
GDH, GLUD	glutamate dehydrogenase
GEF	guanine nucleotide exchange factor
GFP	green fluorescent protein
GPCR	G-protein coupled receptor
HINT-1	histidine triad nucleotide binding protein 1
HIP	haploinsufficiency profiling
HPLC	high performance liquid chromatography
HR	high resolution
HT	hydroxytryptamine
Hz	Hertz
IC_{50}	half maximal inhibitory concentration
IGD	in-gel digest
IP_3	inositol 1,4,5-trisphosphate
J	coupling constant
KG	α-ketoglutarate
LC	liquid chromatography
LC3	light chain 3
LOPAC	library of pharmaceutically active compounds
MAPK	mitogen-activated protein kinase
MKK	mitogen-activated protein kinase kinase
MS	mass spectrometry
mTOR	mammalian target of rapamycin
NBS	*N*-bromosuccinimide
NHS	*N*-hydroxysuccinimide
NMM	*N*-methyl-morpholine
NMR	nuclear manetic resonance
OBD	on-bead digest
PAGE	polyacrylamide gel electrophoresis
PBS	phosphate-buffered saline

PE	phosphatidylethanolamine
PEG	polyethylene glycol
PHD	prolyl hydroxylase
PI3K	phosphoinositide 3-kinase
PI3P	phosphatidylinositol 3-phosphate
pin	pinacol
PIP_2	phosphatidylinositol 4,5-bisphosphate
PK	pyruvate kinase
PKA, PKB, and PKC	protein kinase A, B, and C
PLC	phospholipase C
PyBOP	benzotriazol-1-yl-oxytripyrrolidinophosphonium hexafluorophosphate
qPCR	quantitative polymerase chain reaction
RAF	rapidly accelerated fibrosarcoma
RAS	rat sarcoma
resp.	respectively
RHEB	RAS homolog enriched in brain
rt	room temperature
RTK	receptor tyrosine kinase
SAR	structure–activity relationship
SDS	sodium dodecyl sulfate
SEA	Similarity Ensemble Approach
SH3GLB1	endophilin-B1
SILAC	stable isotope labeling with amino acids in cell culture
siRNA	Small interfering RNA
SIRT4	sirtuin 4
SMM	small-molecule modulator
T3P	propylphosphonic anhydride
TBAF	tetrabutylammonium fluoride
TBDMS	*t*-butyldimethylsilyl
TBS	tris-buffered saline
TCEP	tris(2-carboxyethyl)phosphine
TCF/LEF	T-cell factor/lymphoid enhancer factor
TEAB	triethylammonium bicarbonate
TFA	trifluoroacetic acid
TFEB	transcription factor EB
THF	tetrahydrofuran

TMT10	neutron-encoded isobaric mass tagging reagents
TPP	thermal proteome profiling
TSA	thermal shift assay
TSC	tuberous sclerosis
TXNL1	thioredoxin-like protein 1
ULK1	unc-51 like autophagy activating kinase 1
UVRAG	UV radiation resistance-associated gene protein
VCS	valosin-containing protein
VPS34	vacuolar protein sorting 34 (class III PI3K)
WIPI	WD repeat domain phosphoinositide-interacting protein

8. REFERENCES

[1] H. Spemann, H. Mangold, *W. Roux. Arch. Entw. Organ.* **1924**, *100*, 599–638. Über Induktion von Embryonalanlagen durch Implantation artfremder Organisatoren.

[2] B. Alberts, A. Johnson, J. Lewis, M. Raff, K. Roberts, P. Walter, *Molecular Biology of the Cell*, 4th ed., Garland Science, New York, **2002**.

[3] J. Gerhart, *Teratology* **1999**, *60*, 226–239. 1998 Warkany Lecture: Signaling Pathways in Development.

[4] A. Pires-daSilva, R. J. Sommer, *Nat. Rev. Genet.* **2003**, *4*, 39–49. The evolution of signalling pathways in animal development.

[5] P. Mora-Garcia, K. M. Sakamoto, *Mol. Genet. Metab.* **1999**, *66*, 143–171. Cell signaling defects and human disease.

[6] M. J. Berridge, *Cell Signalling Biology* **2014**, *6*, csb0001012. Module 12: Signalling Defects and Disease.

[7] R. J. DeBerardinis, C. B. Thompson, *Cell* **2012**, *148*, 1132–1144. Cellular metabolism and disease: what do metabolic outliers teach us?

[8] A. Persidis, *Nat. Biotechnol.* **2000**, *18*, It37–It39. Signal transduction as a drug-discovery platform - (Reprinted from Nature Biotechnology, vol 16, pg 1082-1083, 1998).

[9] Y. Ohsumi, *Cell Res.* **2014**, *24*, 9–23. Historical landmarks of autophagy research.

[10] C. de Duve, B. C. Pressman, R. Gianetto, R. Wattiaux, F. Appelmans, *Biochem. J* **1955**, *60*, 604–617. Tissue fractionation studies. 6. Intracellular distribution patterns of enzymes in rat-liver tissue.

[11] S. L. Clark, *J. Biophys. Biochem. Cy.* **1957**, *3*, 349–362. Cellular Differentiation in the Kidneys of Newborn Mice Studied with the Electron Microscope.

[12] A. B. Novikoff, H. Beaufay, C. de Duve, *J. Biophys. Biochem. Cy.* **1956**, *2*, 179–184. Electron Microscopy of Lysosome-Rich Fractions from Rat Liver.

[13] A. U. Arstila, B. F. Trump, *Am. J. Pathol.* **1968**, *53*, 687–733. Studies on cellular autophagocytosis. The formation of autophagic vacuoles in the liver after glucagon administration.

[14] C. de Duve, in *Ciba Foundation Symposium on Lysosomes* (Eds.: A. V. S. de Reuck, M. P. Cameron), J. and A. Churchill, Ltd., London, **1963**.

[15] D. C. Rubinsztein, P. Codogno, B. Levine, *Nat. Rev. Drug Discov.* **2012**, *11*, 709–730. Autophagy modulation as a potential therapeutic target for diverse diseases.

[16] N. Mizushima, B. Levine, A. M. Cuervo, D. J. Klionsky, *Nature* **2008**, *451*, 1069–1075. Autophagy fights disease through cellular self-digestion.

[17] D. J. Klionsky, S. D. Emr, *Science* **2000**, *290*, 1717–1721. Cell biology - Autophagy as a regulated pathway of cellular degradation.

[18] Z. Yang, D. J. Klionsky, *Nat. Cell Biol.* **2010**, *12*, 814–822. Eaten alive: a history of macroautophagy.

[19] N. Mizushima, B. Levine, *Nat. Cell Biol.* **2010**, *12*, 823–308. Autophagy in mammalian development and differentiation.

[20] D. C. Rubinsztein, J. E. Gestwicki, L. O. Murphy, D. J. Klionsky, *Nat. Rev. Drug Discov.* **2007**, *6*, 304–312. Potential therapeutic applications of autophagy.

[21] B. Ravikumar, S. Sarkar, J. E. Davies, M. Futter, M. Garcia-Arencibia, Z. W. Green-Thompson, M. Jimenez-Sanchez, V. I. Korolchuk, M. Lichtenberg, S. Luo, D. C. Massey, F. M. Menzies, K. Moreau, U. Narayanan, M. Renna, F. H. Siddiqi, B. R. Underwood, A. R. Winslow, D. C. Rubinsztein, *Physiol. Rev.* **2010**, *90*, 1383–1435. Regulation of mammalian autophagy in physiology and pathophysiology.

[22] L. Galluzzi, E. H. Baehrecke, A. Ballabio*, et al.*, *EMBO J.* **2017**. Molecular definitions of autophagy and related processes.

[23] D. J. Klionsky, *Nat. Rev. Mol. Cell Biol.* **2007**, *8*, 931–937. Autophagy: from phenomenology to molecular understanding in less than a decade.

[24] N. Mizushima, T. Yoshimori, Y. Ohsumi, *Annu. Rev. Cell Dev. Biol.* **2011**, *27*, 107–132. The role of Atg proteins in autophagosome formation.

[25] J. Kim, M. Kundu, B. Viollet, K. L. Guan, *Nat. Cell Biol.* **2011**, *13*, 132–141. AMPK and mTOR regulate autophagy through direct phosphorylation of Ulk1.

[26] A. Williams, S. Sarkar, P. Cuddon, E. K. Ttofi, S. Saiki, F. H. Siddiqi, L. Jahreiss, A. Fleming, D. Pask, P. Goldsmith, C. J. O'Kane, R. A. Floto, D. C. Rubinsztein, *Nat. Chem. Biol.* **2008**, *4*, 295–305. Novel targets for Huntington's disease in an mTOR-independent autophagy pathway.

[27] S. Pattingre, A. Tassa, X. Qu, R. Garuti, X. H. Liang, N. Mizushima, M. Packer, M. D. Schneider, B. Levine, *Cell* **2005**, *122*, 927–939. Bcl-2 antiapoptotic proteins inhibit Beclin 1-dependent autophagy.

[28] C. Settembre, C. Di Malta, V. A. Polito, M. Garcia Arencibia, F. Vetrini, S. Erdin, S. U. Erdin, T. Huynh, D. Medina, P. Colella, M. Sardiello, D. C. Rubinsztein, A. Ballabio, *Science* **2011**, *332*, 1429–1433. TFEB links autophagy to lysosomal biogenesis.

[29] C. G. Towers, A. Thorburn, *EBioMedicine* **2016**, *14*, 15–23. Therapeutic Targeting of Autophagy.

[30] C. He, M. C. Bassik, V. Moresi*, et al.*, *Nature* **2012**, *481*, 511–515. Exercise-induced BCL2-regulated autophagy is required for muscle glucose homeostasis.

[31] B. Ravikumar, R. Duden, D. C. Rubinsztein, *Hum. Mol. Genet.* **2002**, *11*, 1107–1117. Aggregate-prone proteins with polyglutamine and polyalanine expansions are degraded by autophagy.

[32] Z. Berger, B. Ravikumar, F. M. Menzies, L. G. Oroz, B. R. Underwood, M. N. Pangalos, I. Schmitt, U. Wullner, B. O. Evert, C. J. O'Kane, D. C. Rubinsztein, *Hum. Mol. Genet.* **2006**, *15*, 433–442. Rapamycin alleviates toxicity of different aggregate-prone proteins.

[33] J. L. Webb, B. Ravikumar, J. Atkins, J. N. Skepper, D. C. Rubinsztein, *J. Biol. Chem.* **2003**, *278*, 25009–25013. Alpha-Synuclein is degraded by both autophagy and the proteasome.

[34] B. Levine, G. Kroemer, *Cell* **2008**, *132*, 27–42. Autophagy in the pathogenesis of disease.

[35] T. Shintani, D. J. Klionsky, *Science* **2004**, *306*, 990–905. Autophagy in health and disease: a double-edged sword.

[36] A. Caccamo, S. Majumder, A. Richardson, R. Strong, S. Oddo, *J. Biol. Chem.* **2010**, *285*, 13107–13120. Molecular Interplay between Mammalian Target of Rapamycin (mTOR), Amyloid-β, and Tau: Effects on Cognitive Impairments.

[37] P. Jiang, N. Mizushima, *Cell Res.* **2014**, *24*, 69–79. Autophagy and human diseases.

[38] L. Galluzzi, J. M. Bravo-San Pedro, B. Levine, D. R. Green, G. Kroemer, *Nat. Rev. Drug Discov.* **2017**, *16*, 487–511. Pharmacological modulation of autophagy: therapeutic potential and persisting obstacles.

[39] D. R. Spring, *Chem. Soc. Rev.* **2005**, *34*, 472–482. Chemical genetics to chemical genomics: small molecules offer big insights.

[40] S. Ziegler, V. Pries, C. Hedberg, H. Waldmann, *Angew. Chem. Int. Ed.* **2013**, *52*, 2744–2792. Target identification for small bioactive molecules: finding the needle in the haystack.

[41] J. Lehar, B. R. Stockwell, G. Giaever, C. Nislow, *Nat. Chem. Biol.* **2008**, *4*, 674–681. Combination chemical genetics.

[42] M. Kawasumi, P. Nghiem, *J. Invest. Dermatol.* **2007**, *127*, 1577–1584. Chemical Genetics: Elucidating Biological Systems with Small-Molecule Compounds.

[43] K. Hubel, T. Lessmann, H. Waldmann, *Chem. Soc. Rev.* **2008**, *37*, 1361–1374. Chemical biology—identification of small molecule modulators of cellular activity by natural product inspired synthesis.

[44] P. A. Clemons, *Curr. Opin. Chem. Biol.* **2004**, *8*, 334–338. Complex phenotypic assays in high-throughput screening.

[45] T. L. Riss, R. A. Moravec, A. L. Niles, S. Duellman, H. A. Benink, T. J. Worzella, L. Minor, in *Assay Guidance Manual [Internet]* (Eds.: G. S. Sittampalam, N. P. Coussens, K. Brimacombe, A. Grossman, M. Arkin, D. Auld, C. Austin, J. Baell, B. Bejcek, T. D. Y. Chung, J. L. Dahlin, V. Devanaryan, T. L. Foley, M. Glicksman, M. D. Hall, J. V. Hass, J. Inglese, P. W. Iversen, S. D. Kahl, S. C. Kales, M. Lal-Nag, Z. Li, J. McGee, O. McManus, T. Riss, O. J. Trask Jr., J. R. Weidner, M. Xia, X. Xu), Bethesda (MD): Eli Lilly & Company and the National Center for Advancing Translational Sciences, **2013**.

[46] T. Chiba, T. Tsuchiya, R. Mori, I. Shimokawa, *Sensors (Basel)* **2012**, *12*, 1648–1656. Protein reporter bioassay systems for the phenotypic screening of candidate drugs: a mouse platform for anti-aging drug screening.

[47] X.-Y. Li, Y.-Y. Wang, C.-M. Yuan, X.-J. Hao, Y. Li, *Nat. Prod. Bioprospect.* **2013**, *3*, 24–28. A reporter gene system for screening inhibitors of Wnt signaling pathway.

[48] R. A. G. Cinelli, A. Ferrari, V. Pellegrini, M. Tyagi, M. Giacca, F. Beltram, *Photochem. Photobiol.* **2000**, *71*, 771–776. The Enhanced Green Fluorescent Protein as a Tool for the Analysis of Protein Dynamics and Localization: Local Fluorescence Study at the Single-molecule Level.

[49] G. Zhang, V. Gurtu, S. R. Kain, *Biochem. Biophys. Res. Commun.* **1996**, *227*, 707–711. An Enhanced Green Fluorescent Protein Allows Sensitive Detection of Gene Transfer in Mammalian Cells.

[50] F. Zanella, J. B. Lorens, W. Link, *Trends Biotechnol.* **2010**, *28*, 237–245. High content screening: seeing is believing.

[51] E. A. Ponomarenko, E. V. Poverennaya, E. V. Ilgisonis, M. A. Pyatnitskiy, A. T. Kopylov, V. G. Zgoda, A. V. Lisitsa, A. I. Archakov, *Int. J. Anal. Chem.* **2016**, *2016*, 1–6. The Size of the Human Proteome: The Width and Depth.

[52] Y. Zhang, X. Zou, Y. Ding, H. Wang, X. Wu, B. Liang, *BMC Genomics* **2013**, *14*, 164. Comparative genomics and functional study of lipid metabolic genes in Caenorhabditis elegans.

[53] National Research Council, *Transforming Glycoscience: A Roadmap for the Future*, The National Academies Press, Washington, DC, **2012**.

[54] S.-I. Sato, Y. Kwon, S. Kamisuki, N. Srivastava, Q. Mao, Y. Kawazoe, M. Uesugi, *J. Am. Chem. Soc.* **2007**, *129*, 873–880. Polyproline-Rod Approach to Isolating Protein Targets of Bioactive Small Molecules: Isolation of a New Target of Indomethacin.

[55] T. Shiyama, M. Furuya, A. Yamazaki, T. Terada, A. Tanaka, *Biorg. Med. Chem.* **2004**, *12*, 2831–2841. Design and synthesis of novel hydrophilic spacers for the reduction of nonspecific binding proteins on affinity resins.

[56] M. H. Wright, S. A. Sieber, *Nat. Prod. Rep.* **2016**, *33*, 681–708. Chemical proteomics approaches for identifying the cellular targets of natural products.

[57] S. E. Ong, B. Blagoev, I. Kratchmarova, D. B. Kristensen, H. Steen, A. Pandey, M. Mann, *Molecular & Cellular Proteomics* **2002**, *1*, 376-386. Stable isotope labeling by amino acids in cell culture, SILAC, as a simple and accurate approach to expression proteomics.

[58] S. E. Ong, M. Schenone, A. A. Margolin, X. Y. Li, K. Do, M. K. Doud, D. R. Mani, L. Kuai, X. Wang, J. L. Wood, N. J. Tolliday, A. N. Koehler, L. A. Marcaurelle, T. R. Golub, R. J. Gould, S. L. Schreiber, S. A. Carr, *Proc. Natl. Acad. Sci. USA* **2009**, *106*, 4617–4622. Identifying the proteins to which small-molecule probes and drugs bind in cells.

[59] B. Lomenick, R. W. Olsen, J. Huang, *ACS Chem. Biol.* **2011**, *6*, 34–46. Identification of direct protein targets of small molecules.

[60] M. M. Savitski, F. B. Reinhard, H. Franken, T. Werner, M. F. Savitski, D. Eberhard, D. Martinez Molina, R. Jafari, R. B. Dovega, S. Klaeger, B. Kuster, P. Nordlund, M. Bantscheff, G. Drewes, *Science* **2014**, *346*, 1255784. Tracking cancer drugs in living cells by thermal profiling of the proteome.

[61] M. Schurmann, P. Janning, S. Ziegler, H. Waldmann, *Cell Chem. Biol.* **2016**, *23*, 435–441. Small-Molecule Target Engagement in Cells.

[62] G. Giaever, P. Flaherty, J. Kumm, M. Proctor, C. Nislow, D. F. Jaramillo, A. M. Chu, M. I. Jordan, A. P. Arkin, R. W. Davis, *Proc. Natl. Acad. Sci. USA* **2004**, *101*, 793–798. Chemogenomic profiling: Identifying the functional interactions of small molecules in yeast.

[63] M. J. Keiser, B. L. Roth, B. N. Armbruster, P. Ernsberger, J. J. Irwin, B. K. Shoichet, *Nat. Biotechnol.* **2007**, *25*, 197–206. Relating protein pharmacology by ligand chemistry.

[64] M. J. Keiser, V. Setola, J. J. Irwin, C. Laggner, A. I. Abbas, S. J. Hufeisen, N. H. Jensen, M. B. Kuijer, R. C. Matos, T. B. Tran, R. Whaley, R. A. Glennon, J. Hert, K. L. Thomas, D. D. Edwards, B. K. Shoichet, B. L. Roth, *Nature* **2009**, *462*, 175–181. Predicting new molecular targets for known drugs.

[65] D. Gfeller, O. Michielin, V. Zoete, *Bioinformatics* **2013**, *29*, 3073–3079. Shaping the interaction landscape of bioactive molecules.

[66] A. Cereto-Massagué, M. J. Ojeda, C. Valls, M. Mulero, G. Pujadas, S. Garcia-Vallve, *Methods* **2015**, *71*, 98–103. Tools for in silico target fishing.

[67] J. Joachim, M. Jiang, N. C. McKnight, M. Howell, S. A. Tooze, *Methods* **2015**, *75*, 96–104. High-throughput screening approaches to identify regulators of mammalian autophagy.

[68] N. Mizushima, A. Yamamoto, M. Matsui, T. Yoshimori, Y. Ohsumi, *Mol. Biol. Cell* **2004**, *15*, 1101–1111. In vivo analysis of autophagy in response to nutrient starvation using transgenic mice expressing a fluorescent autophagosome marker.

[69] A. D. Balgi, B. D. Fonseca, E. Donohue, T. C. Tsang, P. Lajoie, C. G. Proud, I. R. Nabi, M. Roberge, *PLoS One* **2009**, *4*, e7124. Screen for chemical modulators of autophagy reveals novel therapeutic inhibitors of mTORC1 signaling.

[70] L. Zhang, J. Yu, H. Pan, P. Hu, Y. Hao, W. Cai, H. Zhu, A. D. Yu, X. Xie, D. Ma, J. Yuan, *Proc. Natl. Acad. Sci. USA* **2007**, *104*, 19023–19028. Small molecule regulators of autophagy identified by an image-based high-throughput screen.

[71] Y. Li, S. McGreal, J. Zhao, R. Huang, Y. Zhou, H. Zhong, M. Xia, W.-X. Ding, *Pharmacol. Res.* **2016**, *110*, 35–49. A cell-based quantitative high-throughput image screening identified novel autophagy modulators.

[72] S. Chauhan, Z. Ahmed, S. B. Bradfute, J. Arko-Mensah, M. A. Mandell, S. Won Choi, T. Kimura, F. Blanchet, A. Waller, M. H. Mudd, S. Jiang, L. Sklar, G. S. Timmins, N. Maphis, K. Bhaskar, V. Piguet, V. Deretic, *Nat. Commun.* **2015**, *6*, 8620–8634. Pharmaceutical screen identifies novel target processes for activation of autophagy with a broad translational potential.

[73] L. Laraia, K. Ohsawa, G. Konstantinidis, L. Robke, Y. W. Wu, K. Kumar, H. Waldmann, *Angew. Chem. Int. Ed.* **2017**, *56*, 2145–2150. Discovery of Novel Cinchona-Alkaloid-Inspired Oxazatwistane Autophagy Inhibitors.

[74] I.-K. Choi, Y. S. Cho, H. J. Jung, H. J. Kwon, *Biochem. Biophys. Res. Commun.* **2010**, *393*, 849–854. Autophagonizer, a novel synthetic small molecule, induces autophagic cell death.

[75] J. V. Peppard, C. Rugg, M. Smicker, C. Dureuil, B. Ronan, O. Flamand, L. Durand, B. Pasquier, *Curr. Chem. Genom. Transl. Med.* **2014**, *8*, 3–15. Identifying Small Molecules which Inhibit Autophagy: a Phenotypic Screen Using Image-Based High-Content Cell Analysis.

[76] S. Lee, E. Kim, S. B. Park, *Chem. Sci.* **2013**, *4*, 3282–3287. Discovery of autophagy modulators through the construction of a high-content screening platform via monitoring of lipid droplets.

[77] Y. Sasazawa, S. Kanagaki, E. Tashiro, T. Nogawa, M. Muroi, Y. Kondoh, H. Osada, M. Imoto, *ACS Chem. Biol.* **2012**, *7*, 892–900. Xanthohumol Impairs Autophagosome Maturation through Direct Inhibition of Valosin-Containing Protein.

[78] F. Gong, X. Peng, Y. Sang, M. Qiu, C. Luo, Z. He, X. Zhao, A. Tong, *Cell Death Dis.* **2013**, *4*, e913. Dichloroacetate induces protective autophagy in LoVo cells: involvement of cathepsin D/thioredoxin-like protein 1 and Akt-mTOR-mediated signaling.

[79] L. Robke, L. Laraia, M. A. Carnero Corrales, G. Konstantinidis, M. Muroi, A. Richters, M. Winzker, T. Engbring, S. Tomassi, N. Watanabe, H. Osada, D. Rauh, H. Waldmann, Y. W. Wu, J. Engel, *Angew. Chem. Int. Ed.* **2017**, *56*, 8153–8157. Phenotypic Identification of a Novel Autophagy Inhibitor Chemotype Targeting Lipid Kinase VPS34.

[80] D. J. Klionsky, K. Abdelmohsen, A. Abe*, et al.*, *Autophagy* **2016**, *12*, 1–222. Guidelines for the use and interpretation of assays for monitoring autophagy (3rd edition).

[81] N. Mizushima, T. Yoshimori, B. Levine, *Cell* **2010**, *140*, 313–326. Methods in mammalian autophagy research.

[82] T. N. Campbell, F. Y. M. Choy, *Mol. Biol. Today* **2001**, *2*, 1–4. The Effect of pH on Green Fluorescent Protein: a Brief Review.

[83] N. Jaber, Z. Dou, J. S. Chen, J. Catanzaro, Y. P. Jiang, L. M. Ballou, E. Selinger, X. Ouyang, R. Z. Lin, J. Zhang, W. X. Zong, *Proc. Natl. Acad. Sci. USA* **2012**, *109*, 2003–2008. Class III PI3K Vps34 plays an essential role in autophagy and in heart and liver function.

[84] C. Burman, N. T. Ktistakis, *FEBS Lett.* **2010**, *584*, 1302–1312. Regulation of autophagy by phosphatidylinositol 3-phosphate.

[85] T. Proikas-Cezanne, S. Waddell, A. Gaugel, T. Frickey, A. Lupas, A. Nordheim, *Oncogene* **2004**, *23*, 9314–9325. WIPI-1alpha (WIPI49), a member of the novel 7-bladed WIPI protein family, is aberrantly expressed in human cancer and is linked to starvation-induced autophagy.

[86] T. R. Jeffries, S. K. Dove, R. H. Michell, P. J. Parker, *Mol. Biol. Cell* **2004**, *15*, 2652–2663. PtdIns-specific MPR pathway association of a novel WD40 repeat protein, WIPI49.

[87] R. C. Russell, Y. Tian, H. Yuan, H. W. Park, Y. Y. Chang, J. Kim, H. Kim, T. P. Neufeld, A. Dillin, K. L. Guan, *Nat. Cell Biol.* **2013**, *15*, 741–750. ULK1 induces autophagy by phosphorylating Beclin-1 and activating VPS34 lipid kinase.

[88] K. Inoki, T. Zhu, K. L. Guan, *Cell* **2003**, *115*, 577–590. TSC2 mediates cellular energy response to control cell growth and survival.

[89] D. M. Gwinn, D. B. Shackelford, D. F. Egan, M. M. Mihaylova, A. Mery, D. S. Vasquez, B. E. Turk, R. J. Shaw, *Mol. Cell* **2008**, *30*, 214–226. AMPK phosphorylation of raptor mediates a metabolic checkpoint.

[90] D. J. Klionsky, *Autophagy* **2012**, *8*, 445-544. Guidelines for the use and interpretation of assays for monitoring autophagy.

[91] O. R. Suarez-Castillo, L. Beiza-Granados, M. Melendez-Rodriguez, A. Alvarez-Hernandez, M. S. Morales-Rios, P. Joseph-Nathan, *J. Nat. Prod.* **2006**, *69*, 1596–1600. Synthesis of bromoindole alkaloids from Laurencia brongniartii.

[92] W. P. Reeves, R. M. King, *Synth. Commun.* **1993**, *23*, 855–859. A Convenient Method for Bromination of Aromatic-Amines.

[93] M. B. Smith, L. Guo, S. Okeyo, J. Stenzel, J. Yanella, E. LaChapelle, *Org. Lett.* **2002**, *4*, 2321–2323. Regioselective one-pot bromination of aromatic amines.

[94] F. M. Moghaddam, D. Zargarani, *Synth. Commun.* **2009**, *39*, 4212–4220. Regioselective Bromination of Aromatic Amines and Phenols UsingN-Benzyl-DABCO Tribromide.

[95] V. Caló, F. Ciminale, L. Lopez, P. E. Todesco, *J. Chem. Soc. C* **1971**, 3652–3654. A Selective Bromination of Aromatic Amines.

[96] A. L. Borror, E. Chinoporos, M. P. Filosa, S. R. Herchen, C. P. Petersen, C. A. Stern, *J. Org. Chem.* **1988**, *53*, 2047–2052. Regioselectivity of Electrophilic Aromatic-Substitution - Syntheses of 6-Sulfamoylindolines and 7-Sulfamoylindolines and Sulpamoylindoles.

[97] M. E. Welsch, S. A. Snyder, B. R. Stockwell, *Curr. Opin. Chem. Biol.* **2010**, *14*, 347–361. Privileged scaffolds for library design and drug discovery.

[98] F. R. D. Alves, E. J. Barreiro, C. A. M. Fraga, *Mini-Rev. Med. Chem.* **2009**, *9*, 782–793. From Nature to Drug Discovery: The Indole Scaffold as a 'Privileged Structure'.

[99] J. A. Burkhard, G. Wuitschik, M. Rogers-Evans, K. Müller, E. M. Carreira, *Angew. Chem. Int. Ed.* **2010**, *49*, 9052–9067. Oxetanes as Versatile Elements in Drug Discovery and Synthesis.

[100] A. A. Estrada, D. G. Shore, E. Blackwood*, et al.*, *J. Med. Chem.* **2013**, *56*, 3090–3101. Pyrimidoaminotropanes as potent, selective, and efficacious small molecule kinase inhibitors of the mammalian target of rapamycin (mTOR).

[101] G. A. Patani, E. J. LaVoie, *Chem. Rev.* **1996**, *96*, 3147–3176. Bioisosterism: A Rational Approach in Drug Design.

[102] S. Marriott, W. F. Reynolds, R. W. Taft, R. D. Topsom, *J. Org. Chem.* **1984**, *49*, 959–965. Substituent Electronegativity Parameters.

[103] A. R. Campanelli, A. Domenicano, F. Ramondo, I. Hargittai, *J. Phys. Chem. A* **2004**, *108*, 4940–4948. Group electronegativities from benzene ring deformations: A quantum chemical study.

[104] T. T. Talele, *J. Med. Chem.* **2016**, *59*, 8712–8756. The "Cyclopropyl Fragment" is a Versatile Player that Frequently Appears in Preclinical/Clinical Drug Molecules.

[105] N. A. Meanwell, *J. Med. Chem.* **2011**, *54*, 2529–2591. Synopsis of some recent tactical application of bioisosteres in drug design.

[106] H. Dückert, V. Pries, V. Khedkar, S. Menninger, H. Bruss, A. W. Bird, Z. Maliga, A. Brockmeyer, P. Janning, A. Hyman, S. Grimme, M. Schurmann, H. Preut, K. Hubel, S. Ziegler, K. Kumar, H. Waldmann, *Nat. Chem. Biol.* **2011**, *8*, 179–184. Natural product-inspired cascade synthesis yields modulators of centrosome integrity.

[107] N. P. Grimster, C. Gauntlett, C. R. A. Godfrey, M. J. Gaunt, *Angew. Chem. Int. Ed.* **2005**, *117*, 3185–3189. Palladium-Catalyzed Intermolecular Alkenylation of Indoles by Solvent-Controlled Regioselective C–H Functionalization.

[108] C. Bonnefous, J. E. Payne, N. D. Smith, T. Z. Hoffman, M. Sertic, P. L. Wash, J. W. Malecha (K. Inc.), WO/2007/067994, **2007**. Inhibitors of Histone Deacetylase for the Treatment of Disease

[109] “Heterocyclic Scaffolds II: Reactions and Applications of Indoles,” in *Topics in Heterocyclic Chemistry, Vol. 26* (Ed.: G. W. Gribble), **2010**.

[110] A. E. Lanzilotti, R. Littell, W. J. Fanshawe, T. C. Mckenzie, F. M. Lovell, *J. Org. Chem.* **1979**, *44*, 4809–4813. Stereoselective Reduction of Some Indoles with Triethylsilane-Trifluoroacetic Acid.

[111] J. S. Ward, R. W. Fuller, L. Merritt, H. D. Snoddy, J. W. Paschal, N. R. Mason, J. S. Horng, *J. Med. Chem.* **1988**, *31*, 1512–1519. Ergolines as Selective 5-HT1 Agonists.

[112] I. Yanovsky, E. Finkin-Groner, A. Zaikin, L. Lerman, H. Shalom, S. Zeeli, T. Weill, I. Ginsburg, A. Nudelman, M. Weinstock, *J. Med. Chem.* **2012**, *55*, 10700–10715. Carbamate derivatives of indolines as cholinesterase inhibitors and antioxidants for the treatment of Alzheimer's disease.

[113] R. V. Duran, E. D. MacKenzie, H. Boulahbel, C. Frezza, L. Heiserich, S. Tardito, O. Bussolati, S. Rocha, M. N. Hall, E. Gottlieb, *Oncogene* **2013**, *32*, 4549–4556. HIF-independent role of prolyl hydroxylases in the cellular response to amino acids.

[114] R. V. Duran, W. Oppliger, A. M. Robitaille, L. Heiserich, R. Skendaj, E. Gottlieb, M. N. Hall, *Mol. Cell* **2012**, *47*, 349–358. Glutaminolysis activates Rag-mTORC1 signaling.

[115] A. Csibi, S. M. Fendt, C. Li, G. Poulogiannis, A. Y. Choo, D. J. Chapski, S. M. Jeong, J. M. Dempsey, A. Parkhitko, T. Morrison, E. P. Henske, M. C. Haigis, L. C. Cantley, G. Stephanopoulos, J. Yu, J. Blenis, *Cell* **2013**, *153*, 840–854. The mTORC1 pathway stimulates glutamine metabolism and cell proliferation by repressing SIRT4.

[116] S. Lorin, M. J. Tol, C. Bauvy, A. Strijland, C. Pous, A. J. Verhoeven, P. Codogno, A. J. Meijer, *Autophagy* **2013**, *9*, 850–860. Glutamate dehydrogenase contributes to leucine sensing in the regulation of autophagy.

[117] C. Spanaki, I. Zaganas, K. A. Kleopa, A. Plaitakis, *J. Biol. Chem.* **2010**, *285*, 16748–16756. Human GLUD2 glutamate dehydrogenase is expressed in neural and testicular supporting cells.

[118] J. V. Rodrigues, V. Prosinecki, I. Marrucho, L. P. Rebelo, C. M. Gomes, *Phys. Chem. Chem. Phys.* **2011**, *13*, 13614–13616. Protein stability in an ionic liquid milieu: on the use of differential scanning fluorimetry.

[119] A. Sener, W. J. Malaisse, *Nature* **1980**, *288*, 187–189. L-leucine and a nonmetabolized analogue activate pancreatic islet glutamate dehydrogenase.

[120] C. Li, A. Allen, J. Kwagh, N. M. Doliba, W. Qin, H. Najafi, H. W. Collins, F. M. Matschinsky, C. A. Stanley, T. J. Smith, *J. Biol. Chem.* **2006**, *281*, 10214–10221. Green tea polyphenols modulate insulin secretion by inhibiting glutamate dehydrogenase.

[121] Y. Huang, K. K. Wang, *Trends Mol. Med.* **2001**, *7*, 355–362. The calpain family and human disease.

[122] F. Demarchi, C. Bertoli, T. Copetti, I. Tanida, C. Brancolini, E. L. Eskelinen, C. Schneider, *J. Cell Biol.* **2006**, *175*, 595–605. Calpain is required for macroautophagy in mammalian cells.

[123] H. G. Xia, L. Zhang, G. Chen, T. Zhang, J. Liu, M. Jin, X. Ma, D. Ma, J. Yuan, *Autophagy* **2010**, *6*, 61–66. Control of basal autophagy by calpain1 mediated cleavage of ATG5.

[124] W. Zhang, J. Liu, R. Sun, L. Zhao, J. Du, C. Ruan, K. Dai, *Int. J. Mol. Sci.* **2011**, *12*, 2125–2137. Calpain activator dibucaine induces platelet apoptosis.

[125] S. Mehdi, *Trends Biochem. Sci* **1991**, *16*, 150–153. Cell-penetrating inhibitors of calpain.

[126] D. Donnelly-Roberts, S. McGaraughty, C. C. Shieh, P. Honore, M. F. Jarvis, *J. Pharmacol. Exp. Ther.* **2008**, *324*, 409–415. Painful purinergic receptors.

[127] N.-i.-H. Syed, C. Kennedy, *Wiley Interdiscip. Rev. Membr. Transp. Signal* **2012**, *1*, 16–30. Pharmacology of P2X receptors.

[128] R. Fischer, B. Kalthof, E. Rank, B. Stelte-Ludwig, M. Wuttke DE 10312969A1, **2004**. Preparation of benzofuro-1,4-diazepin-2-ones as P2X4 receptor antagonists for the treatment of arteriosclerosis and restenosis

[129] D. Draganov, S. Gopalakrishna-Pillai, Y. R. Chen, N. Zuckerman, S. Moeller, C. Wang, D. Ann, P. P. Lee, *Sci. Rep.* **2015**, *5*, 16222–16239. Modulation of P2X4/P2X7/Pannexin-1 sensitivity to extracellular ATP via Ivermectin induces a non-apoptotic and inflammatory form of cancer cell death.

[130] A. Kondratskyi, M. Yassine, K. Kondratska, R. Skryma, C. Slomianny, N. Prevarskaya, *Front. Physiol.* **2013**, *4*, 272. Calcium-permeable ion channels in control of autophagy and cancer.

[131] D. A. East, M. Campanella, *Autophagy* **2013**, *9*, 1710–1719. Ca2+ in quality control: an unresolved riddle critical to autophagy and mitophagy.

[132] M. Høyer-Hansen, L. Bastholm, P. Szyniarowski, M. Campanella, G. Szabadkai, T. Farkas, K. Bianchi, N. Fehrenbacher, F. Elling, R. Rizzuto, I. S. Mathiasen, M. Jaattela, *Mol. Cell* **2007**, *25*, 193–205. Control of macroautophagy by calcium, calmodulin-dependent kinase kinase-beta, and Bcl-2.

[133] J. E. Gonzalez, K. Oades, Y. Leychkis, A. Harootunian, P. A. Negulescu, *Drug Discov. Today* **1999**, *4*, 431–439. Cell-based assays and instrumentation for screening ion-channel targets.

[134] H. B. Yu, M. Li, W. P. Wang, X. L. Wang, *Acta Pharmacol. Sin.* **2016**, *37*, 34–43. High throughput screening technologies for ion channels.

[135] O. B. McManus, M. L. Garcia, D. Weaver, M. Bryant, S. Titus, J. B. Herrington, in *Assay Guidance Manual* (Ed.: O. B. McManus), Bethesda (MD): Eli Lilly & Company and the National Center for Advancing Translational Sciences, **2012**.

[136] T. Kawate, J. C. Michel, W. T. Birdsong, E. Gouaux, *Nature* **2009**, *460*, 592–598. Crystal structure of the ATP-gated P2X(4) ion channel in the closed state.

[137] A. R. Ase, N. S. Honson, H. Zaghdane, T. A. Pfeifer, P. Seguela, *Mol. Pharmacol.* **2015**, *87*, 606–616. Identification and characterization of a selective allosteric antagonist of human P2X4 receptor channels.

[138] C. A. Jones, I. P. Chessell, J. Simon, E. A. Barnard, K. Miller, J., A. D. Michel, P. P. A. Humphrey, *Br. J. Pharmacol.* **2000**, *129*, 388–394. Functional characterization of the P2X4 receptor orthologues.

[139] L. Bar-Peled, L. D. Schweitzer, R. Zoncu, D. M. Sabatini, *Cell* **2012**, *150*, 1196–1208. Ragulator Is a GEF for the Rag GTPases that Signal Amino Acid Levels to mTORC1.

[140] SciFinder, available at http://scifinder.cas.org/, Chemical Abstracts Service: Columbus, OH (accessed Oct. 2013).

[141] M. Enriqueta Muñoz, E. Ponce, *Comp. Biochem. Phys. B* **2003**, *135*, 197–218. Pyruvate kinase: current status of regulatory and functional properties.

[142] S. Mazurek, C. B. Boschek, F. Hugo, E. Eigenbrodt, *Semin. Cancer Biol.* **2005**, *15*, 300–308. Pyruvate kinase type M2 and its role in tumor growth and spreading.

[143] M. G. Vander Heiden, H. R. Christofk, E. Schuman, A. O. Subtelny, H. Sharfi, E. E. Harlow, J. Xian, L. C. Cantley, *Biochem. Pharmacol.* **2010**, *79*, 1118–1124. Identification of small molecule inhibitors of pyruvate kinase M2.

[144] B. Chiavarina, D. Whitaker-Menezes, U. E. Martinez-Outschoorn, A. K. Witkiewicz, R. Birbe, A. Howell, R. G. Pestell, J. Smith, R. Daniel, F. Sotgia, M. P. Lisanti, *Cancer Biol. Ther.* **2011**, *12*, 1101–1113. Pyruvate kinase expression (PKM1 and PKM2) in cancer-associated fibroblasts drives stromal nutrient production and tumor growth.

[145] S. Sridharan, K. Jain, A. Basu, *Cancers (Basel)* **2011**, *3*, 2630–2654. Regulation of autophagy by kinases.

[146] N. Verma, S. K. Manna, *J. Biol. Chem.* **2016**, *291*, 1481–1491. Advanced Glycation End Products (AGE) Potently Induce Autophagy through Activation of RAF Protein Kinase and Nuclear Factor κB (NF-κB).

[147] B. Liu, J.-M. Wu, J. Li, J.-J. Liu, W.-W. Li, C.-Y. Li, H.-L. Xu, J.-K. Bao, *Biochimie* **2010**, *92*, 1934–1938. Polygonatum cyrtonema lectin induces murine fibrosarcoma L929 cell apoptosis and autophagy via blocking Ras–Raf and PI3K–Akt signaling pathways.

[148] J. L. Armstrong, M. Corazzari, S. Martin, V. Pagliarini, L. Falasca, D. S. Hill, N. Ellis, S. Al Sabah, C. P. F. Redfern, G. M. Fimia, M. Piacentini, P. E. Lovat, *Clin. Cancer. Res.* **2011**, *17*, 2216–2226. Oncogenic B-RAF Signaling in Melanoma Impairs the Therapeutic Advantage of Autophagy Inhibition.

[149] O. Hantschel, *Genes & Cancer* **2012**, *3*, 436–446. Structure, Regulation, Signaling, and Targeting of Abl Kinases in Cancer.

[150] D. Cilloni, G. Saglio, *Clin. Cancer. Res.* **2012**, *18*, 930–937. Molecular Pathways: BCR-ABL.

[151] G. Yogalingam, A. M. Pendergast, *J. Biol. Chem.* **2008**, *283*, 35941–35953. Abl Kinases Regulate Autophagy by Promoting the Trafficking and Function of Lysosomal Components.

[152] Z. Sheng, L. Ma, J. E. Sun, L. J. Zhu, M. R. Green, *Blood* **2011**, *118*, 2840. BCR-ABL suppresses autophagy through ATF5-mediated regulation of mTOR transcription.

[153] D. E. Nichols, C. D. Nichols, *Chem. Rev.* **2008**, *108*, 1614–1641. Serotonin receptors.

[154] R. A. Glennon, *J. Med. Chem.* **1987**, *30*, 1–12. Central Serotonin Receptors as Targets for Drug Research.

[155] D. Hoyer, *Pharmacol. Rev.* **1994**, *46*, 157–203. VII: International Union of Pharmacology Classification of Receptors for 5-Hydroxytryptamine (Serotonin).

[156] M. Popiolek, D. P. Nguyen, V. Reinhart, J. R. Edgerton, J. Harms, S. M. Lotarski, S. J. Steyn, J. E. Davoren, S. Grimwood, *Biochemistry* **2016**, *55*, 7073–7085. Inositol Phosphate Accumulation in Vivo Provides a Measure of Muscarinic M1 Receptor Activation.

[157] R. Zhang, X. Xie, *Acta Pharmacol. Sin.* **2012**, *33*, 372–384. Tools for GPCR drug discovery.

[158] F. Ye, G. F. Anthony, V. Ronald, *Combinatorial Chem. High Throughput Screening* **2008**, *11*, 357–369. Label-Free Cell-Based Assays for GPCR Screening.

[159] E. M. Wauson, H. A. Dbouk, A. B. Ghosh, M. H. Cobb, *Trends Endocrinol. Metab.* **2014**, *25*, 274–282. G protein-coupled receptors and the regulation of autophagy.

[160] Y. Baqi, K. Atzler, M. Kose, M. Glanzel, C. E. Muller, *J. Med. Chem.* **2009**, *52*, 3784–3793. High-affinity, non-nucleotide-derived competitive antagonists of platelet P2Y12 receptors.

[161] C. Chatterjee, D. L. Sparks, *PLoS One* **2012**, *7*, e36916. Extracellular nucleotides inhibit insulin receptor signaling, stimulate autophagy and control lipoprotein secretion.

[162] E. Harlow, D. Lane, *Antibodies: A Laboratory Manual*, Cold Spring Harbor Laboratory Press, New York, **1988**.

[163] J. Cox, M. Mann, *Nat. Biotechnol.* **2008**, *26*, 1367–1372. MaxQuant enables high peptide identification rates, individualized p.p.b.-range mass accuracies and proteome-wide protein quantification.

[164] G. Vendrell-Navarro, A. Brockmeyer, H. Waldmann, P. Janning, S. Ziegler, "Identification of the Targets of Biologically Active Small Molecules Using Quantitative Proteomics," in *Chemical Biology: Methods and Protocols, Vol. 1263*, Springer New York, **2015**, pp. 263–286.

[165] J. Rappsilber, M. Mann, Y. Ishihama, *Nat. Protocols* **2007**, *2*, 1896–1906. Protocol for micro-purification, enrichment, pre-fractionation and storage of peptides for proteomics using StageTips.

[166] M. M. Bradford, *Anal. Biochem.* **1976**, *72*, 248–254. A rapid and sensitive method for the quantitation of microgram quantities of protein utilizing the principle of protein-dye binding.

[167] U. K. Laemmli, *Nature* **1970**, *227*, 680–685. Cleavage of structural proteins during the assembly of the head of bacteriophage T4.

[168] K. E. Beatty, J. D. Fisk, B. P. Smart, Y. Y. Lu, J. Szychowski, M. J. Hangauer, J. M. Baskin, C. R. Bertozzi, D. A. Tirrell, *ChemBioChem* **2010**, *11*, 2092-2095. Live-Cell Imaging of Cellular Proteins by a Strain-Promoted Azide–Alkyne Cycloaddition.

[169] L. Yang, Q. Liang, K. Shen, L. Ma, N. An, W. Deng, Z. Fei, J. Liu, *Biomed. Pharmacother.* **2015**, *71*, 70–78. A novel class I histone deacetylase inhibitor, I-7ab, induces apoptosis and arrests cell cycle progression in human colorectal cancer cells.

9. APPENDIX

Curriculum Vitae

PERSONAL INFORMATION

Surname: Rummelt
Maiden Name: Carnero Corrales
Name: Marjorie Alessandra
Date of Birth: 08.08.1988
Place of Birth: Chiclayo, Peru
Citizenship: Dual Swiss/Peruvian

EDUCATION

Oct. 2013 – Sept. 2017 **PhD student at Max Planck Institute of Molecular Physiology** (Germany)
Research topic: Biological target identification of autophagy inhibitors (chemical biology).
Advisor: Prof. Dr. Dr. Herbert Waldmann

May 2013 – Aug. 2013 **Internship at F. Hoffmann-La Roche** (Basel, Switzerland)
Research topic: Batch synthesis of chemical libraries for known targets (medicinal chemistry).
Advisor: Dr. Rainer E. Martin

Sept. 2011 – Mar. 2013 **Master's at Swiss Federal Institute of Technology Zurich (ETH)**
Biology with major in Biological Chemistry (Zurich, Switzerland)

Master thesis:
Research topic: Using Rebek-imide receptors to study amide–aromatic interactions (supramolecular chemistry).
Advisor: Prof. Dr. François Diederich

Additional research projects:
Research fields: Medicinal chemistry and directed evolution.
Advisors: Prof. Dr. François Diederich and Prof. Dr. Donald Hilvert

Sept. 2008 – Aug. 2011 **Bachelor's at Swiss Federal Institute of Technology (ETH)**
Biology, Chemical Direction (Zurich, Switzerland)

Eidesstattliche Versicherung (Affidavit)

Rummelt, Marjorie Alessandra
Name, Vorname
(Surname, first name)

173202
Matrikel-Nr.
(Enrolment number)

Belehrung:

Wer vorsätzlich gegen eine die Täuschung über Prüfungsleistungen betreffende Regelung einer Hochschulprüfungsordnung verstößt, handelt ordnungswidrig. Die Ordnungswidrigkeit kann mit einer Geldbuße von bis zu 50.000,00 € geahndet werden. Zuständige Verwaltungsbehörde für die Verfolgung und Ahndung von Ordnungswidrigkeiten ist der Kanzler/die Kanzlerin der Technischen Universität Dortmund. Im Falle eines mehrfachen oder sonstigen schwerwiegenden Täuschungsversuches kann der Prüfling zudem exmatrikuliert werden, § 63 Abs. 5 Hochschulgesetz NRW.

Die Abgabe einer falschen Versicherung an Eides statt ist strafbar.

Wer vorsätzlich eine falsche Versicherung an Eides statt abgibt, kann mit einer Freiheitsstrafe bis zu drei Jahren oder mit Geldstrafe bestraft werden, § 156 StGB. Die fahrlässige Abgabe einer falschen Versicherung an Eides statt kann mit einer Freiheitsstrafe bis zu einem Jahr oder Geldstrafe bestraft werden, § 161 StGB.

Die oben stehende Belehrung habe ich zur Kenntnis genommen:

Official notification:

Any person who intentionally breaches any regulation of university examination regulations relating to deception in examination performance is acting improperly. This offence can be punished with a fine of up to EUR 50,000.00. The competent administrative authority for the pursuit and prosecution of offences of this type is the chancellor of the TU Dortmund University. In the case of multiple or other serious attempts at deception, the candidate can also be unenrolled, Section 63, paragraph 5 of the Universities Act of North Rhine-Westphalia.

The submission of a false affidavit is punishable.

Any person who intentionally submits a false affidavit can be punished with a prison sentence of up to three years or a fine, Section 156 of the Criminal Code. The negligent submission of a false affidavit can be punished with a prison sentence of up to one year or a fine, Section 161 of the Criminal Code.

I have taken note of the above official notification.

Dortmund, den 03. Juli 2017
Ort, Datum
(Place, date)

Unterschrift
(Signature)

Titel der Dissertation:
(Title of the thesis):

Identification and biological characterization of indoline-based autophagy inhibitors

Ich versichere hiermit an Eides statt, dass ich die vorliegende Dissertation mit dem Titel selbstständig und ohne unzulässige fremde Hilfe angefertigt habe. Ich habe keine anderen als die angegebenen Quellen und Hilfsmittel benutzt sowie wörtliche und sinngemäße Zitate kenntlich gemacht.
Die Arbeit hat in gegenwärtiger oder in einer anderen Fassung weder der TU Dortmund noch einer anderen Hochschule im Zusammenhang mit einer staatlichen oder akademischen Prüfung vorgelegen.

I hereby swear that I have completed the present dissertation independently and without inadmissible external support. I have not used any sources or tools other than those indicated and have identified literal and analogous quotations.

The thesis in its current version or another version has not been presented to the TU Dortmund University or another university in connection with a state or academic examination.*

*Please be aware that solely the German version of the affidavit ("Eidesstattliche Versicherung") for the PhD thesis is the official and legally binding version.

Dortmund, den 03. Juli 2017
Ort, Datum
(Place, date)

Unterschrift
(Signature)